CR 152345

A CORRELATION METHOD TO PREDICT THE SURFACE PRESSURE DISTRIBUTION ON AN INFINITE PLATE OR A BODY OF REVOLUTION FROM WHICH A JET IS ISSUING

by

Stanley C. Perkins, Jr. and
Michael R. Mendenhall

NEAR TR 211

January 1980

Prepared under Contract No. NAS2-10125

for

NATIONAL AERONAUTICS AND SPACE ADMINISTRATION
Ames Research Center

by

NIELSEN ENGINEERING & RESEARCH, INC.
510 Clyde Avenue, Mountain View, CA 94043
Telephone (415) 968-9457

1. Report No.	2. Government Accession No.	3. Recipient's Catalog No.
NASA CR-152,345		

4. Title and Subtitle	5. Report Date
A CORRELATION METHOD TO PREDICT THE SURFACE PRESSURE DISTRIBUTION ON AN INFINITE PLATE OR A BODY OF REVOLUTION FROM WHICH A JET IS ISSUING	May 1980
	6. Performing Organization Code 549/C
7. Author(s) Stanley C. Perkins, Jr. and Michael R. Mendenhall	8. Performing Organization Report No. NEAR TR 211
	10. Work Unit No.
9. Performing Organization Name and Address Nielsen Engineering & Research, Inc. 510 Clyde Avenue Mountain View, CA 94043	11. Contract or Grant No. NAS2-10125
	13. Type of Report and Period Covered FINAL 12/7/78 - 5/1/80
12. Sponsoring Agency Name and Address National Aeronautics and Space Administration Ames Research Center Moffett Field, CA 94035	14. Sponsoring Agency Code

15. Supplementary Notes

Ames Technical Monitor, K. Aoyagi

16. Abstract A correlation method to predict pressures induced on an infinite plate by a jet exhausting normal to the plate into a subsonic free stream has been extended to jets exhausting at angles to the plate and to jets exhausting normal to the surface of a body of revolution. The complete method consists of an analytical method which models the blockage and entrainment properties of the jet and an empirical correlation which accounts for viscous effects. For the flat plate case, the method is applicable to jet velocity ratios up to ten, jet inclination angles up to 45° from the normal, and radial distances up to five diameters from the jet. For the body of revolution case, the method is applicable to a body at zero degrees angle of attack, jet velocity ratios 1.96 and 3.43, circumferential angles around the body up to 25° from the jet, axial distances up to seven diameters from the jet, and jet-to-body diameter ratios less than 0.1. Correlation curves and data comparisons are presented for inclined jets issuing from a flat plate with velocity ratios one to twelve. Correlation curves are presented for jets issuing normally from the surface of a body of revolution for velocity ratios 1.96 and 3.43.

17. Key Words (Suggested by Author(s))	18. Distribution Statement
Subsonic Crossflow Jet in a Crossflow Pressure Distribution V/STOL	Unclassified - Unlimited

19. Security Classif. (of this report)	20. Security Classif. (of this page)	21. No. of Pages	22. Price*
Unclassified	Unclassified	198	

*For sale by the National Technical Information Service, Springfield, Virginia 22161

TABLE OF CONTENTS

A CORRELATION METHOD TO PREDICT THE SURFACE PRESSURE DISTRIBUTION ON AN INFINITE PLATE OR A BODY OF REVOLUTION FROM WHICH A JET IS ISSUING

by

Stanley C. Perkins, Jr. and Michael R. Mendenhall

SUMMARY

A correlation method to predict pressures induced on an infinite plate by a jet exhausting normal to the plate into a subsonic free stream has been extended to jets exhausting at angles to the plate and to jets exhausting normal to the surface of a body of revolution. The complete method consists of an analytical method which models the blockage and entrainment properties of the jet and an empirical correlation which accounts for viscous effects. For the flat plate case, the method is applicable to jet velocity ratios up to ten, jet inclination angles up to 45° from the normal, and radial distances up to five diameters from the jet. For the body of revolution case, the method is applicable to a body at zero degrees angle of attack, jet velocity ratios 1.96 and 3.43, circumferential angles around the body up to 25° from the jet, axial distances up to seven diameters from the jet, and jet-to-body diameter ratios less than 0.1. Correlation curves and data comparisons are presented for inclined jets issuing from a flat plate with velocity ratios one to twelve. Correlation curves are presented for jets issuing normally from the surface of a body of revolution for velocity ratios 1.96 and 3.43.

INTRODUCTION

Increased interest in V/STOL configurations which utilize lift-jet engines mounted in the wing, pod, or the fuselage has prompted experimental and analytical studies of jet interference effects on infinite flat plates and bodies of revolution. Experimental studies on infinite flat plates (refs. 1-7) and bodies of revolution (refs. 3, and 8-12) have shown that the jet produces a region of positive pressure upstream of the jet and regions of negative pressure downstream and to the side of the jet. These studies also show a very strong viscous region immediately downstream of the jet. It is in this viscous-dominated region that inviscid analytic methods, such as those presented in references 13-17, have not been successful in predicting surface pressures. As an alternative to purely inviscid methods, an empirical method to predict surface pressures on a flat plate in a crossflow with a jet exhausting normal to the surface was developed by Nielsen Engineering & Research, Inc. (NEAR) and is presented in reference 18. This method consists of an analytical jet model for the inviscid part and empirically-derived factors to account for viscous effects. These factors, which are obtained from a correlation of the difference between analytically predicted surface pressures and measured results, are presented as a function of jet velocity ratio and position on the plate.

In this report, results of a two-phase study to extend the empirical method of reference 18 are presented. The first phase deals with jets exhausting at an angle to an infinite plate. The analytical jet model of reference 18 is used in conjunction with available experimental data to obtain empirical correlation factors. These viscous correlation factors are presented for a range of jet inclination angles and jet velocity ratios, and

predicted pressure distributions are compared with experimental data from several sources. Also included as a part of the first phase are comparisons of new normal-jet data from NASA/Ames Research Center and results obtained using the prediction method with the viscous correlation factors.

The second phase deals with jets exhausting normal to the surface of a body of revolution. The analytical model utilizes the NSRDC version of the Douglas-Neumann program (refs. 19 and 20) to model the body/jet-surface mutual interference effects and the sink distribution model of reference 14 to represent entrainment effects. The jet boundary and position are determined from empirical observations. Development of viscous correlation factors for jets exhausting from a body of revolution are presented for a limited range of jet velocity ratios. Recommendations for improving the present correlation method for jets exhausting from a body of revolution are discussed.

LIST OF SYMBOLS

C_p	pressure coefficient, $p - p_\infty/q_\infty$
D	jet diameter at the exit plane
$\vec{n}$	unit normal at a point, see figure 4
p	static pressure
q_∞	dynamic pressure, $\frac{1}{2}\rho_\infty V_\infty^2$
r	radial distance along the plate from the center of the jet to any field point on the plate
R	jet radius at the exit plane
S_a	curve length of the jet axis
S_{pc}	curve length of potential core
t	local jet radius
u,v,w	velocity components in the x,y, and z directions, respectively
V_j	jet velocity at the exit plane
V_∞	constant free-stream velocity
x,y,z	plate coordinate system fixed at the center of the jet exit plane, positive x is upstream
x_j,y_j,z_j	jet coordinate system fixed at center of the jet exit plane, positive x_j is downstream
β	polar angle, measured clockwise from the positive x-axis in the plate x-y plane, see figure 1
$(\Delta C_p)_{viscous}$	correlation increment of pressure coefficient
δ_j	initial inclination angle of jet centerline, measured from the positive x-axis in the x-z plane, $\delta_j = 90° - \theta$; see figure 1
θ	initial inclination angle of jet centerline, measured from the positive z_j axis in the x_j-z_j plane, $\theta = 0°$ for a jet issuing normal to the free stream, see figure 1

LIST OF SYMBOLS (Concluded)

ρ_∞	density
ϕ	circumferential angle, measured from top of body of revolution, see figure 17

Subscripts

j	jet quantity
max	maximum value
∞	free-stream quantity

APPROACH

The problem of interest is the prediction of the surface pressure distribution in the vicinity of a jet issuing from a flat or curved surface in the presence of a free-stream flow along the surface. The flat plate case is illustrated in figure 1. If one uses a potential flow model to describe the flow, including jet entrainment, blockage and curvature, one can predict the surface pressures upstream of the jet (β less than 60°) reasonably well, but the discrepancies become increasingly large as β increases beyond 90°. The source of the differences is a viscous interaction between the flow around the jet and the surface flow, which cannot be modeled properly with present analytical methods due to lack of detailed flow data in the interaction region.

In the work of reference 18, an approach was adopted for the flat plate case in which a potential model was selected which gave good agreement with surface pressures upstream of the jet, and the differences between the predicted and measured pressures around the jet were correlated into a viscous correction. Accordingly, the pressure coefficient at every point on the plate can be expressed as

$$C_p = C_p\Big|_{\text{potential}} + \Delta C_p\Big|_{\text{viscous}} \qquad (1)$$

where $\Delta C_p\big|_{\text{viscous}}$ is the correlation factor which represents viscous or non-potential effects. The potential portion of the above equation is calculated using the Bernoulli equation in the form

$$C_p = 1 - \left\{ \frac{(V_\infty + u)^2 + v^2}{V_\infty^2} \right\} \qquad (2)$$

In the current work, the same approach is taken. The first task, then, is to establish a potential jet model that agrees well with the upstream pressures, considering first the case of the flat plate with the jet issuing at an angle δ_j other than 90° and secondly the case of a jet issuing normally from the surface of a body of revolution. After the model is selected and verified, the viscous correlations are obtained. In the following sections, the development of the jet model and correlation for the two cases is described.

Flat Plate

A sketch of an expanding jet of initial velocity V_j and initial inclination angle θ emerging from an infinite plate into a subsonic crossflow of velocity V_∞ is shown in figure 1. The flat plate method presented herein is applicable to low speed crossflow velocities and jet Mach numbers less than one.

Jet model.- Details concerning the specification of the jet centerline path, the blockage and entrainment models, and the spreading rate of a jet exhausting normal to a flat plate are presented in reference 18. The same basic jet model, with some modifications made to the blockage and entrainment models, is used for a jet exhausting at an angle to a flat plate. A general description of the various components of the jet model is presented in the following paragraphs.

The path of the jet centerline is specified using the empirical relation developed by Margason (ref. 21):

$$\frac{x_j}{D} = \frac{1}{4\sin^2\delta_j}\left[\frac{V_\infty}{V_j}\right]^2\left[\frac{z_j}{D}\right]^3 + \frac{z_j}{D}\cot\delta_j \qquad (3)$$

Figure 2 shows jet centerline shapes given by equation (3) for a range of velocity ratios with $\delta_j = 75^\circ$, 60°, 45°, and 30°. As shown in this figure, the spread in centerline position with velocity ratio is reduced as the jet becomes more parallel to the crossflow.

A comparison of measured and predicted jet centerline shapes is shown in figure 3 for $V_j/V_\infty = 12$ and $\theta = 0^\circ$, 15°, 30°, 45°, and 60°. The good agreement between the measured centerline shapes, which were determined by locating the position of maximum total pressure in successive $y_j - z_j$ planes behind the jet, and those obtained using equation (3) lends confidence to the use of this equation for obtaining centerline shapes for jets in a crossflow.

Blockage effects of the jet are modeled by representing the specified wake surface with a series of vortex quadrilateral panels on which a boundary condition of flow tangency due to the free stream is enforced. The vortex quadrilateral panel blockage model described herein is based on a method developed by Maskew (ref. 22).

The boundary of the jet wake, specified by the centerline path and the wake radius along the centerline, is divided into length segments as illustrated in figure 4. Each length segment is further divided into a number of circumferential segments. A slice through the wake, normal to the centerline, shows the circular cross section wake to be represented by a series of

straight segments. The control point on each panel is located at the centroid of the panel, and the vector $\vec{n}$ is the unit normal to the panel, positive when directed outward. The boundary condition satisfied at each control point is

$$\vec{V} \cdot \vec{n} = 0 \qquad (4)$$

where $\vec{V}$ is the vector sum of the free-stream velocity and the velocity induced at a panel control point by all vortex quadrilateral panels making up the blockage model. Implementation of this boundary condition results in a set of linear simultaneous equations which can be solved for the unknown vortex quadrilateral strengths.

After obtaining the vortex strengths for each panel, the field point velocity induced by a single vortex quadrilateral is obtained by summing the contribution from each of the four sides of the quadrilateral. A summation over all the panels representing the jet surface produces the velocity induced at a point by the complete blockage model.

As a jet is inclined from the normal to the plate, the shape of the jet exit at the plate becomes elliptical. In order to model this shape, modification of the panel layout in the region near the plate is necessary. Figure 5 shows a side view of the panel layout of a jet in the region near the plate for V_j/V_∞ = 12.0, $\theta = 45^\circ$. The "transition" disc between the elliptical disc at the plate and the first circular disc is required to maintain panels of reasonable aspect ratio (height/width) in the front part of the jet. A disc, as indicated in the figure, is a slice through the jet cross-section at the end of a row of panels. Each disc following the third disc is circular.

It is noted that the predicted plate pressures in the region immediately behind the jet become very sensitive to panel length for large jet inclination angles. This is a numerical problem due to end effects from vortex quadrilateral panels which come closer to the plate in the region behind the jet as the inclination angle increases. It is necessary that low aspect ratio panels be used for jets exhausting at large angles to a flat plate.

The spreading rate for a jet exhausting from a flat plate is calculated using a method described in reference 18. This method utilizes the empirical method of reference 23 and data from reference 24. The empirical method of Bowley and Sucec (ref. 23) is directly applicable to a jet exhausting at an angle. It is assumed, due to lack of data, that the local centerline velocity data of reference 24 for jets exhausting normal to the plate can be used for jets exhausting at an angle. Total pressure profiles presented in reference 7 for a jet exhausting at a range of inclination angles to a plate indicate that this assumption is valid.

Assumptions are also made, as discussed in detail in reference 18, that the jet is axisymmetric and the potential core length is three jet diameters. It is generally accepted that potential core length is a function of jet velocity ratio and inclination angle; however, the variation of experimentally-determined potential core length with these parameters, as shown in figure 6, is considerable for different tests and there is insufficient data on which to base a functional relation. Consequently, a potential core length of three jet diameters was selected as a reasonable average length based on the range of data shown.

Figure 7 presents a series of expansion rate curves which show nondimensional jet radius (t/D) versus nondimensional distance along the jet centerline (S_a/R). These curves are used to represent the expansion of the circular cross section of the jet (ref. 18). Some comments regarding the curves in figure 7 follow. First, data from reference 24 were used to obtain expansion curves for V_j/V_∞ = 4.0, 6.0, and 8.0. All other expansion curves were obtained by interpolation or extrapolation of these curves. Second, the V_j/V_∞ = 12.0 expansion rate curve is not shown, since the expansion curves for V_j/V_∞ = 10.0 and 12.0 are essentially identical.

Figure 8 presents plots of $(t/D)_{max}$ versus V_j/V_∞, where $(t/D)_{max}$ is the value of t/D at S_a/R = 20. This value of jet centerline length (S_a/R) is used as the upper integration limit for the jet entrainment model and represents the total length of the jet modeled. It was found (ref. 18) that increasing the length of the jet beyond 20 initial jet radii increased computation time without affecting change in the final results. Choosing S_a/R = 20 as the length of the jet centerline and assuming $(t/D)_{max} \to 1.0$ as $V_j/V_\infty \to 0$, a curve is faired through this point and the values of $(t/D)_{max}$ for V_j/V_∞ = 4.0, 6.0, and 8.0. These plots are then used when interpolating or extrapolating the V_j/V_∞ = 4.0, 6.0, and 8.0 expansion curves to obtain a spreading rate for arbitrary V_j/V_∞ (see ref. 18).

Jet entrainment effects for a jet exhausting at an angle to a plate are obtained using a modified version of an empirical method developed by Yeh (ref. 14). Experimental data from reference 7 indicate that the entrainment rate of a jet is lowered as jet inclination angle (θ) is increased; however, the amount by which entrainment is reduced is not known. Since Yeh's method was developed for jets exhausting normal to a flat

plate, it was decided to use an effective velocity ratio given by the normal component of the initial jet velocity ratio. This relationship is given by:

$$\left(\frac{V_j}{V_\infty}\right)_{\text{effective}} = \frac{V_j}{V_\infty} \cos \theta \qquad (5)$$

where θ is the initial inclination angle of the jet measured from the normal to the plate (see fig. 1).

Predicted results were obtained using these entrainment and blockage models, and comparisons with experimental data over a wide range of velocity ratios and inclination angles were made. These data comparisons, shown in figures 9 through 12, are for the region of the plate where viscous effects are believed to be small ($0^\circ \leq \beta \leq 60^\circ$) based on experimental observations (ref. 5). Data comparisons in this region are a true test of the ability of the potential flow model to accurately predict pressures on the plate in the absence of large viscous effects.

As can be seen in these figures, varying degrees of success were obtained using the reduced entrainment model. In general, predicted results compare well with experimental results for low velocity ratios ($V_j/V_\infty \leq 7$) and poorly with experimental results for high velocity ratios, especially for $\theta = 15^\circ$ and 45°. For cases in which good agreement between theory and experiment were obtained, differences in the trends exhibited by the data comparisons make it difficult to assess the reduced entrainment model. For example, data comparisons for $V_j/V_\infty = 4.0$, $\theta = 30^\circ$ [fig. 10(b)], indicate good agreement between the data of reference 6 and predicted results obtained using the standard entrainment model. However, this same figure shows that further reduction of the effective velocity ratio is needed

to improve agreement between predicted results and data from reference 28 for $\beta = 0^{\circ}$ and 30°. Differences between data sets and between data and theory, as seen in this figure, may be due to real jet effects, such as initial velocity profile, turbulence level, and potential core length which are not included in the present jet model.

Other low velocity ratio cases were found in which the differences between predicted and experimental results may be due to real jet effects or plate edge effects. For example, figure 13 shows a comparison between measured and predicted pressures for $V_j/V_\infty = 6.67$, $\theta = 15^{\circ}$, $\beta = 60^{\circ}$. The increment between theory and experiment at $r/D = 5.0$ is $\Delta C_p = .074$. Applying this increment to the theory improves the comparison between theory and experiment over the entire r/D range. This phenomena may be due to edge effects or real jet effects, since the increment is usually constant in the region of the plate where viscous effects are small ($\beta = 60^{\circ}$). Since such effects probably vary with distance from the jet or edge of the plate, the increment probably varies with r/D and cannot simply be added to every theoretical value. Further investigation of this phenomena is necessary before applying such techniques to the theory.

In addition to poor agreement between theory and experiment for high velocity ratios, it was found that in many cases the differences between data sets exceeded the differences between theory and experiment. For example, figure 9(f) presents a comparison of predicted and experimental results from references 6 and 28 for $V_j/V_\infty = 10.0$, $\theta = 15^{\circ}$. As this figure shows, the predicted results split the difference between the two sets of data.

The disagreement between different sets of data at higher velocity ratios suggested the need for further examination of the available data. To do this, data from several sources were plotted in a systematic fashion to allow direct comparisons of trends between data sets. Figures 14 and 15 show the effects of inclination angle at nearly constant velocity ratio and the effects of velocity ratio at constant inclination angle, respectively, on experimental pressure distributions at $\beta = 0^{\circ}$. Examination of these figures and of other similar data plots produced the results discussed in the following paragraphs.

First, as exemplified in figures 14(b) and (c), the high velocity ratio data of reference 28 indicate more effect of inclination angle than is shown by the data from references 6 and 7. Second, the high velocity ratio data of reference 28 for $\theta = 15^{\circ}$ and 45° are nearly identical in the region upstream of the jet. This second result illustrates the reason for the large differences between data from references 6 and 28 at $\theta = 15^{\circ}$. Note that the data of reference 28 are still undergoing examination and should be considered preliminary at this time.

Third, the trends exhibited by the data of references 4 and 6 in figure 15 (i.e., decrease in pressure level with increase in jet velocity ratio), are not exhibited by most of the high velocity ratio data of reference 28 for $\theta > 15^{\circ}$. These same data from reference 28 appear to be asymptotic to a value of C_p other than 0 in the region upstream of the jet. Adjusting the pressure level of these data such that it is consistent with the trends exhibited by the data of references 4, 6, and 7 (i.e., making it more negative and asymptotic to $C_p = 0$) would greatly improve comparisons with predicted pressures.

Since data comparisons using the reduced entrainment model are usually poor only for cases in which there appear to be inconsistencies in the data, this model is used to obtain viscous correlation factors for jets exhausting at an angle to a flat plate. Based on the previous discussion of the reference 28 data, the correlation factors for $V_j/V_\infty \geq 7$, $\theta = 15^\circ$ and 45° are to be considered preliminary until the apparent inconsistencies in these data are resolved.

Correlation.- The purpose of the correlation is to isolate the viscous or non-potential effects of the jet on the plate. It is expected that the predicted potential pressure distribution away from the jet and within the range $0^\circ \leq \beta \leq 60^\circ$ will be in good agreement with experiment. The predicted pressures near the jet and within the range $60^\circ \leq \beta \leq 180^\circ$ will likely be in poor agreement with experiment due to viscous effects. Assuming that the measured pressure distribution can be represented by a potential part and a viscous part, the viscous part can be determined by a differencing technique.

$$\Delta C_p\Big|_{\text{viscous}} = C_p\Big|_{\text{experiment}} - C_p\Big|_{\text{potential}} \tag{6}$$

Correlating this quantity as a function of jet velocity ratio and position on the plate, the predicted pressure induced by a jet exhausting from the plate into a crossflow is given by

$$C_p = C_p\Big|_{\text{potential}} + \Delta C_p\Big|_{\text{viscous}} \tag{7}$$

The correlation curves presented for a jet exhausting at an angle to a plate were obtained in the same manner as those presented in reference 18. In cases where more than one data

set is available for a given jet velocity ratio/jet inclination angle combination, $(\Delta C_p)_{viscous}$ is found by averaging the correlation values obtained from each data set. In this report the inclination angle has been included, along with the jet velocity ratio, as a dominant parameter in determining pressures on the plate. This results in a data base which consists of a (ΔC_p) array as a function of β and r/D for each jet velocity ratio and jet inclination angle. Linear interpolation is used to determine correlation values at any V_j/V_∞, θ, β, and r/D values for which correlation curves have not been determined. These results are described in the RESULTS section.

Body of Revolution

The general problem of interest for the body of revolution case is a subsonic jet exhausting normally from the surface of a body at zero degrees angle of attack into an incompressible crossflow. The parameters of interest are jet velocity ratio, body shape, and jet-to-body diameter ratio. The general method for the body of revolution case is applicable over a wide range of these parameters; however, the present method has been verified for only a limited range of parameters because of the small quantity of available data. The present method has been applied to a cone-cylinder model with a small jet-to-body diameter ratio for two low jet velocity ratios. Further discussion of extending the method to larger jet-to-body diameters and higher velocity ratios is found in following sections.

Body model.- The NSRDC version of the Douglas-Neumann program (refs. 19 and 20) is used to model the specified body of revolution geometry. This program approximates the surface of the body by a set of plane quadrilaterals. The solution is

constructed in terms of a source density, which is assumed to be constant in each quadrilateral element. The solution satisfies Laplace's equation in the free-stream and a zero normal-flow condition on the surface of the body. The program presently utilizes a maximum of 650 panels to model a three-dimensional body.

As a check of the accuracy of the NSRDC program, predicted pressures on an ogive-cylinder body with a fineness ratio 3 nose at $\alpha = 10^{\circ}$ were compared with measured data (ref. 29). The agreement between theory and experiment is good over the entire length of the body, as shown in figure 16. The difference between experiment and theory near $\phi = 60^{\circ}$ for x/D = 4.5 and 6.0 may be due to viscous effects, which are not accounted for in the NSRDC program. These comparisons lend confidence to the use of the NSRDC method for developing viscous correlation factors for the body of revolution case.

A cone-cylinder model with a jet exhausting normal to the surface (ref. 3) is shown in figure 17. The model was tested at zero angle of attack and low free-stream velocity over a range of jet velocity ratios. Pressures were measured on the cylinder surface in the vicinity of the jet. The row of pressure taps shown in figure 17 was rotated to obtain pressure data from the top of the body ($\phi = 0^{\circ}$) to $\phi = 25^{\circ}$.

Due to the close proximity of the jet to the aft end of the body, a parametric study of the effects of modeling the downstream end of the body for the jet-off case was carried out. One model incorporated an ogive extension or boattail to close the body at the downstream end, and a second model incorporated an open end on the cylinder. Since the first model is a closed body, the sum of the source strengths is zero, resulting in

zero net flow inside the body. The second model essentially models the wake behind the cylinder since a net flow is produced due to the open end.

Jet-off pressure distributions (fig. 18) showed a large effect of the ogive, such that the pressure coefficient did not recover to zero downstream of the cone-cylinder junction. Without the ogive extension, the predicted pressure coefficient approaches zero toward the end of the cylinder, as would be expected. Data comparisons for the jet-off case in figure 19 show reasonably good agreement between the measured and predicted results for the model without an ogive extension. These comparisons indicate that the measured pressures recover more quickly than the predicted pressures, probably due to the separation at the cone-cylinder junction, which is located at $x/D = 12.9$. Such effects are not accounted for in the NSRDC program. As a result of this investigation, the aft end of the body is modeled as an open-ended cylinder.

Jet model.- Details concerning the specification of the jet centerline path, the blockage and entrainment models, and the spreading rate of a jet exhausting normal to the surface of a body of revolution are presented in the following paragraphs.

The path of the jet centerline is specified using an empirical relation developed by Viehweger (ref. 12). This relation, obtained by correlating results for a low pressure jet with a short potential core exhausting from a body of revolution, is written as

$$x_j/D = 1.727(z_j/D \cdot \sqrt{q_\infty/q_j})^{2.65} \qquad (8)$$

This centerline result is based on data in the range $16 \leq q_j/q_\infty \leq 290$. For practical purposes, the assumption is made that $\sqrt{q_\infty/q_j}$ is approximately equal to V_∞/V_j, so the range of velocity ratios represented is 4.0 to 17.0. The jet centerline data from reference 12 is the only available data for a jet exhausting from a body of revolution.

Figure 20 shows centerline shapes for velocity ratios 1.96 and 3.43 as given by equation (8). Although the velocity ratios of interest are outside the range used to obtain equation (8), this equation has the advantage of having its origin in body-of-revolution data. Since references 3 and 12 both consider similar low pressure jets with short potential cores, it is assumed that the above centerline relation will provide accurate centerline shapes in the velocity ratio range of interest.

Blockage effects of the jet were obtained by modeling the jet surface as an integral part of the cone-cylinder model. In this manner, the mutual interference effects between the jet surface and the body are accounted for simultaneously. With respect to the panel layout in the region of the body/jet intersection, the edges of the body panels are matched to the edges of the jet surface panels, thereby providing a smooth transition from the cylinder surface to the jet surface.

The cone-cylinder configuration (fig. 17) was modeled using the symmetry option of the NSRDC program, which necessitated modeling only one-half of the jet/body combination. A total of 632 panels were used to model the configuration; 532 panels on the body and 100 panels on the jet surface. The jet is divided into 20 circumferential segments (10 segments per half plane) with panels near the body having an aspect ratio (height/width)

of 3.18. A fine grid on the body was utilized in the region of the jet in order to get better resolution of the pressures in that region. Predicted results could not be obtained at exactly $\phi = 0$, since results cannot be obtained along a line of symmetry when the symmetry option is exercised.

Jet entrainment effects are modeled using the empirical method of Yeh, which is described in detail in reference 14. Although this method was developed for a jet exhausting from a flat plate, lack of an available entrainment model for a jet exhausting from a body of revolution necessitated the use of a flat plate model. The entrainment-induced velocities are included with the jet blockage model induced velocities in the boundary condition on the body surface. The entrainment induced velocities are not included in the boundary conditions on the jet surface.

The spreading rate for a jet exhausting from a body of revolution is calculated using the same method used for the flat plate case (ref. 18). Once again, lack of spreading rate data or theory for a jet exhausting from a body of revolution necessitates the use of a flat plate method.

It is noted here that the flat plate models for entrainment rate and spreading rate should give accurate results for the small jet-to-body diameter ratio (.064) of the cone-cylinder model on which data is available. The flat plate model may become less accurate as the jet diameter increases to an appreciable fraction of the body diameter, and it will be necessary to have additional data to evaluate differences between flat plate and body jets as the relative jet size increases.

Static jet dynamic-pressure decay data are available in reference 3 and indicate that the potential core extends approximately two jet diameters from the nozzle exit for all jet velocities. As a test of the sensitivity of predicted surface pressures to potential core length, a parametric study using potential core lengths of 1.5 and 3.0 jet diameters was carried out for $V_j/V_\infty = 3.43$. Results of this study indicate nearly identical predicted pressures using both potential core lengths. Since flat plate data have shown (ref. 7) that a jet in a crossflow has a shorter potential core length than a jet under static conditions, 1.5 jet diameters was selected as the potential core length for all calculations included in this report.

A series of expansion rate curves corresponding to a potential core length of 1.5 jet diameters is shown in figure 21. The $V_j/V_\infty = 1.96$ and 3.43 curves were obtained by extrapolating the $V_j/V_\infty = 4$, 6, and 8 expansion curves using information from figure 22. This figure presents (t/D) vs. V_j/V_∞ where $(t/D)_{max}$ is the value of t/D at $S_a/R = 20$. This curve is utilized in the same fashion as outlined in reference 18.

Correlation.- The purpose of the correlation for the body of revolution case is the same as that for the flat plate case; that is, to isolate the viscous or non-potential effects on the jet on the body. It is expected that the predicted potential pressure distribution away from and upstream of the jet will be in good agreement with experiment. The predicted pressures near the jet and downstream of the jet will likely be in poor agreement with experiment due to viscous effects. Equations (6) and (7), which apply to the flat plate correlation, are also applicable to the body of revolution correlation.

In a manner similar to that done for the flat plate case, $(\Delta C_p)_{viscous}$ values are obtained by comparing theoretical pressure coefficients with experimental data at chosen ϕ and x/D stations for each V_j/V_∞. A data base is set up which consists of a $(\Delta C_p)_{viscous}$ array for each jet velocity ratio. Linear interpolation is used to determine the correlation factor at any V_j/V_∞, ϕ, and x/D values for which correlation curves have not been determined.

RESULTS

Flat Plate

Correlation curves are presented in figures 23, 24, 25, and 26 for jet inclination angles 15°, 30°, 45°, and 60°, respectively. The number of jet velocity ratios for which correlation curves are presented for θ = 45° and 60° are limited by the available data. The correlation values were determined for most velocity ratios at β = 0°, 30°, 60°, 90°, 120°, 150°, and 180° and r/D = .75, 1.0, 1.5, 2.0, 3.0, and 5.0. Correlation curves obtained using data from reference 6 only do not contain correlation factors for r/D = .75 and 1.0 due to the absence of data at these radial positions. Also, correlation factors for all r/D values could not be obtained at each β value for the data from reference 7 due to lack of data at various r/D positions. For cases in which two independent sets of data were used to obtain correlation curves, the given velocity ratio is the average of the velocity ratios from the two sets of data and each correlation value is the average of the correlation values obtained using each data set. In most cases, multiple data sets were not available and the correlation curves were obtained using only one independent set of data (refs. 6, 7, or 28).

The results shown in figures 23 through 26 are similar in form to those presented in reference 18 for jets exhausting normal to a flat plate. The $(\Delta C_p)_{viscous}$ values are usually smallest in the region upstream and away from the jet and largest in the region immediately downstream of the jet and in close proximity to the jet, as would be expected. It is noted that the erratic behavior of the r/D = .75 correlation curves for the region $90^o \leq \beta \leq 150^o$ is very similar to that seen in the $\theta = 0^o$ case in reference 18. As was previously discussed, the correlating factors are maintained in a data base form as shown in figures 23 through 26. Any required factor can be obtained by interpolating between curves for a given velocity ratio and inclination angle combination.

The pressure prediction method, made up of the blockage model, the entrainment model, and the viscous correction factors, has been applied to jet velocity ratio and inclination angle cases for which two independent sets of data are available. Since these data are the same data used to obtain the correlation factors, the purpose of these results is not strictly to show comparisons of predicted and experimental results, but more so to show how close the predicted values are to the data relative to differences between the two sets of data. Obviously, it would be more useful to compare the prediction method with independent data, but adequate additional data are not available at the present time.

Data comparisons of C_p vs. r/D at β = constant are presented in figures 27 and 28 for the following jet velocity ratio and inclination angle combinations: $3.9/15^o$, $5.0/15^o$, $4.0/30^o$, and $8.15/30^o$. Data are not available at r/D = .75 and 1.0 from reference 6, and therefore the correlation factors at these radial positions reflect the data of reference 28 only.

As discussed in reference 18, the success of the prediction method is dependent on how well the various sets of data agree with one another. In regions where the data set are in good agreement with one another, such as $V_j/V_\infty = 3.9$, $\theta = 15^\circ$, $\beta = 60^\circ$ [fig. 27(a)], the predicted results agree well with both sets of experimental results. In regions where the data sets are not in good agreement, such as $V_j/V_\infty = 5.0$, $\theta = 15^\circ$, $\beta = 30^\circ$ [fig. 27(b)], the predicted results show an average of the two sets of data. Perhaps the most significant aspect of these results is that for $\beta > 90^\circ$, the viscous and inviscid contributions are of comparable size (see, for example, figs. 24(b) and 28(a)) and the separation of the phenomena into a predicted potential and an empirical viscous correction results in uniformly good results over a wide parameter range for engineering calculation purposes.

Pressure distribution data on a flat plate with a jet exhausting normal to the plate were also obtained in the NASA/ARC tests of reference 28. These data, in conjunction with data previously used to obtain the correlation factors presented in reference 18, were used to improve the viscous correction factors at $\theta = 0^\circ$. These correlation curves are presented in figure 29 for jet velocity ratios 2.2, 3.9, 5.0, 6.1, 7.0, 8.0, and 10.0. New correlation curves for $V_j/V_\infty = 1.0$, 1.67, and 3.33 were not obtained, since the new experimental results did not include these velocity ratios.

Comparisons of the NASA/ARC data and predicted results obtained with and without the NASA/ARC data included in the viscous correction factors are shown in figure 30. Comparison of the new correlation curves with those presented in reference 18 indicates that the addition of the NASA/ARC data, in general, had little effect on the correlation curves for $\theta = 0^\circ$. The largest effects are seen for $r/D \leq 1.0$, where experimental

pressure data are difficult to obtain due to large unsteady effects near the jet. It is noted that correlation curves had not been previously obtained for $V_j/V_\infty = 7.0$; therefore, predicted results presented in figure 30(e) are available only with the NASA/ARC data included.

Body of Revolution

To verify that the potential model results give good agreement with data in the region of the body of revolution where viscous effects are small, data comparisons of surface pressures were made for $V_j/V_\infty = 1.96$ and 3.43. These velocity ratios are the lowest and highest velocity ratios for which data are presently available (ref. 3).

Comparisons of measured and predicted surface pressures for $V_j/V_\infty = 1.96$ are shown in figures 31 and 32. The predicted results at this velocity ratio were obtained using the blockage model alone, since Yeh's entrainment model is singular when $V_j/V_\infty < 2.35$ (see refs. 14 and 18 for details). Figure 31 presents axial pressure distributions for several constant positions, and figure 32 presents circumferential pressure distributions at several axial stations. These comparisons indicate good agreement between theory and data in the regions upstream of the jet ($x/D \geq 0$), although the jump in experimental pressures between $x/D = 7.0$ and 6.0 is not shown by the predicted pressures. This may be due to separation at the cone/cylinder junction ($x/D = 12.9$), which cannot be predicted using the NSRDC program. In the strong viscous region downstream of the jet, predicted pressures compare poorly with measured pressures, as would be expected. In regions aft of the jet where viscous effects, and jet effects in general, are small

($x/D < -5$), measured and predicted pressures are in good agreement.

Predicted pressures for $V_j/V_\infty = 3.43$, obtained using both the blockage and entrainment models, are compared with measured pressures in figures 33 and 34. These comparisons indicate the same general trends seen for $V_j/V_\infty = 1.96$, although comparisons between predicted and measured pressures at $x/D = 1.0$ and 1.5 are not as good as those seen for $V_j/V_\infty = 1.96$. This may be due to inaccuracies associated with the use of a flat plate entrainment model to predict entrainment effects on a body of revolution. For the flat plate case, it was found that entrainment effects on surface pressures become important at large jet velocity ratios. This is most likely true for the body of revolution case as well. Lack of body of revolution data at higher velocity ratios prevents further investigation of the adequacy of the flat plate entrainment model for use with a body of revolution.

Correlation curves are presented in figures 35 and 36 for jet velocity ratios 1.96 and 3.43, respectively. The correlation values were determined at a range of ϕ values from 0° to 25° and a range of x/D values from ± 1.0 to ± 7.0, where "+" and "-" represent positions upstream and downstream of the jet, respectively. Since predicted pressures could not be obtained at $\phi = 0^\circ$, $(\Delta C_p)_{viscous}$ values for this angle were obtained by extrapolating the theoretical results to $\phi = 0^\circ$ at each x/D position. For $|x/D| > 7$ and $\phi > 25^\circ$, $(\Delta C_p)_{viscous}$ has been set equal to 0.0, since jet effects are negligible in these regions. Also, since data are not available in the region $|x/D| < 1$, $(\Delta C_p)_{viscous}$ values are obtained by interpolation for x/D values in this region.

As these correlation curves show, $(\Delta C_p)_{viscous}$ values are small in the regions upstream and away from the jet and large in the strong viscous region immediately downstream of the jet. Also, the large correlation factors decrease with increasing ϕ, as would be expected.

Since these correlation factors have been obtained using data from only one source (ref. 3), these factors are not used here to calculate new pressure distributions on the cone-cylinder model. It would be useful to compare predicted results with independent data, but adequate additional data are not available at the present time.

CONCLUSIONS

A correlation method to predict surface pressures on a flat plate in a crossflow with a jet exhausting normal to the surface was extended to jets exhausting at an angle to a plate and to jets exhausting normal to the surface of a body of revolution. As in the previous method, the correlation values of viscous-induced pressure coefficients are defined as the difference between pressures predicted by a potential model and those obtained from experimental data.

For the flat plate case, blockage and entrainment effects are accounted for using modified versions of the vortex quadrilateral panel model and the sink distribution model, respectively, of reference 18. The viscous effects of the jet are represented by the correlation values.

Comparisons of measured and predicted plate pressures in the vicinity of inclined jets over a wide range of jet velocity

ratios and inclination angles are generally good. Correlation values for certain ranges of jet velocity ratio and inclination angle are to be considered preliminary due to inconsistencies in the available data (ref. 28) for those ranges.

For the body of revolution case, mutual interference effects between the body and the jet surface are modeled using a source panel method. Entrainment effects are accounted for using the flat plate sink distribution model due to lack of an available method for a body of revolution. The viscous effects are once again represented by the correlation values.

Predicted surface pressures, which were obtained for $V_j/V_\infty = 1.96$ and 3.43 using the potential method, were compared with measured pressures in the vicinity of the jet and showed good agreement for regions where viscous effects are small. Lack of available data made it impossible to assess the method for jet velocity ratios greater than 4 and jet-to-body diameter ratios greater than 0.1.

In addition to extending the normal-jet correlation method in the aforementioned cases, new normal-jet data were compared with results obtained using the normal-jet empirical prediction method with and without the new data included in the viscous correlation factors. In general, the new data had little effect on the predicted results, which lends confidence to the use of the method for normal-jet cases.

In summary, the following comments are made regarding the applicability and use of the viscous correlation prediction method. First, the correlation factors for subsonic jets exhausting normal to an infinite flat plate can be used with confidence. These factors were obtained using data over a wide range of flow parameters and from several sources. Data

comparisons indicate that differences between predicted and measured pressures are usually less than the differences between different sets of data. This indicates that the correlation method should give accurate flat plate pressure distributions for the normal-jet case. For jets exhausting at an angle to a flat plate, the correlation factors for low and medium jet velocity ratios ($V_j/V_\infty \leq 7$) and jet inclination angles (θ) less than 45° can be used with confidence. Inconsistencies in the data for high velocity ratio jets suggest that the prediction method be used with caution for $V_j/V_\infty \geq 7.0$. For jets exhausting from the surface of a body of revolution, the correlation method is to be considered strictly preliminary. This is due to the lack of available data, which limits the applicability of the present method to jet velocity ratios less than 4.0 and jet-to-body diameter ratios less than 0.1. Additional data are needed to extend the method to higher jet velocity ratios and to larger jet-to-body diameter ratios typical of full-scale fan-in-fuselage configurations.

RECOMMENDATIONS

It is clear that the prediction method described in this report (and in reference 18) depends heavily on experimental data for determining the viscous correlations, evaluating the potential model, and assessing the accuracy of the overall prediction method. In many cases, the available data are very limited, and the recommendations have to do principally with the need for further data.

For the flat plate case, it is encouraging that inclusion of the most recent NASA data for normal jets has little effect on the viscous correlation developed previously. The principal need at this time is for additional data for jets inclined at

angles other than 90 degrees to the plate. Two types of data are required. First, data on the jet properties (centerline location, expansion rate and entrainment) over a range of jet inclination angles and velocity ratios are required to assess the accuracy of the jet model and its ability to predict surface pressures upstream of the jet. Secondly, data on surface pressures are required both to add to the data base for deducing viscous correlations and to independently check the overall method.

The body of revolution case has been investigated much less extensively, and the two types of data mentioned above for the flat plate are required also for bodies. The body case also introduces more geometry parameters, in the form of hole-to-body diameter ratio and shape of the body (cross-section and axial changes). The most important need is data on configurations with larger diameter ratios than are currently available.

Finally, as noted in the previous report (ref. 18), measurement of jet turbulence level and mean velocity profile, in addition to induced surface pressure measurements, would be desirable. Such data could aid in the understanding of real jet effects and in the improvement of the present prediction method.

REFERENCES

1. Vogler, R. D.: Surface Pressure Distributions Induced on a Flat Plate by a Cold Air Jet Issuing Perpendicularly from the Plate and Normal to a Low-Speed Free-Stream Flow. NASA TN D-1629, Mar. 1963.

2. Bradbury, L. J. S. and Wood, M. N.: The Static Pressure Distribution Around a Circular Jet Exhausting Normally from a Plane Wall into an Airstream. Aeronaut. Res. Council C. P. No. 882, Aug. 1965.

3. Ousterhout, D. S.: An Experimental Investigation of a Cold Jet Emitting from a Body of Revolution into a Subsonic Free Stream. NASA CR-2089, Aug. 1972.

4. Fearn, R. L. and Weston, R. P.: Induced Pressure Distribution of a Jet in a Crossflow. NASA TN D-7916, June 1975.

5. Mosher, D. K.: An Experimental Investigation of a Turbulent Jet in a Cross Flow. Georgia Inst. of Tech. Rept. GIT-AER-70-715, Dec. 1970 (Ph.D. Thesis).

6. Fricke, L. B., Wooler, P. T., and Ziegler, H.: A Wind Tunnel Investigation of Jets Exhausting into a Crossflow. Vol. I - Test Description and Data Analysis. Vol. II - Additional Data for the One-Jet Configuration. AFFDL-TR-70-154, Dec. 1970.

7. Taylor, P.: An Investigation of an Inclined Jet in a Crosswind. Aeronautical Quarterly, Vol. XXVIII, Part I, Feb. 1977.

8. Spring, D. J. and Street, T. A.: Experimental Investigation of the Pressure Distributions Induced upon a Body of Revolution by Several Transverse Jets at Low Speeds. U. S. Army Missile Command Rept. No. RD-TM-68-7, Aug. 1968.

9. Spring, D. J.: An Experimental Investigation of the Interference Effects Due to a Lateral Jet Issuing from a Body of Revolution over the Mach Number Range of 0.8 to 4.5. U.S. Army Missile Command Rept. No. RD-TR-68-10, Aug. 1968.

10. Mineck, R. E. and Margason, R. J.: Pressure Distribution on a Vectored-Thrust V/STOL Fighter in the Transition-Speed Range. NASA TM X-2867, Mar. 1974.

REFERENCES (Continued)

11. Practical Problems on Longitudinal and Cross-Blown Free Jets: The Simulation of Engine Jets in Wind Tunnels. Rept. on the Conference of the D.G.L.R. Technical Committee 2A1 on Fixed-Wing Aircraft held at Porz-Wahn, W. Germany, Dec. 6, 1973. ESA TT-206, Nov. 1975.

12. Viehweger, G.: Flow Effects with Cross-Blown Lifting Jets of V/STOL Aircraft and their Reaction on Aerodynamical Forces and Moments of the Nacelle. NASA TM-75143, July 1976.

13. Dietz, W. E., Jr.: A Method for Calculating the Induced Pressure Distribution Associated with a Jet in a Crossflow. NASA CR-146434, 1975.

14. Yeh, B. T.: Calculation of the Pressure Distribution Induced by a Jet on a Flat Plate. ESRO-TT-159, May 1975.

15. Heltsley, F. L. and Parker, R. L., Jr.: Application of the Vortex Lattice Method to Represent a Jet Exhausting from a Flat Plate into a Crossflowing Stream. AEDC-TR-73-57, June 1973.

16. Hackett, J. E. and Miller, H. R.: A Theoretical Investigation of a Circular Lifting Jet in a Cross-Flowing Mainstream. AFFDL-TR-70-170, Jan. 1971.

17. Chang, H. S. and Werner, J. E.: Analysis of an Entrainment Model of the Jet in a Crossflow. NASA CR-132324, Nov. 1972.

18. Perkins, S. C., Jr. and Mendenhall, M. R.: A Correlation Method to Predict the Surface Pressure Distribution on an Infinite Plate from Which a Jet is Issuing. NASA CR 152,160, May 1978.

19. Dawson, C. W. and Dean, J. S.: The XYZ Potential Flow Program. NSRDC Report 3892, June 1972.

20. Dawson, C. W. and Dean, J. S.: The Calculation of Streamline Data for Boundary Layer Input. NSRDC Report CMD-7-74, Jan. 1974.

REFERENCES (Concluded)

21. Margason, R. J.: The Path of a Jet Directed at Large Angles to a Subsonic Free Stream. NASA TN D-4919, Nov. 1968.

22. Maskew, B.: Calculation of the Three-Dimensional Potential Flow Around Lifting Nonplanar Wings and Wing-Bodies Using a Surface Distribution of Quadrilateral Vortex Rings. Report TT-7009, Loughborough University of Technology, Sept. 1970.

23. Bowley, W. W. and Sucec, J.: Trajectory and Spreading of a Turbulent Jet in the Presence of a Crossflow of Arbitrary Velocity Distribution. Presented at 14th Annual Gas Turbine Conf. and Products Show, ASME Paper 69-GT-33, Mar. 1969.

24. Keffer, J. F. and Baines, W. D.: The Round Turbulent Jet in a Cross-Wind. J. Fluid Mech., Vol. 15, Part. 4, Apr. 1963, pp. 481-497.

25. Camelier, I. and Karamcheti, K.: An Experimental Study of the Structure and Acoustic Field of a Jet in a Cross Stream. JIAA Rept. TR-2, Jan. 1976.

26. Pratte, B. D. and Baines, W. D.: Profiles of the Round Turbulent Jet in a Cross Flow. Proc. of the ASCE Hydraulic Division, Vol. 92, No. HY6, Nov. 1967, pp. 53-65.

27. Platten, J. L. and Keffer, J. F.: Entrainment in Deflected Axisymmetric Jets at Various Angles to the Stream. UTME-TP 6808, June 1978.

28. Aoyagi, K: NASA/Ames Research Center, work in preparation.

29. Tinling, B. E. and Allen, C. Q.: An Investigation of the Normal-Force and Vortex-Wake Characteristics of an Ogive-Cylinder Body at Subsonic Speeds. NASA TN D-1297, Apr. 1962.

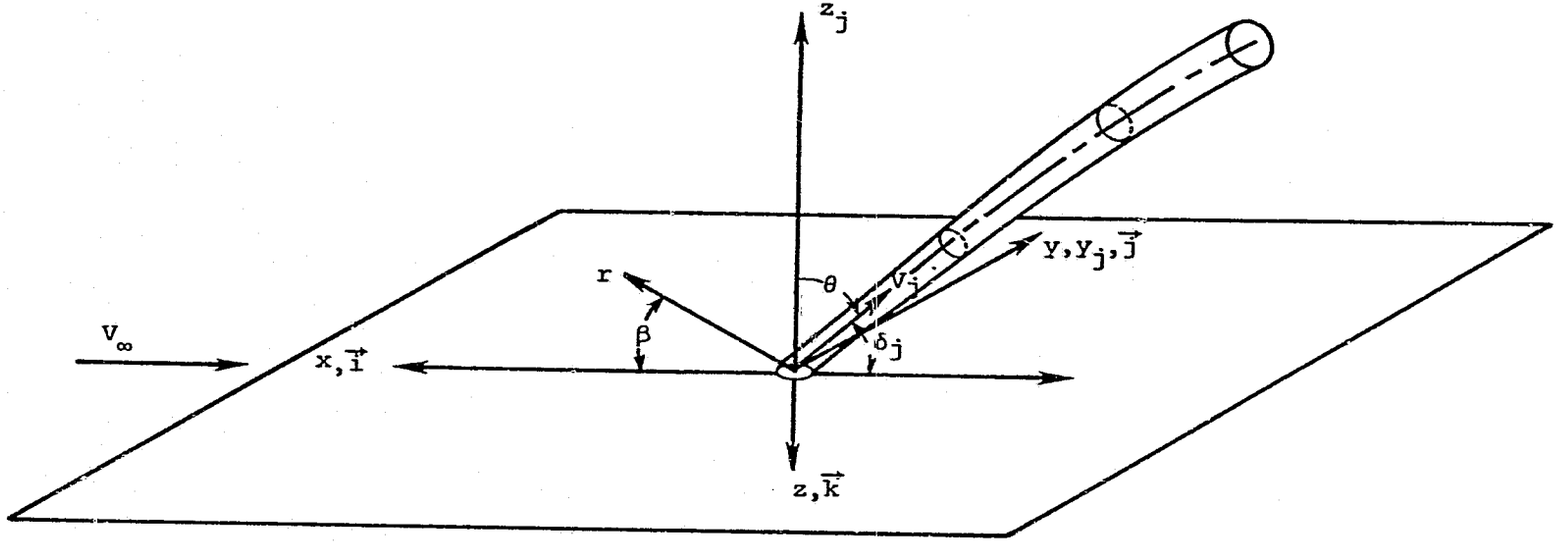

Figure 1.- Coordinate system for a jet issuing from a flat plate into a subsonic crossflow (isometric view).

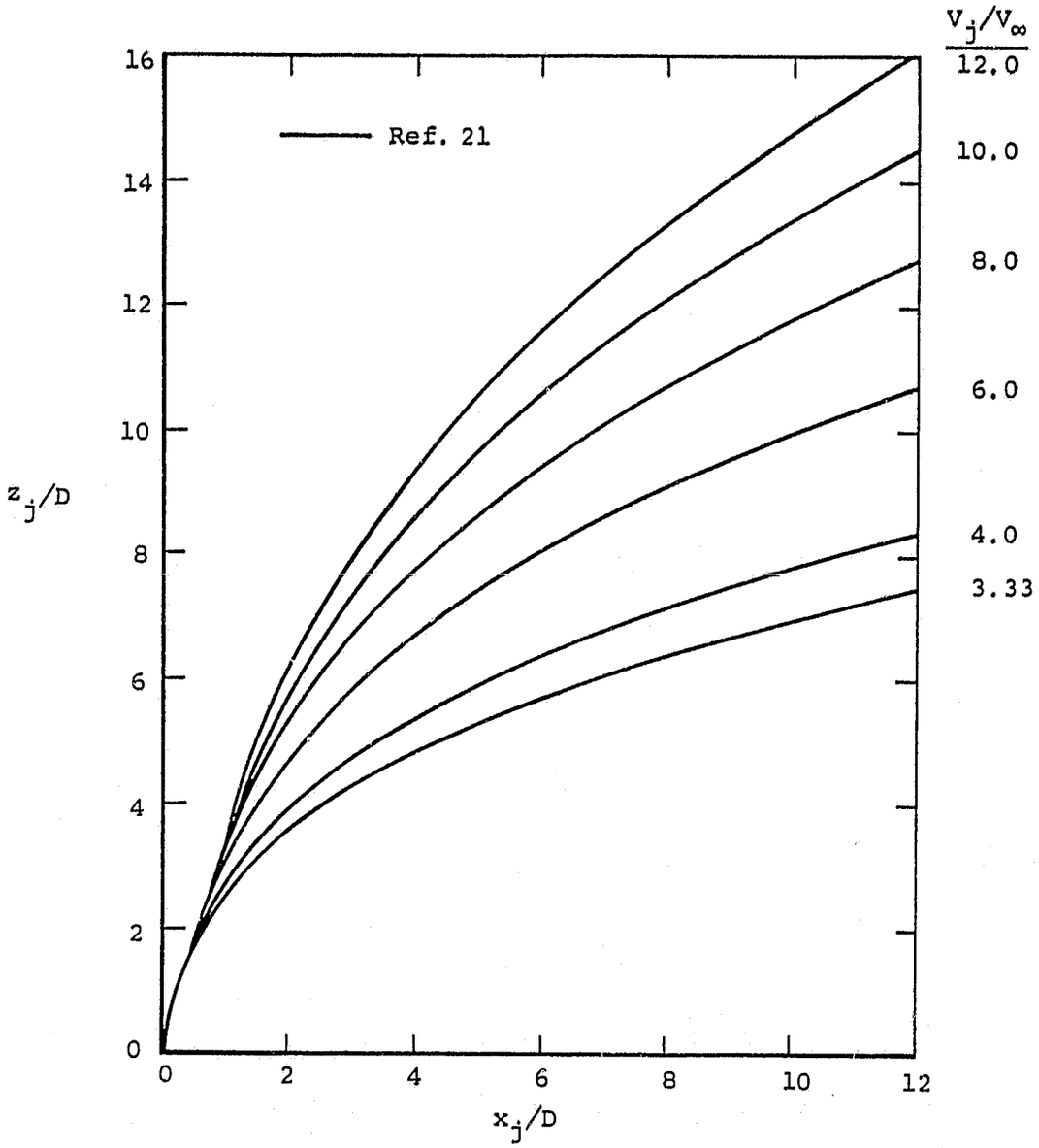

(a) $\delta_j = 75^\circ$ ($\theta = 15^\circ$).

Figure 2.- Centerline shapes for a jet exhausting at an angle to a flat plate.

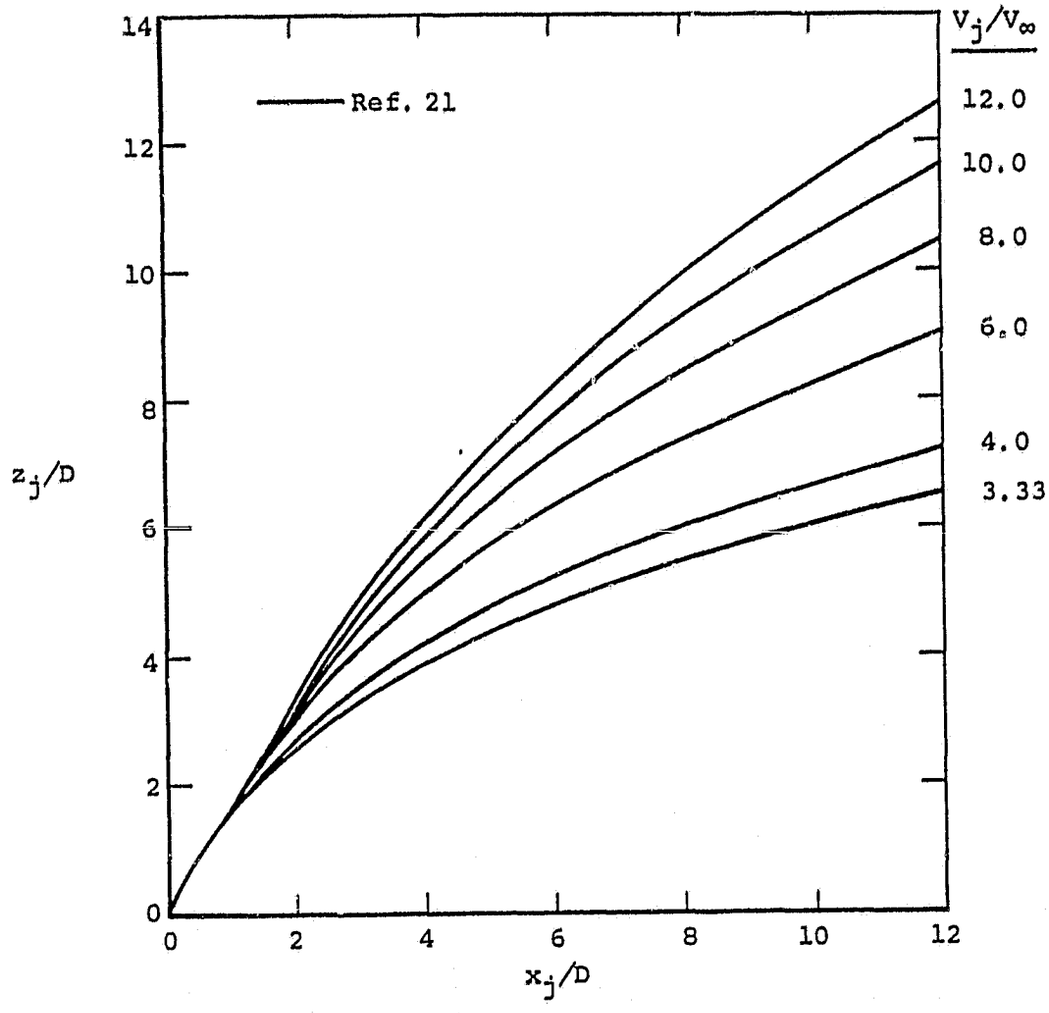

(b) $\delta_j = 60^\circ$ ($\theta = 30^\circ$).

Figure 2.- Continued.

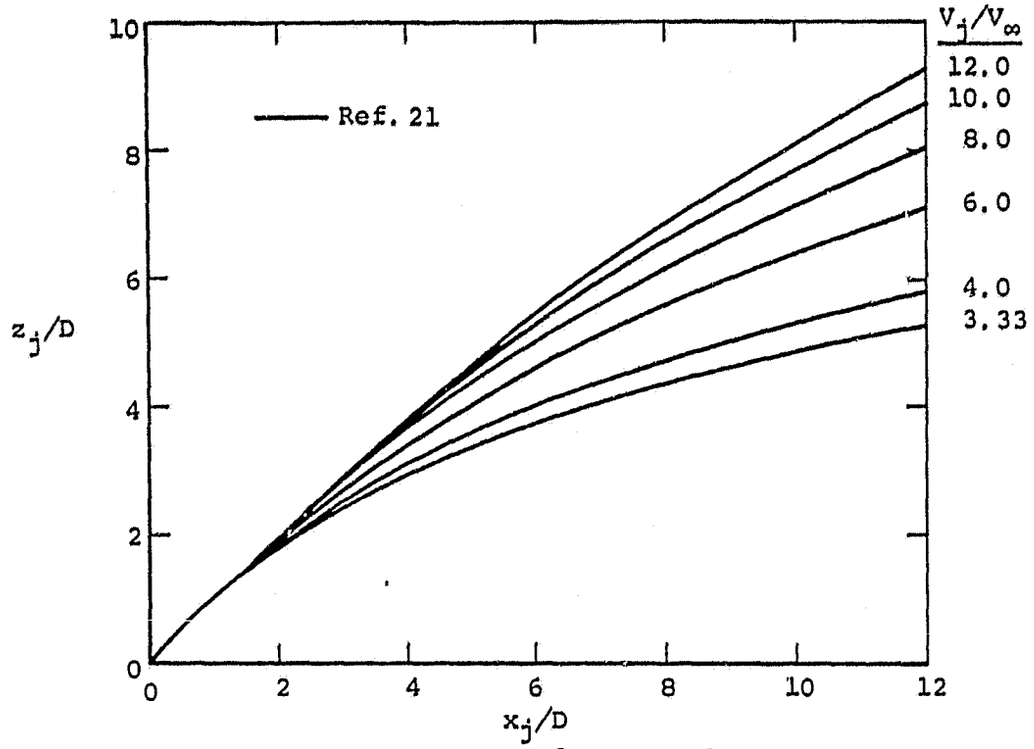

(c) $\delta_j = 45^\circ$ ($\theta = 45^\circ$)

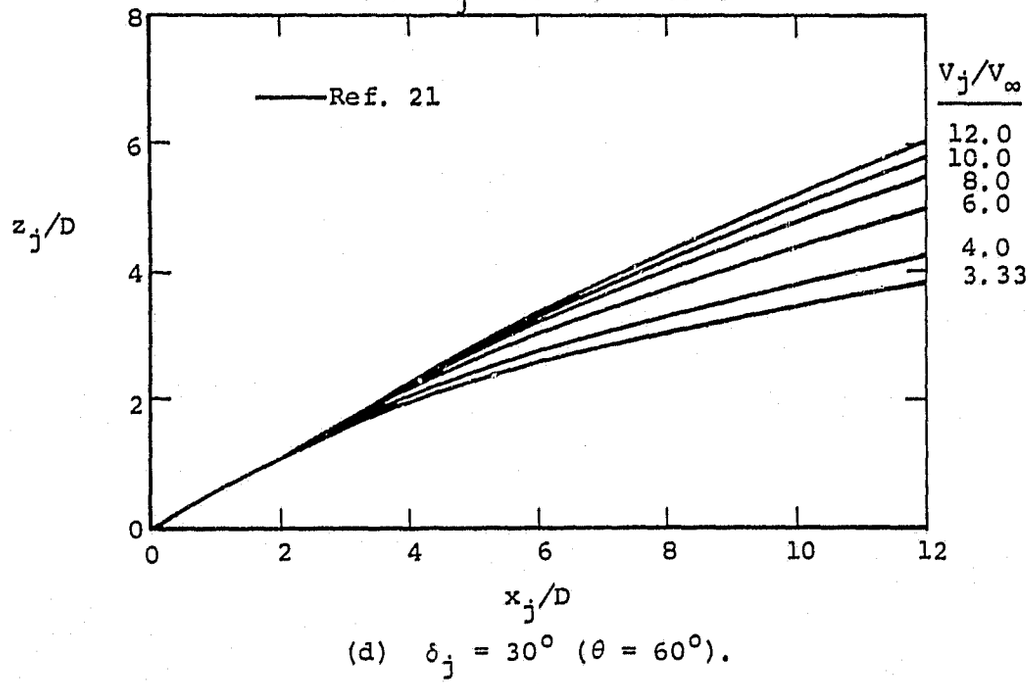

(d) $\delta_j = 30^\circ$ ($\theta = 60^\circ$).

Figure 2.- Concluded.

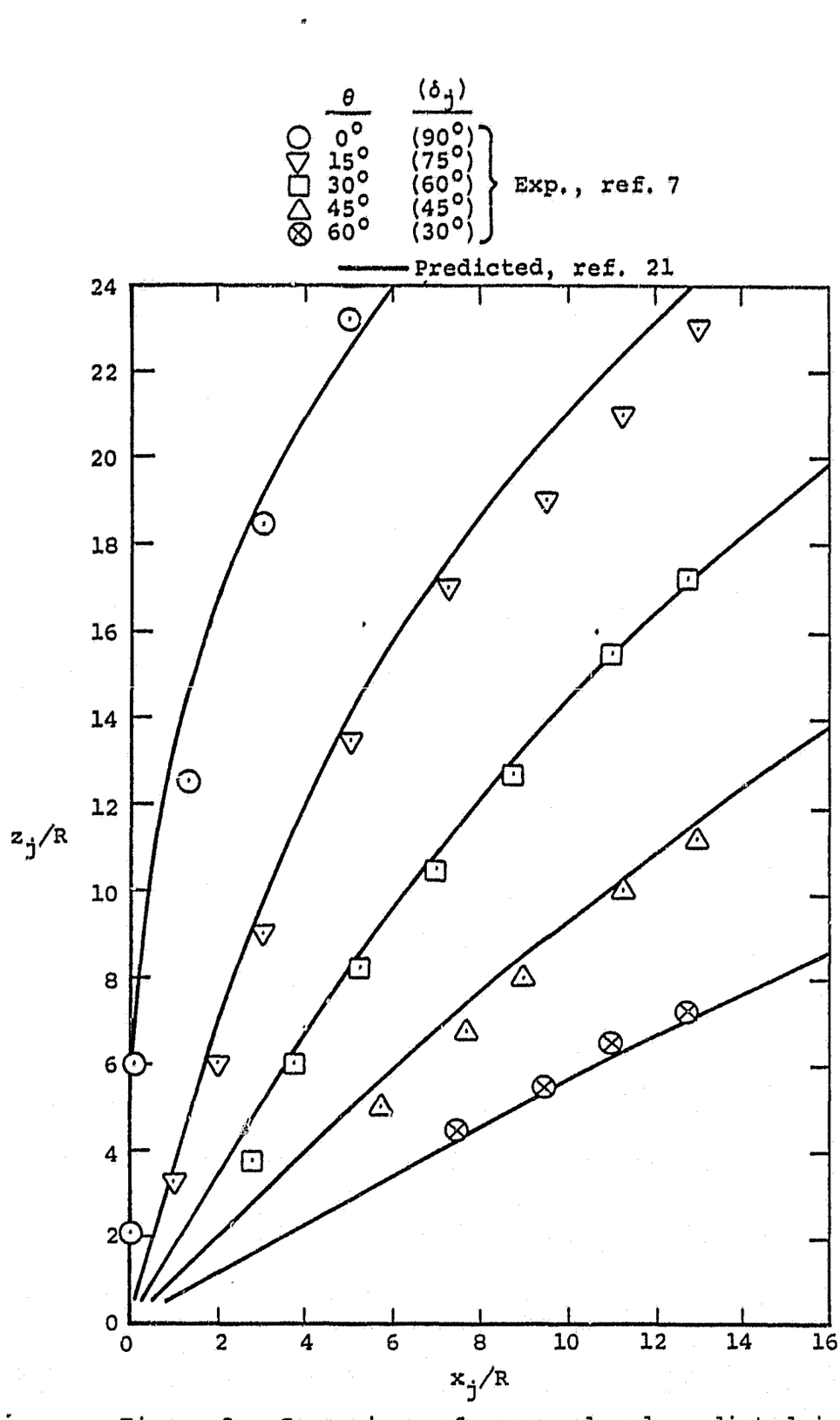

Figure 3.- Comparison of measured and predicted jet centerline shapes, $V_j/V_\infty = 12.0$.

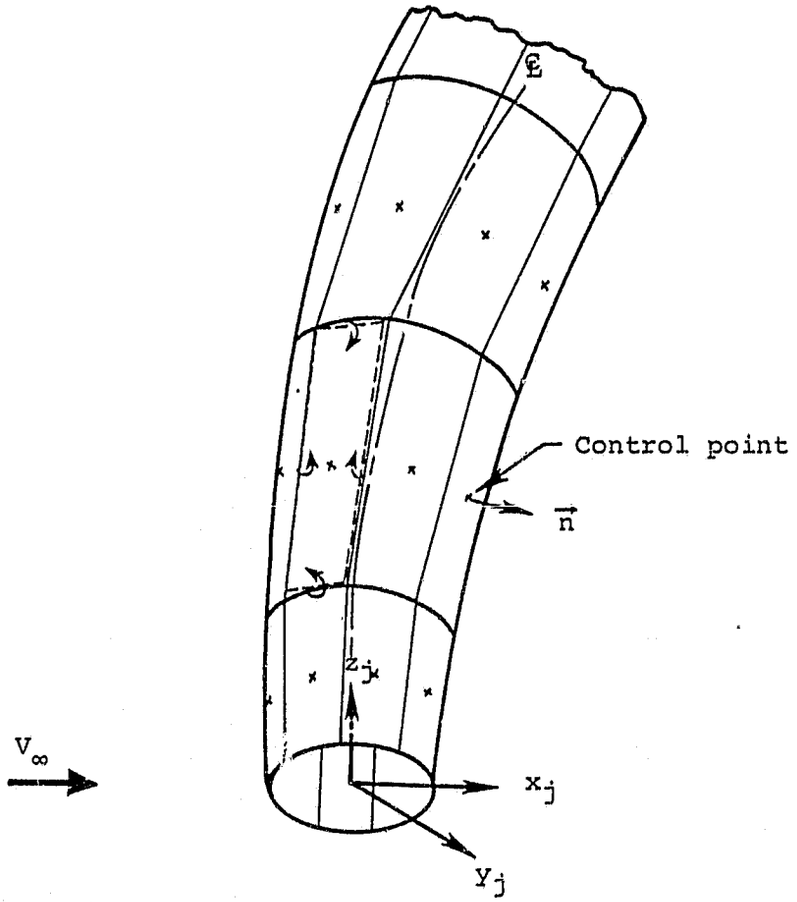

Figure 4.- Vortex quadrilaterals on wake surface.

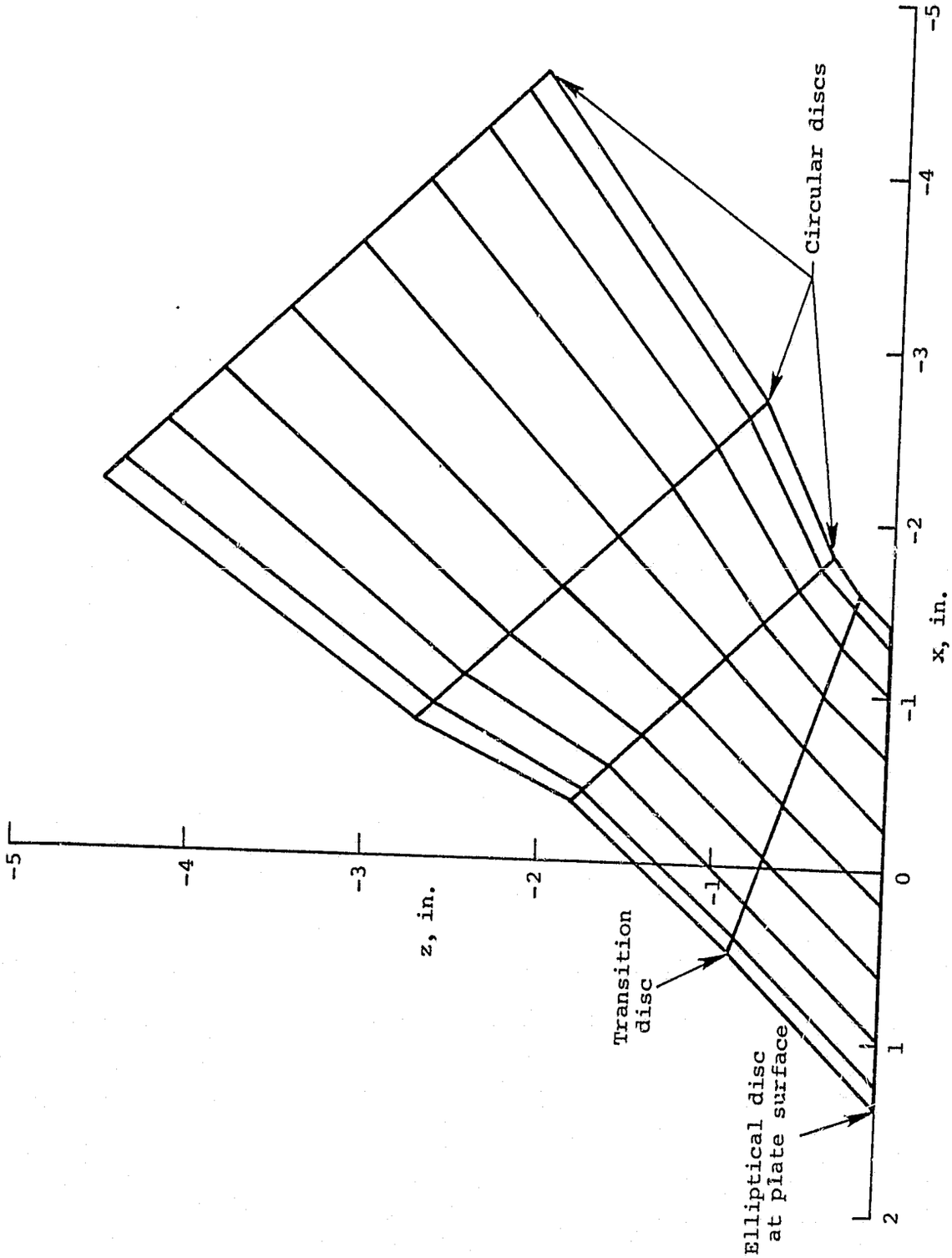

Figure 5.- Side view of the blockage model panel layout for a jet exhausting from a flat plate; $V_j/V_\infty = 12.0$, $\theta = 45^o$.

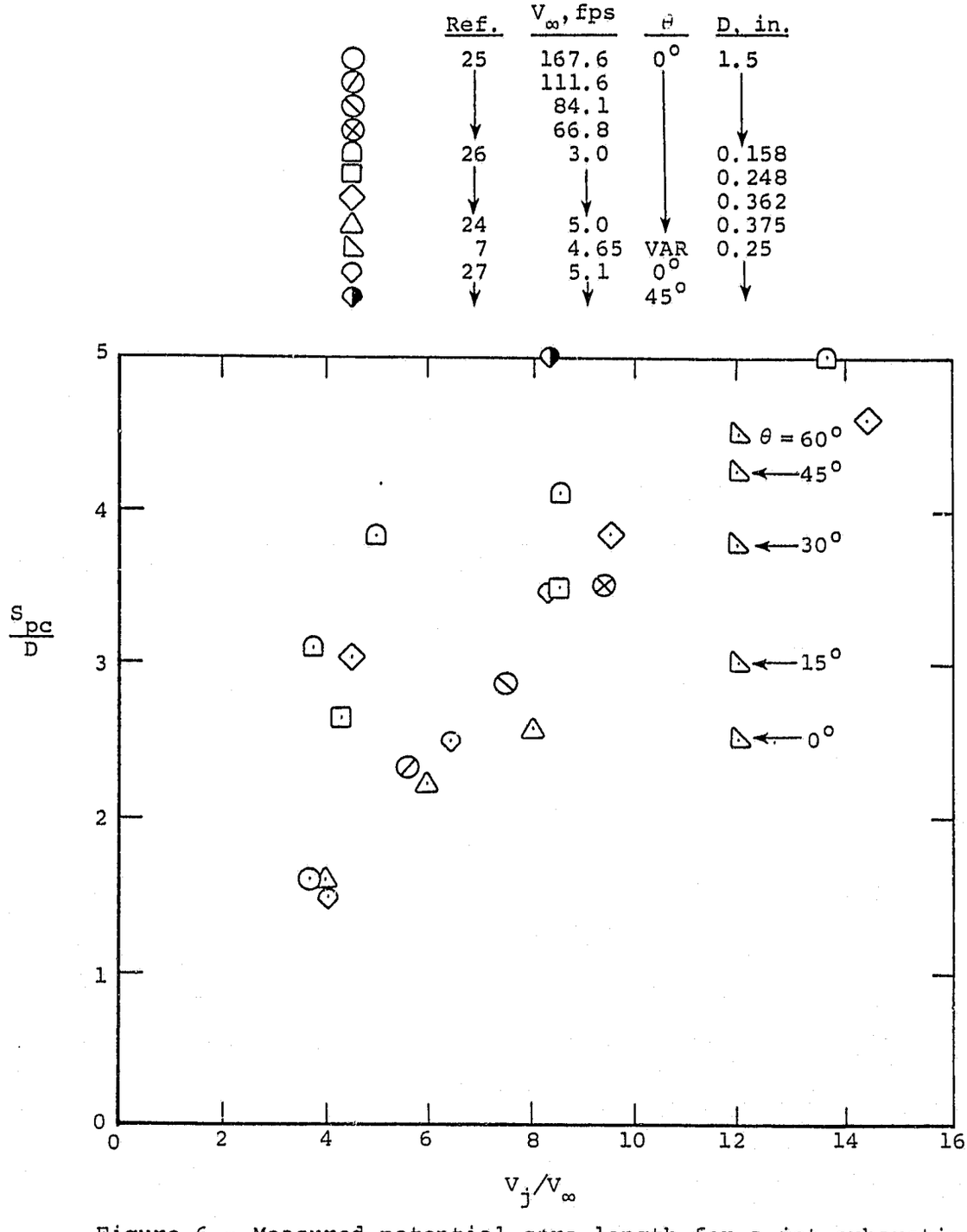

Figure 6.- Measured potential core length for a jet exhausting from a flat plate into a subsonic crossflow.

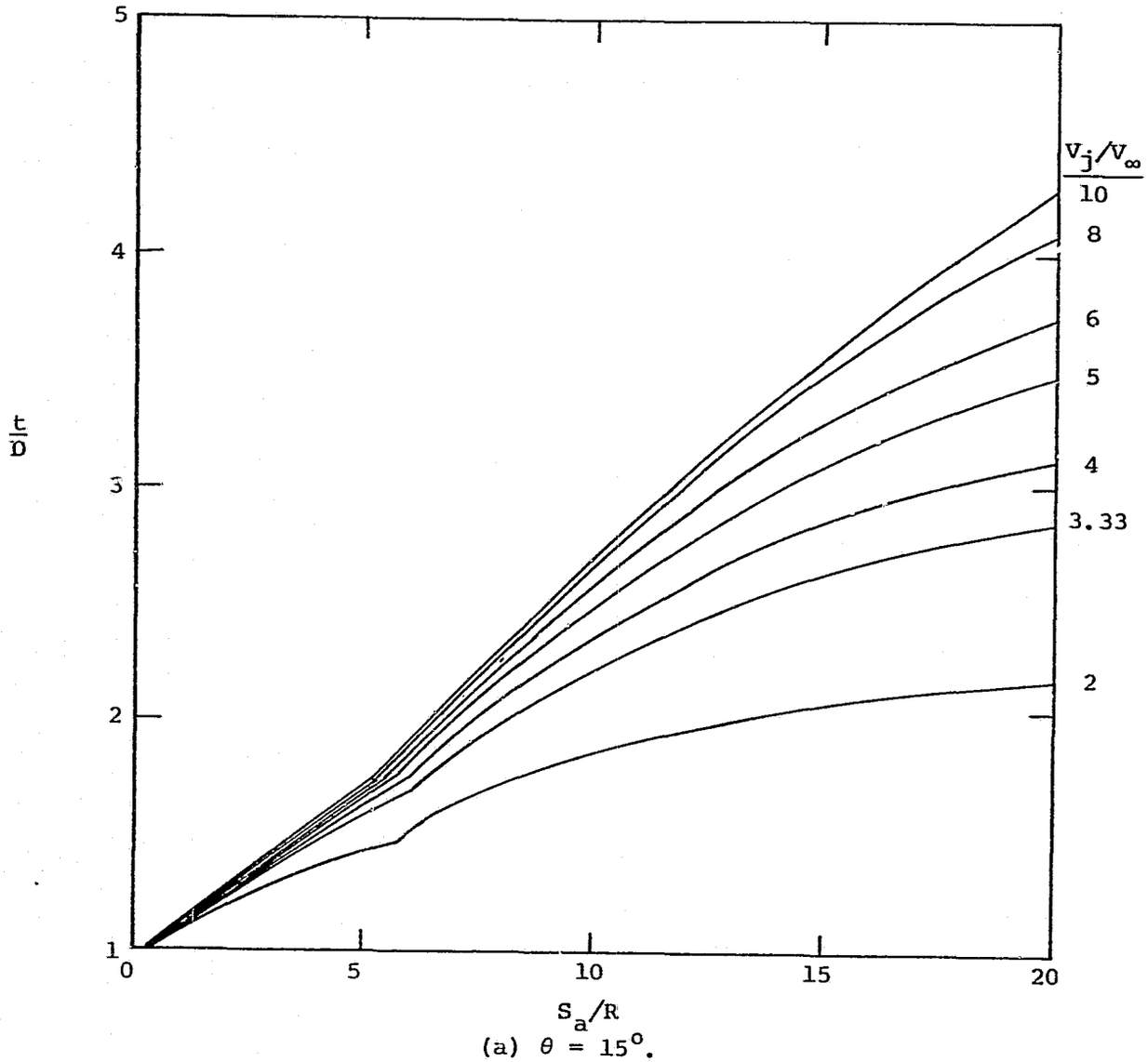

(a) $\theta = 15^{\circ}$.

Figure 7.- Jet expansion curves for a jet exhausting at an angle to a flat plate.

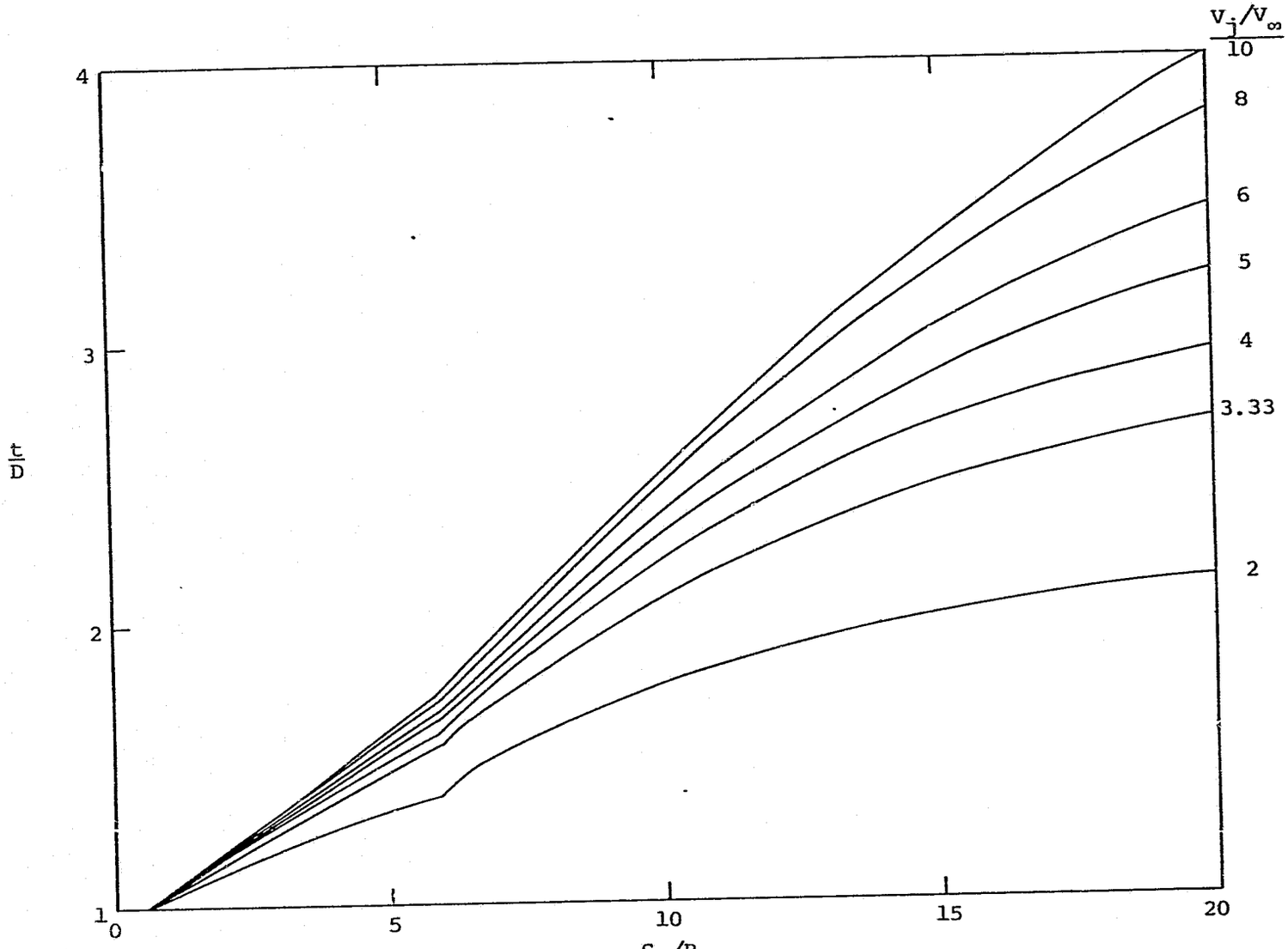

(b) $\theta = 30^\circ$.

Figure 7.- Continued.

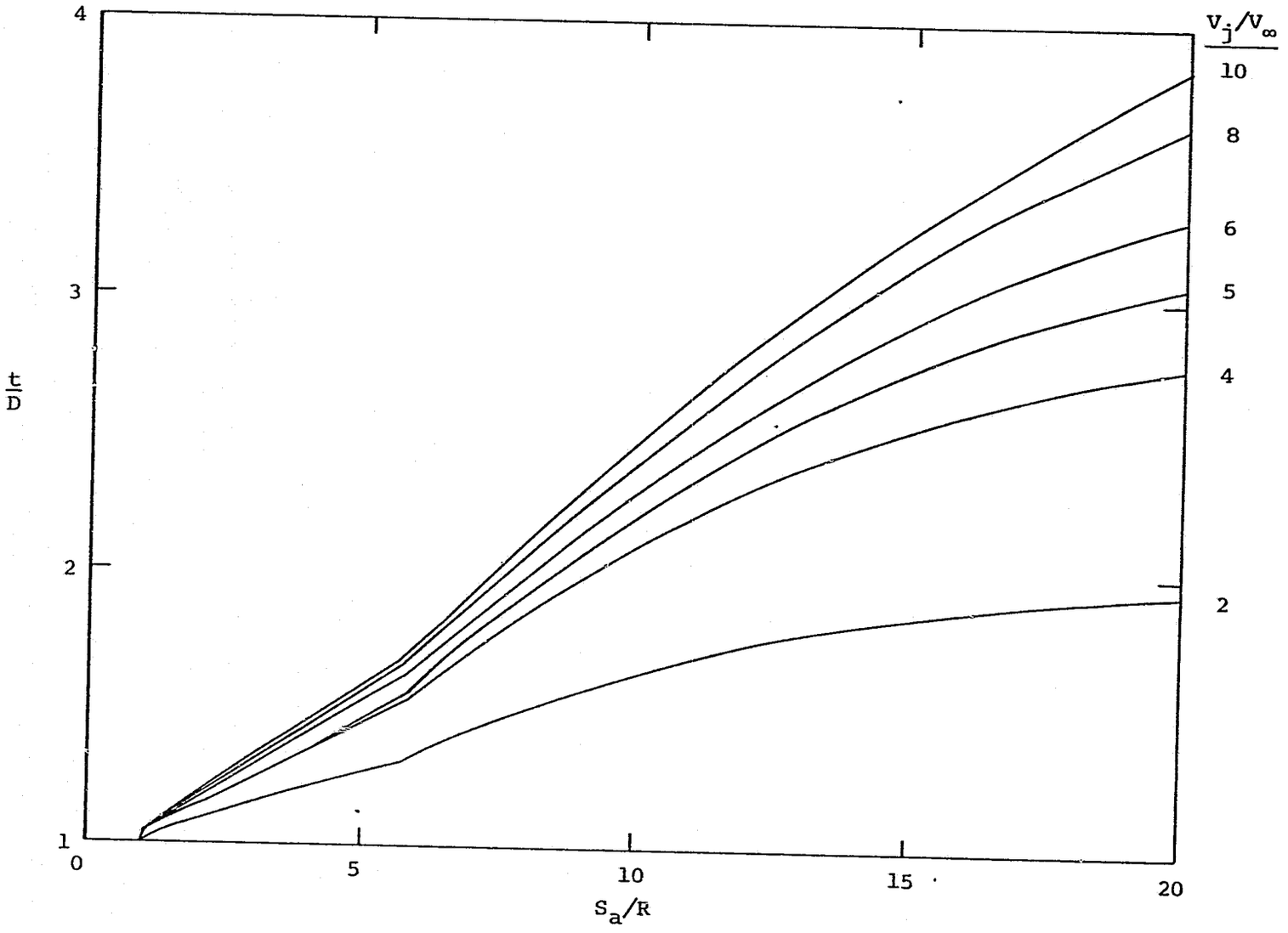

(c) $\theta = 45°$.

Figure 7.- Continued.

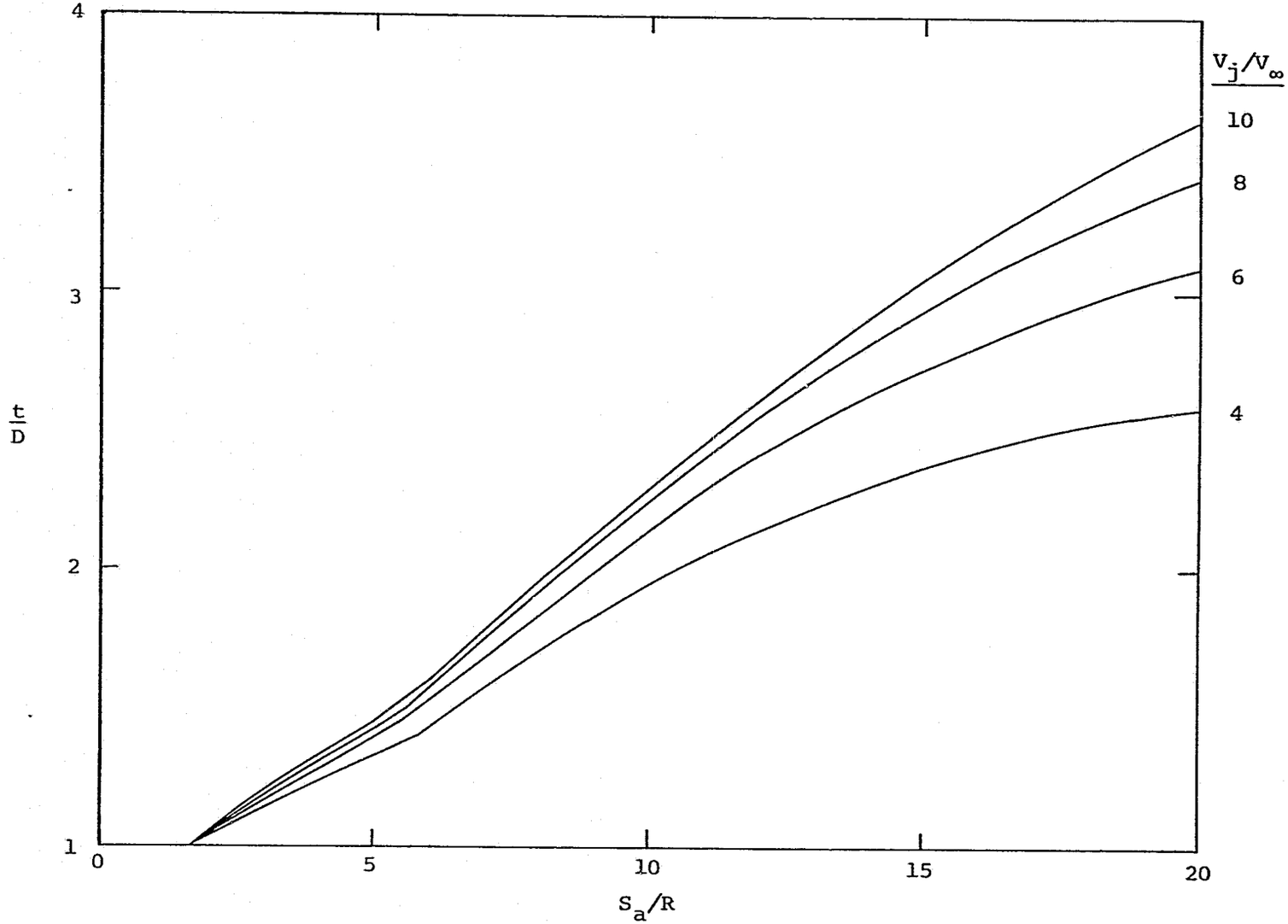

(d) $\theta = 60^\circ$.

Figure 7.- Concluded.

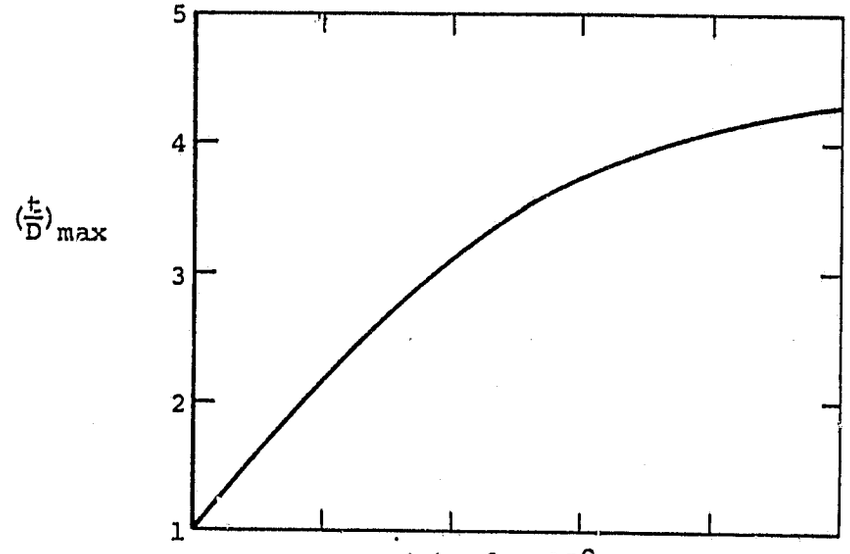

(a) $\theta = 15^{\circ}$.

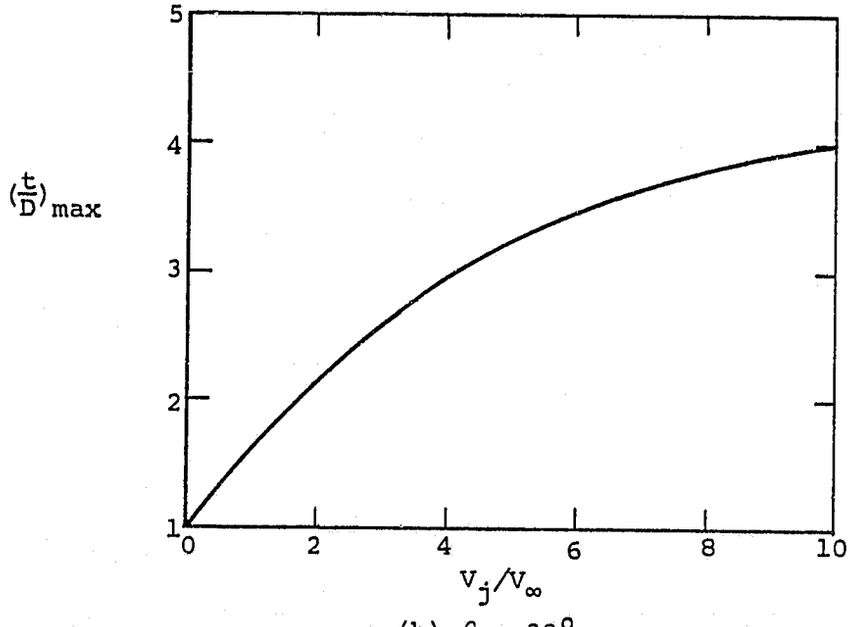

(b) $\theta = 30^{\circ}$.

Figure 8.- Maximum jet radius variation with jet velocity ratio for a jet exhausting at an angle to a flat plate, $S_a/R = 20$.

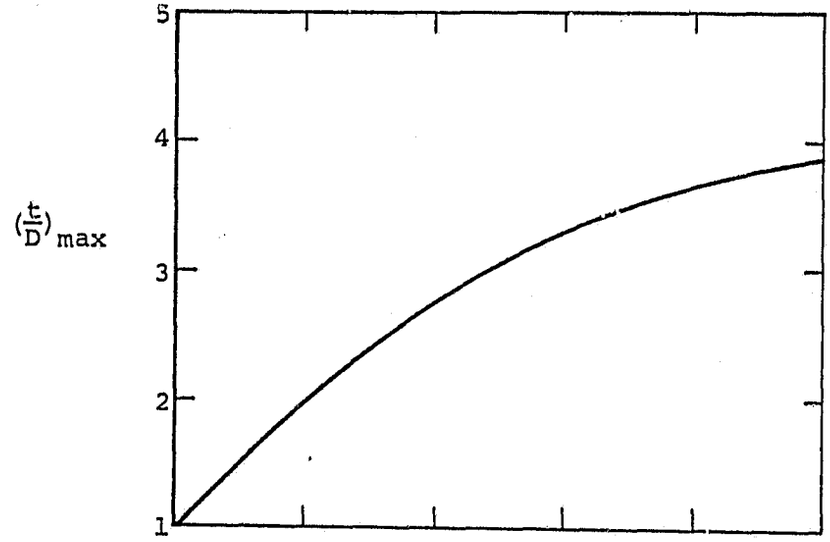

(c) $\theta = 45°$.

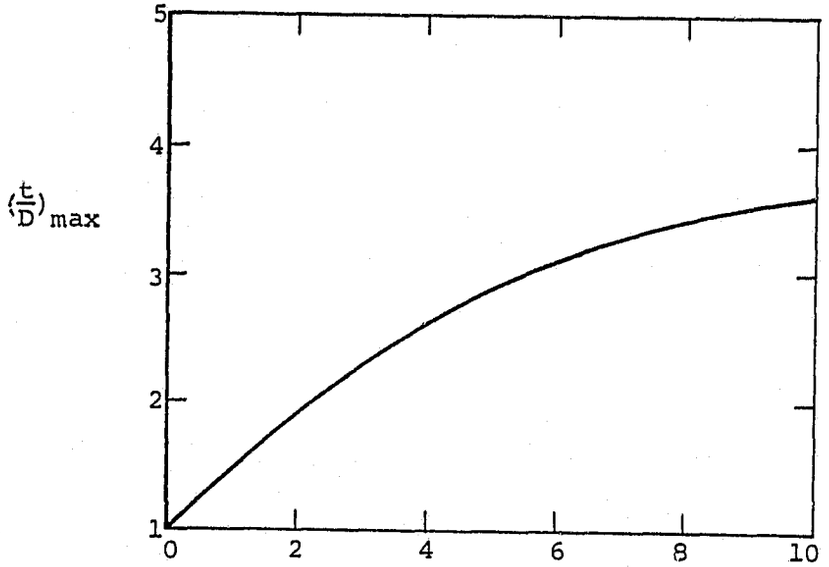

(d) $\theta = 60°$.

Figure 8.- Concluded.

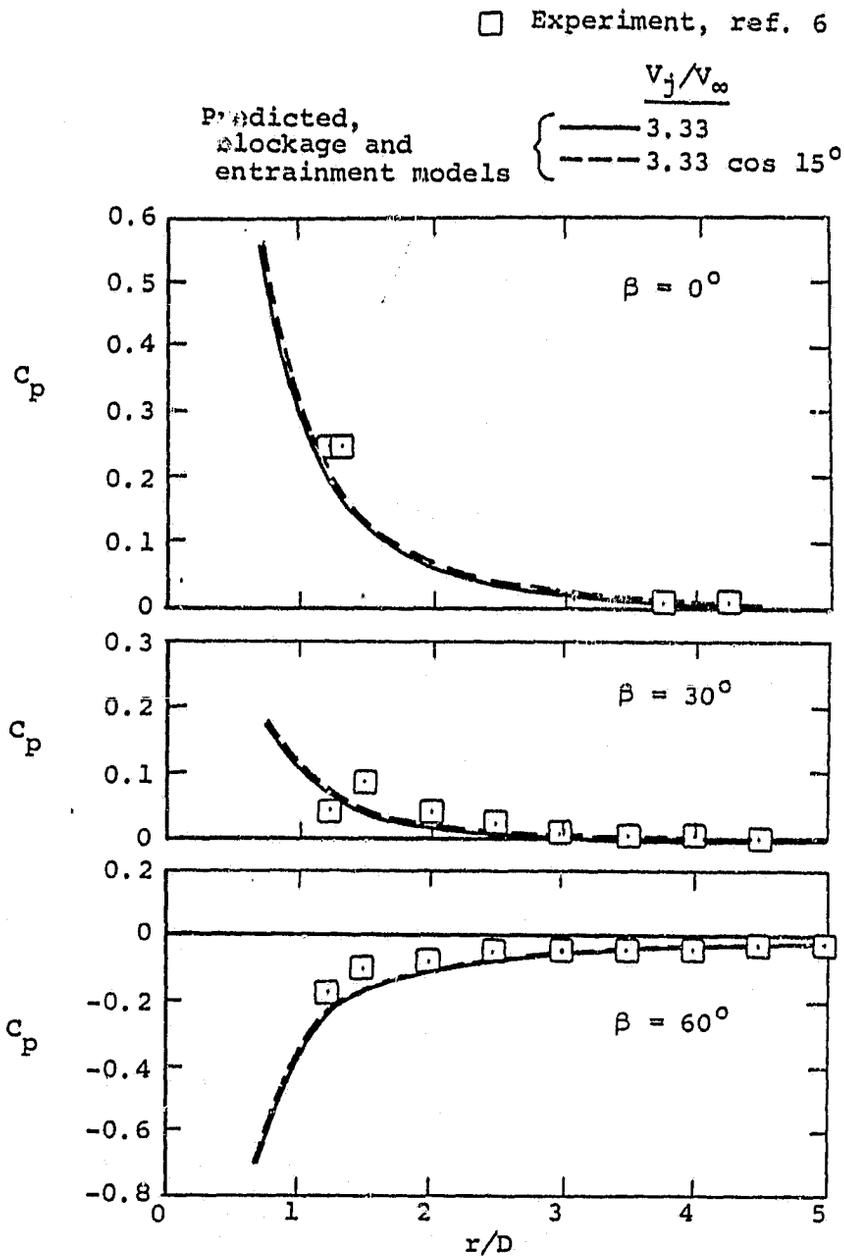

(a) $V_j/V_\infty = 3.33$

Figure 9.- Comparison of measured and predicted pressures on a flat plate from which a jet is exhausting into a crossflow, $\theta = 15°$.

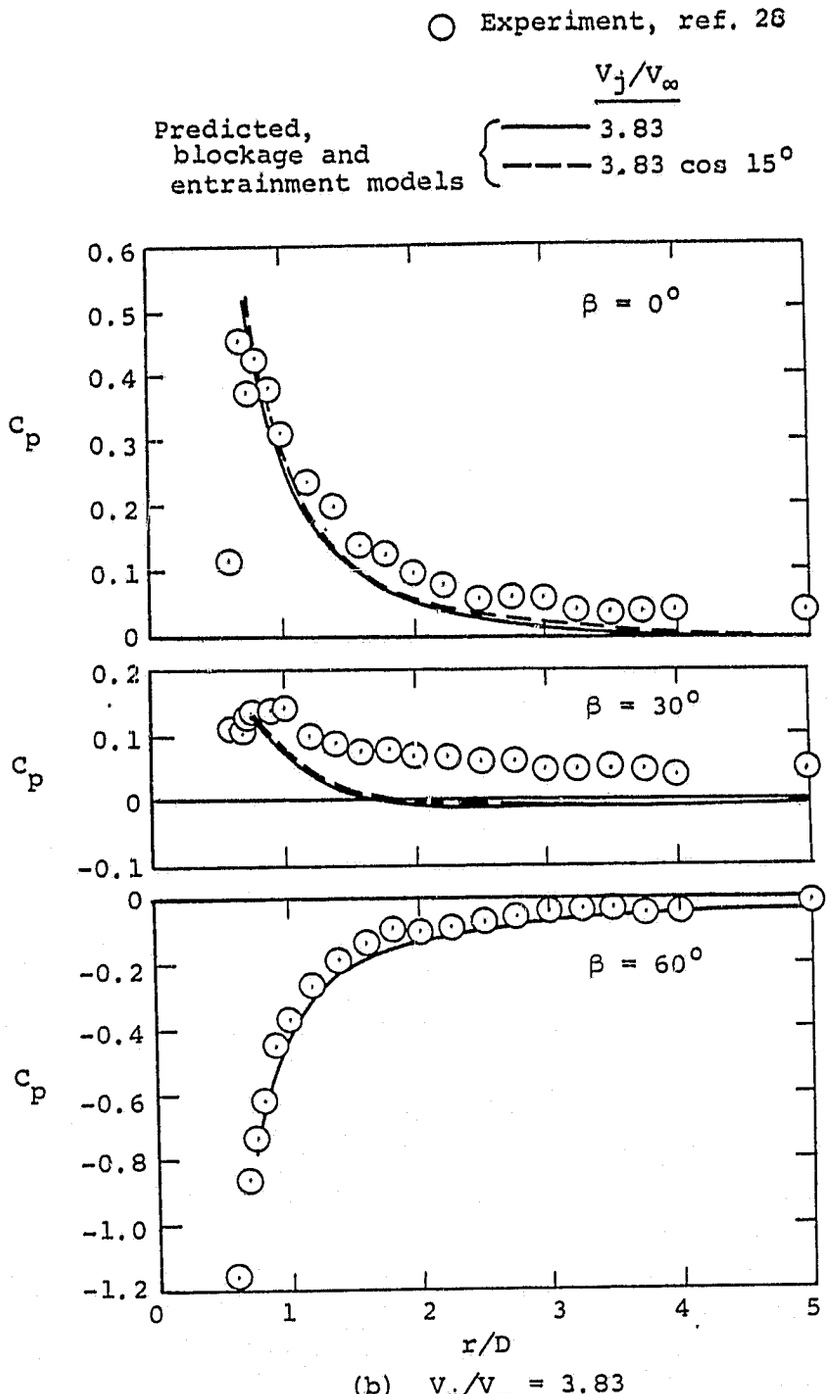

(b) $V_j/V_\infty = 3.83$

Figure 9.- Continued.

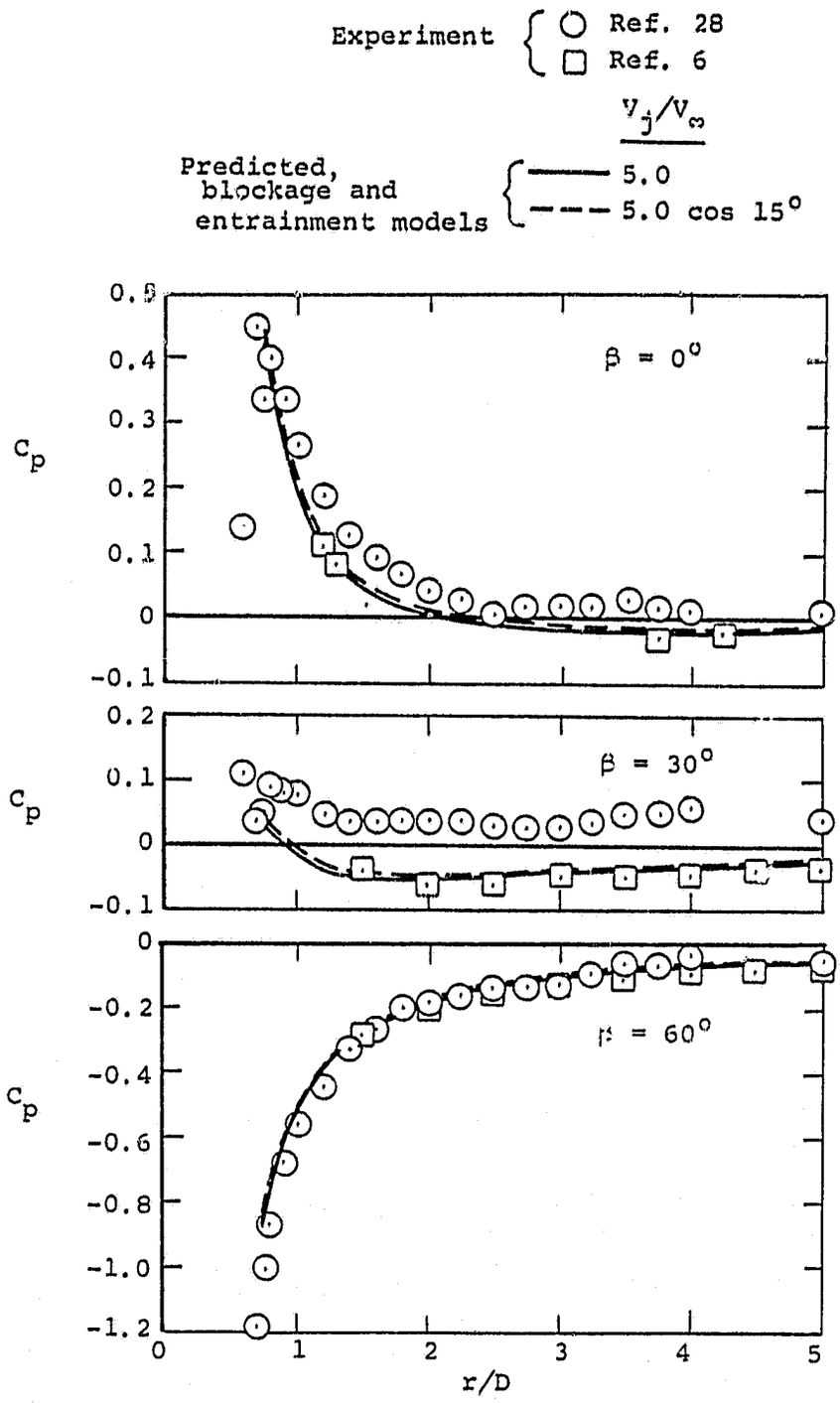

(c) $V_j/V_\infty = 5.0$

Figure 9.- Continued.

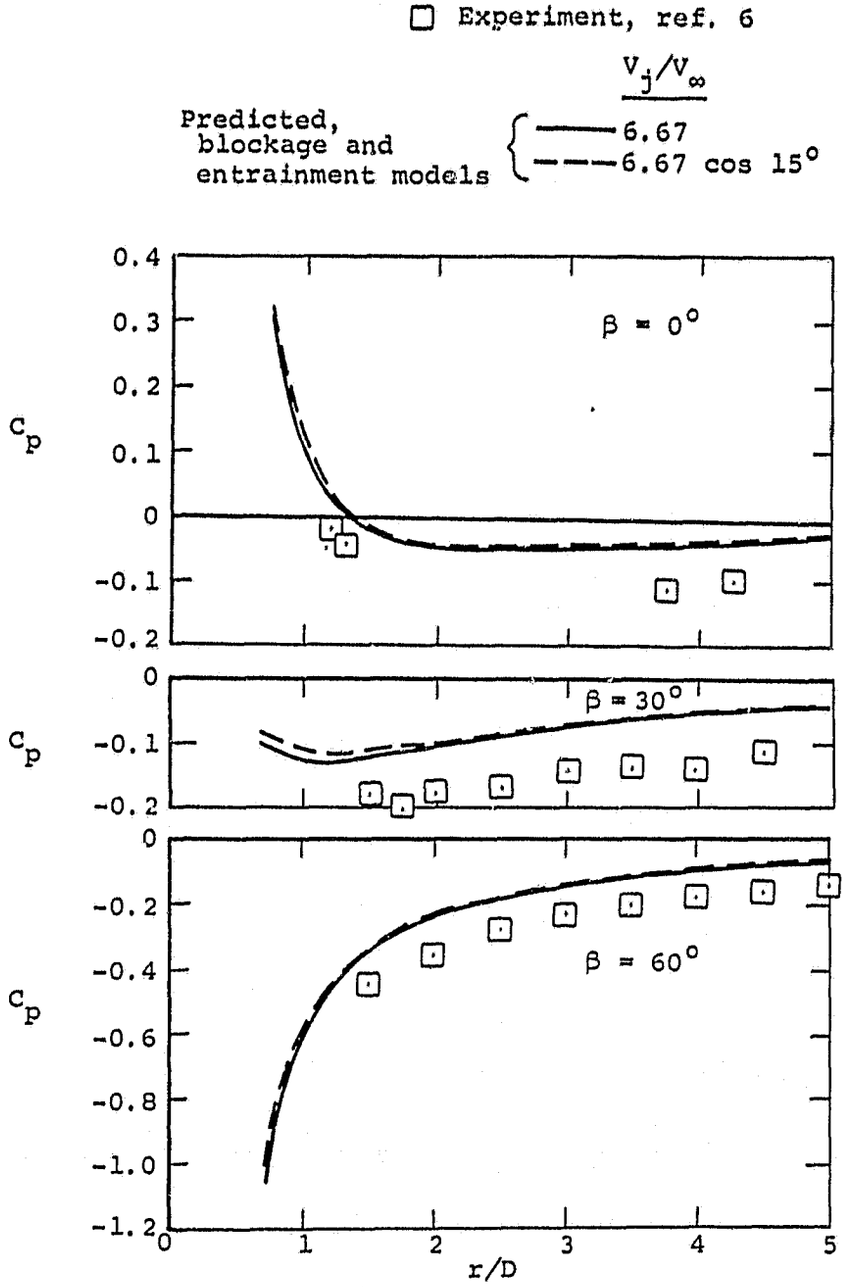

(d) $V_j/V_\infty = 6.67$

Figure 9.- Continued.

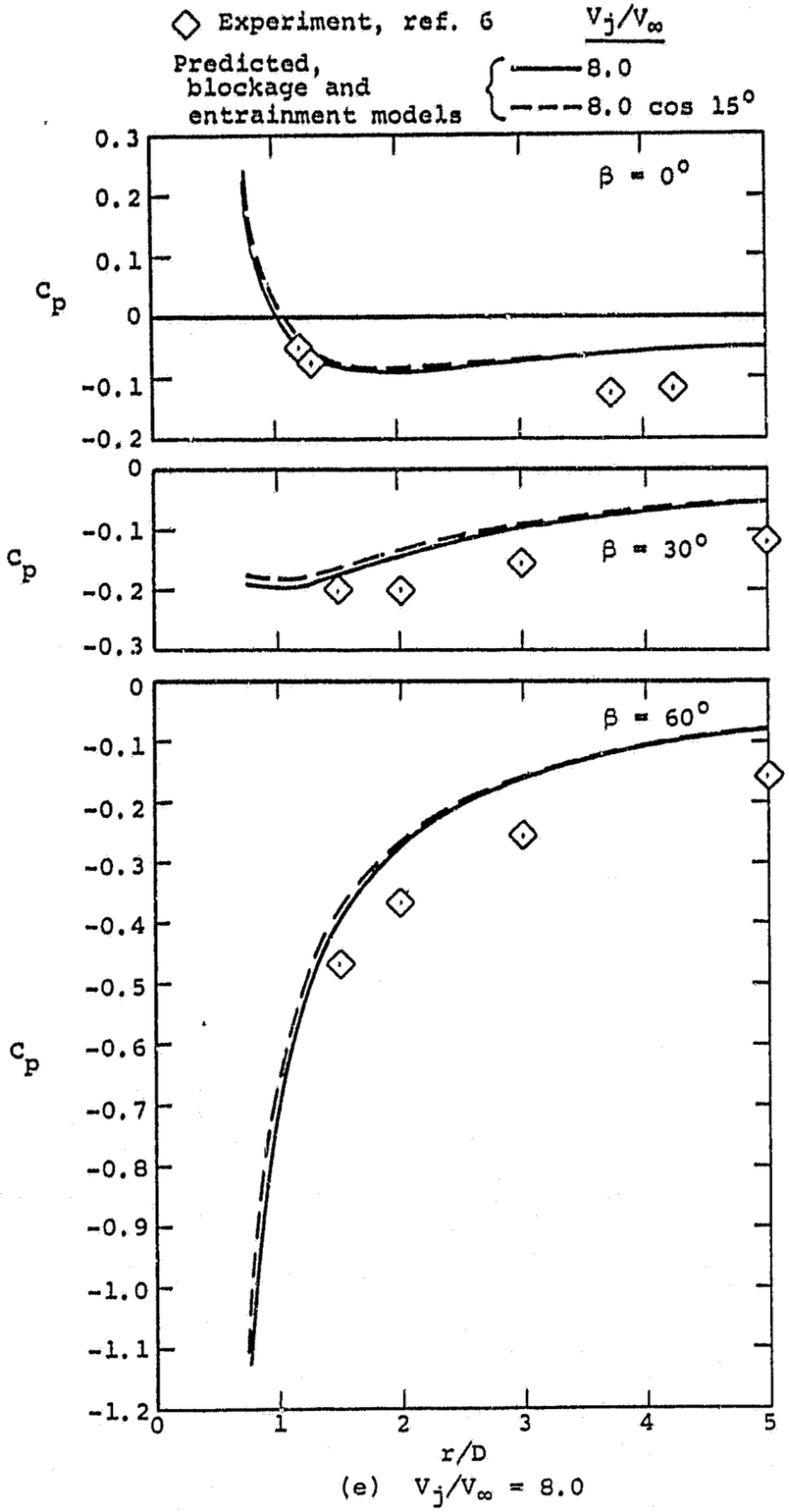

(e) V_j/V_∞ = 8.0

Figure 9.- Continued.

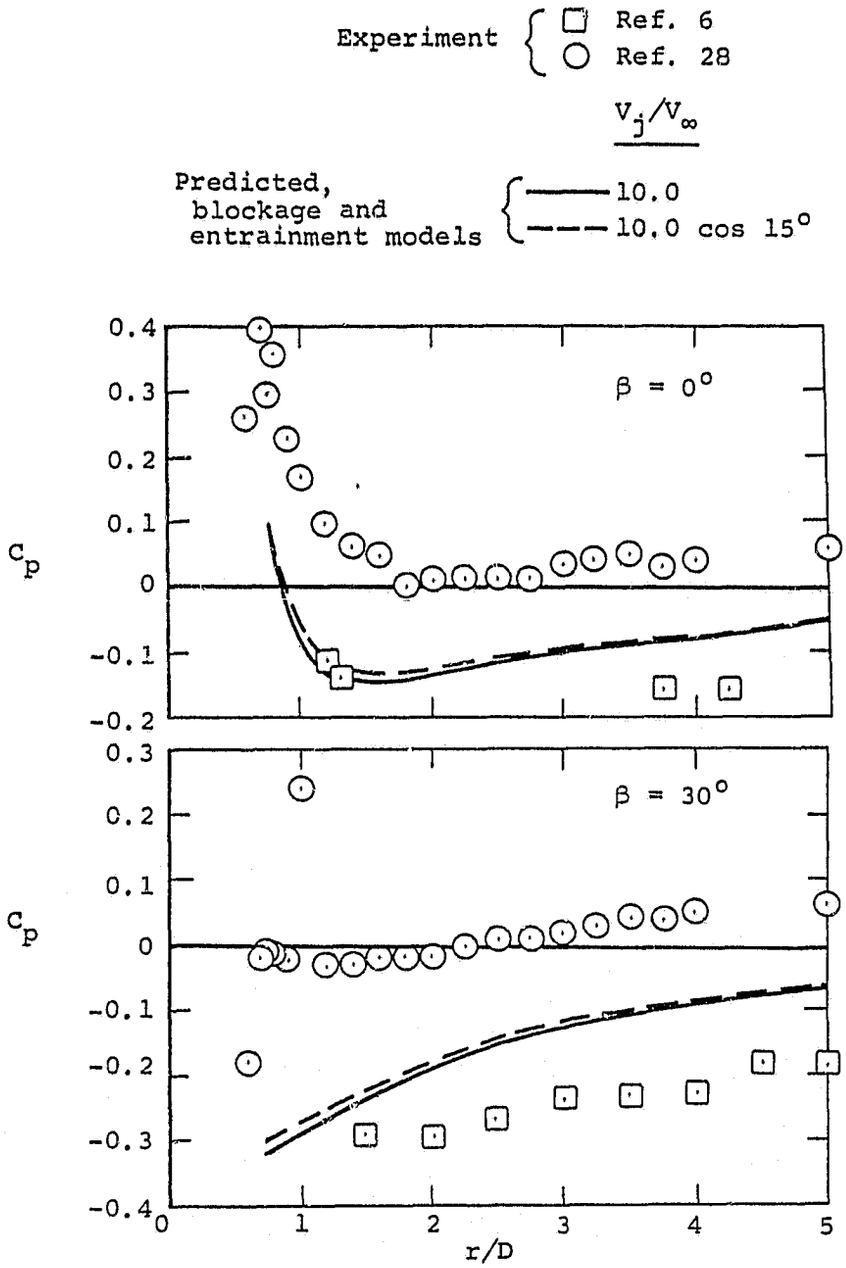

(f) $V_j/V_\infty = 10.0$

Figure 9.- Continued.

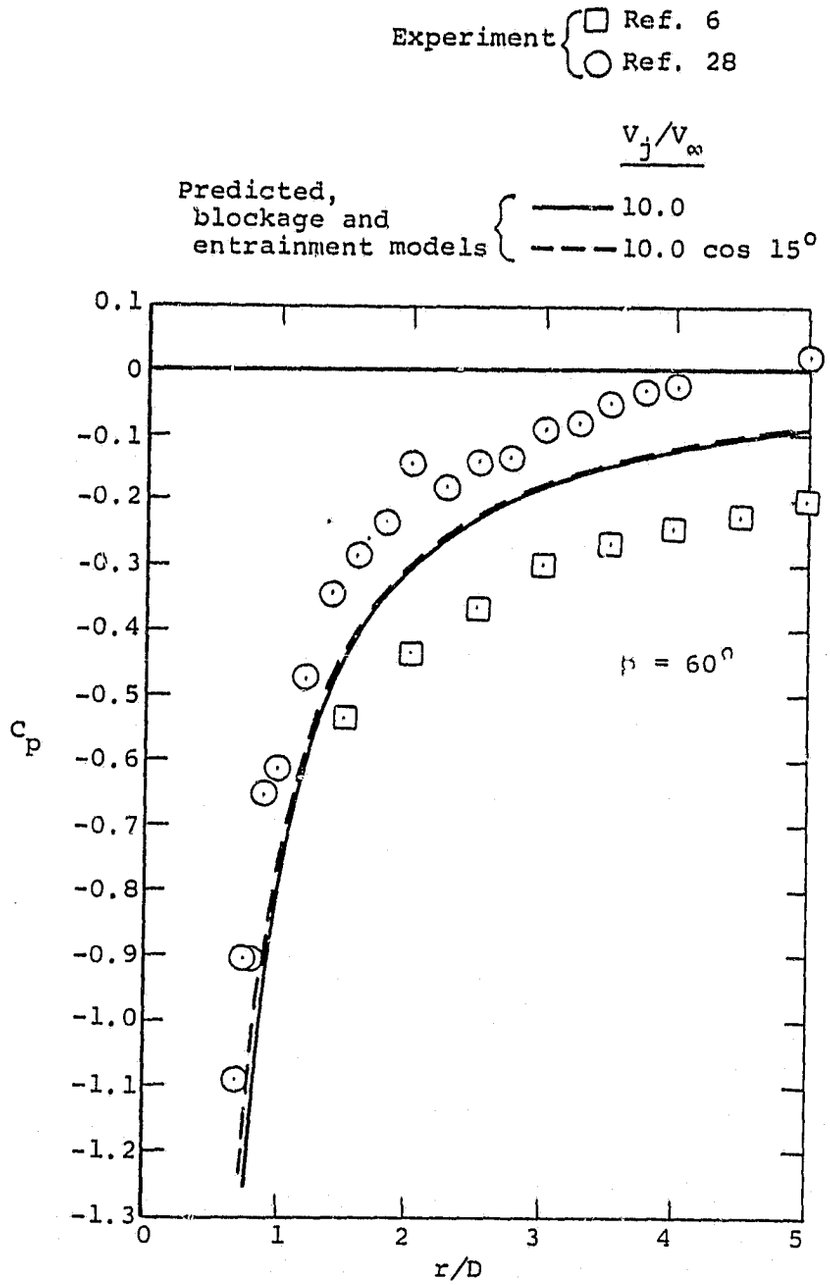

(f) Concluded.

Figure 9.- Continued.

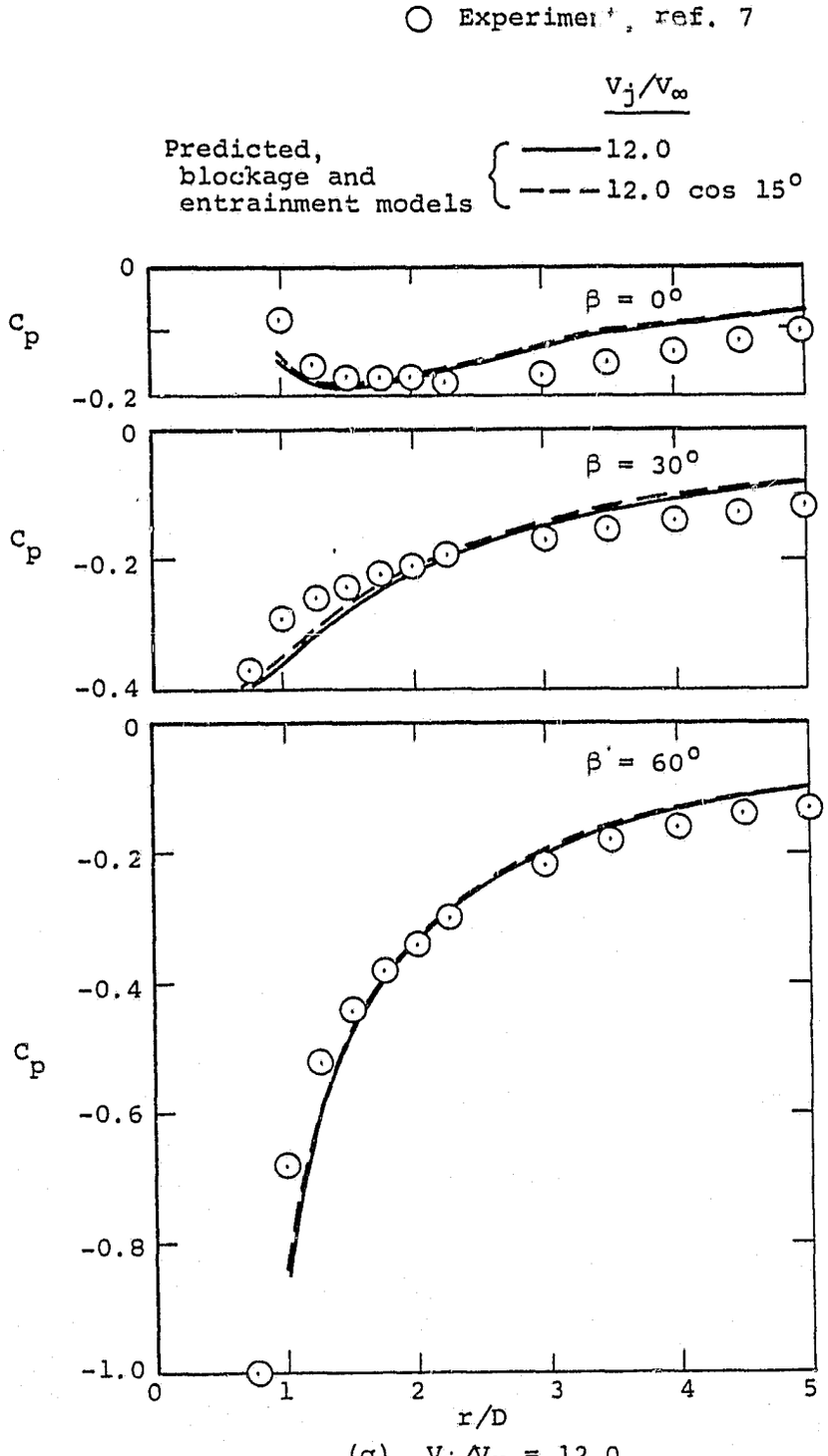

(g) $V_j/V_\infty = 12.0$

Figure 9.- Concluded.

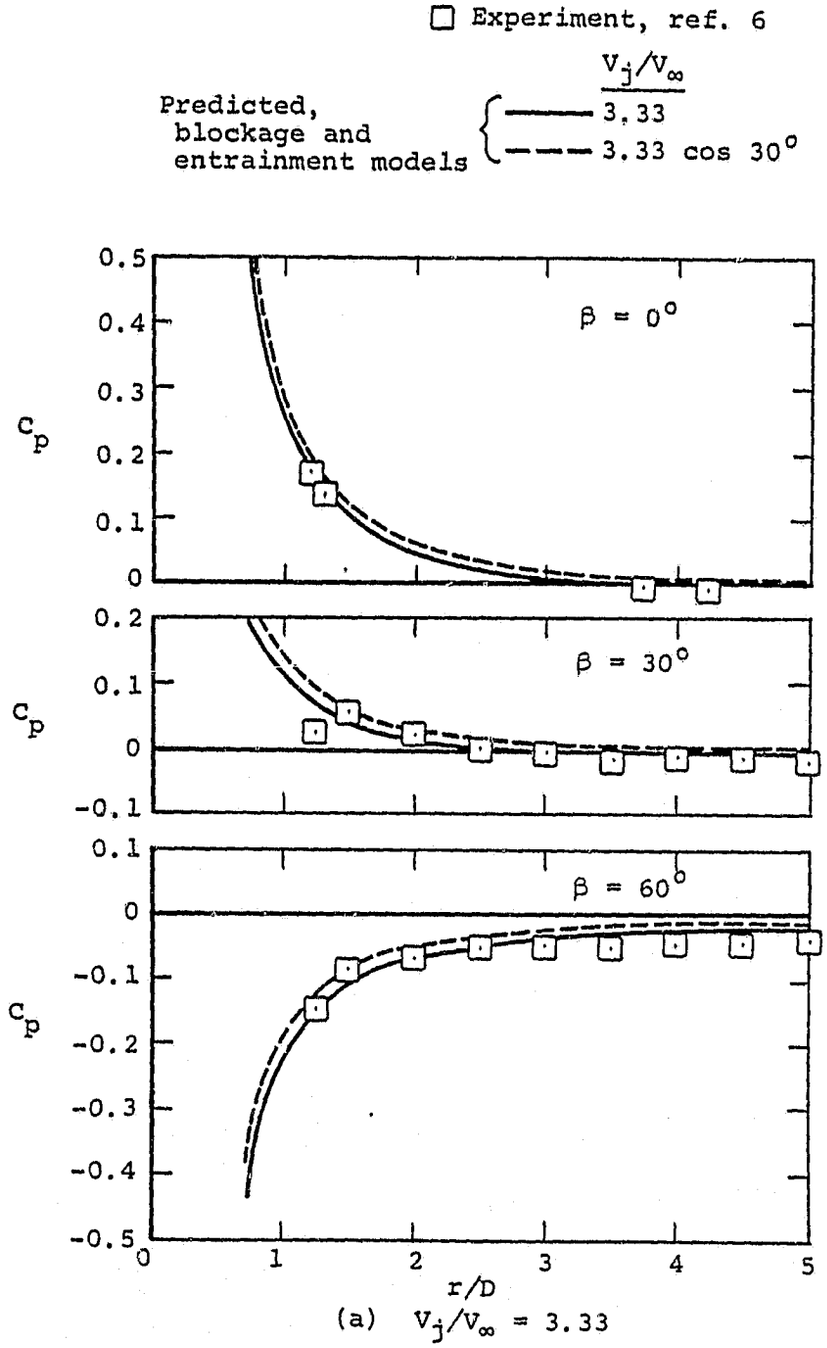

(a) $V_j/V_\infty = 3.33$

Figure 10.- Comparison of measured and predicted pressures on a flat plate from which a jet is exhausting into a crossflow, $\theta = 30°$.

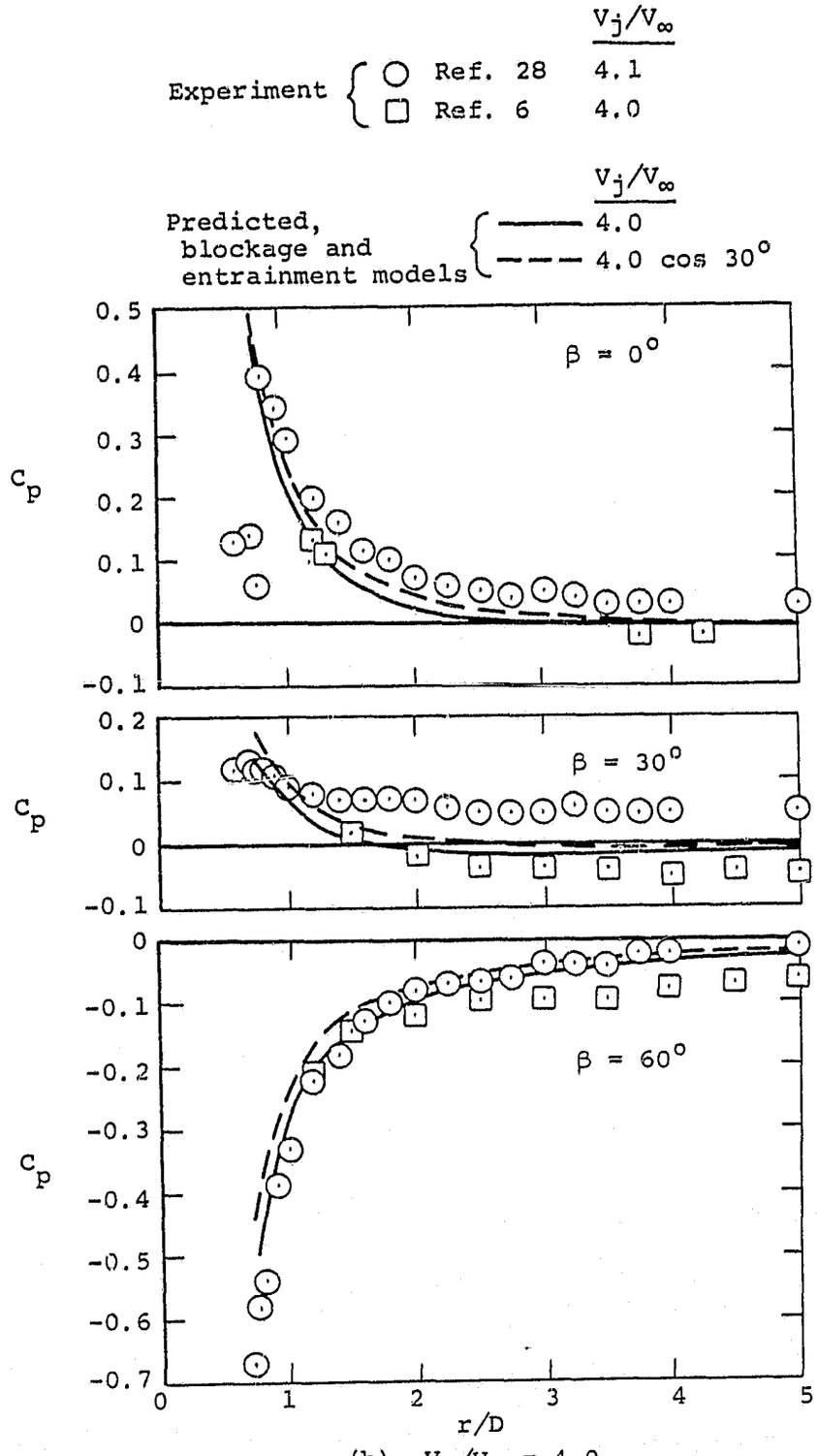

(b) $V_j/V_\infty = 4.0$

Figure 10.- Continued.

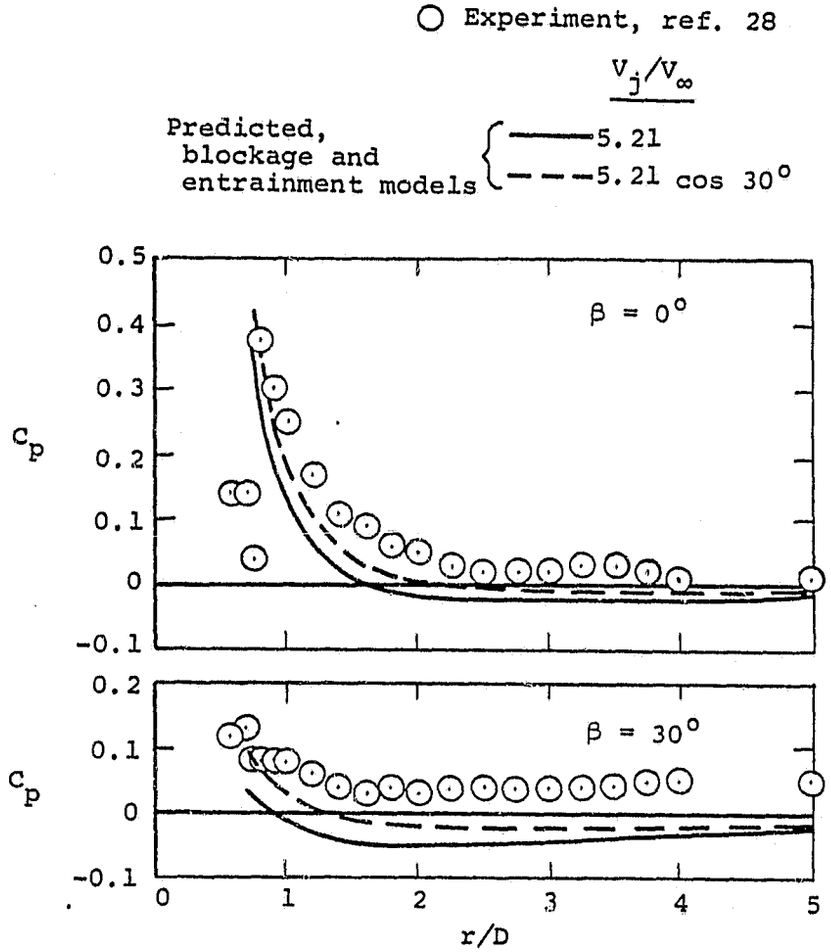

(c) $V_j/V_\infty = 5.21$

Figure 10.- Continued.

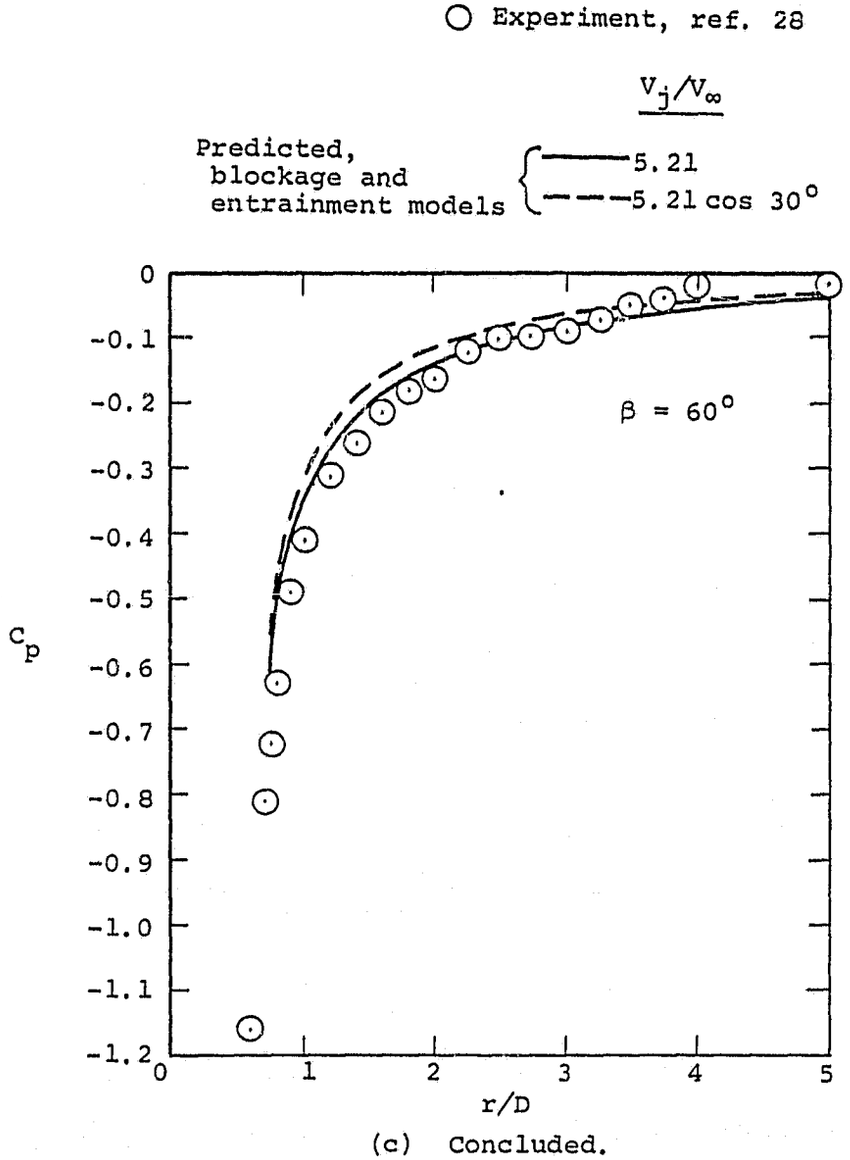

(c) Concluded.

Figure 10.- Continued.

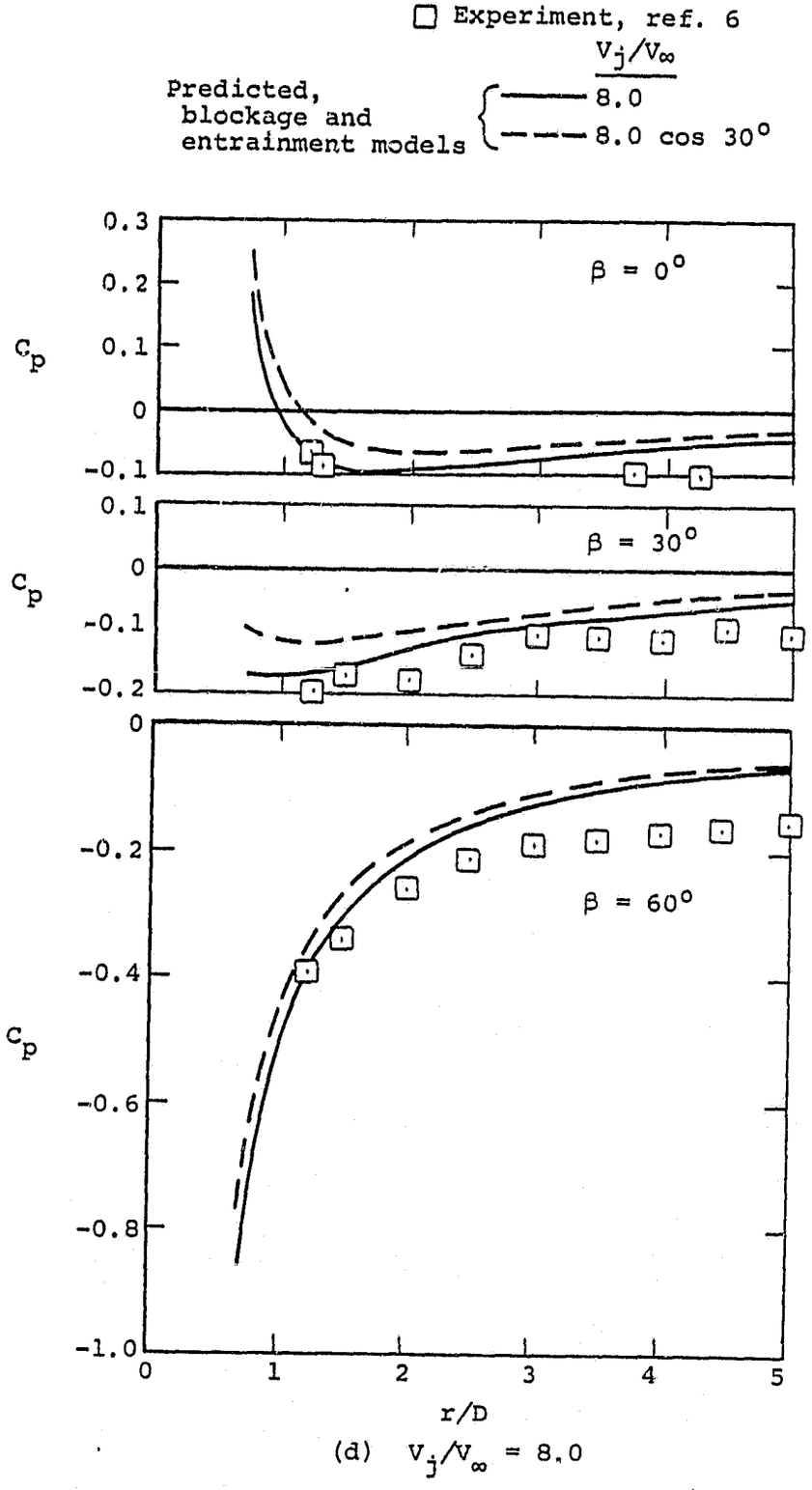

(d) $V_j/V_\infty = 8.0$

Figure 10.- Continued.

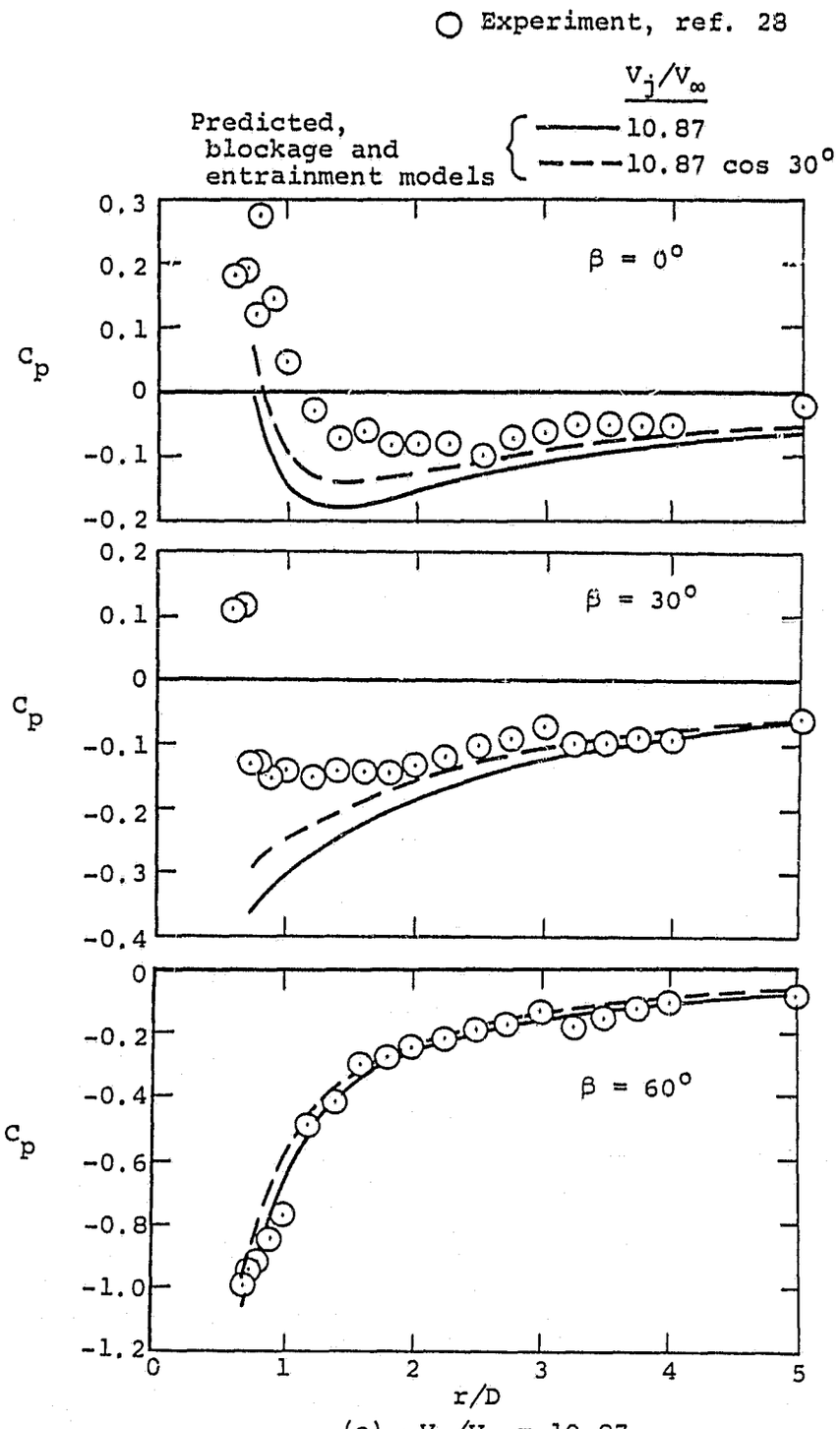

(e) V_j/V_∞ = 10.87

Figure 10.- Continued.

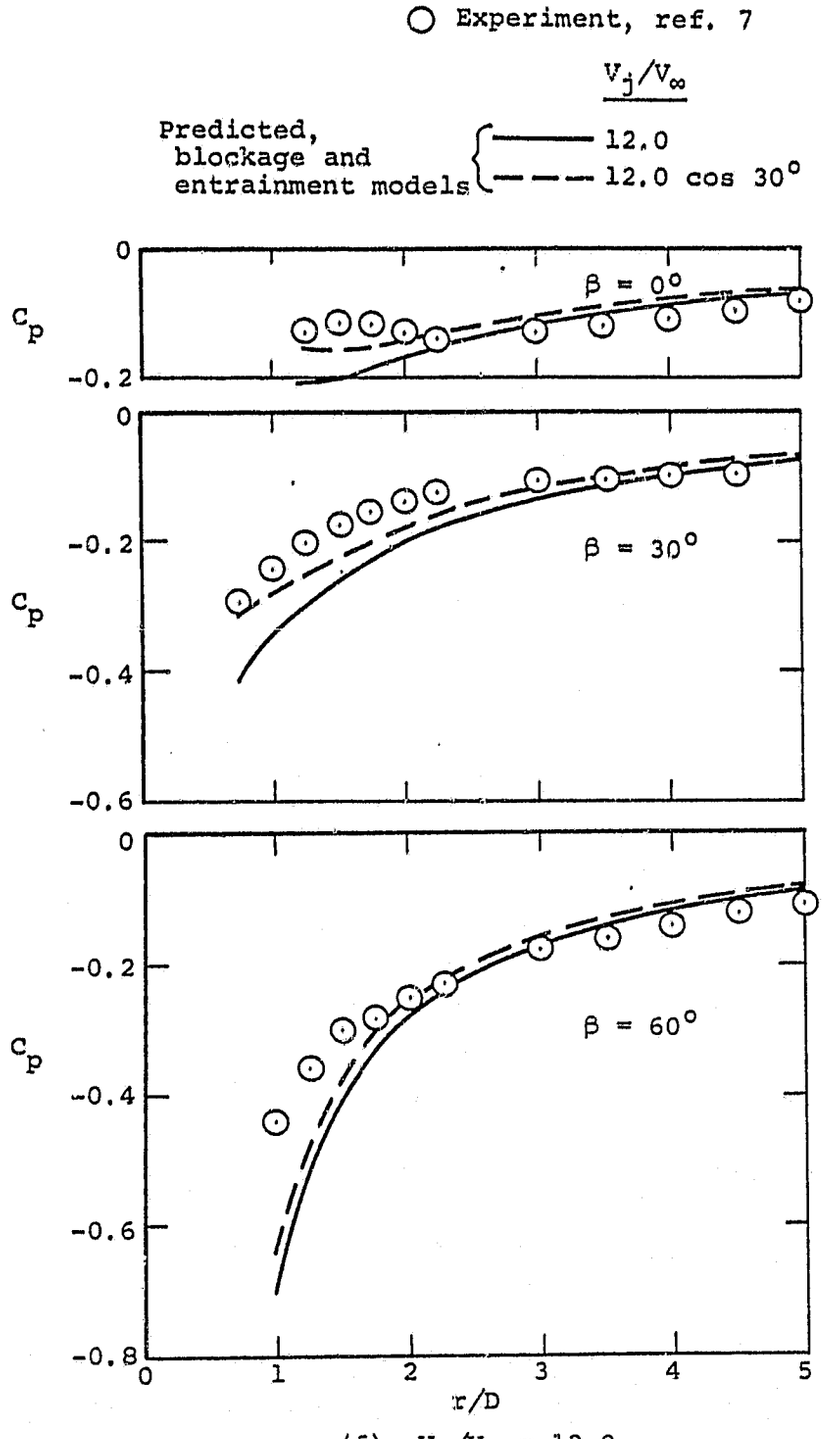

(f) $V_j/V_\infty = 12.0$

Figure 10.- Concluded.

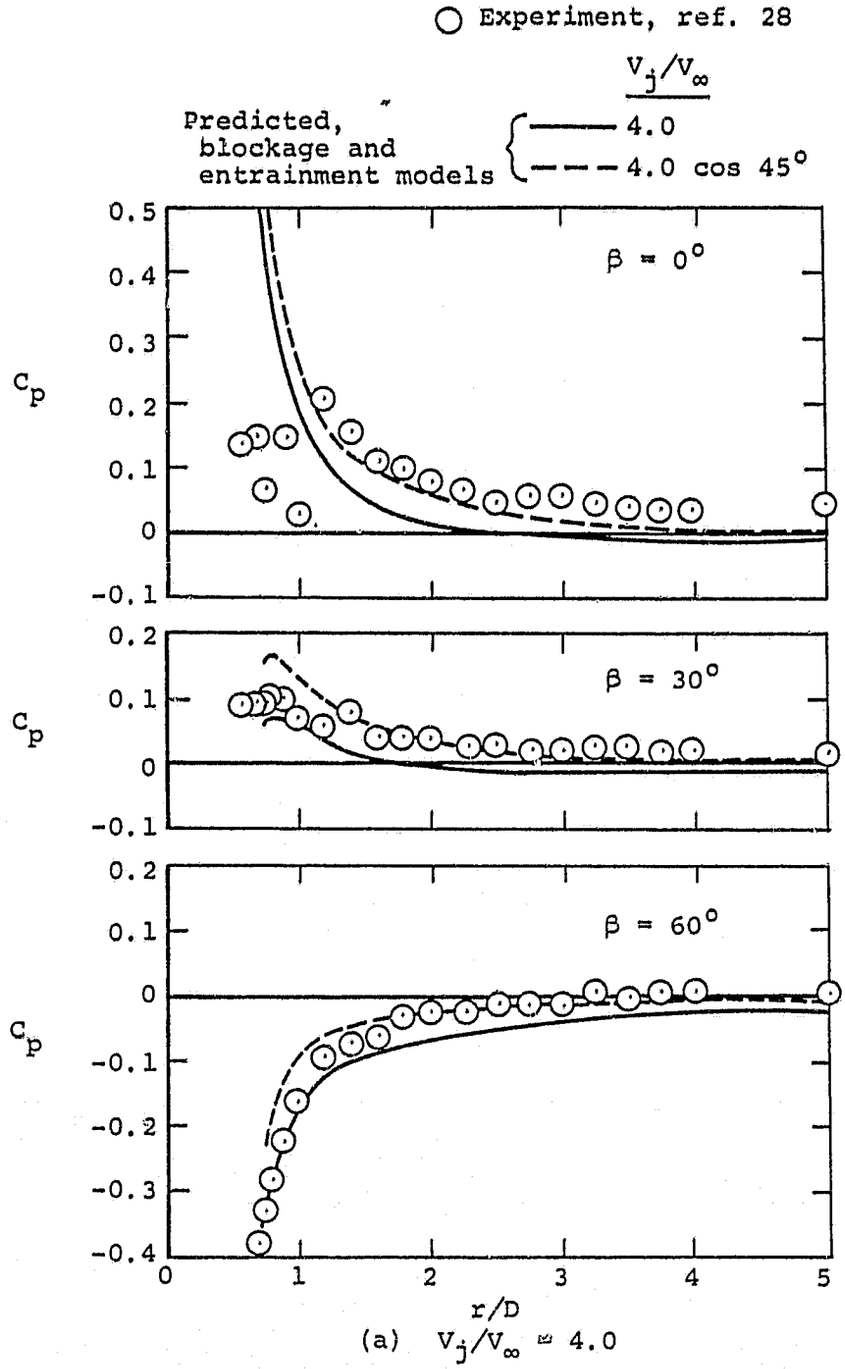

(a) $V_j/V_\infty \approx 4.0$

Figure 11.- Comparison of measured and predicted pressures on a flat plate from which a jet is exhausting into a crossflow, $\theta = 45°$.

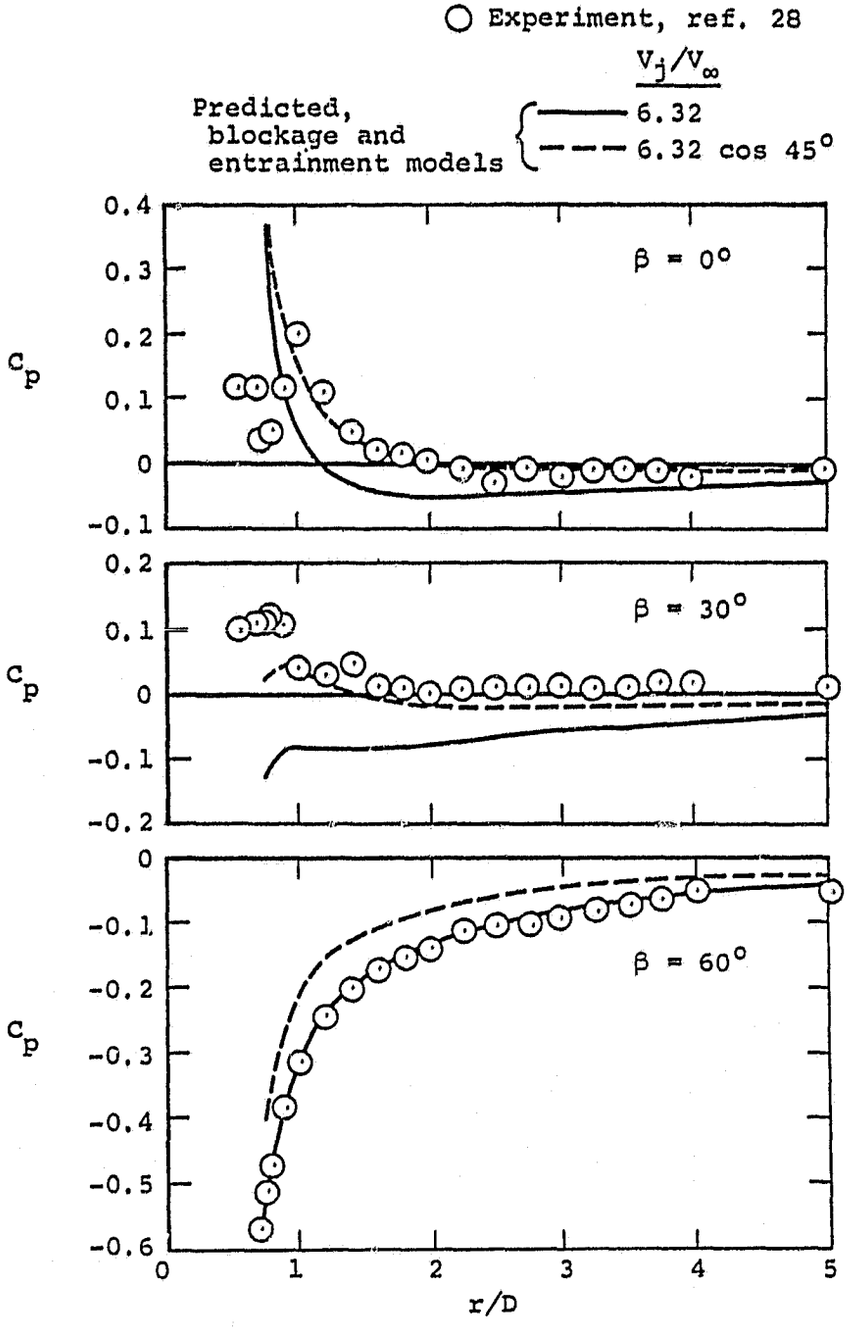

(b) $V_j/V_\infty = 6.32$

Figure 11.- Continued.

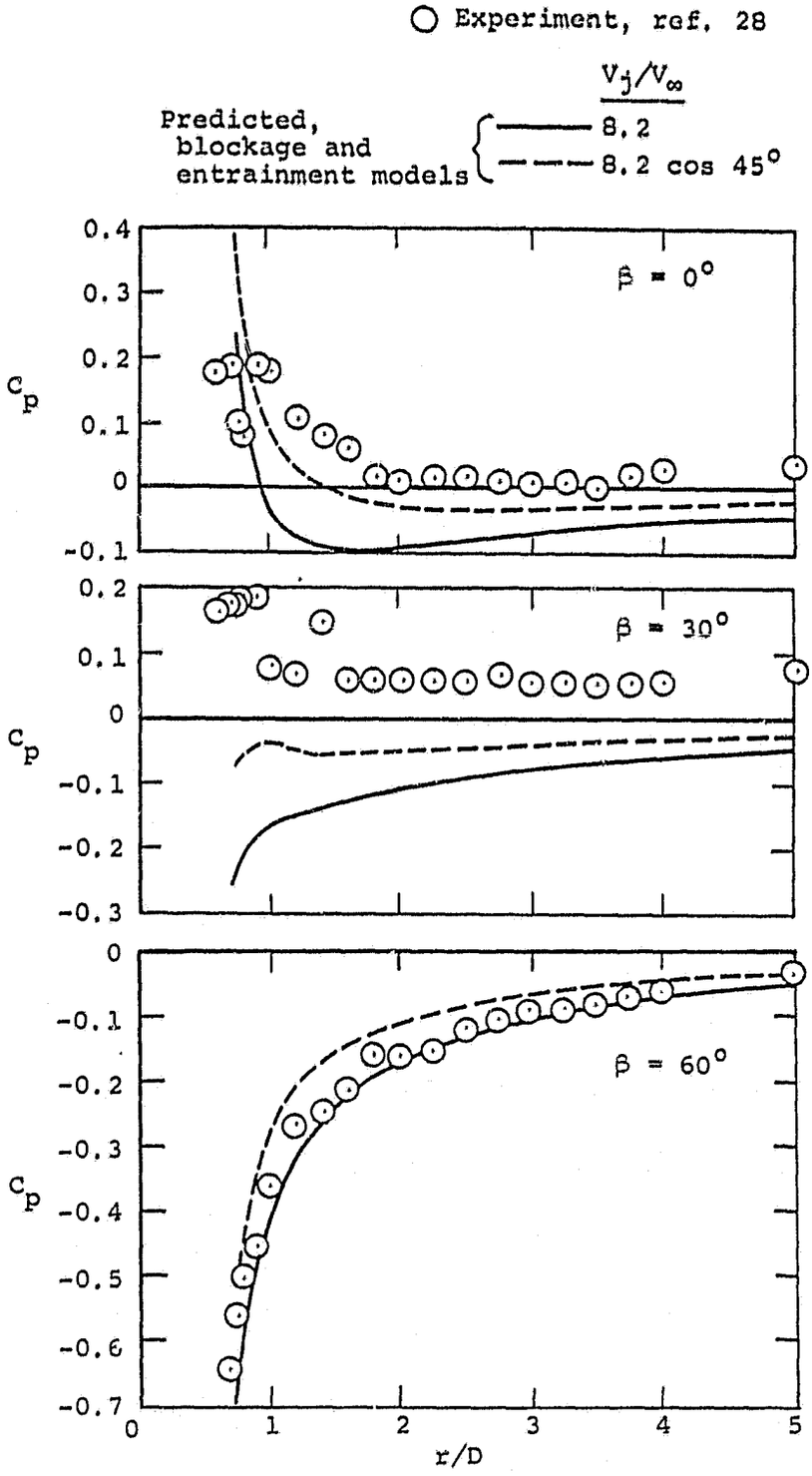

(c) V_j/V_∞ = 8.2

Figure 11.- Continued.

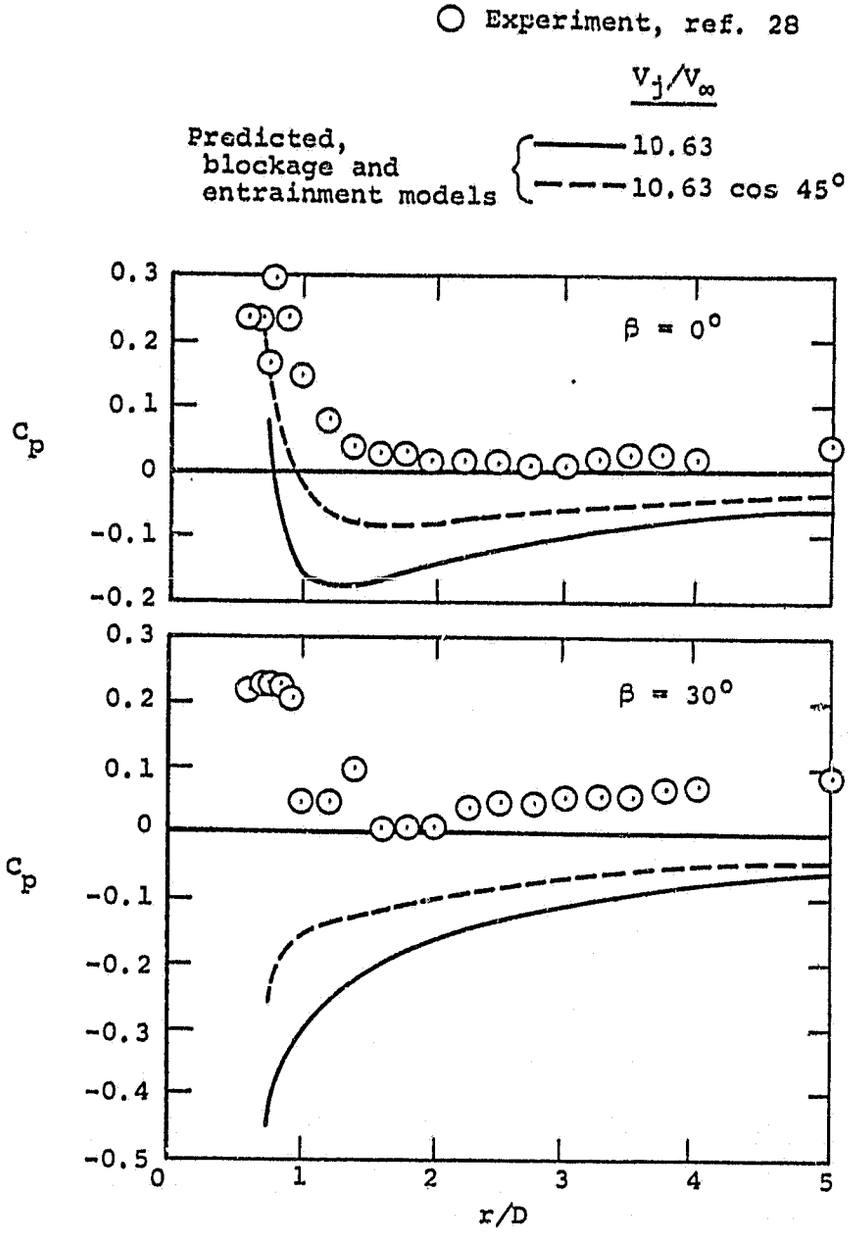

(d) $V_j/V_\infty = 10.63$

Figure 11.- Continued.

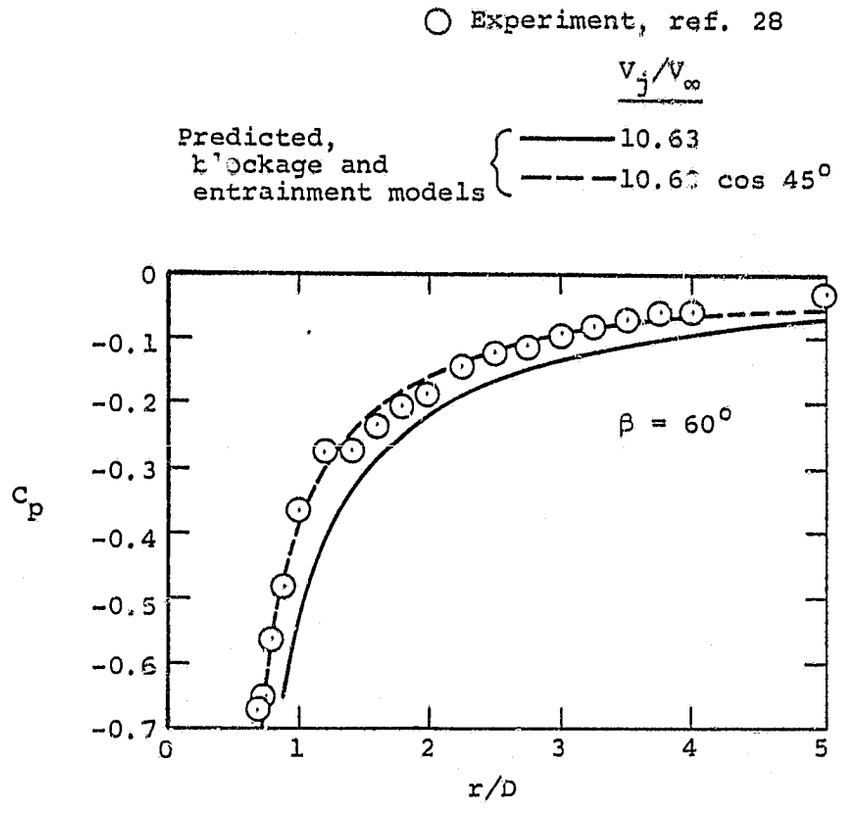

(d) Concluded.

Figure 11.- Continued.

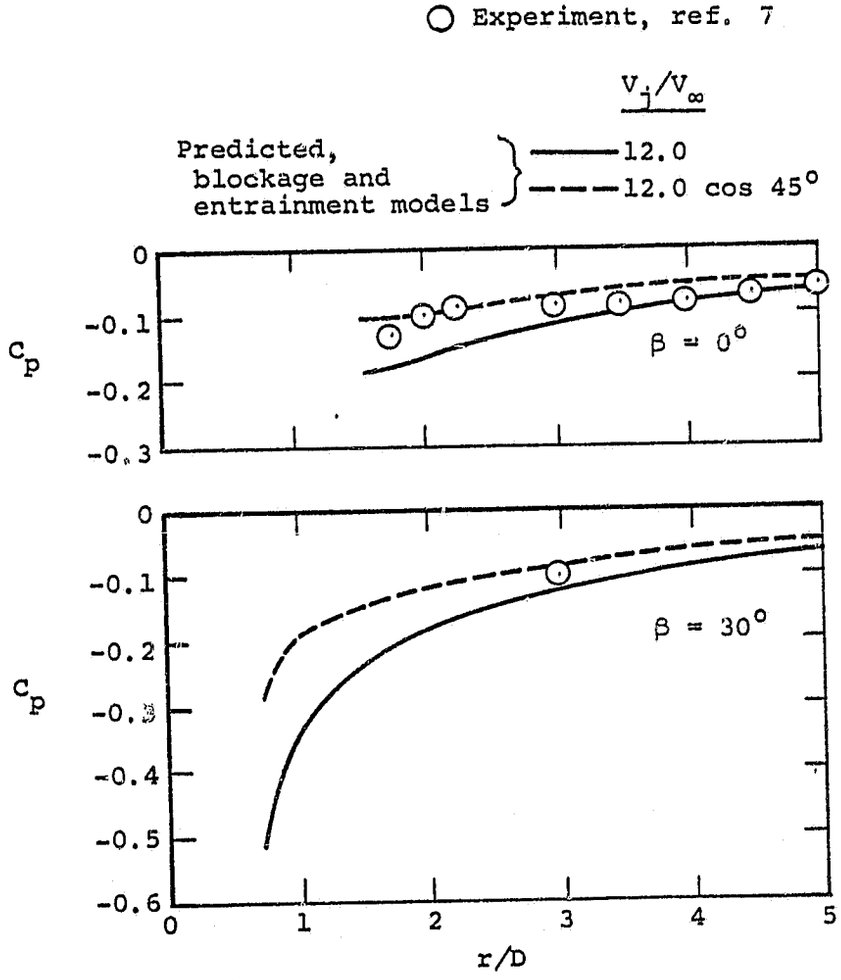

(e) $V_j/V_\infty = 12.0$

Figure 11.- Continued.

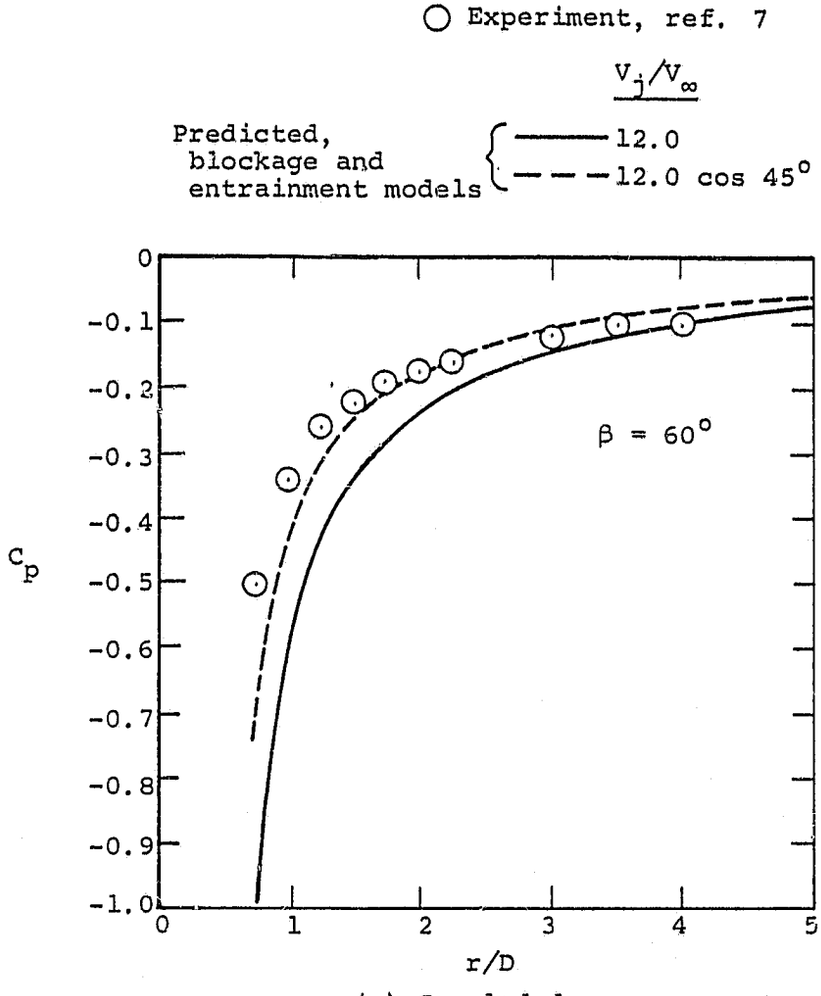

(e) Concluded.

Figure 11.- Concluded.

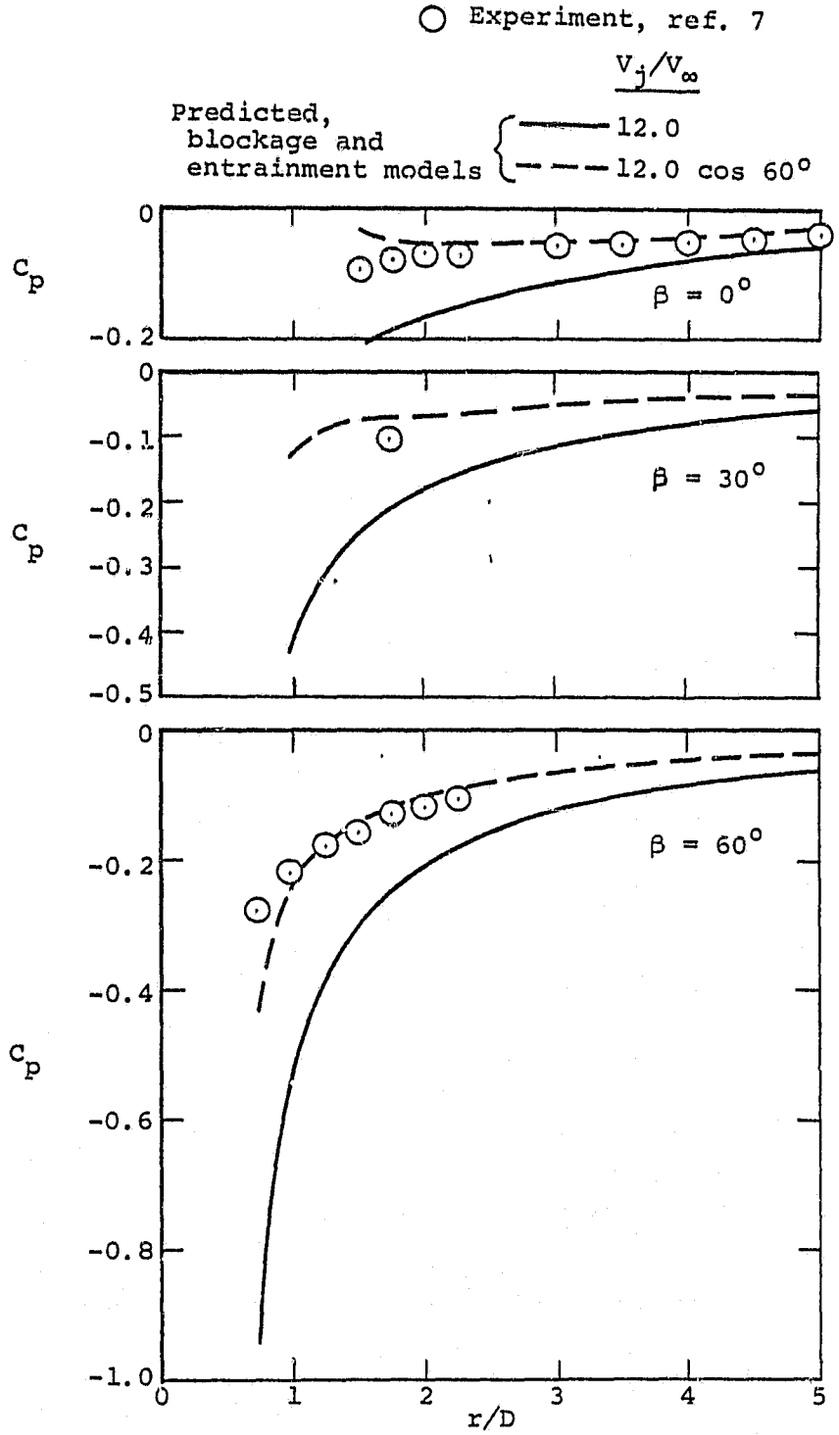

Figure 12.- Comparison of measured and predicted pressures on a flat plate from which a jet is exhausting into a crossflow, $V_j/V_\infty = 12.0$, $\theta = 60^\circ$.

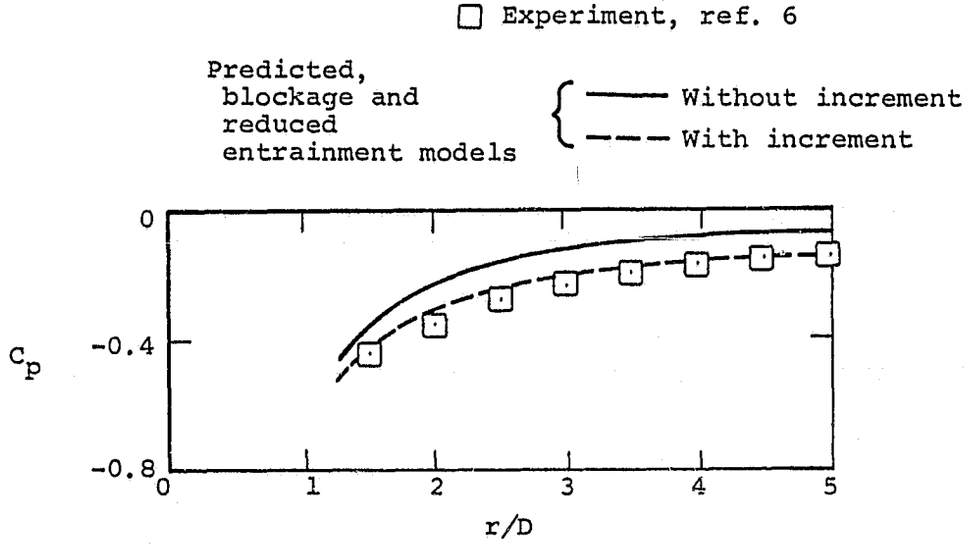

Figure 13.- Comparison of measured and predicted pressures on a flat plate from which a jet is issuing, $V_j/V_\infty = 6.67$, $\theta = 15^\circ$, $\beta = 60^\circ$.

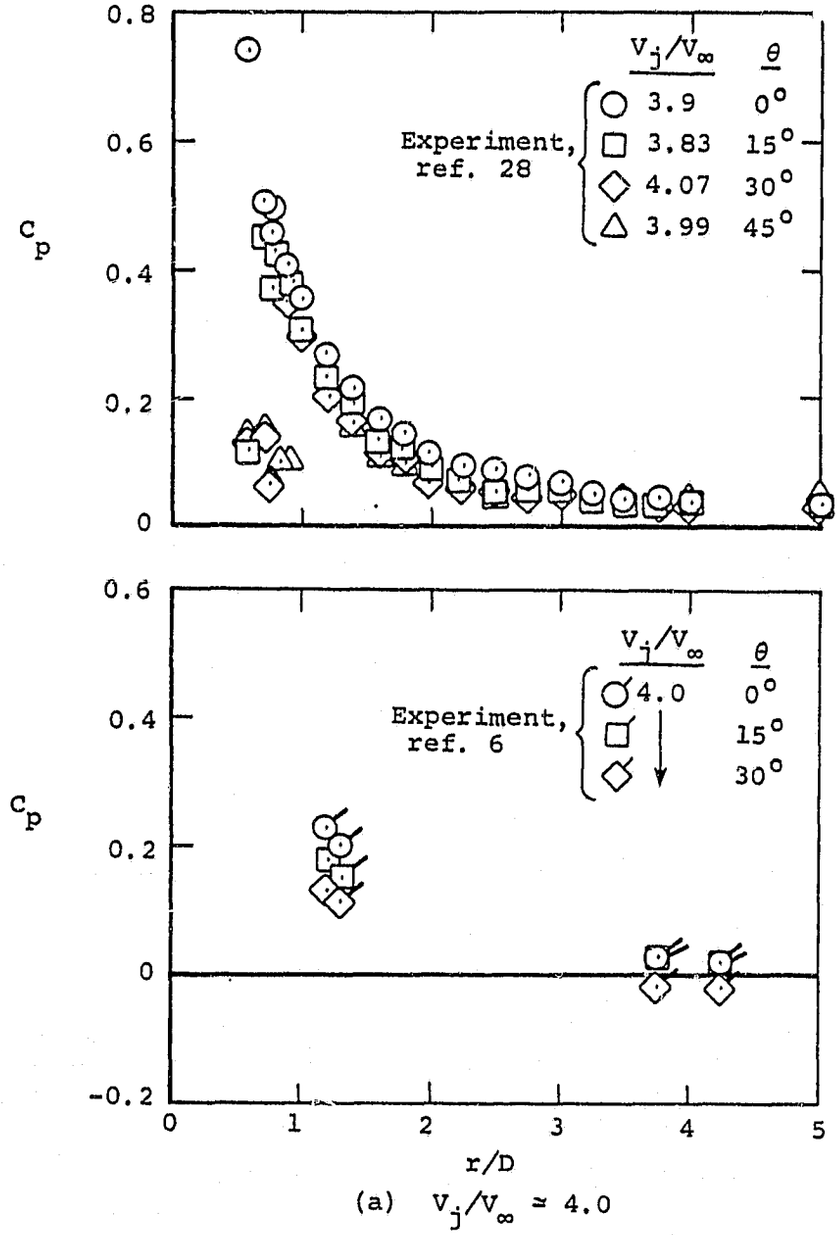

(a) $V_j/V_\infty \simeq 4.0$

Figure 14.- Effect of inclination angle on measured pressure distribution on a flat plate from which a jet is exhausting into a crossflow, $\beta = 0^\circ$.

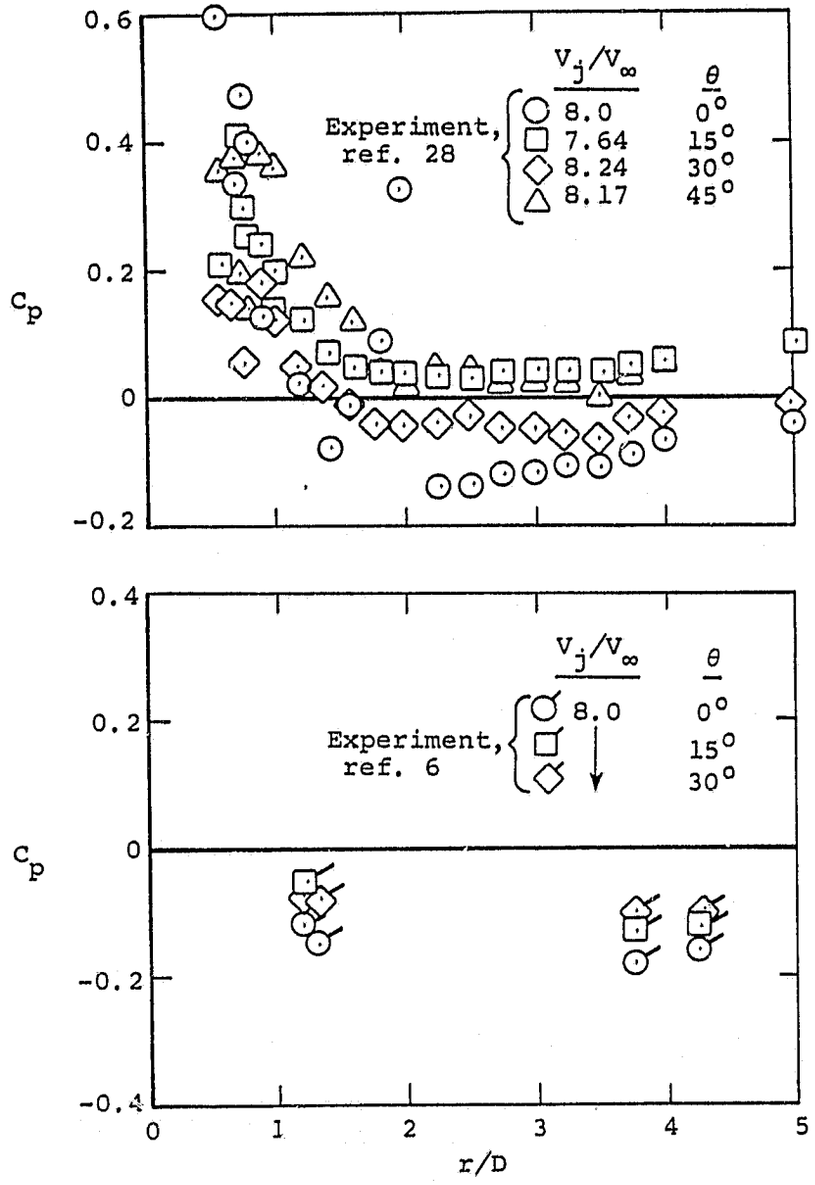

(b) $V_j/V_\infty \approx 8.0$

Figure 14.- Continued.

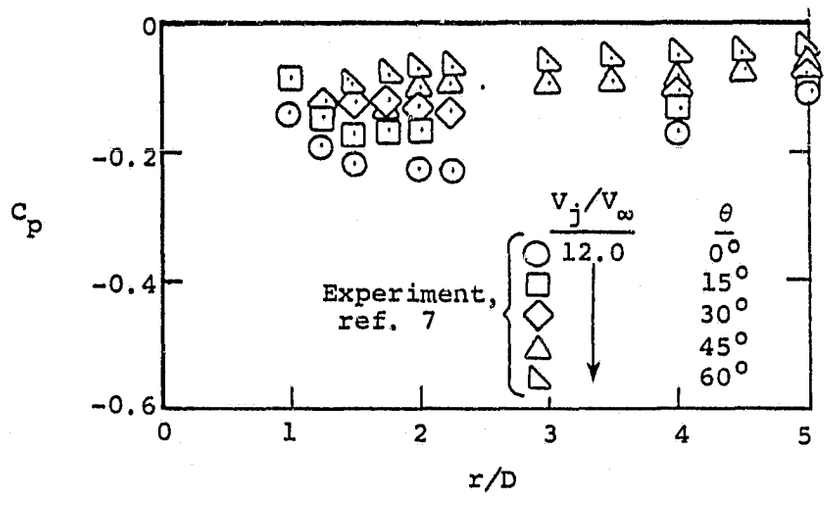

(c) $V_j/V_\infty = 12.0$

Figure 14.- Concluded.

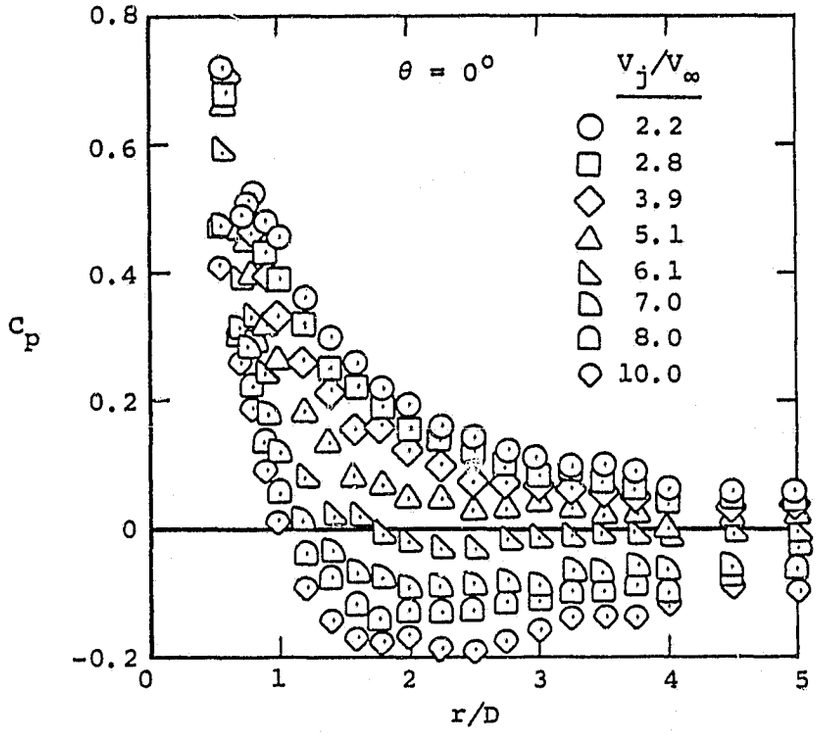

(a) Reference 4 data.

Figure 15.- Effect of jet velocity ratic on measured pressure distribution on a flat plate from which a jet is exhausting into a crossflow, $\beta = 0^\circ$.

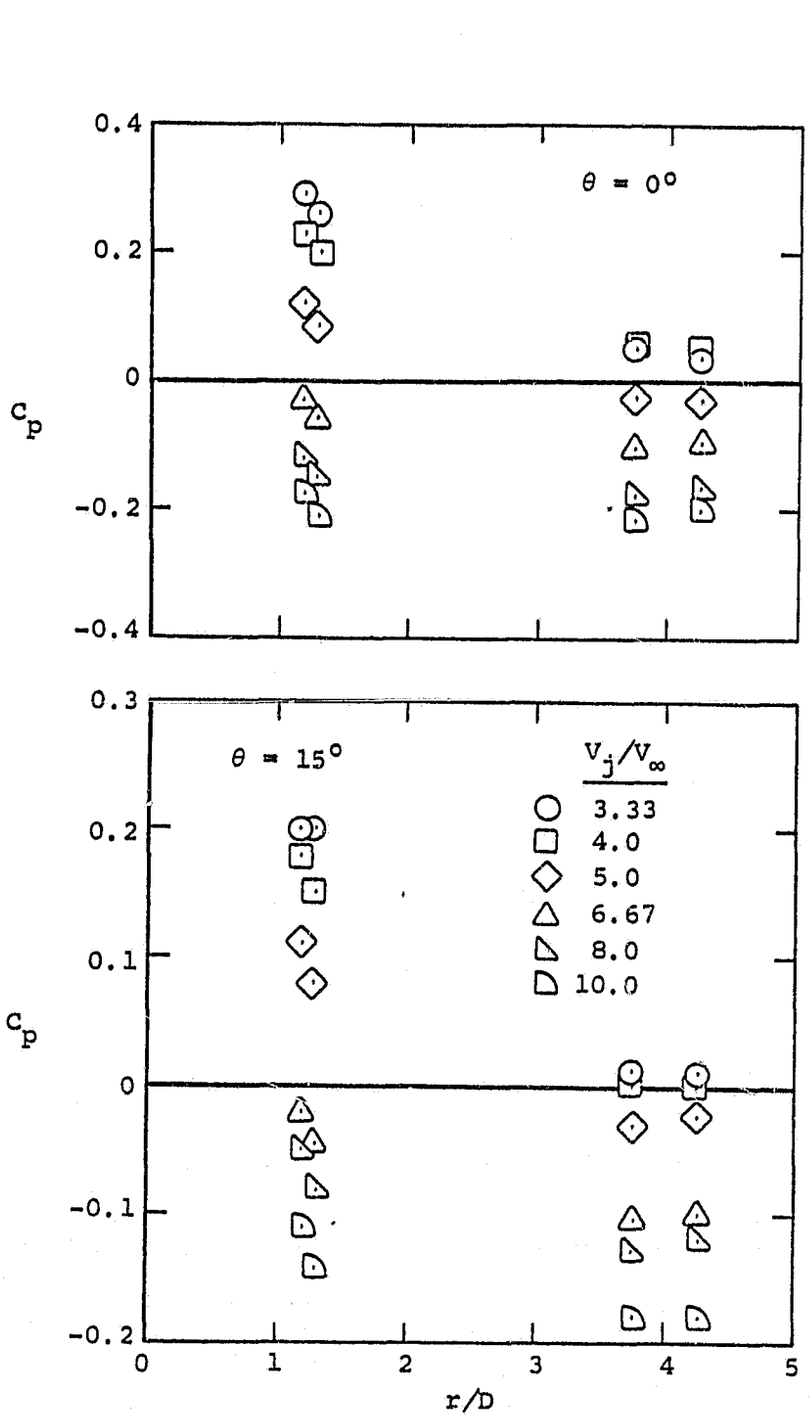

(b) Reference 6 data.

Figure 15.- Continued.

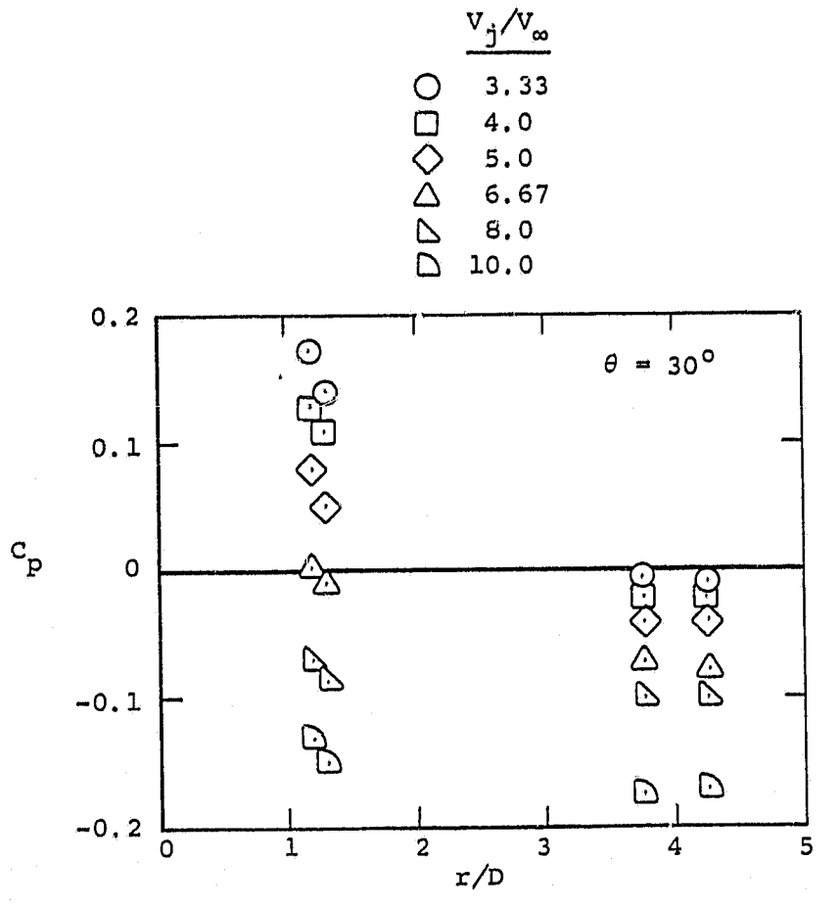

(b) Concluded.

Figure 15 .- Continued.

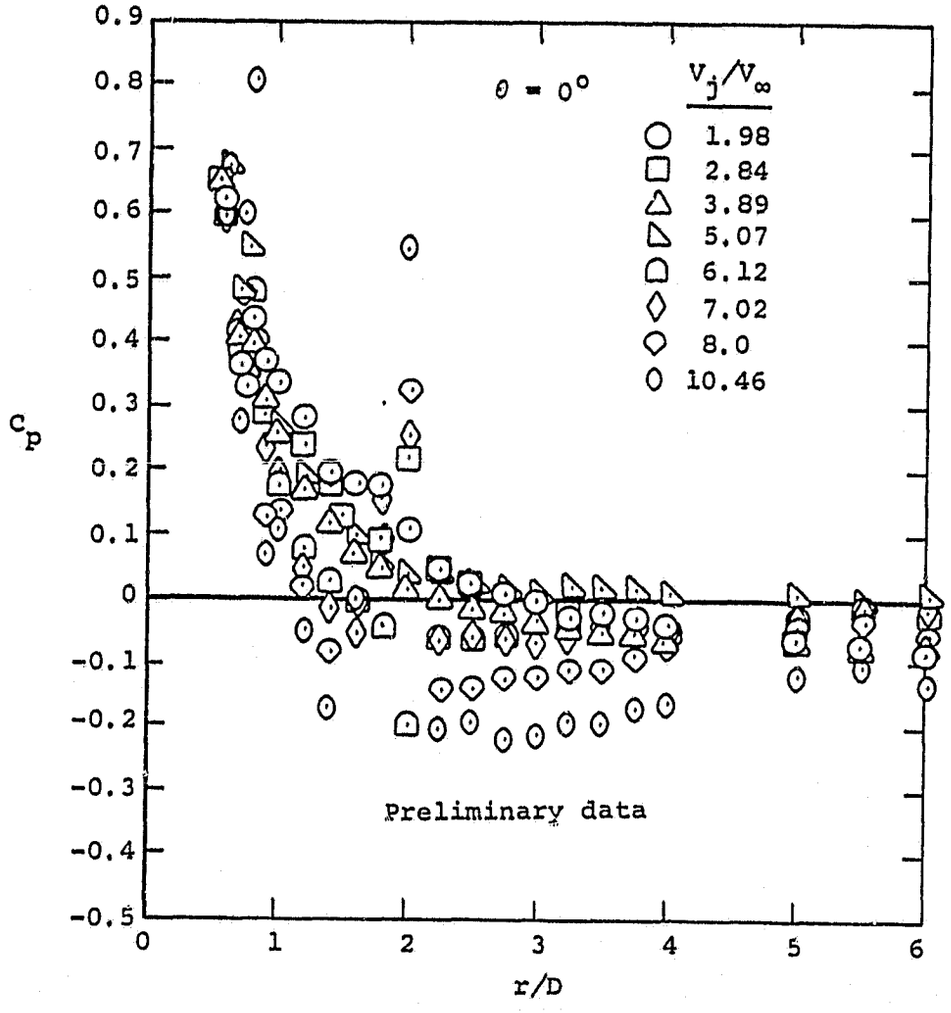

(c) Reference 28 data.

Figure 15.- Continued.

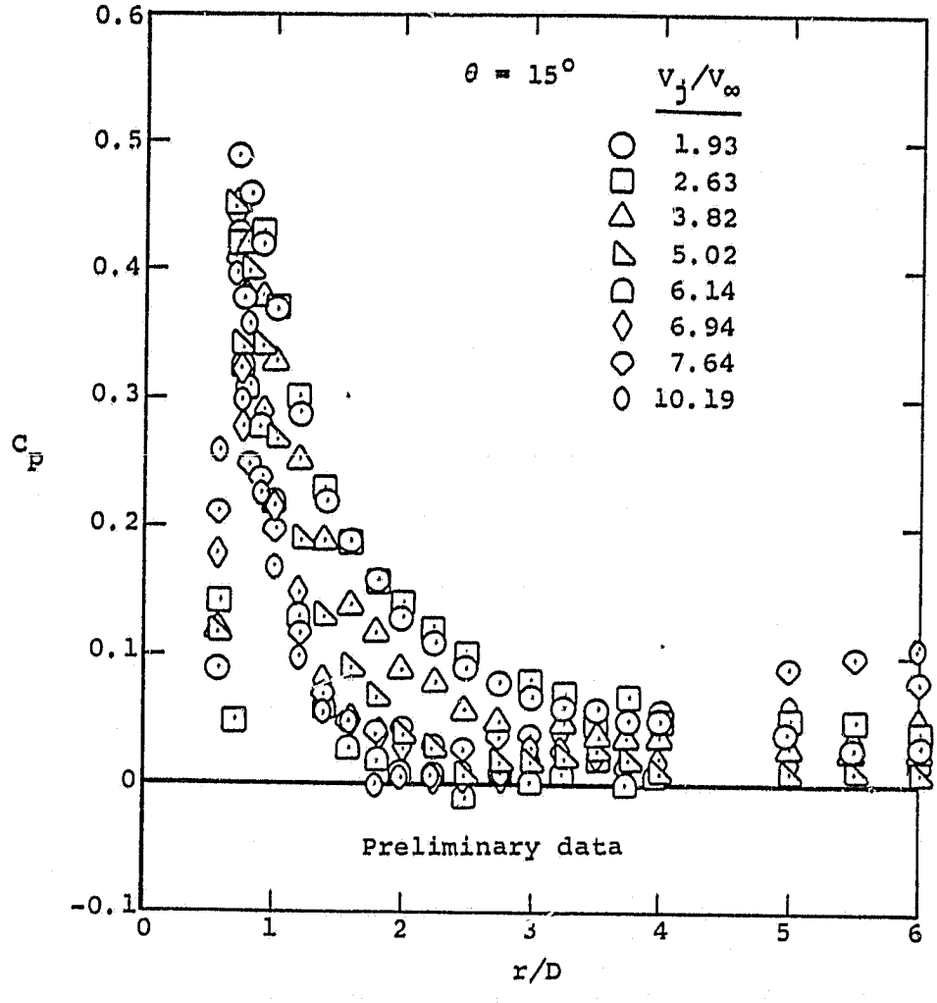

(c) Reference 28 data, continued.

Figure 15.- Continued.

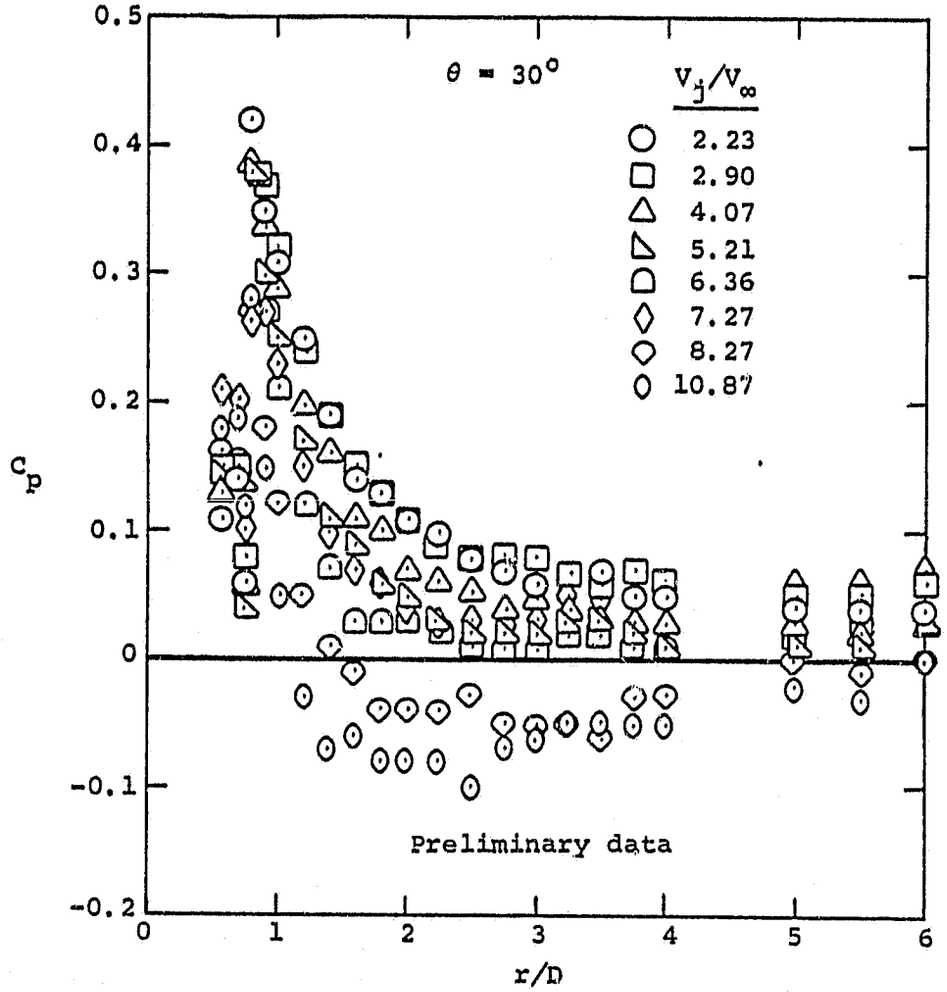

(c) Reference 28 data, continued.

Figure 15.- Continued.

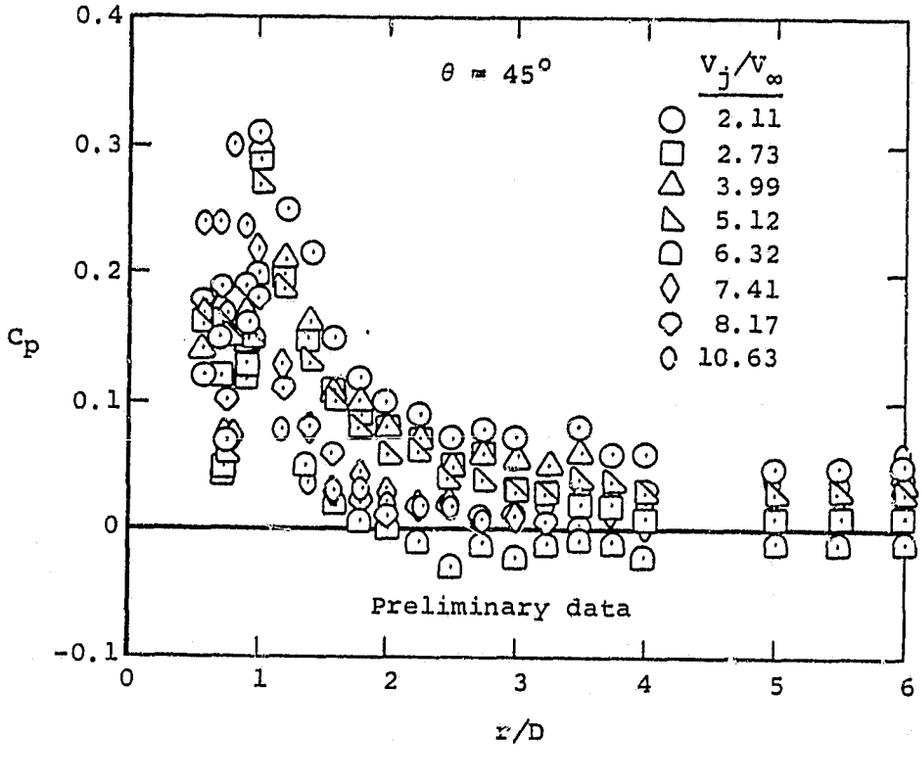

(c) Reference 28, concluded.

Figure 15.- Concluded.

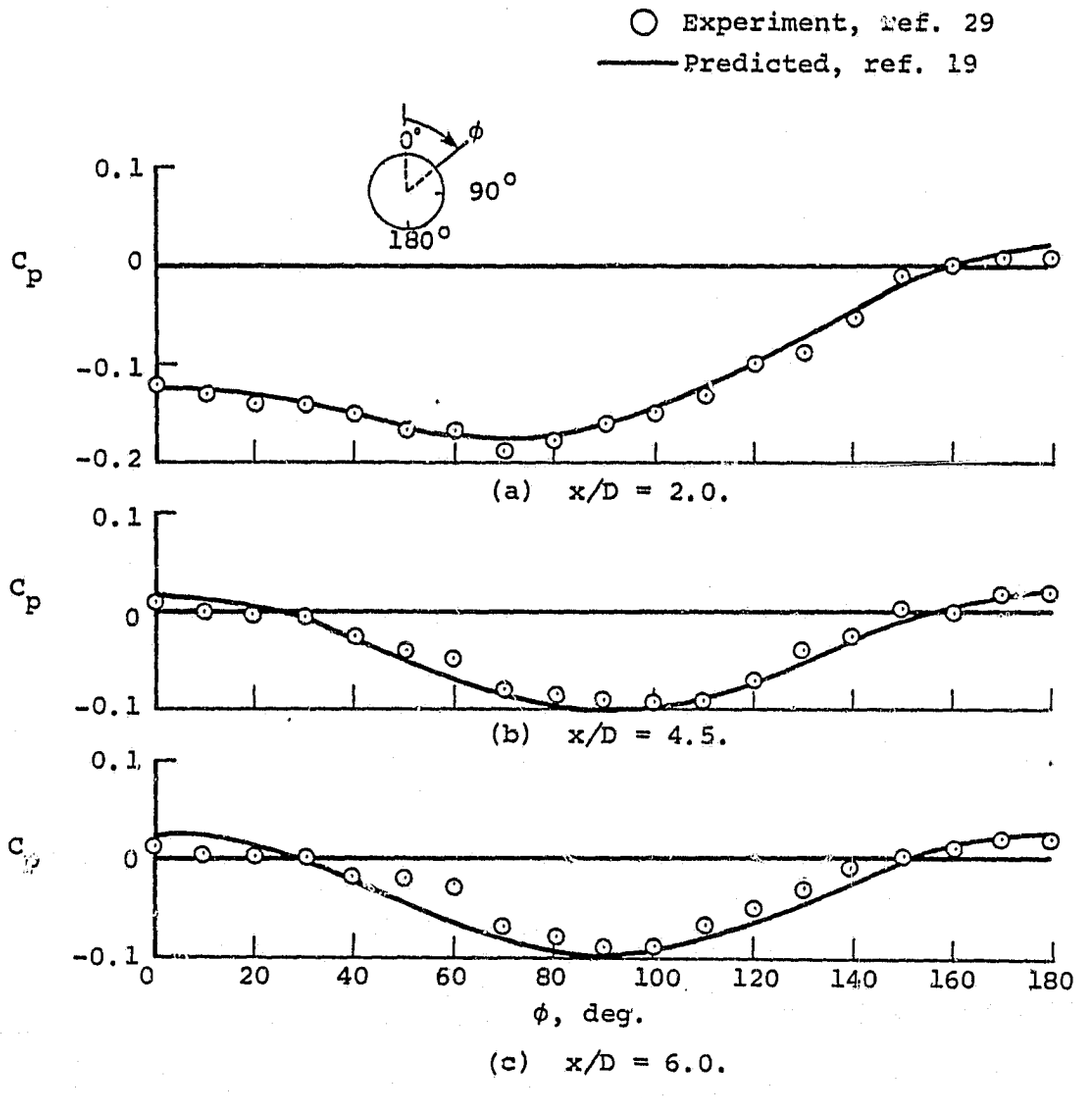

Figure 16.- Comparison of measured and predicted circumferential pressure distributions on an ogive-cylinder body, $\alpha = 10°$, $q_\infty \approx 88$ psf.

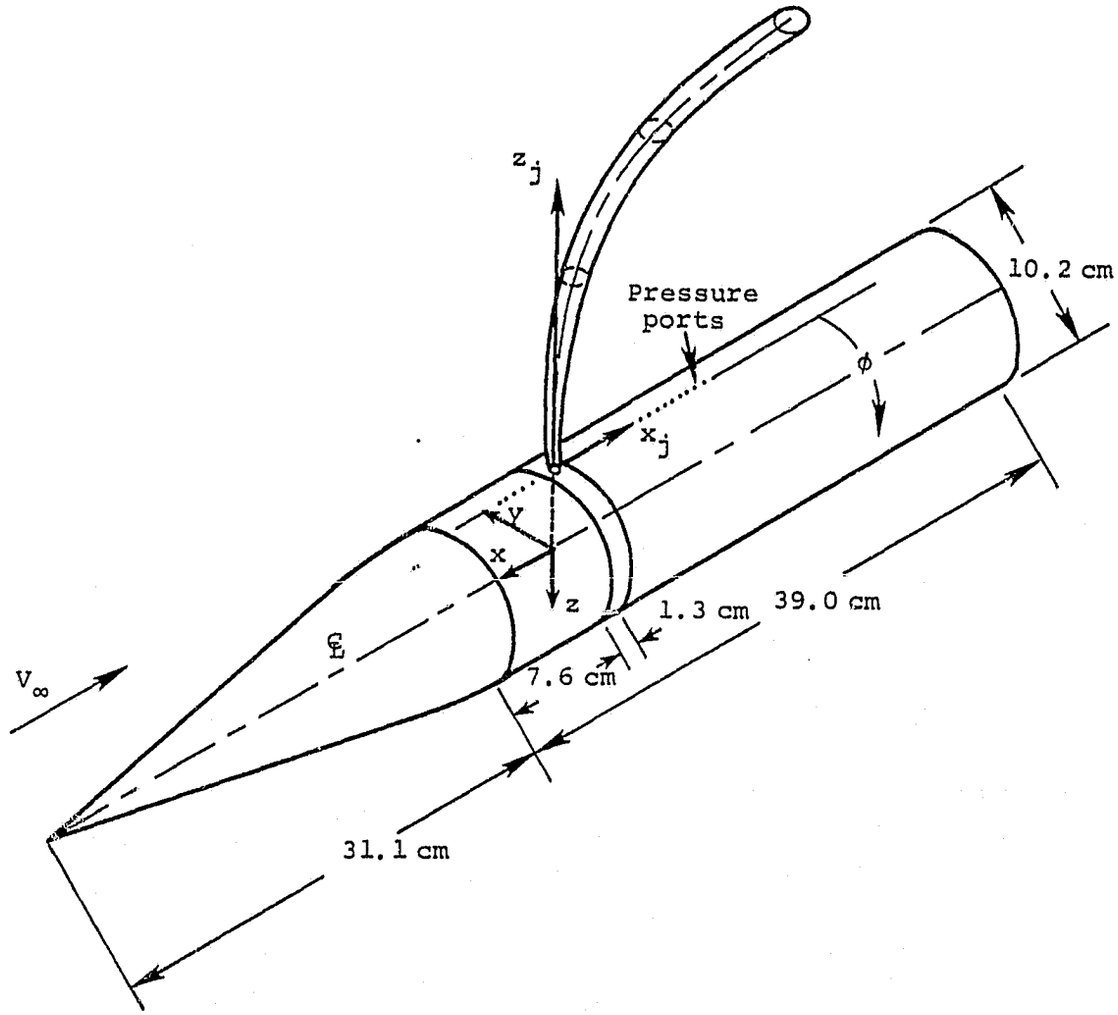

Figure 17.- Cone-cylinder model with jet exhausting from top of body.

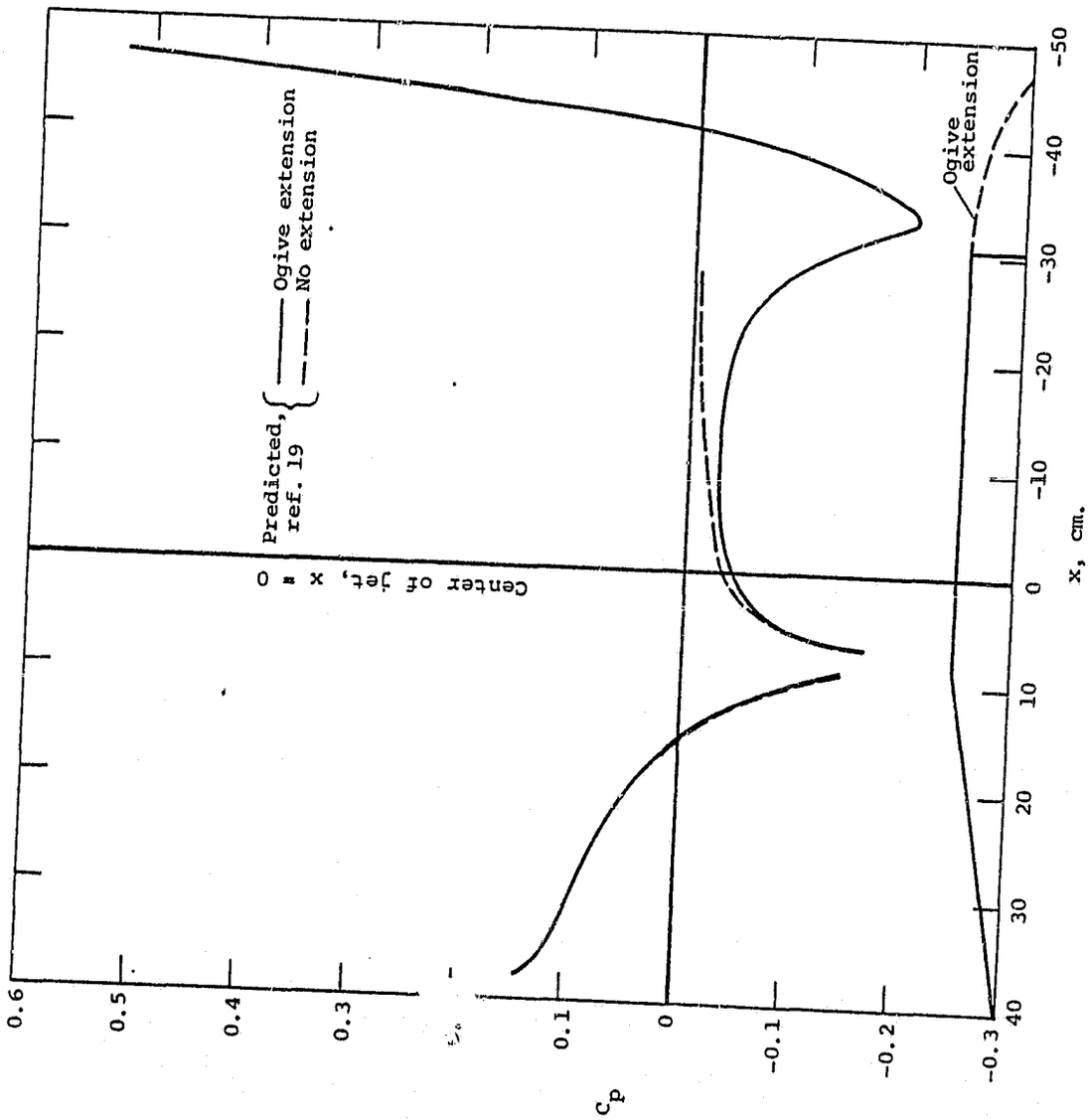

Figure 18.- Predicted pressure distributions on cone-cylinder model of reference 3, $V_j/V_\infty = 0$, $\alpha = 0°$.

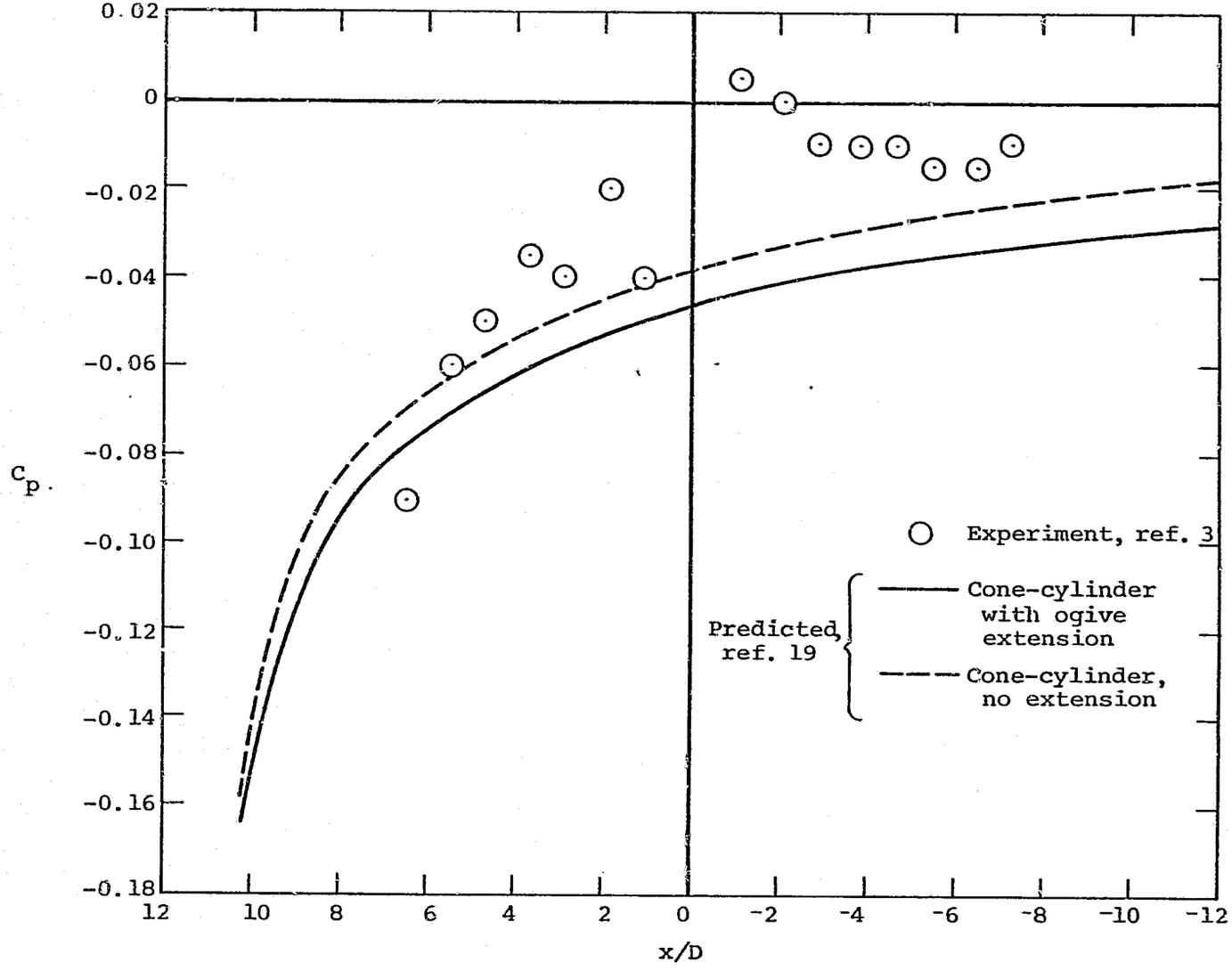

Figure 19.- Comparison of measured and predicted pressure distributions on the cone-cylinder in the region of the jet, $V_j/V_\infty = 0$, $\alpha = 0^\circ, \phi = 0^\circ$

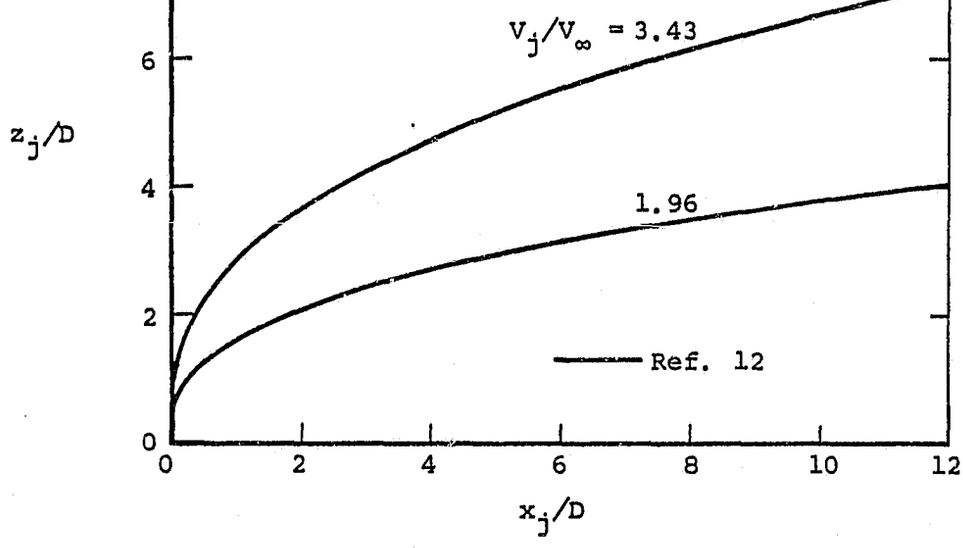

Figure 20.- Centerline shapes for a jet exhausting normal to the surface of a body of revolution.

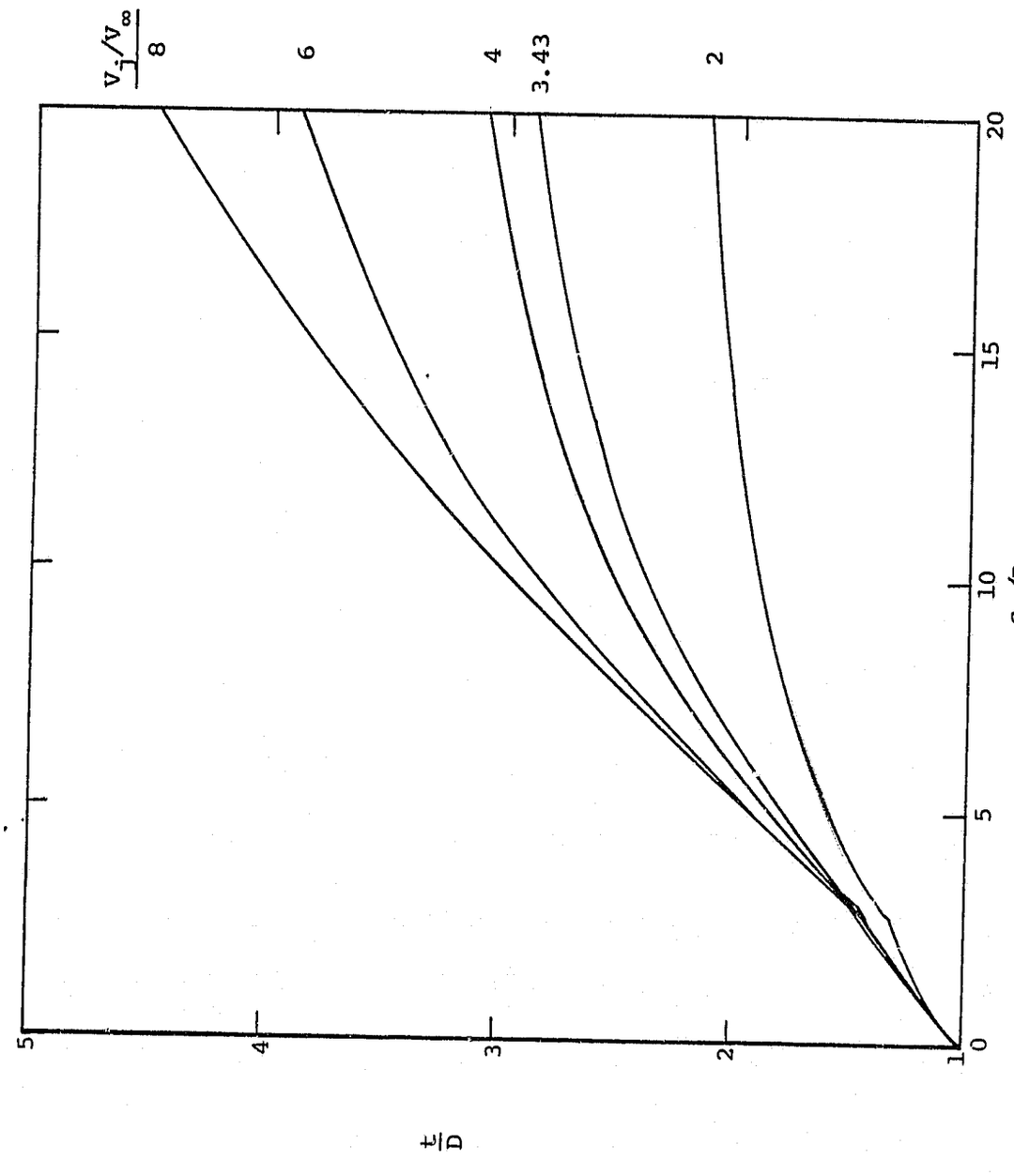

Figure 21.- Jet expansion curves for a jet exhausting normal to the surface of a body of revolution, $\theta = 0$.

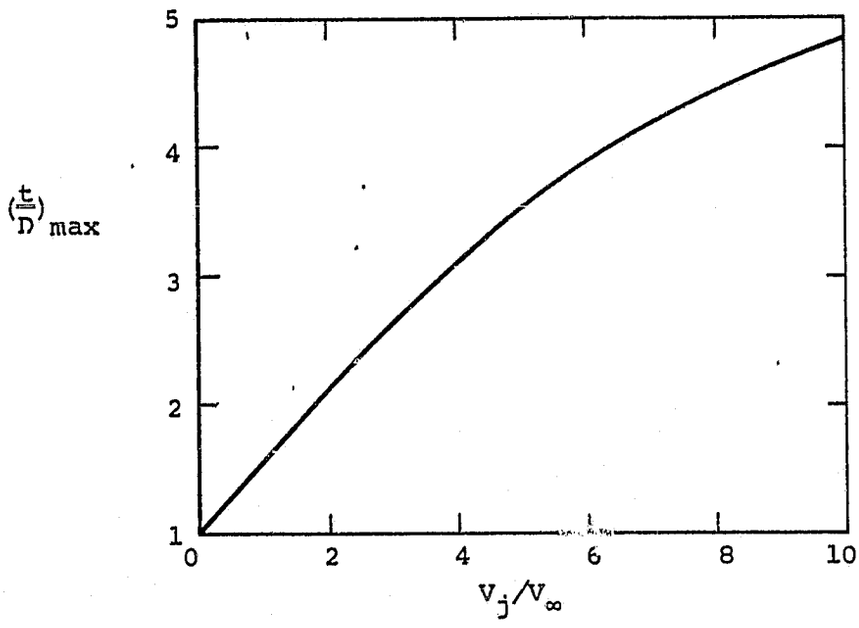

Figure 22.- Maximum jet thickness variation with jet velocity ratio for a jet exhausting normal to the surface of a body of revolution, $S_a/R = 20$.

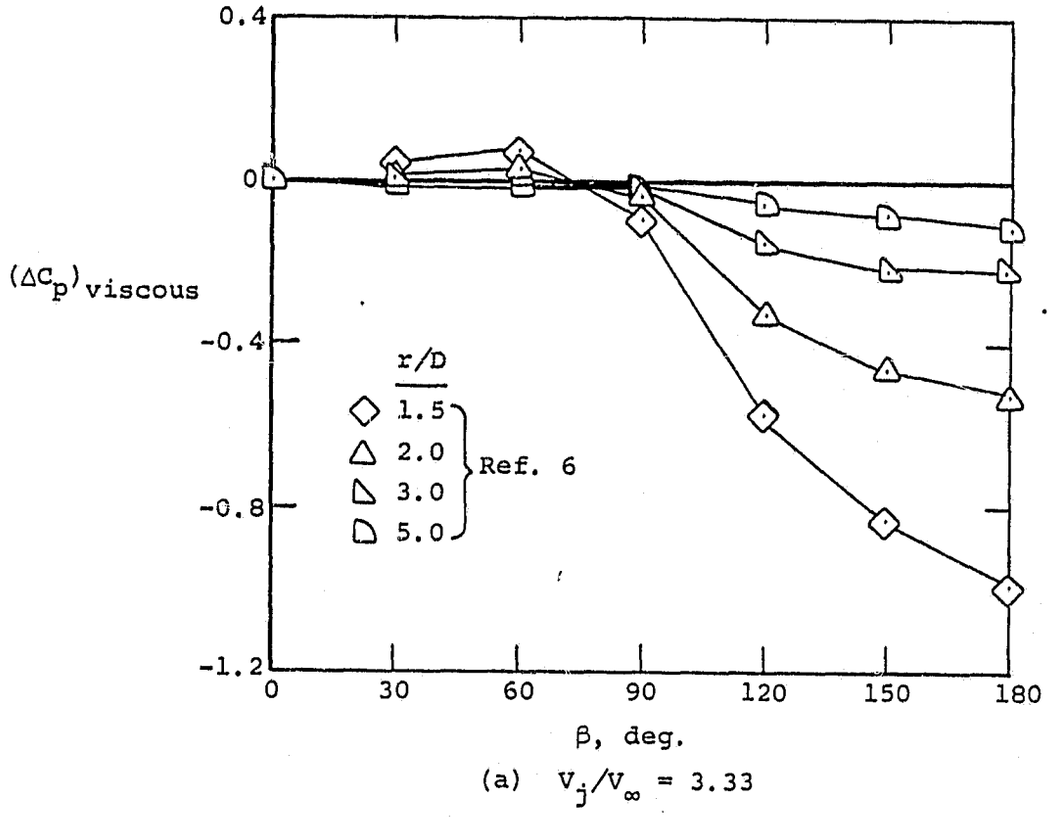

(a) $V_j/V_\infty = 3.33$

Figure 23.- Correlation factors for viscous portion of the pressure coefficient induced on a flat plate by a jet exhausting into a crossflow, $\theta = 15^\circ$.

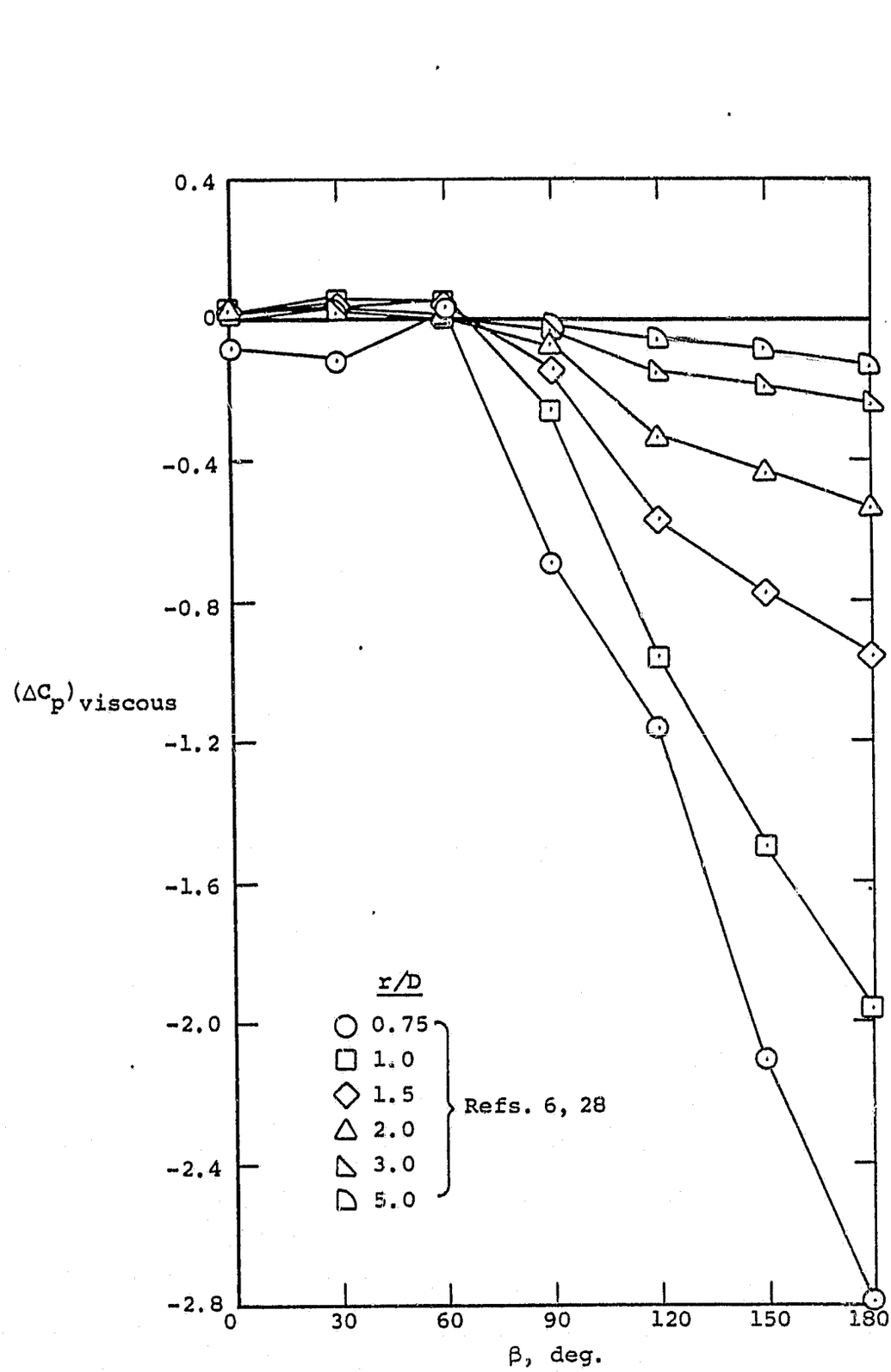

(b) $V_j/V_\infty = 3.9$

Figure 23.- Continued.

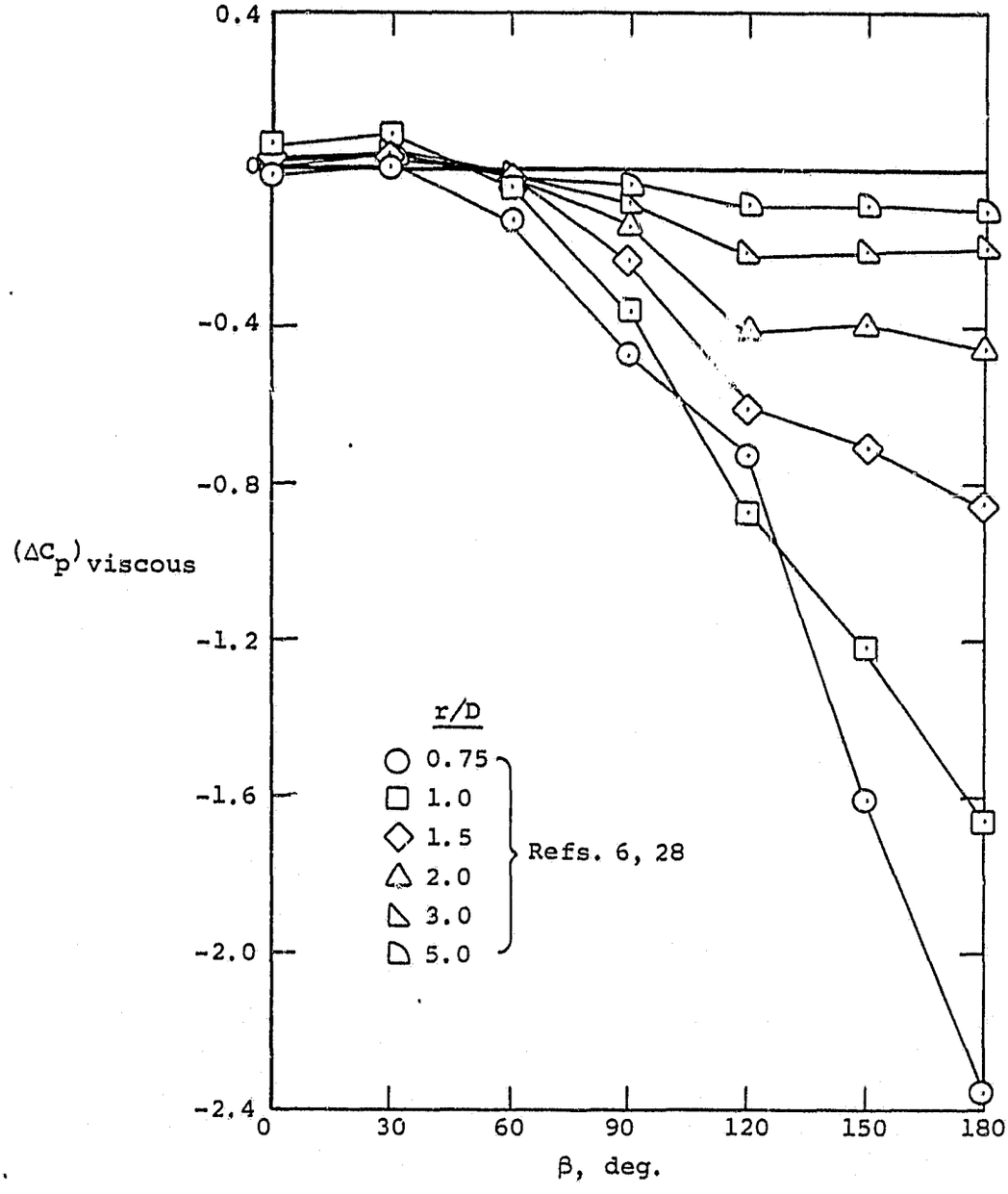

(c) $V_j/V_\infty = 5.0$

Figure 23.- Continued.

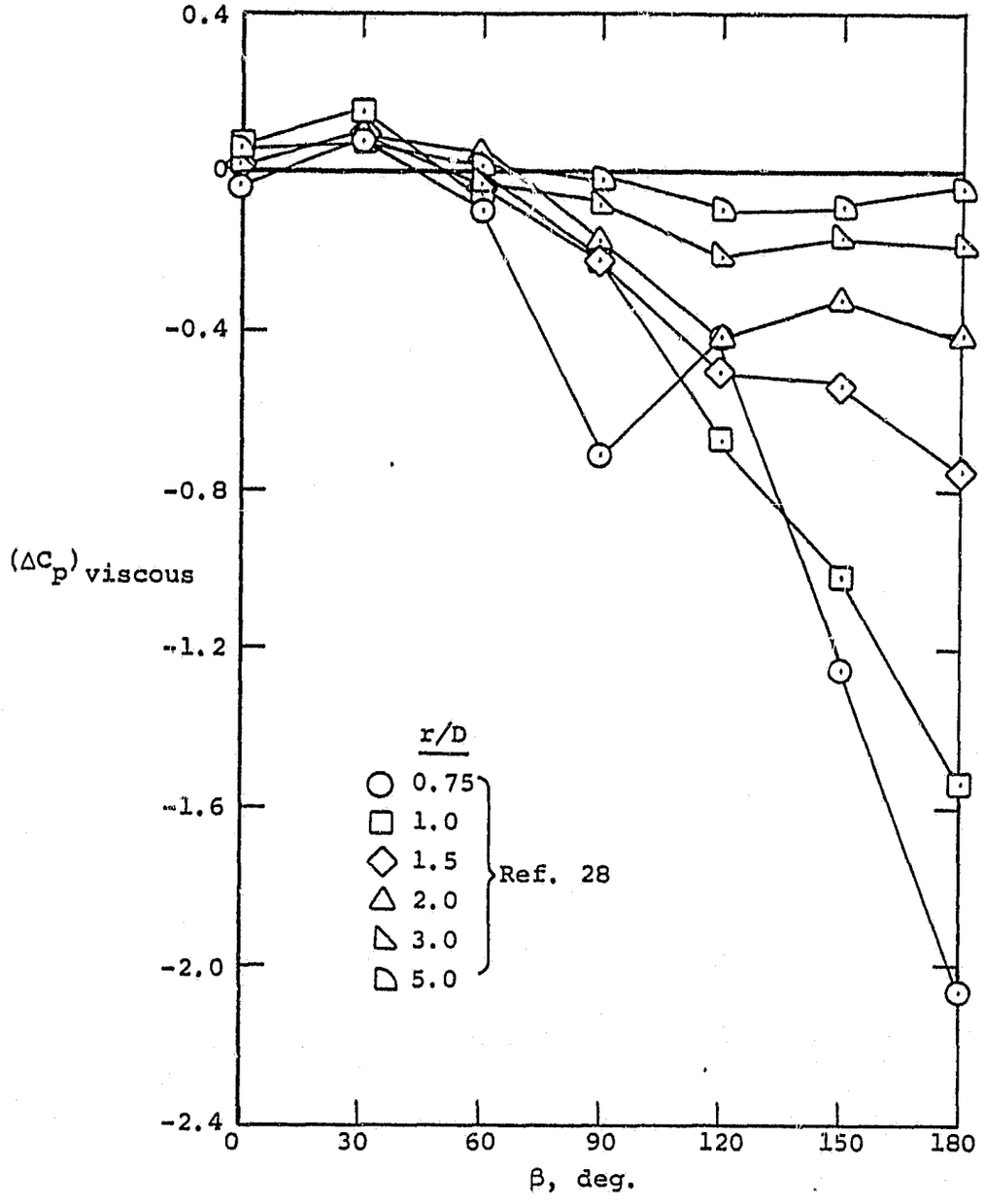

(d) $V_j/V_\infty = 6.14$

Figure 23 .- Continued.

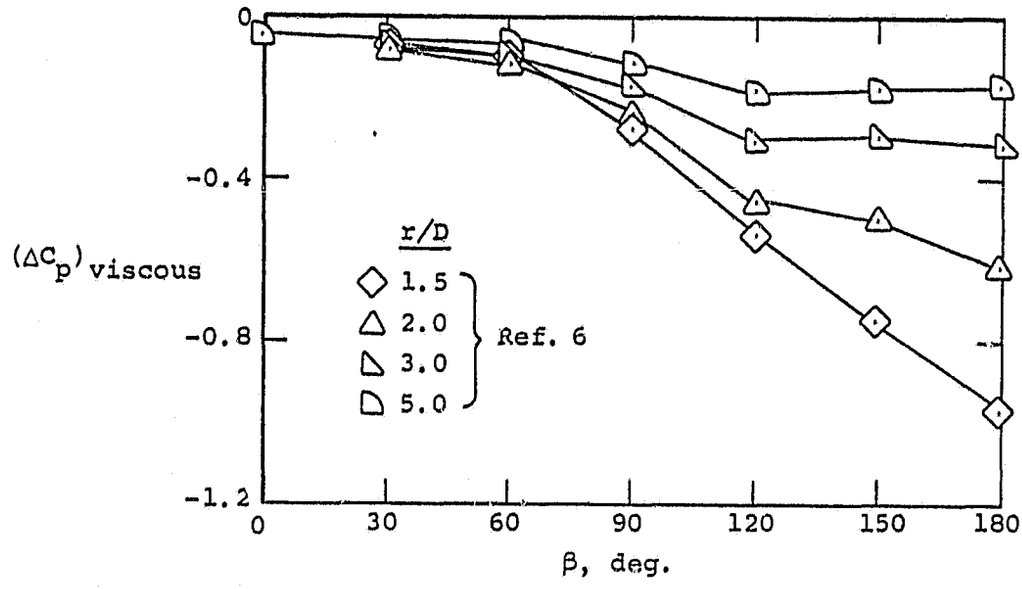

(e) $V_j/V_\infty = 6.67$

Figure 23.- Continued.

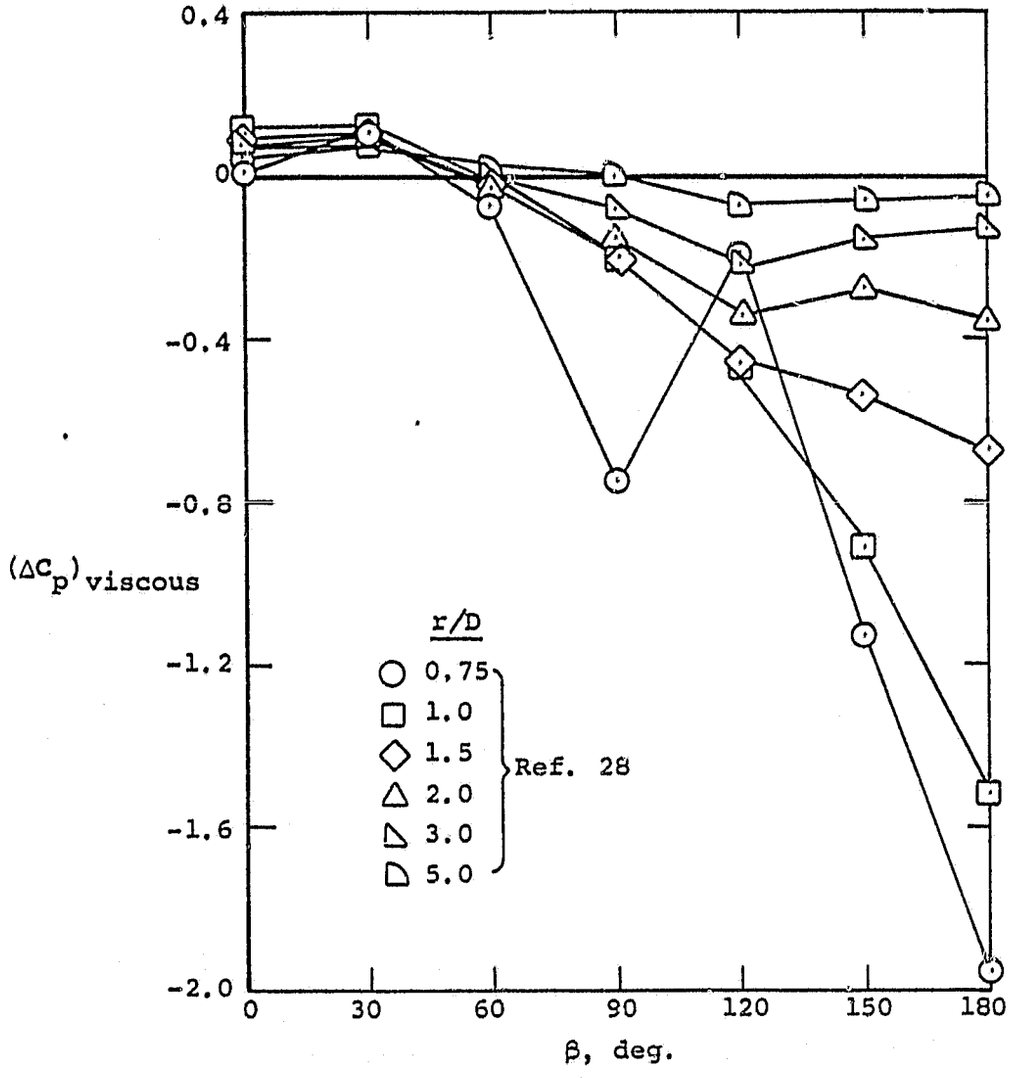

(f) $V_j/V_\infty = 6.94$

Figure 23.- Continued.

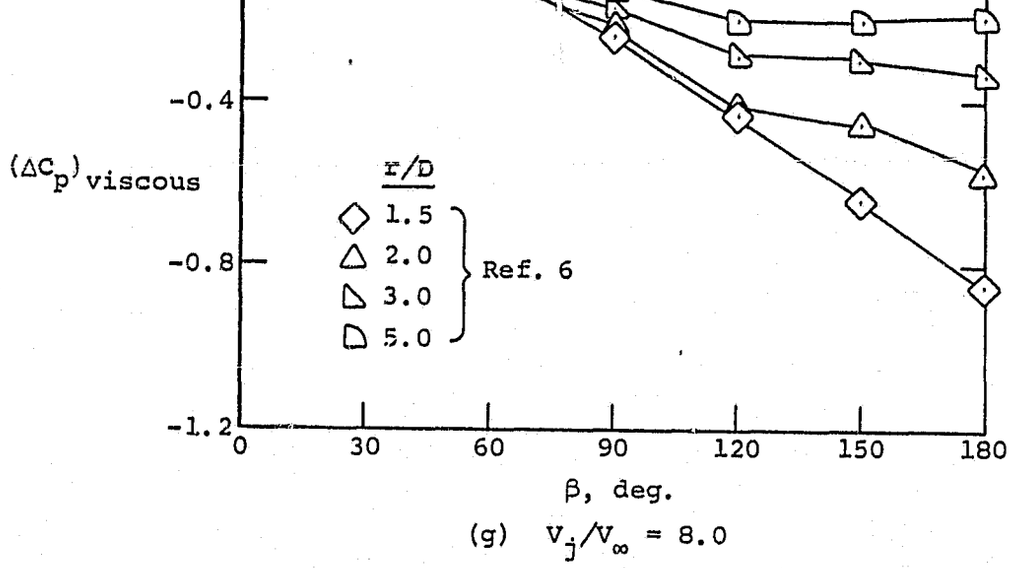

(g) $V_j/V_\infty = 8.0$

Figure 23.- Continued.

C-2

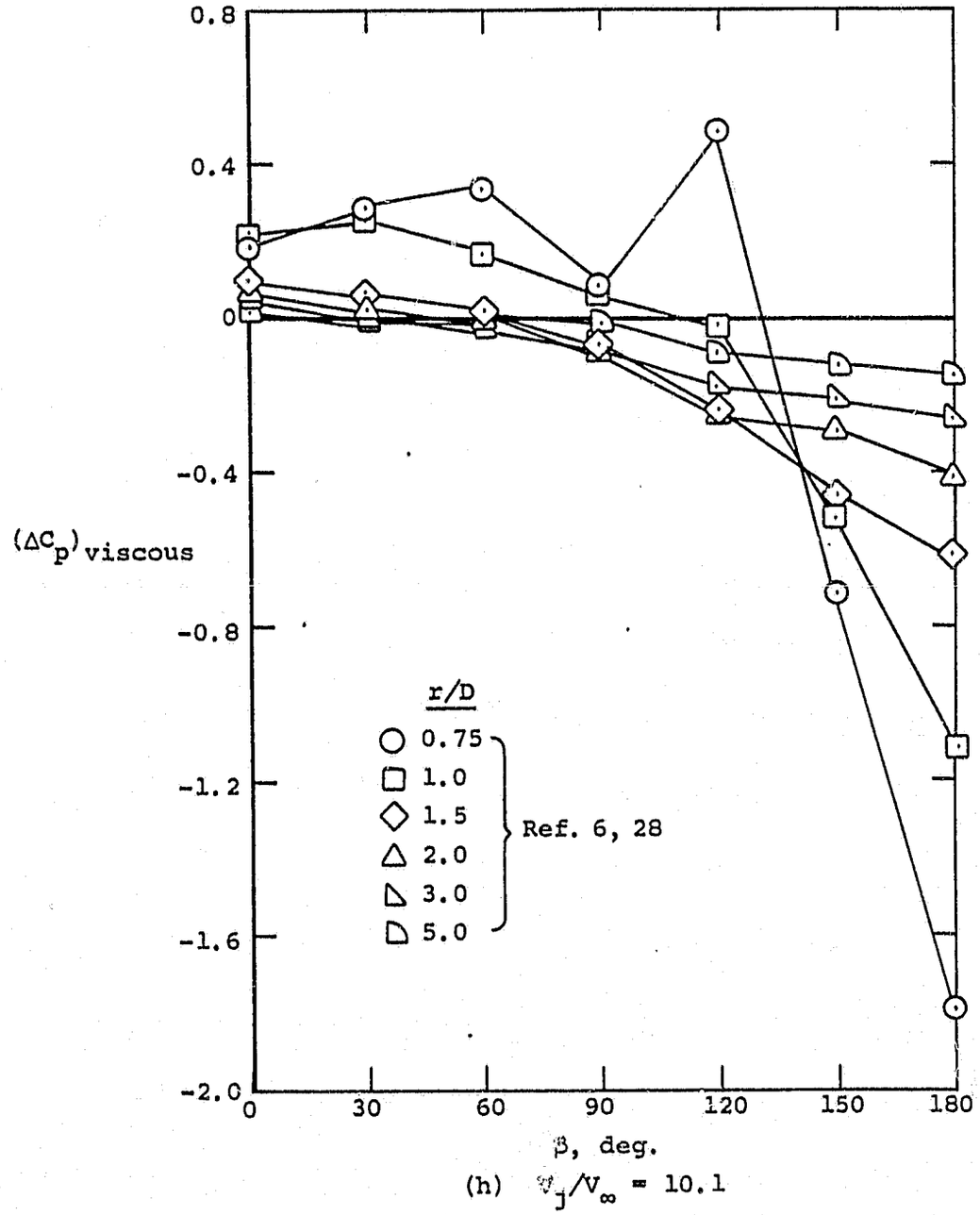

(h) $V_j/V_\infty = 10.1$

Figure 23.- Continued.

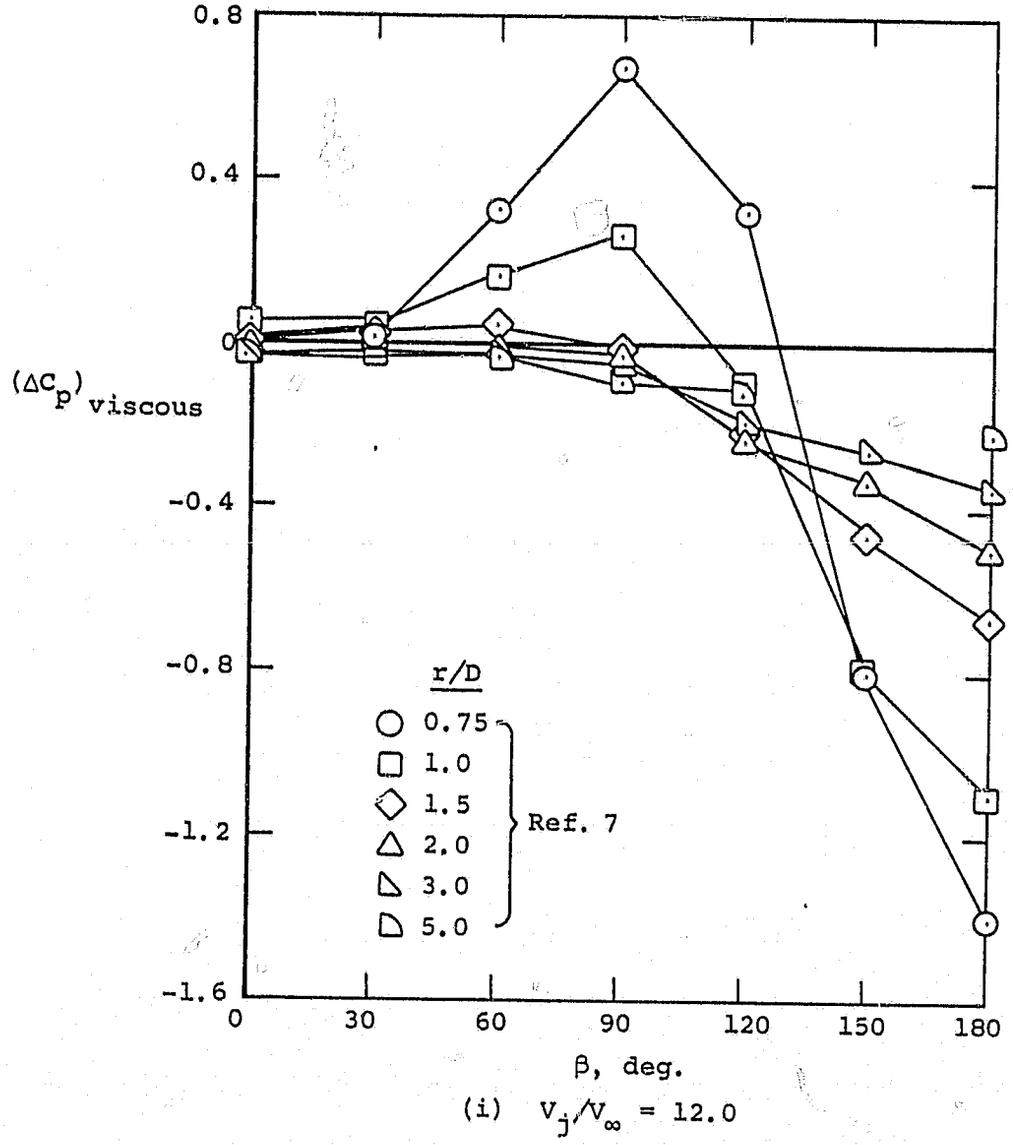

(i) $V_j/V_\infty = 12.0$

Figure 23.- Concluded.

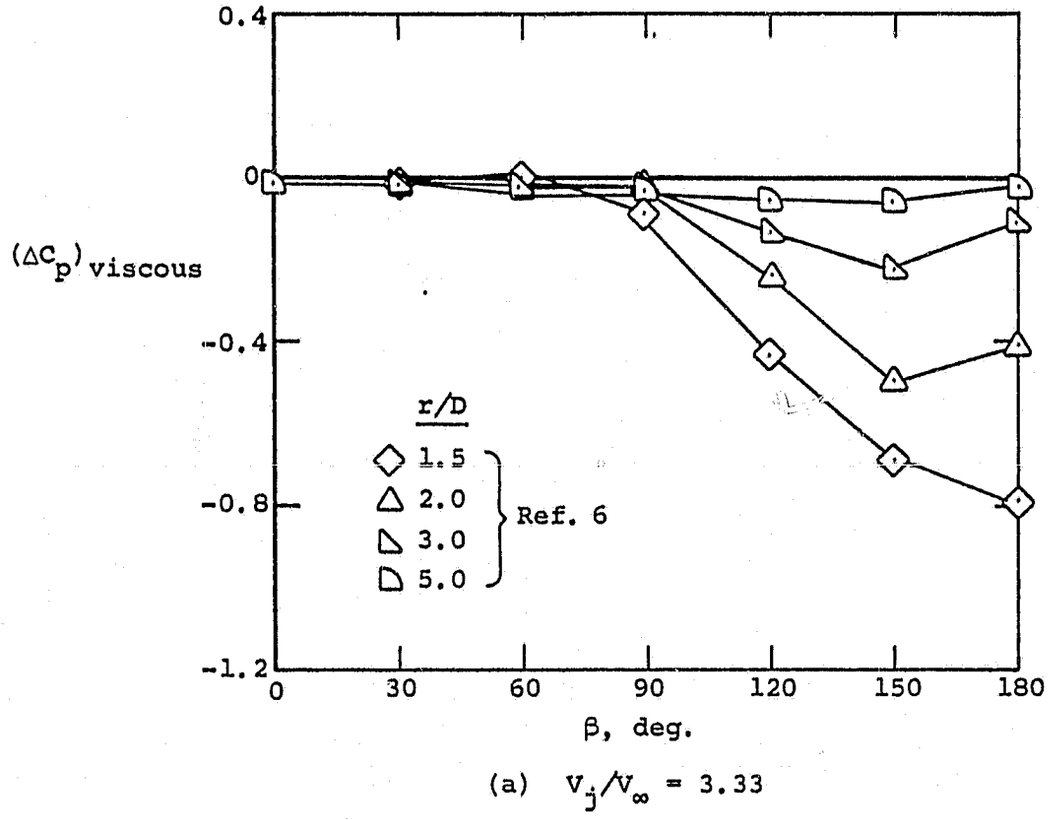

(a) $V_j/V_\infty = 3.33$

Figure 24.- Correlation factors for viscous portion of the pressure coefficient induced on a flat plate by a jet exhausting into a crossflow, $\theta = 30^\circ$.

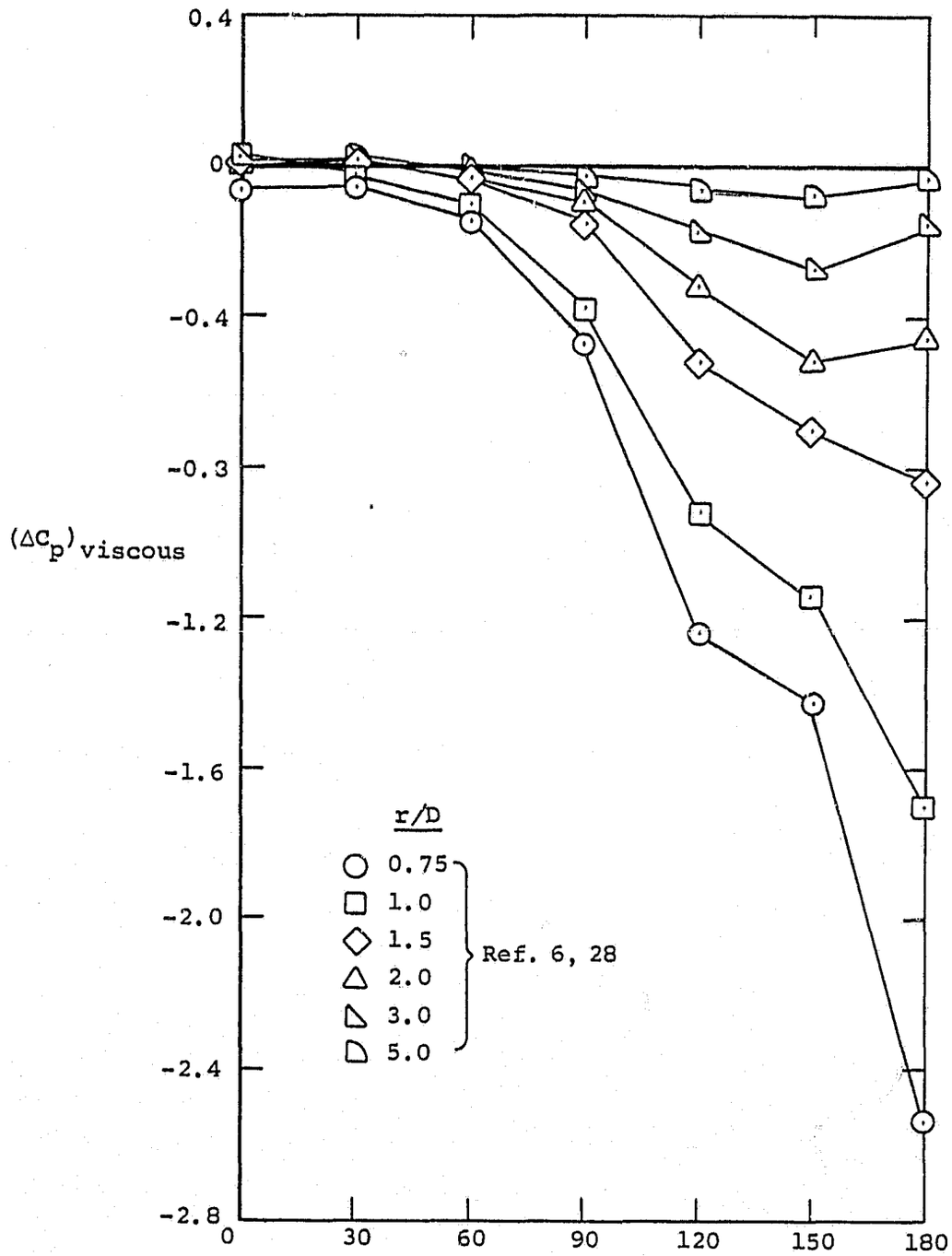

(b) $V_j/V_\infty = 4.0$

Figure 24.- Continued.

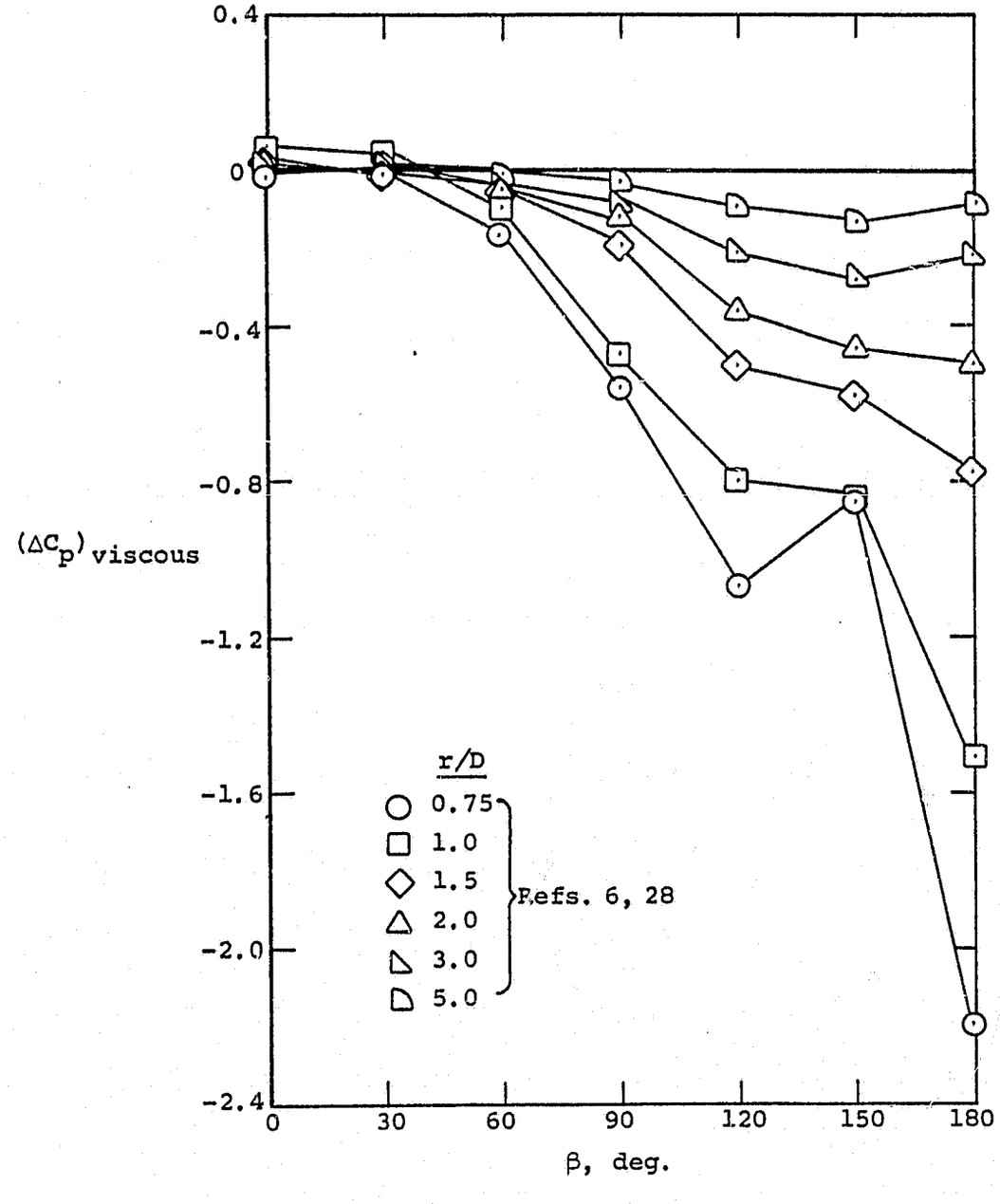

(c) $V_j/V_\infty = 5.0$

Figure 24.- Continued.

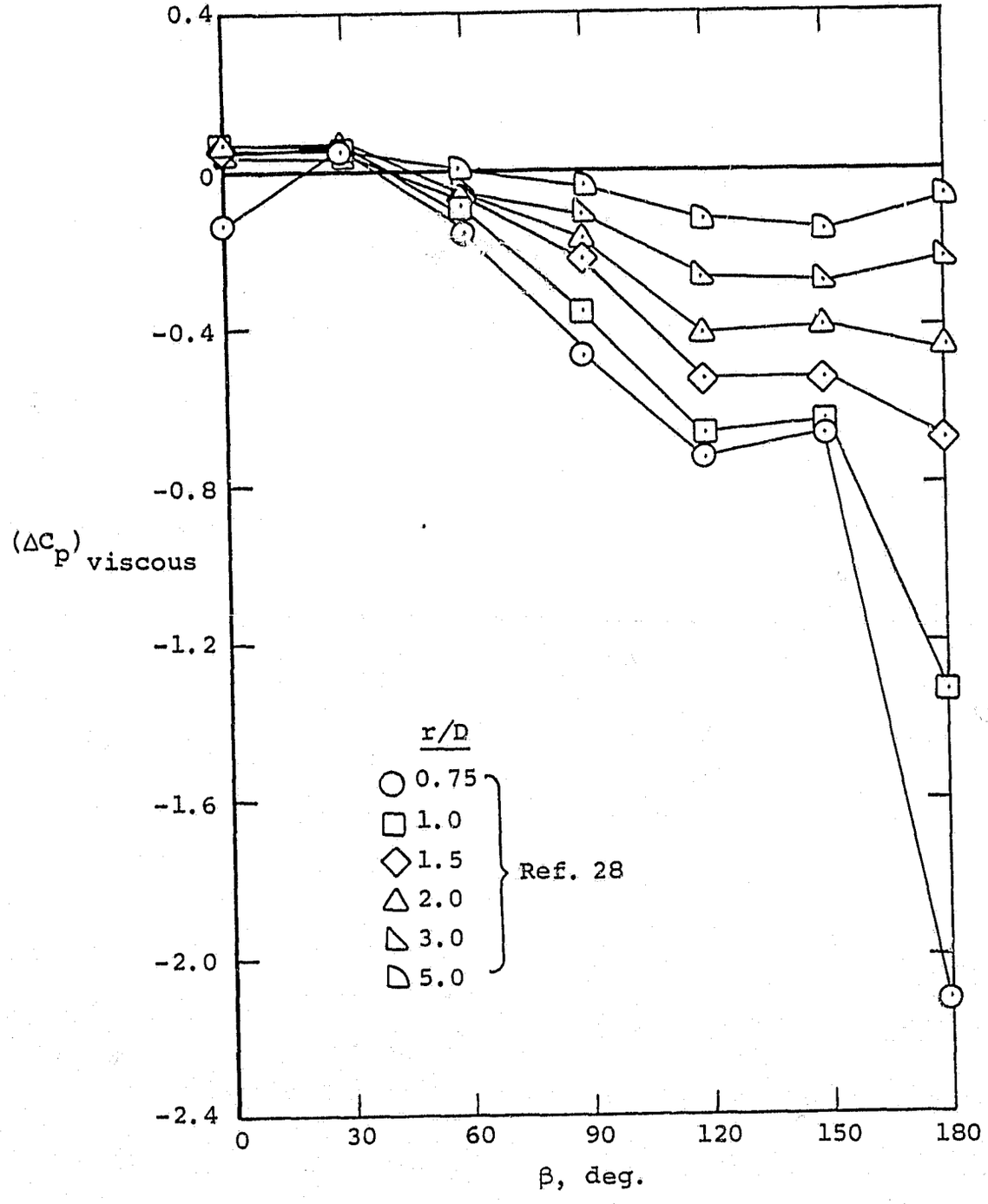

(d) $V_j/V_\infty = 6.36$

Figure 24.- Continued.

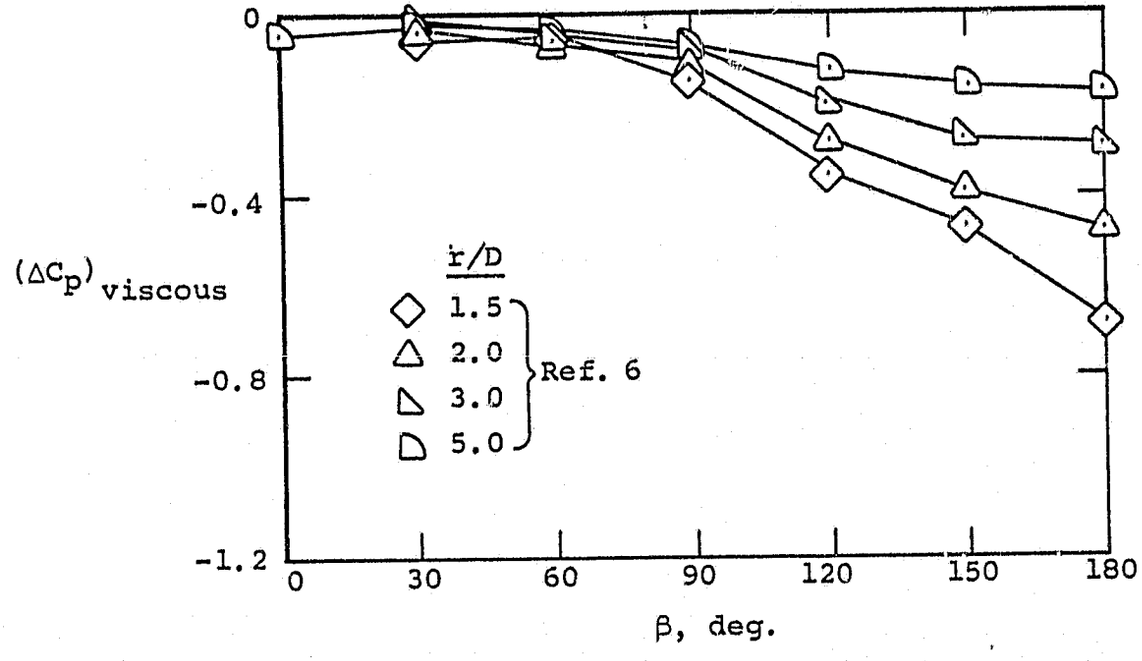

(e) $V_j/V_\infty = 6.67$

Figure 24.- Continued.

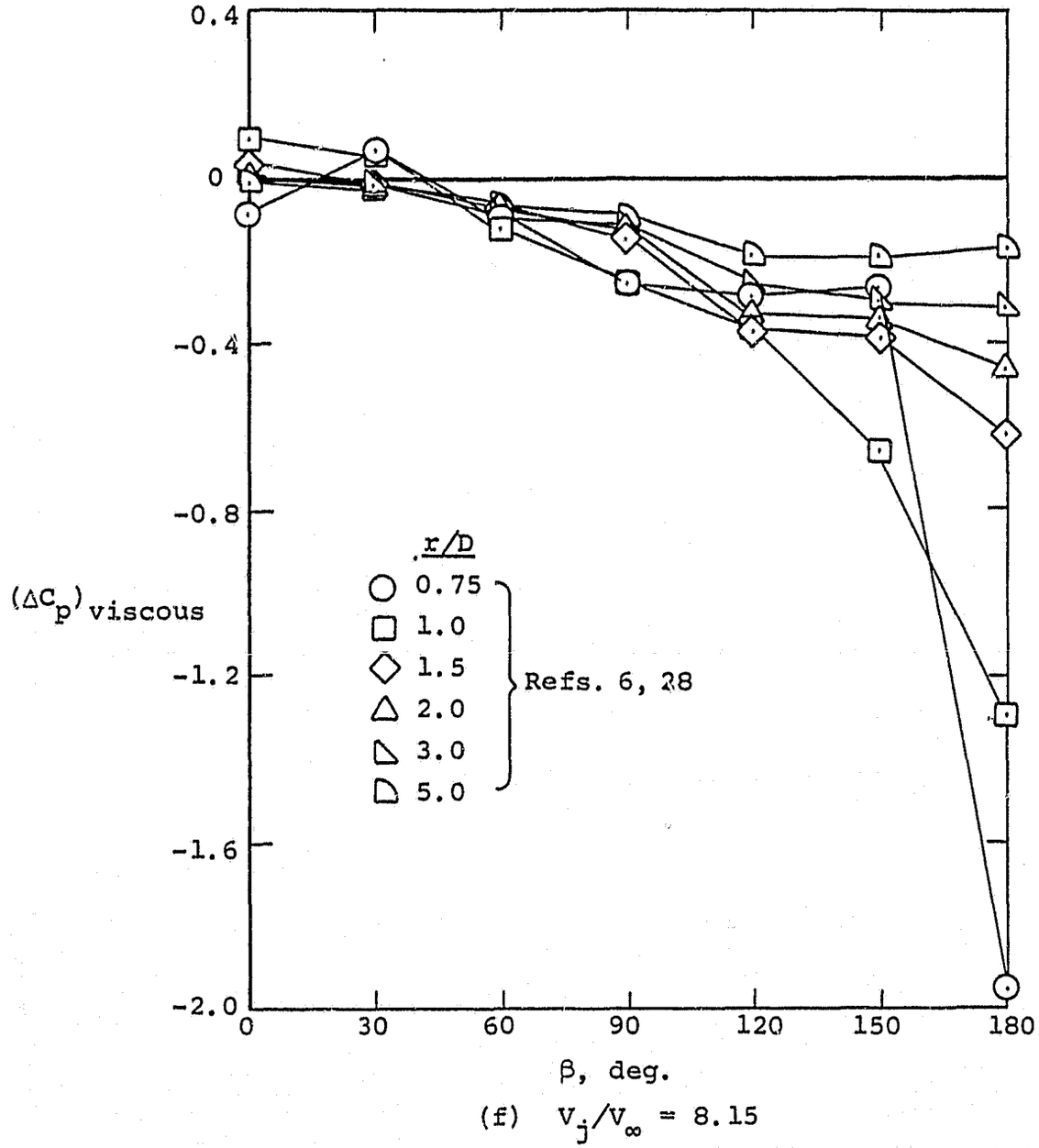

(f) $V_j/V_\infty = 8.15$

Figure 24.- Continued.

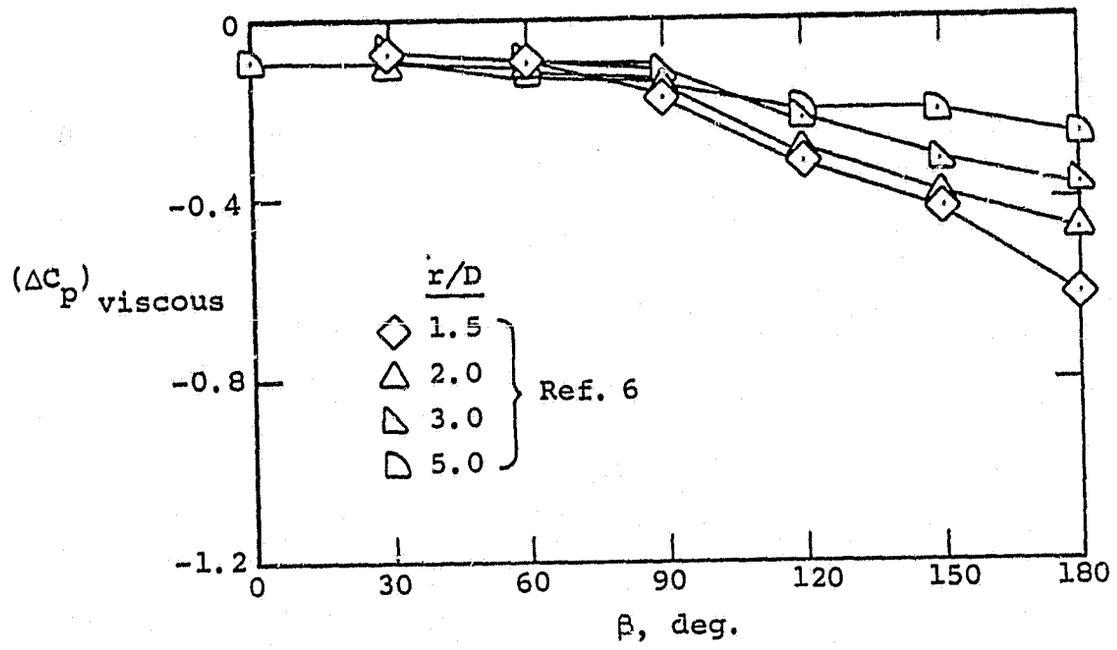

(g) $V_j/V_\infty = 10.0$

Figure 24.- Continued.

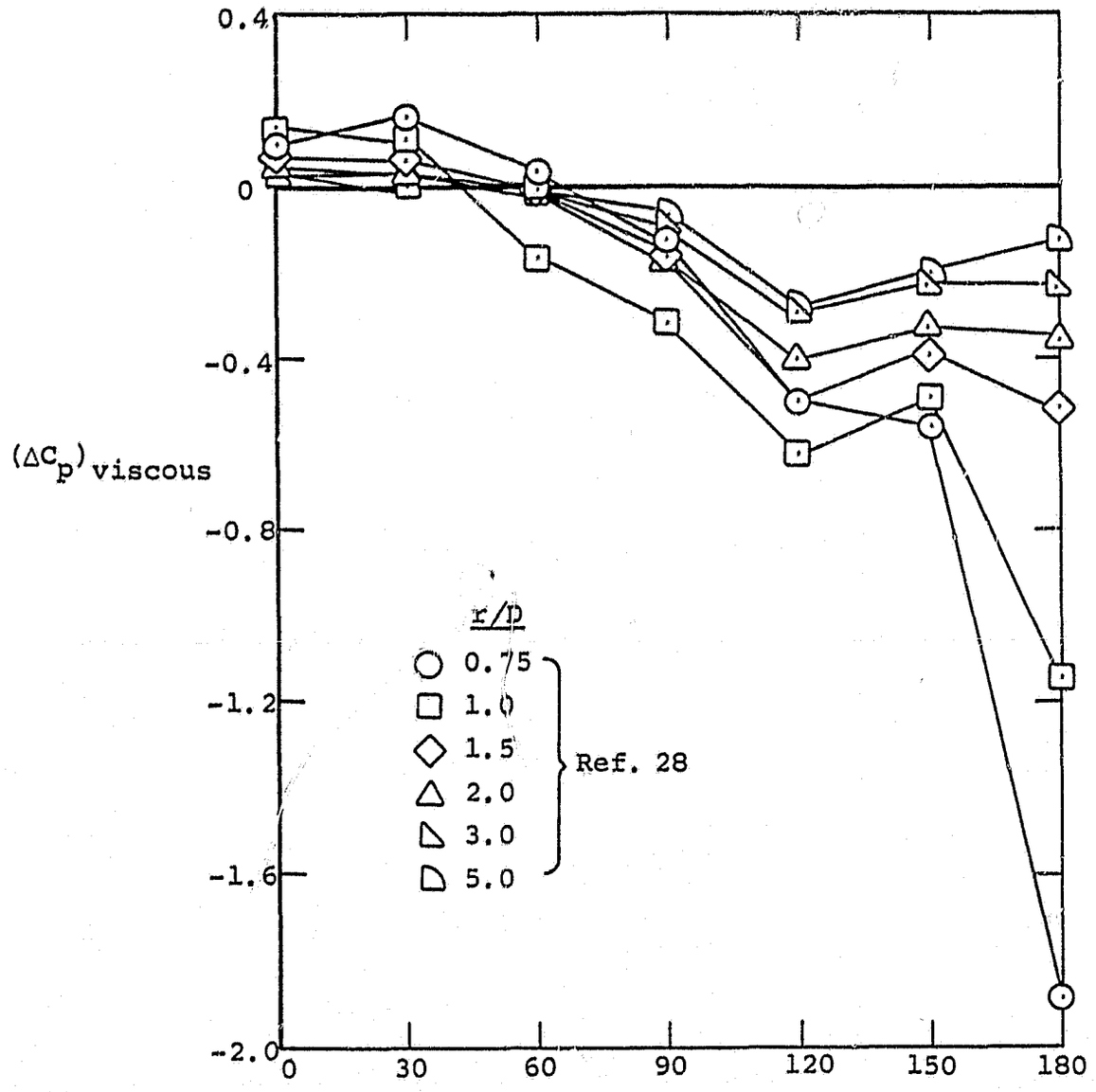

(h) $V_j/V_\infty = 10.87$

Figure 24.- Continued.

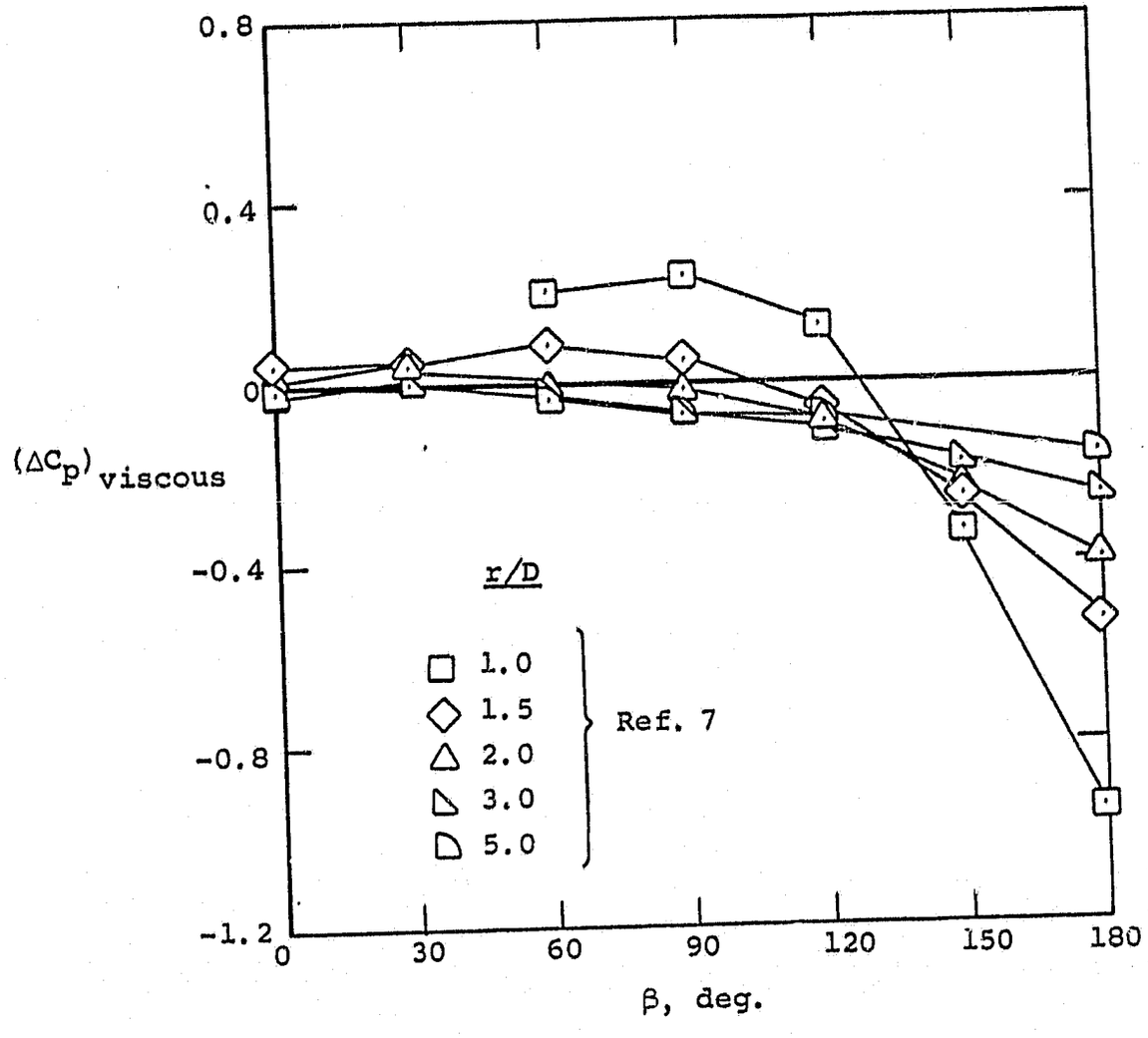

(i) V_j/V_∞ = 12.0

Figure 24.- Concluded.

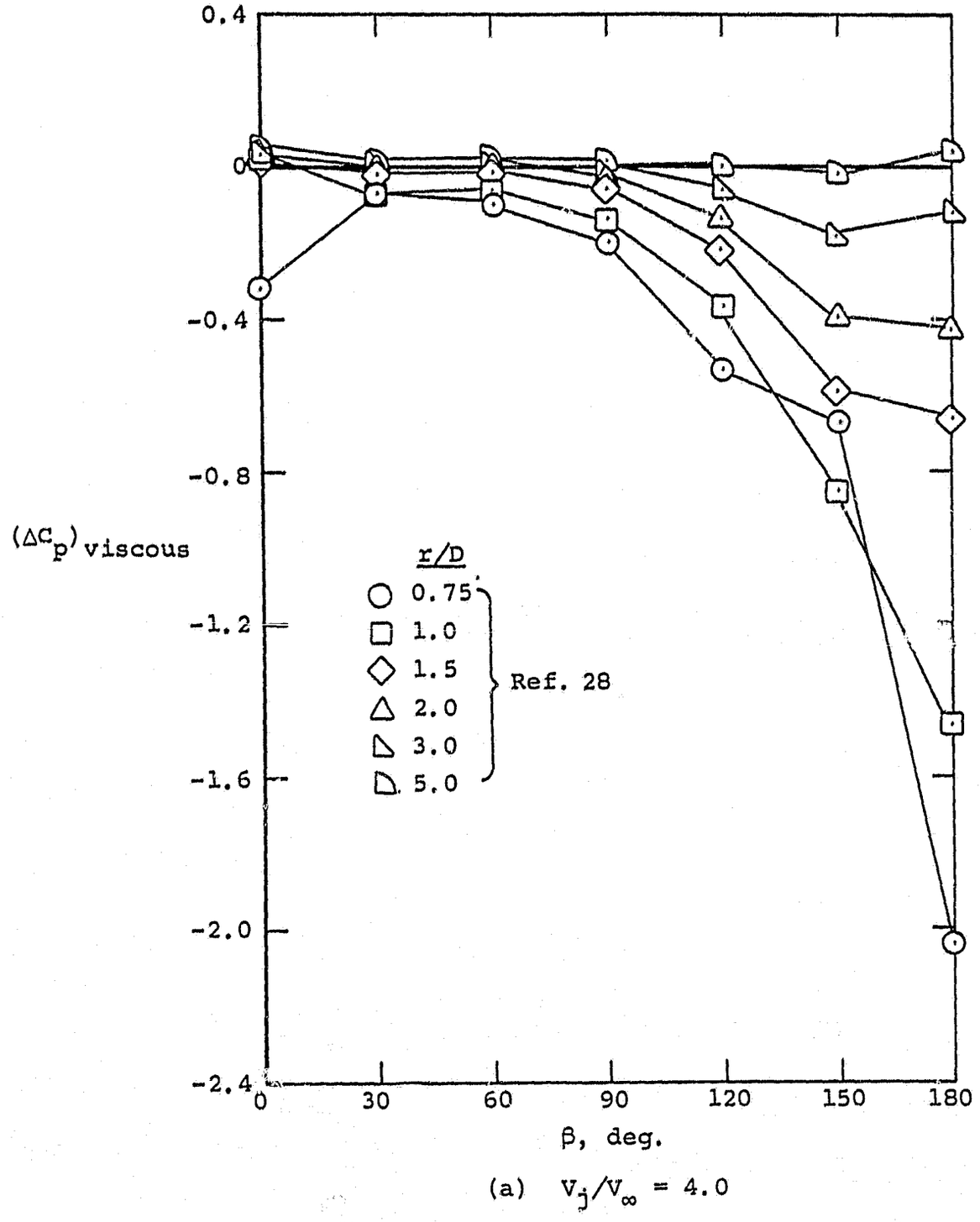

(a) $V_j/V_\infty = 4.0$

Figure 25 .- Correlation factors for viscous portion of the pressure coefficient induced on a flat plate by a jet exhausting into a crossflow, $\theta = 45^\circ$.

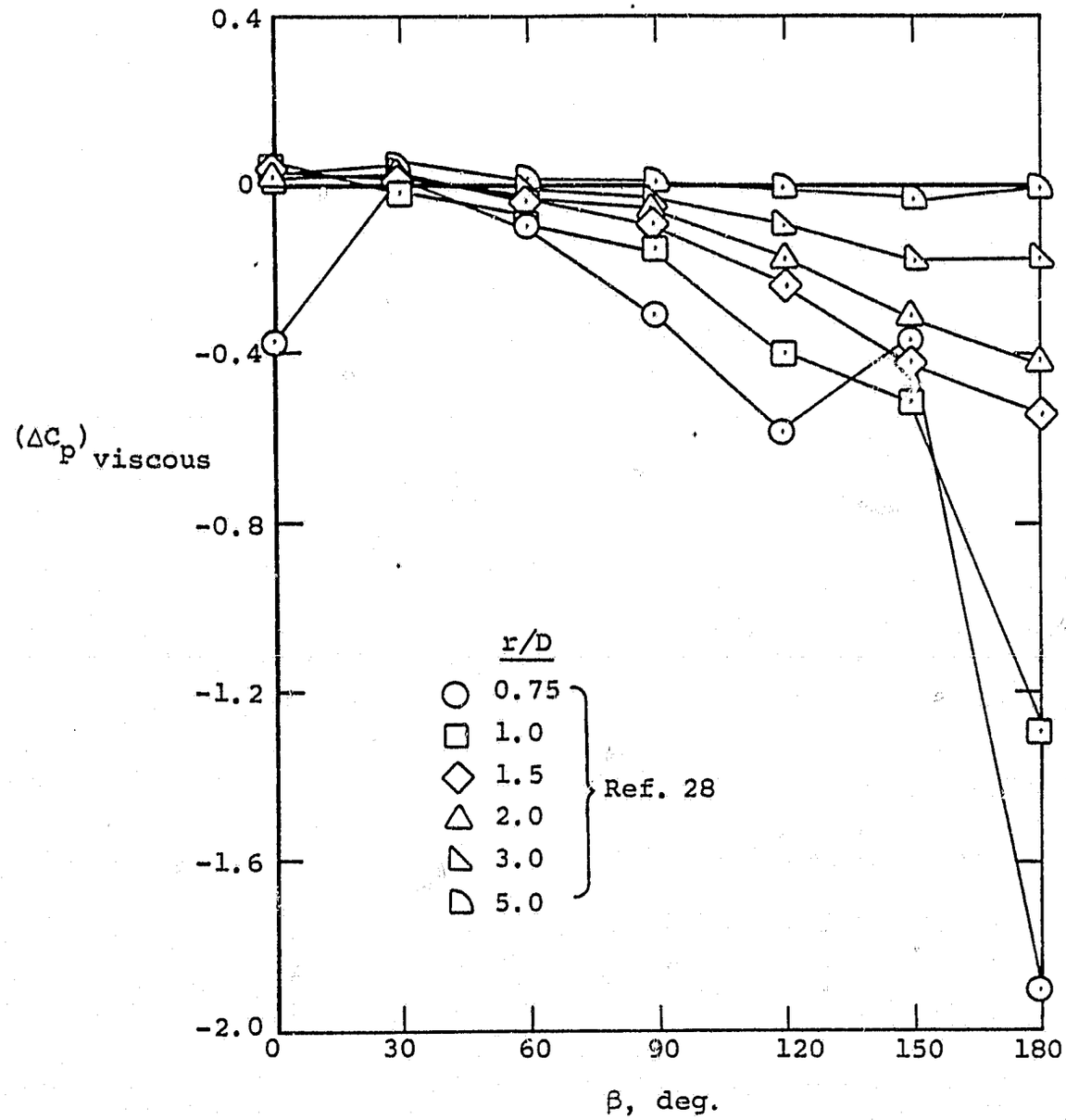

(b) $V_j/V_\infty = 5.1$

Figure 25.- Continued.

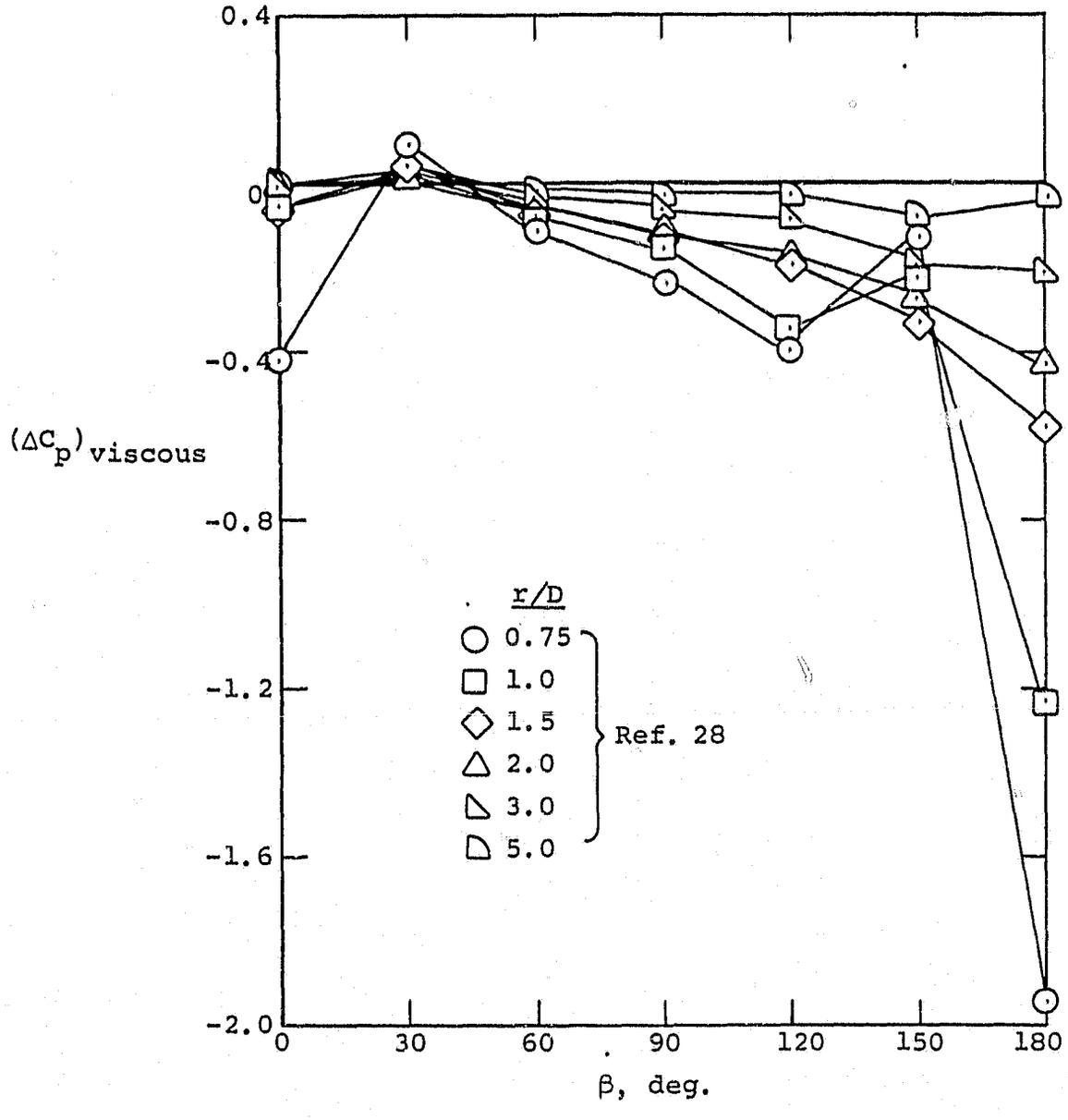

(c) $V_j/V_\infty = 6.32$

Figure 25.- Continued.

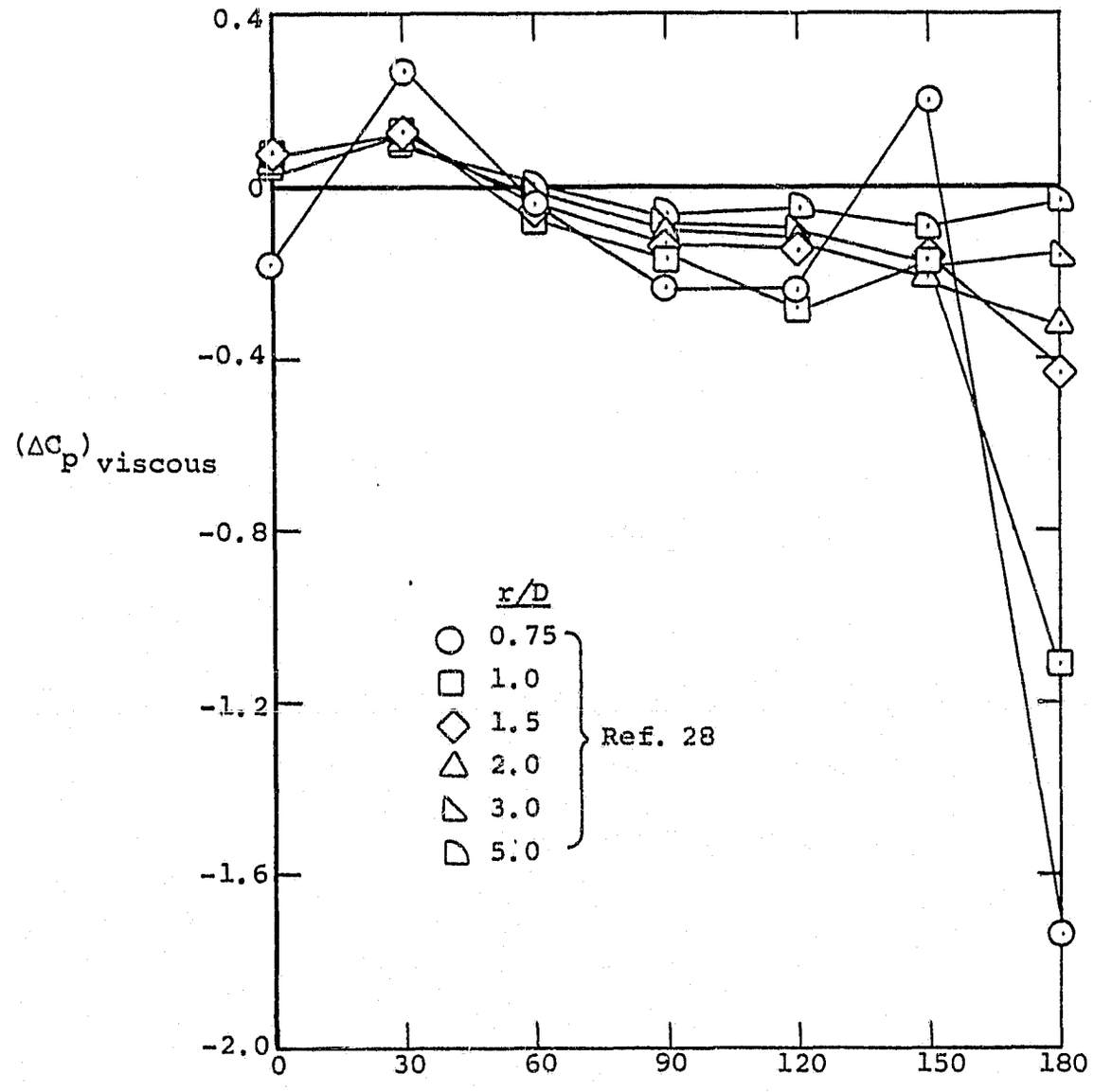

(d) $V_j/V_\infty = 8.17$

Figure 25.- Continued.

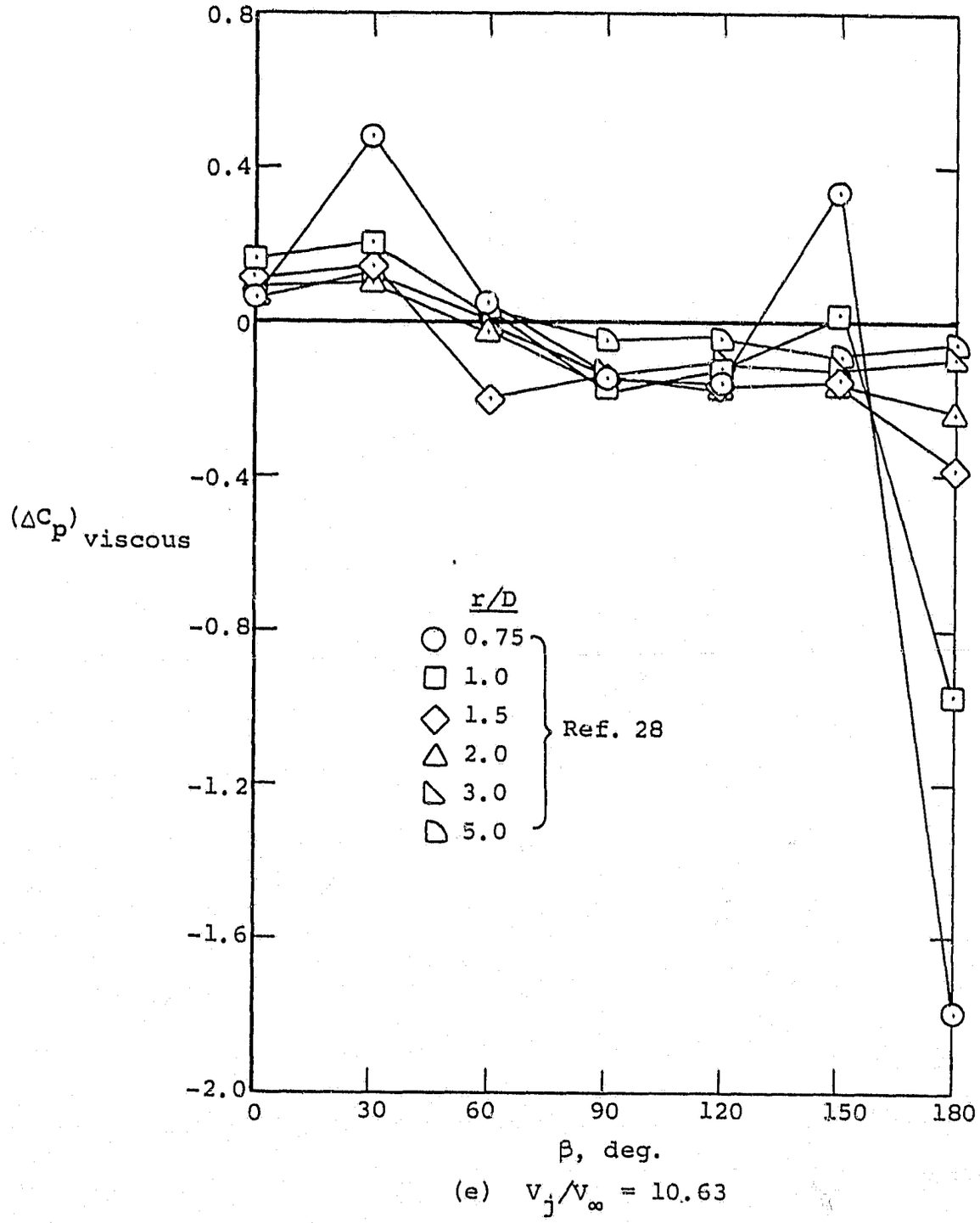

(e) $V_j/V_\infty = 10.63$

Figure 25.- Continued.

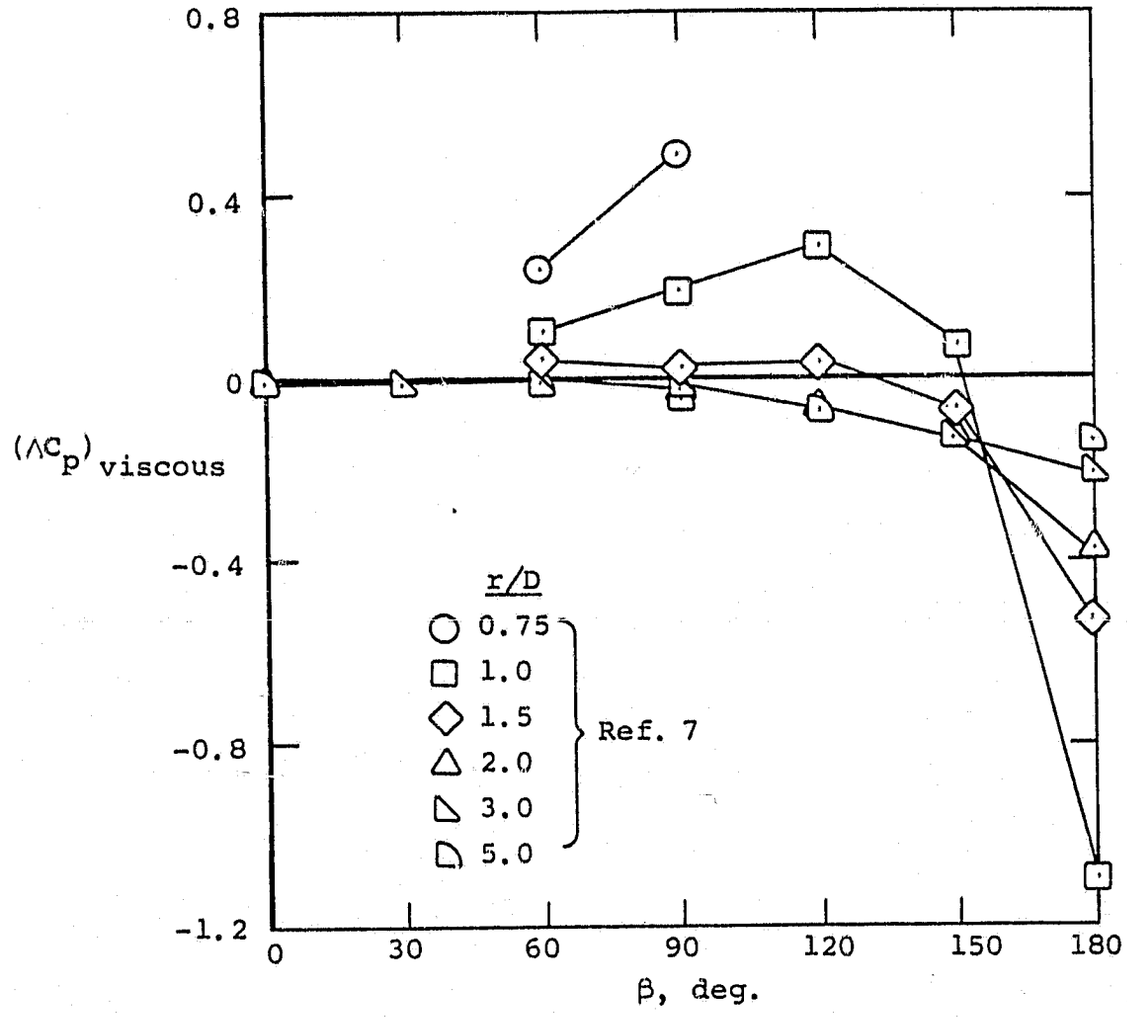

(f) $V_j/V_\infty = 12.0$

Figure 25.- Concluded.

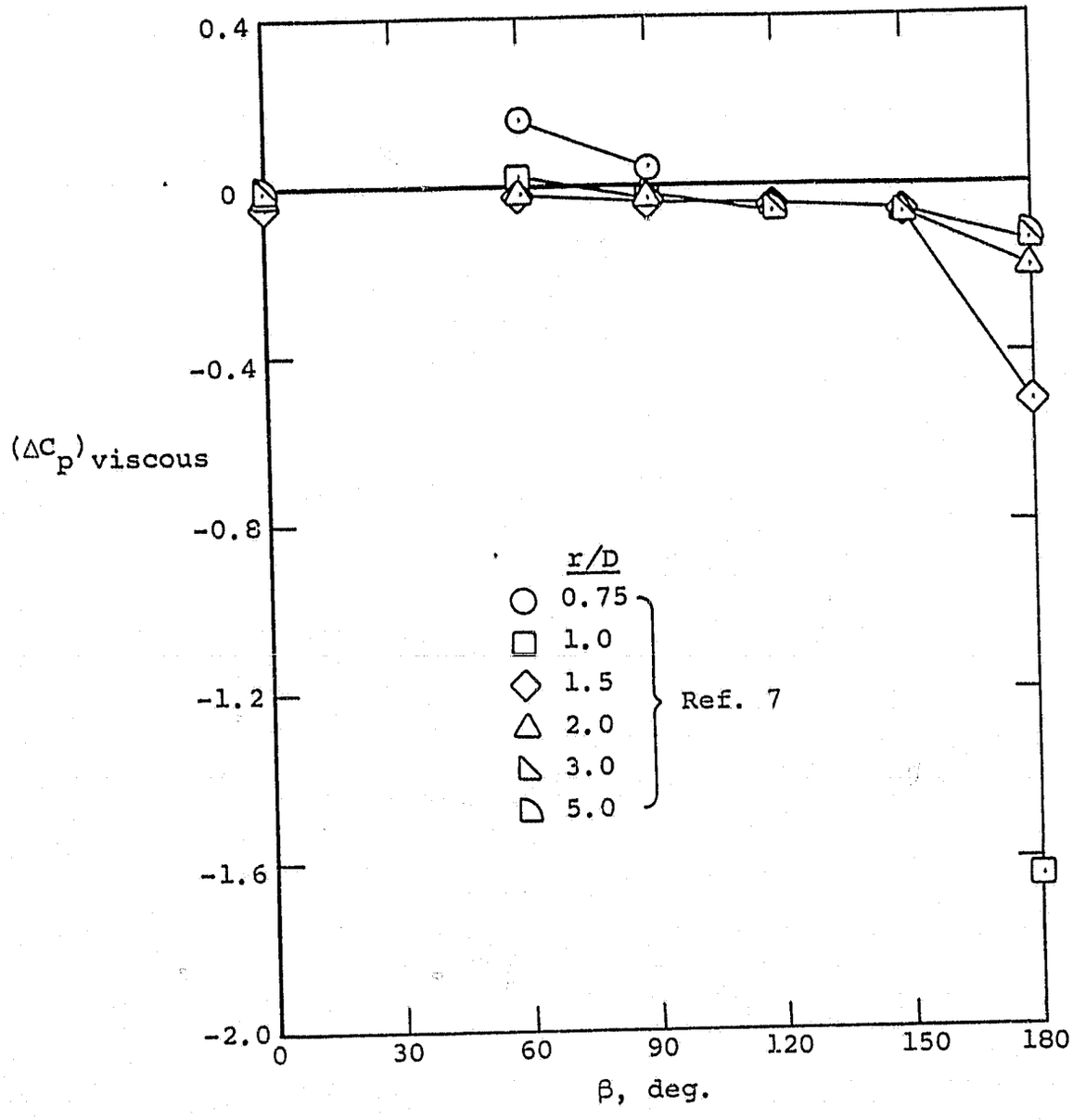

Figure 26.- Correlation factors for viscous portion of the pressure coefficient induced on a flat plate by a jet exhausting into a crossflow, $V_j/V_\infty = 12.0$, $\theta = 60^\circ$.

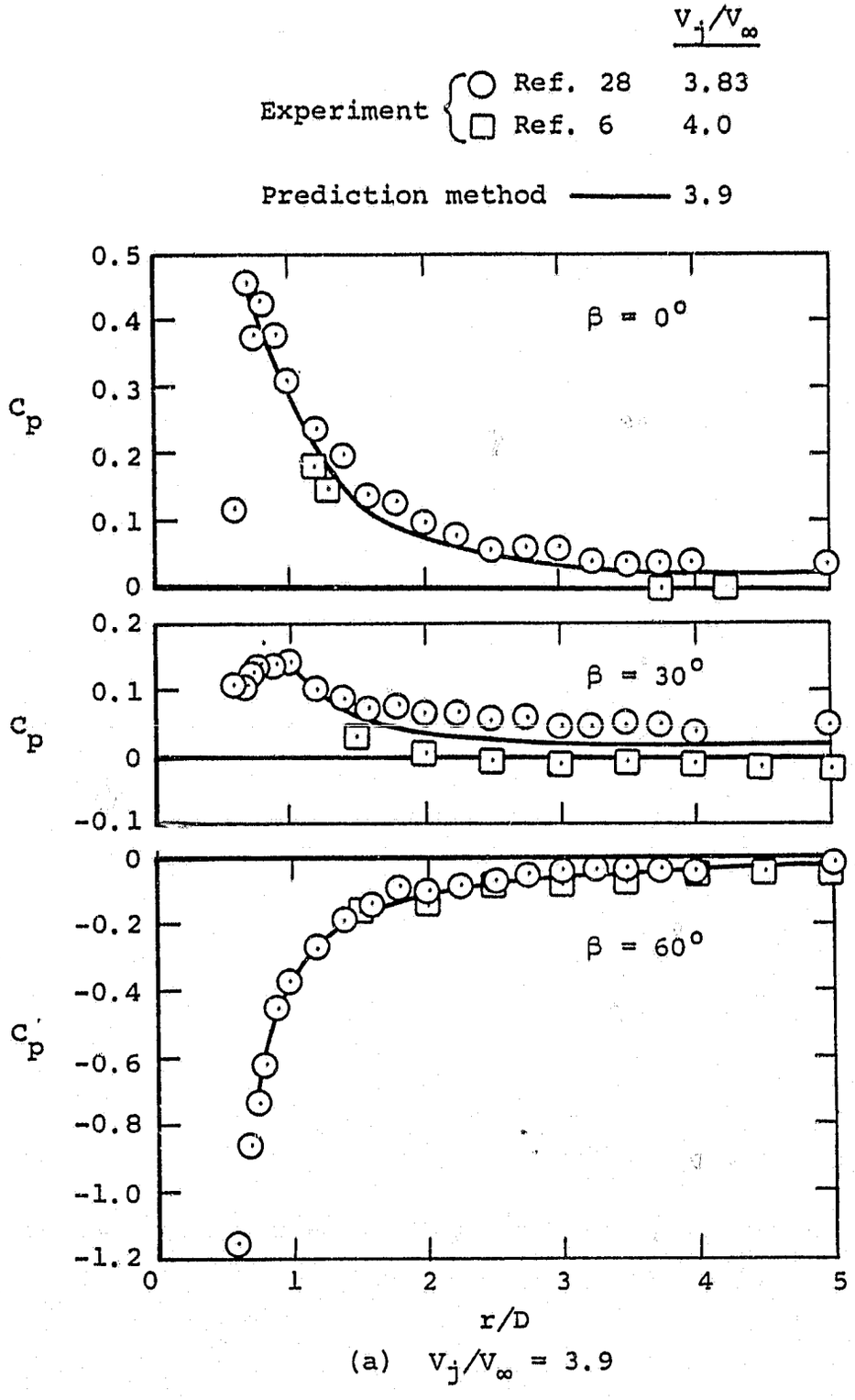

(a) $V_j/V_\infty = 3.9$

Figure 27.- Comparison of measured and predicted pressures on a flat plate from which a jet is exhausting into a crossflow, $\theta = 15^\circ$.

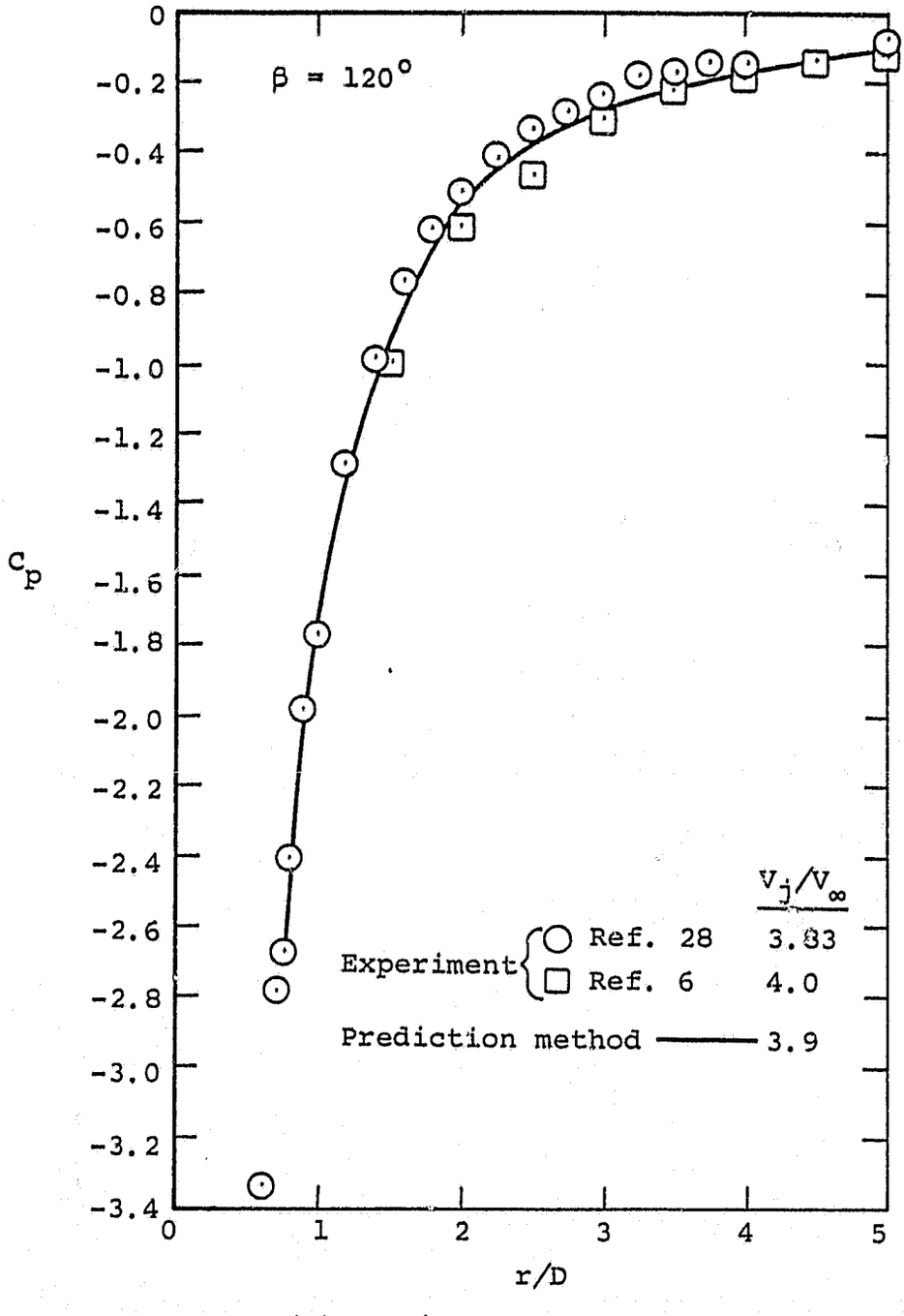

(a) V_j/V_∞ = 3.9, continued.

Figure 27.- Continued.

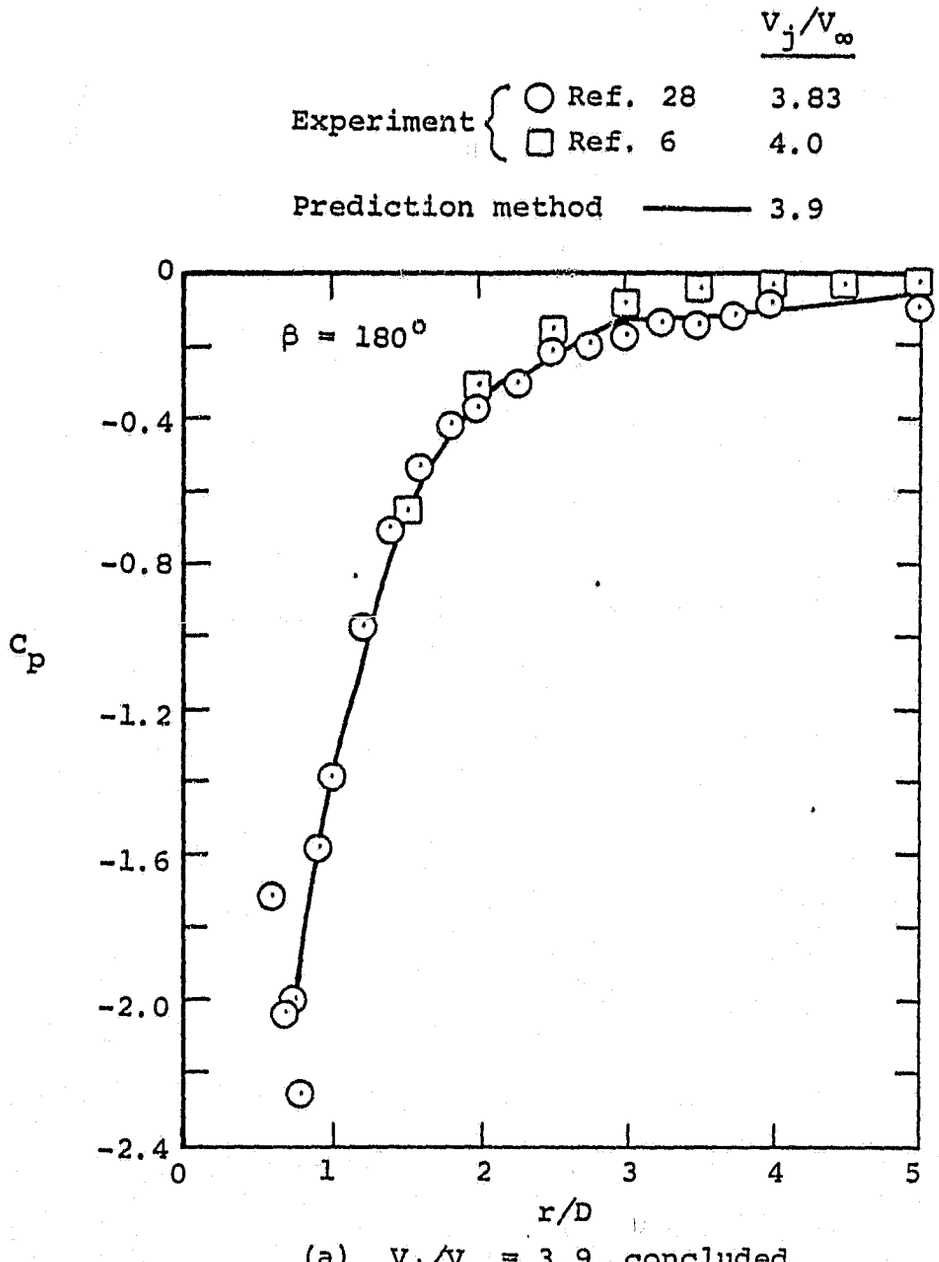

(a) V_j/V_∞ = 3.9, concluded.

Figure 27.- Continued.

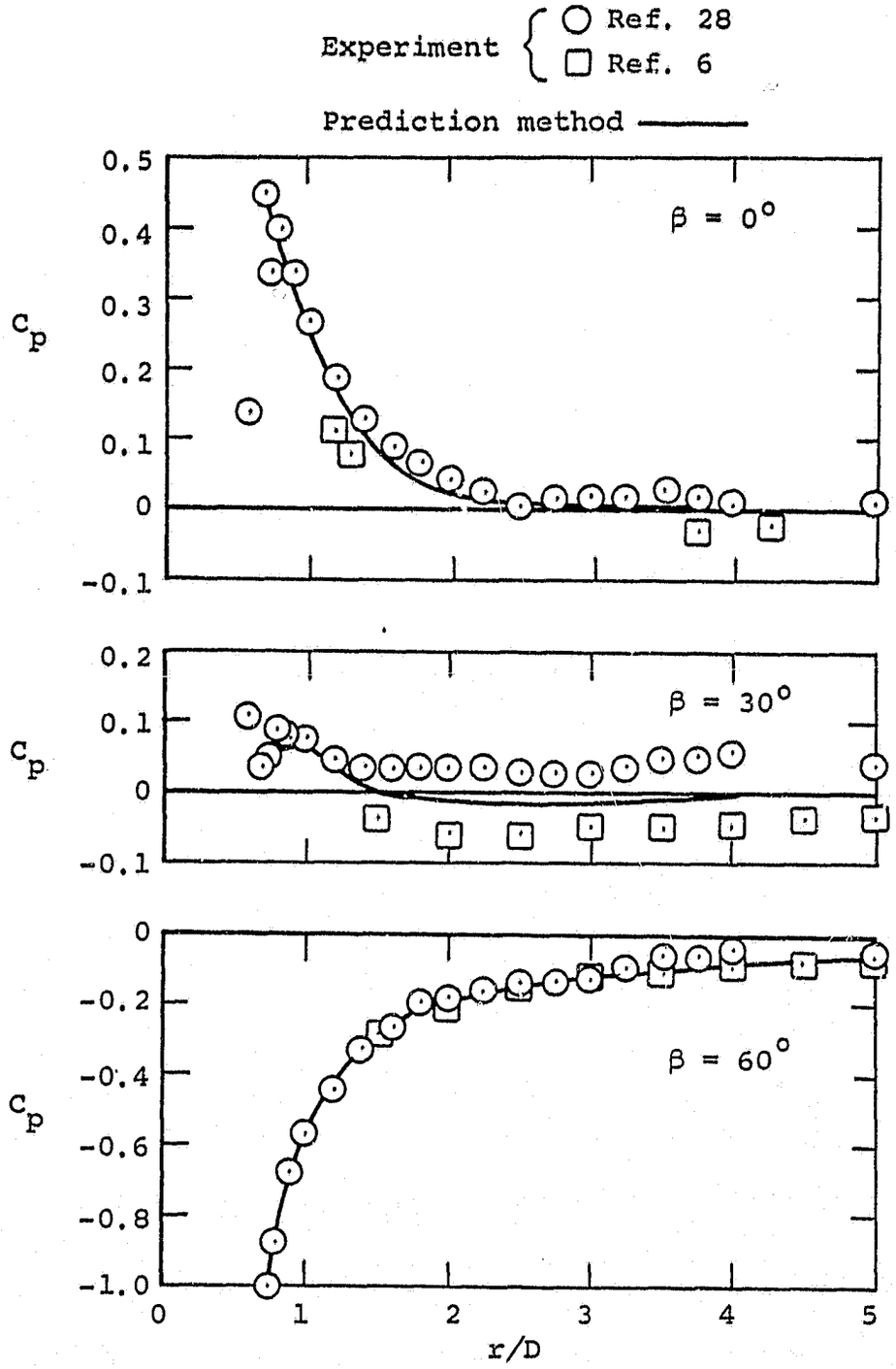

(b) $V_j/V_\infty = 5.0$

Figure 27.- Continued.

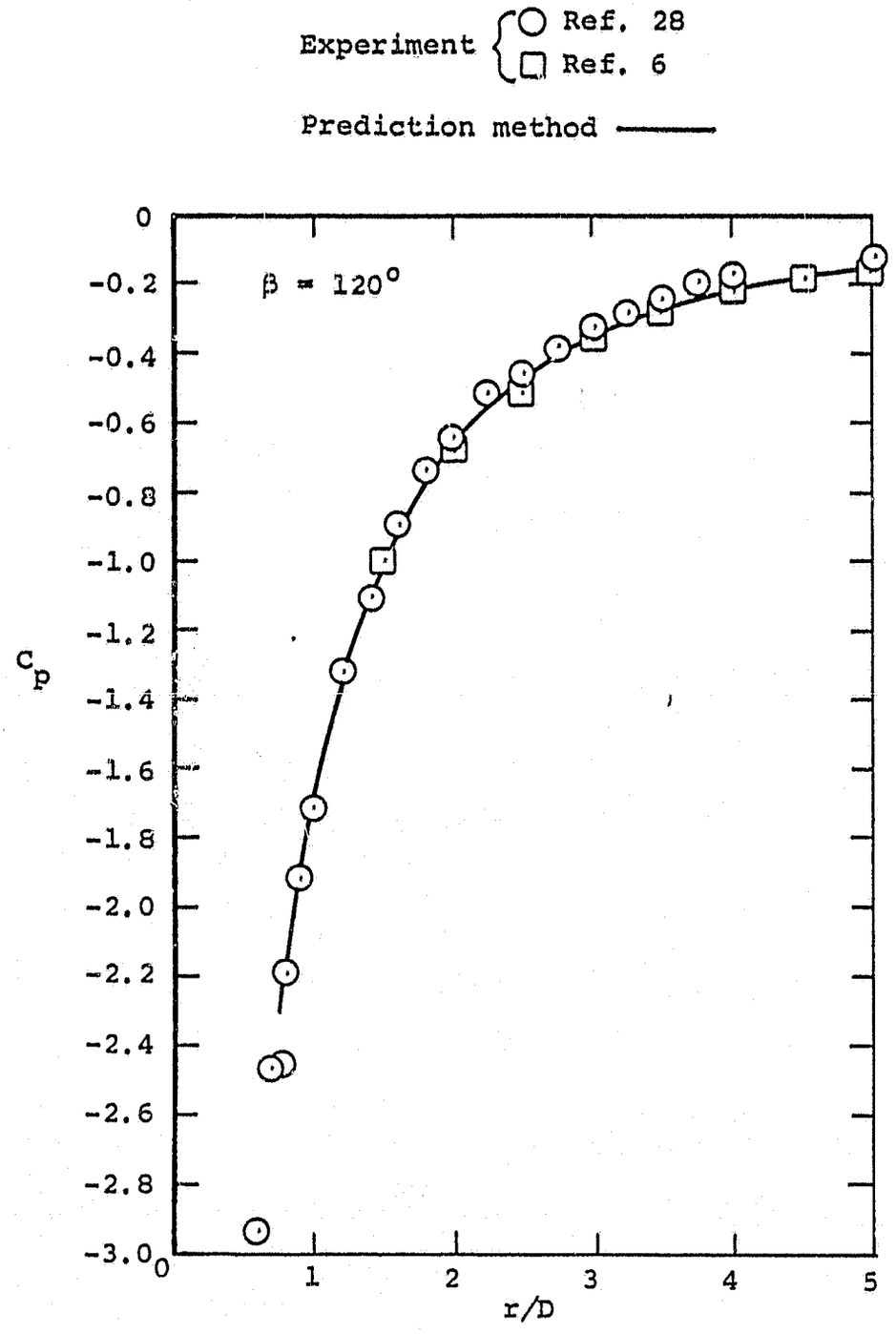

(b) V_j/V_∞ = 5.0, continued.

Figure 27.- Continued.

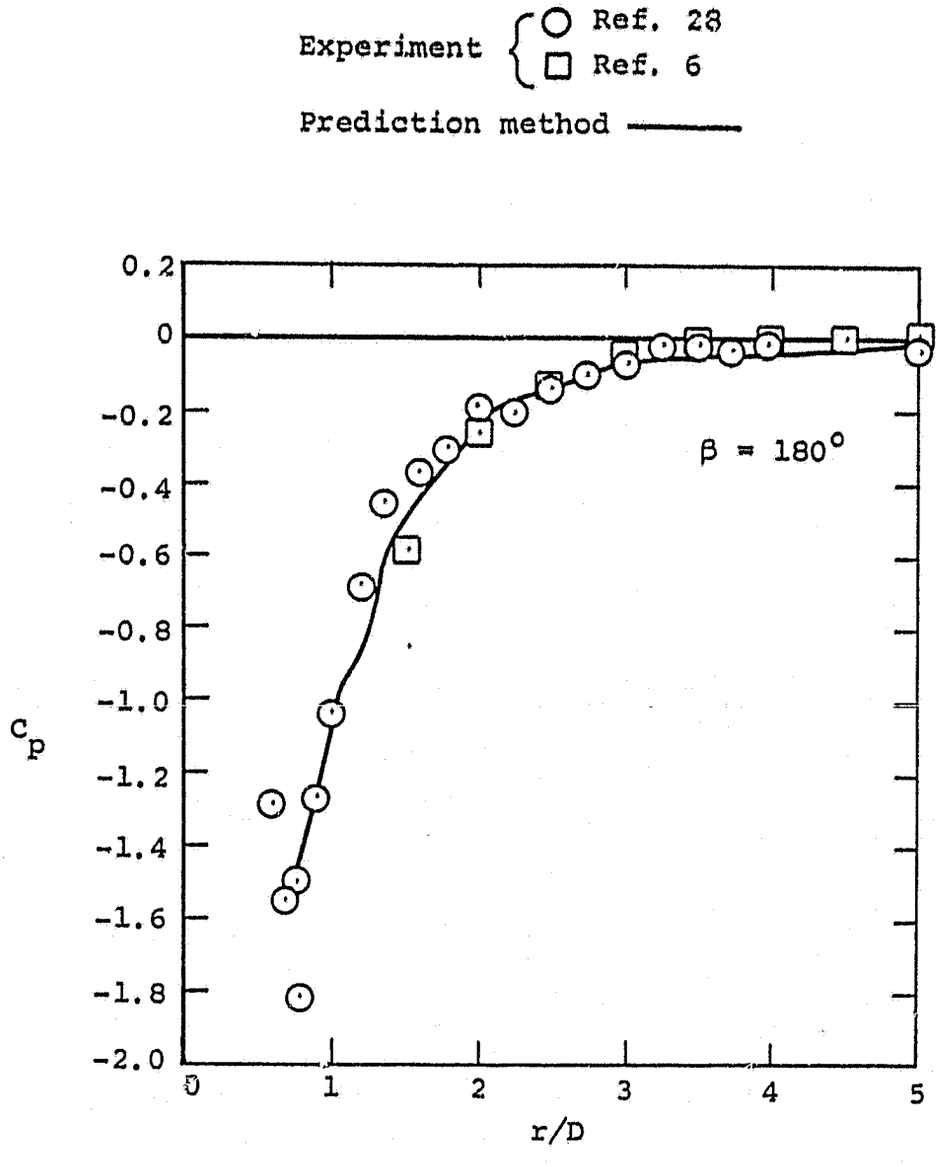

(b) V_j/V_∞ = 5.0, concluded.

Figure 27.- Concluded.

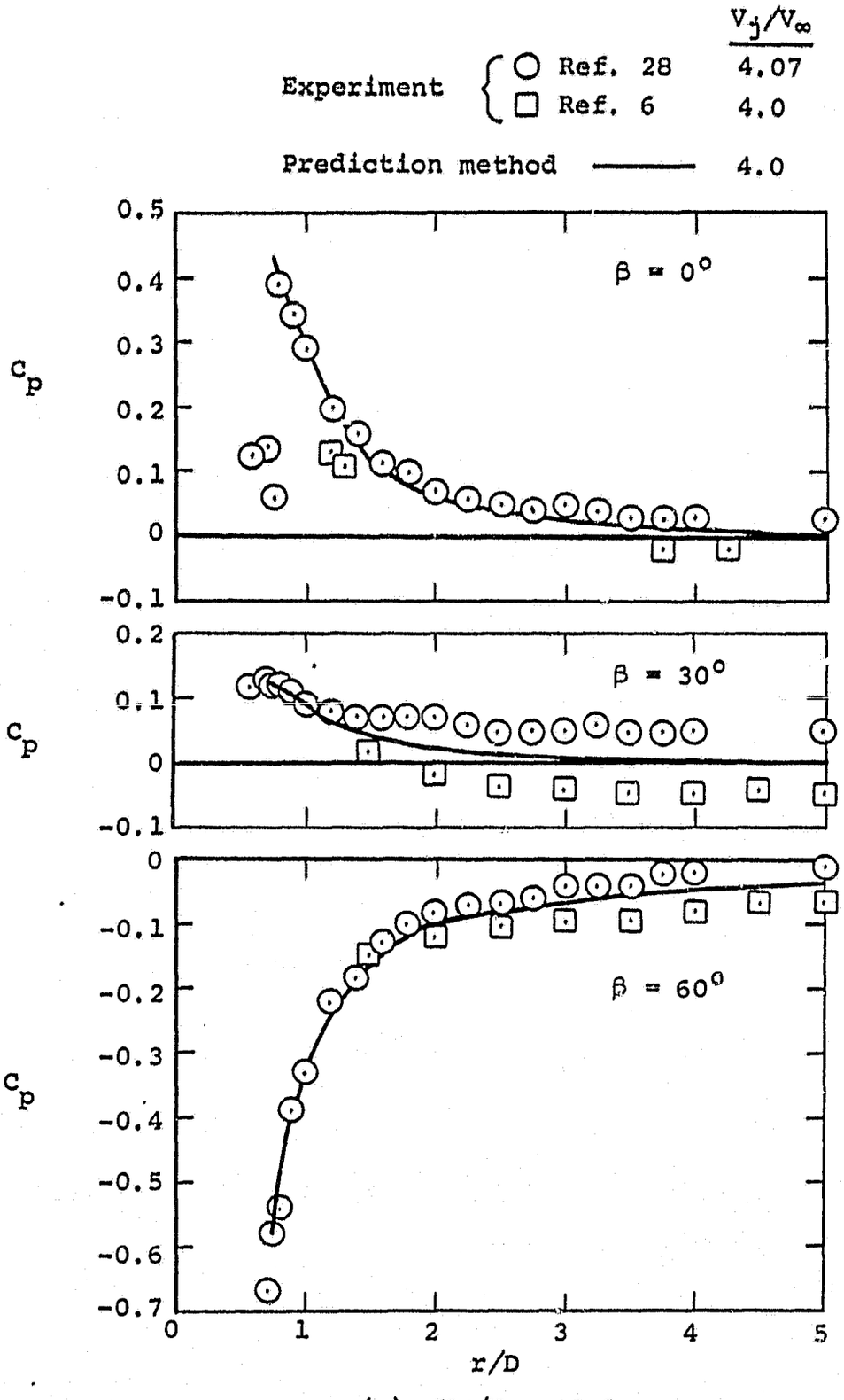

(a) $V_j/V_\infty = 4.0$

Figure 28.- Comparison of measured and predicted pressures on a flat plate from which a jet is exhausting into a crossflow, $\theta = 30^\circ$.

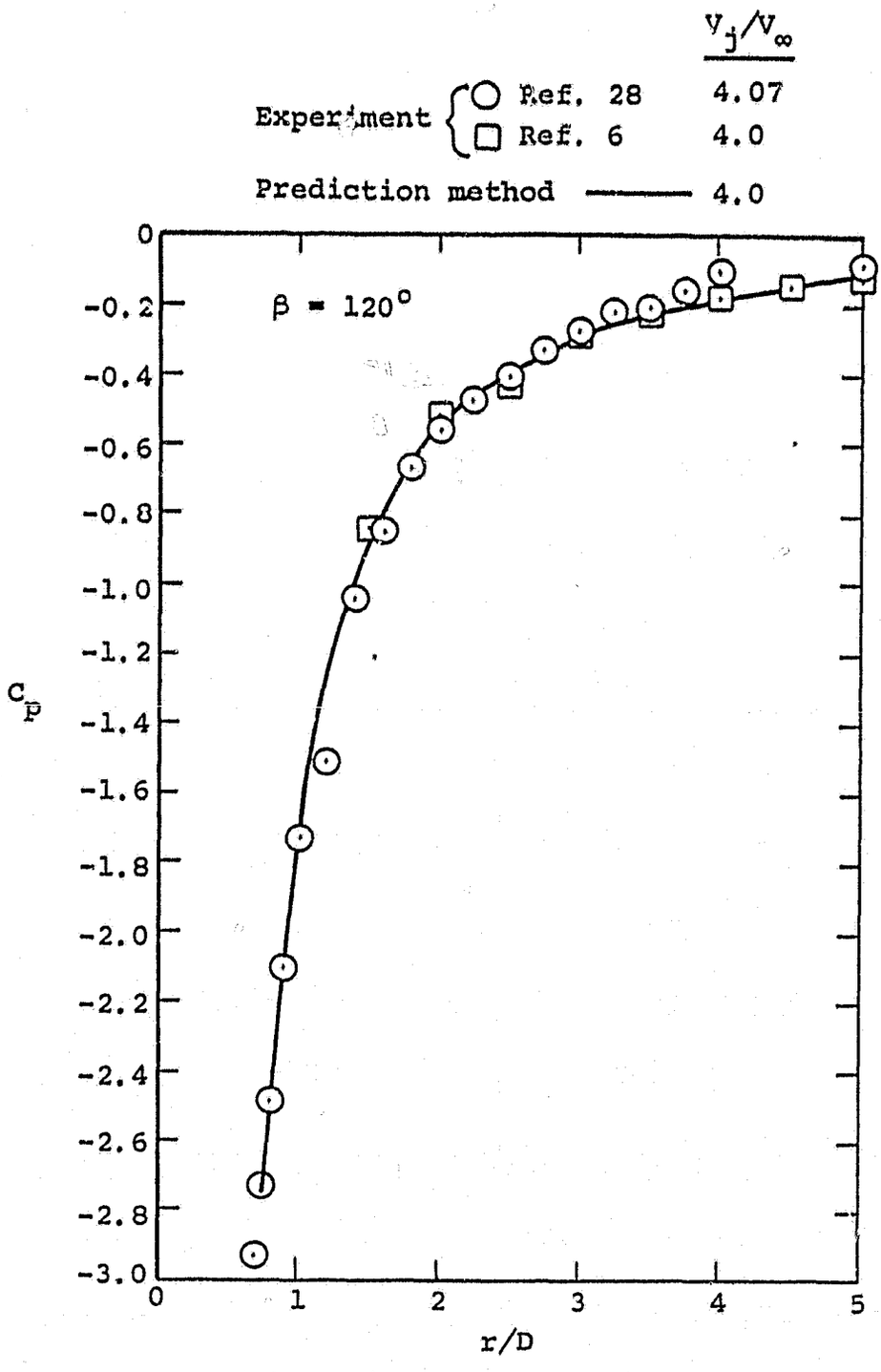

(a) V_j/V_∞ = 4.0, continued.

Figure 28.- Continued.

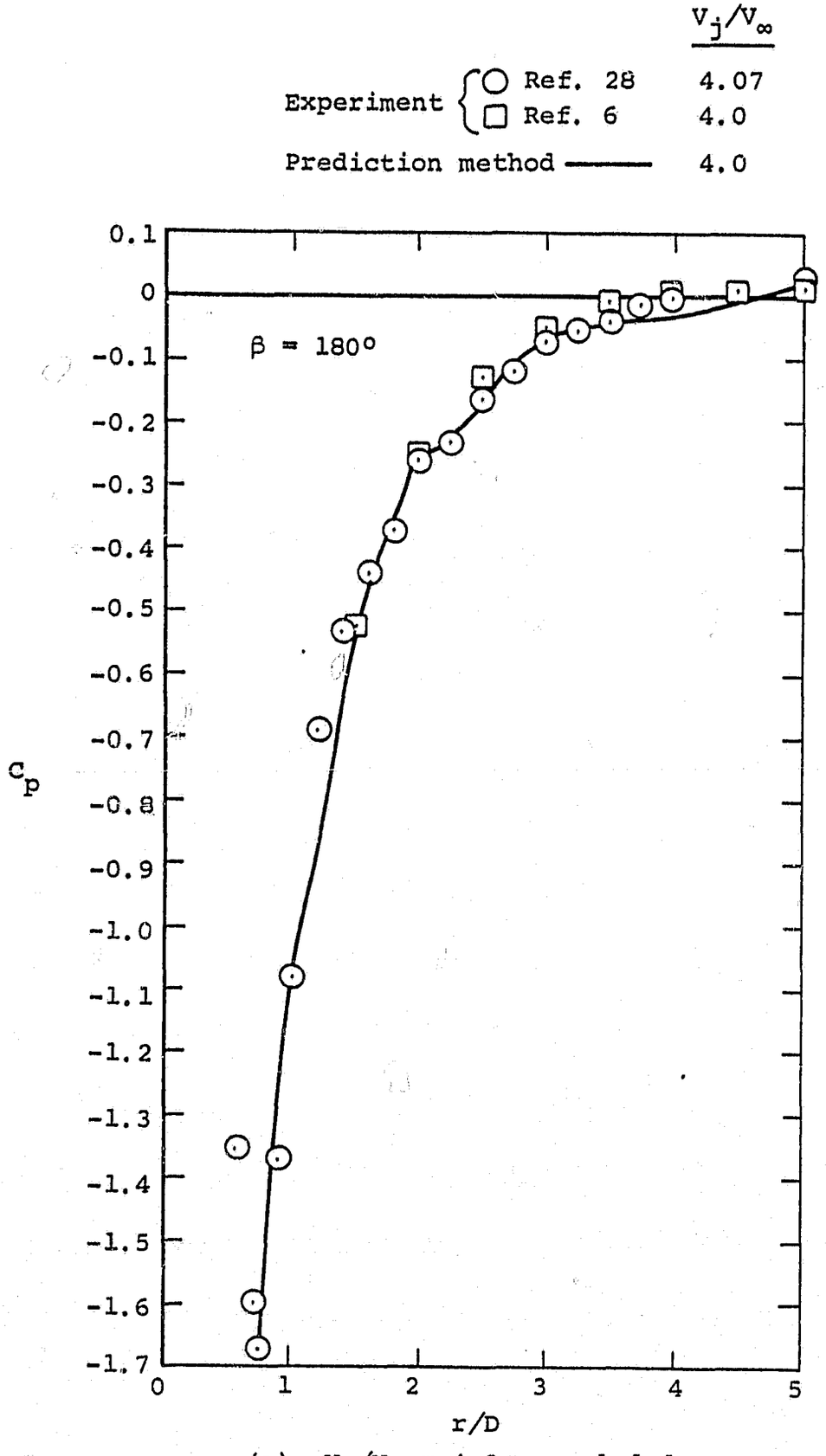

(a) V_j/V_∞ = 4.0, concluded.

Figure 28.- Continued.

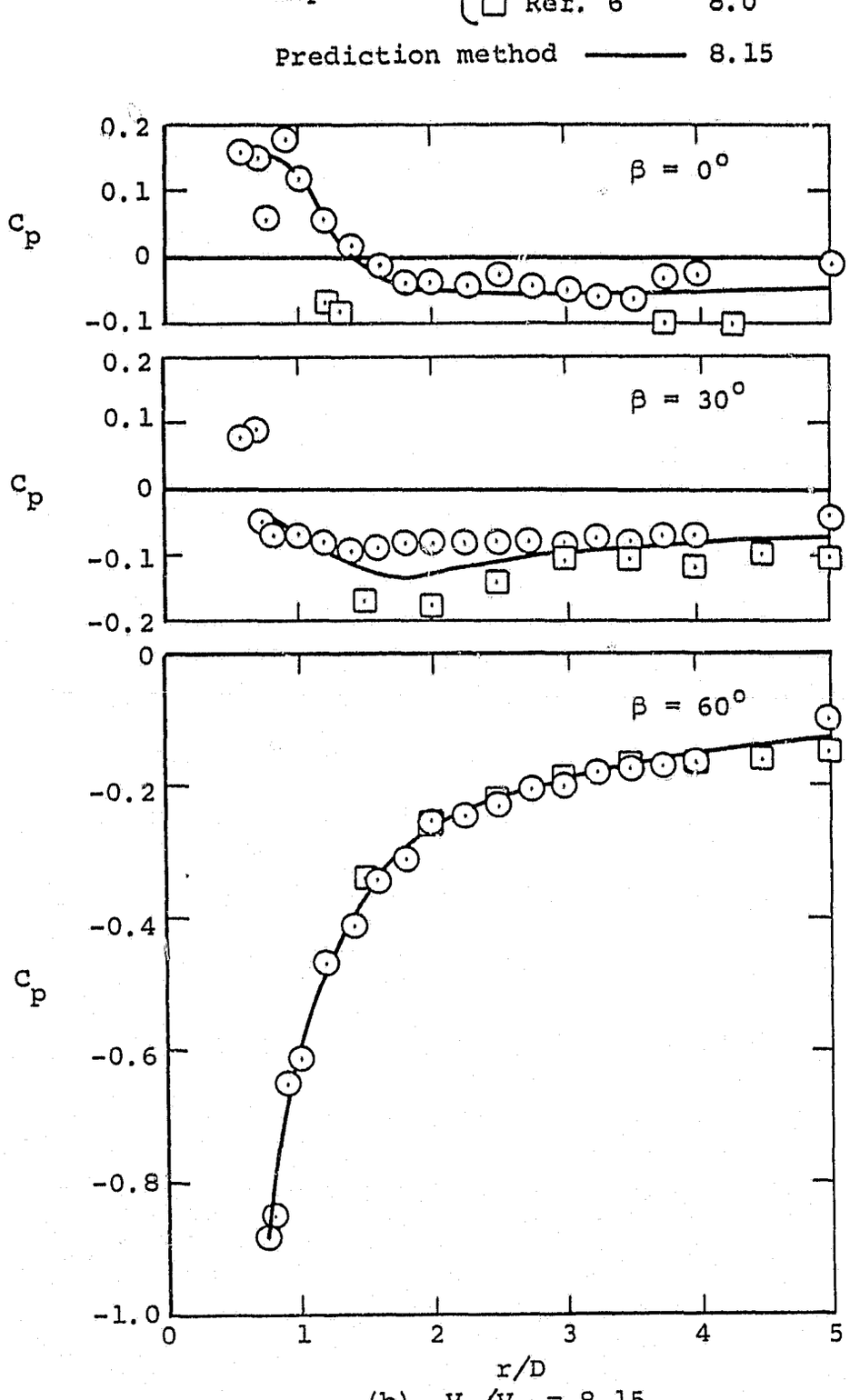

(b) $V_j/V_\infty = 8.15$

Figure 28.- Continued.

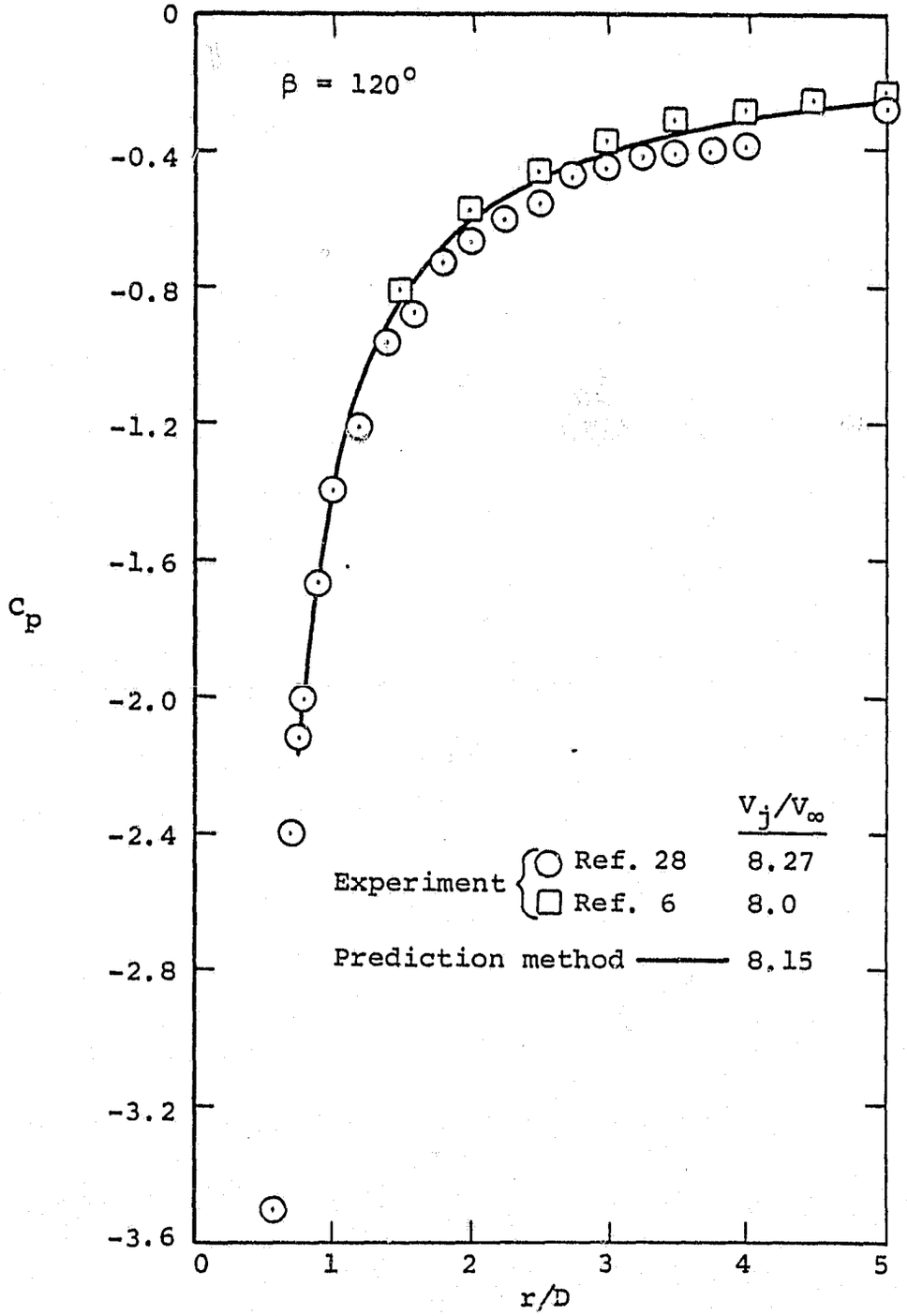

(b) V_j/V_∞ = 8.15, continued.

Figure 28.- Continued.

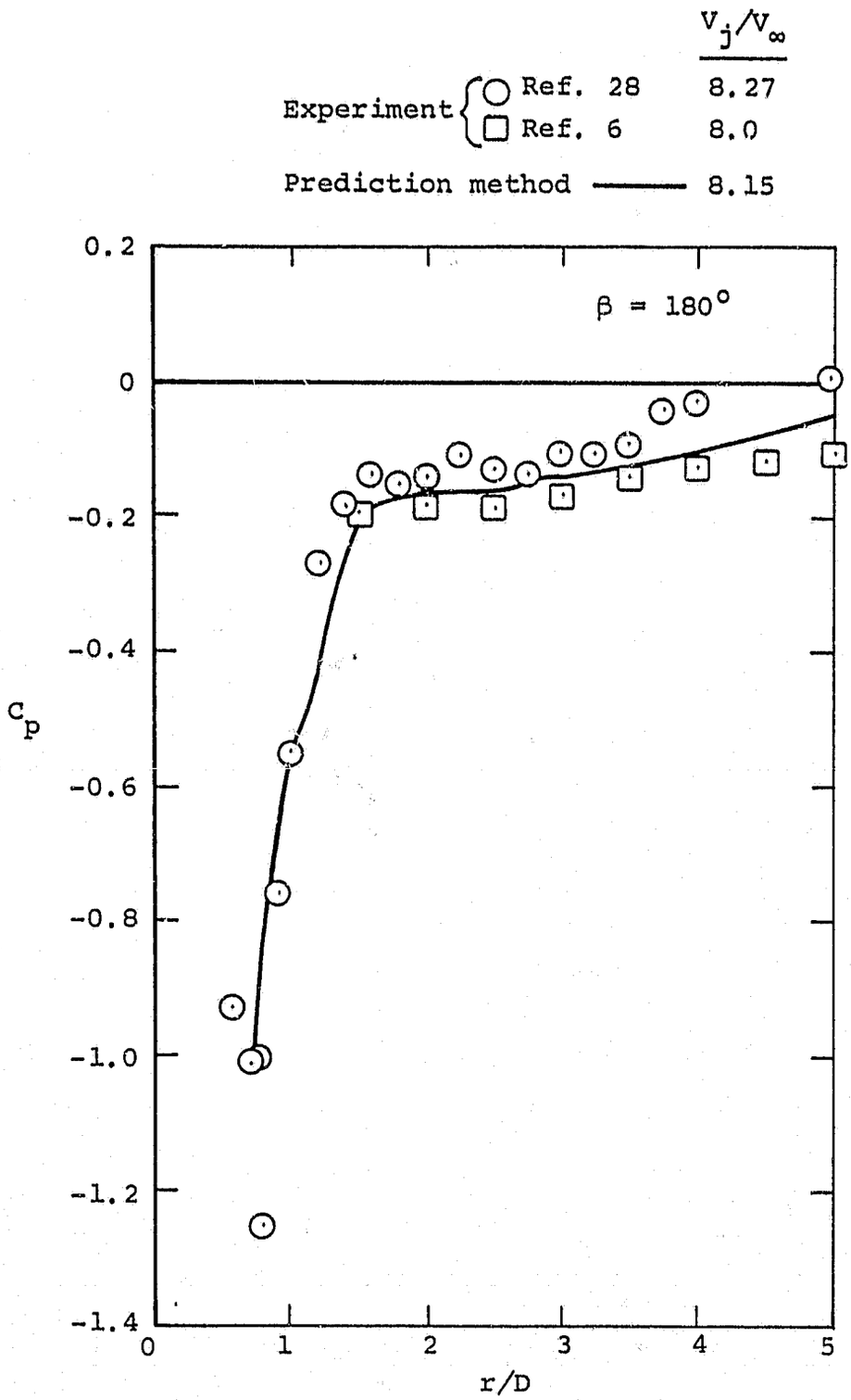

(b) $V_j/V_\infty = 8.15$, concluded.

Figure 28.- Concluded.

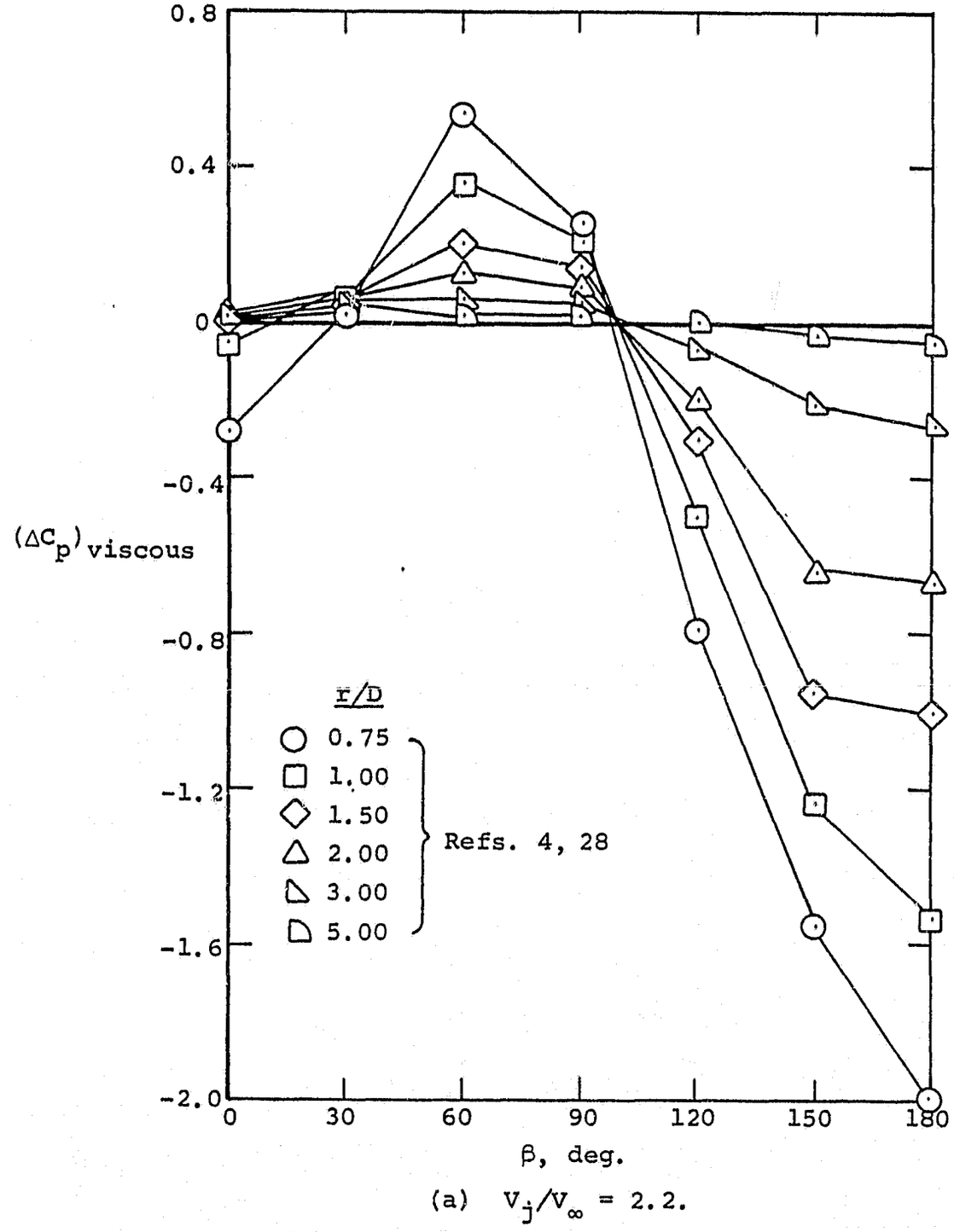

(a) $V_j/V_\infty = 2.2$.

Figure 29.-Correlation factor for viscous portion of the pressure-coefficient induced on a flat plate by a jet exhausting into a crossflow, $\theta = 0^\circ$.

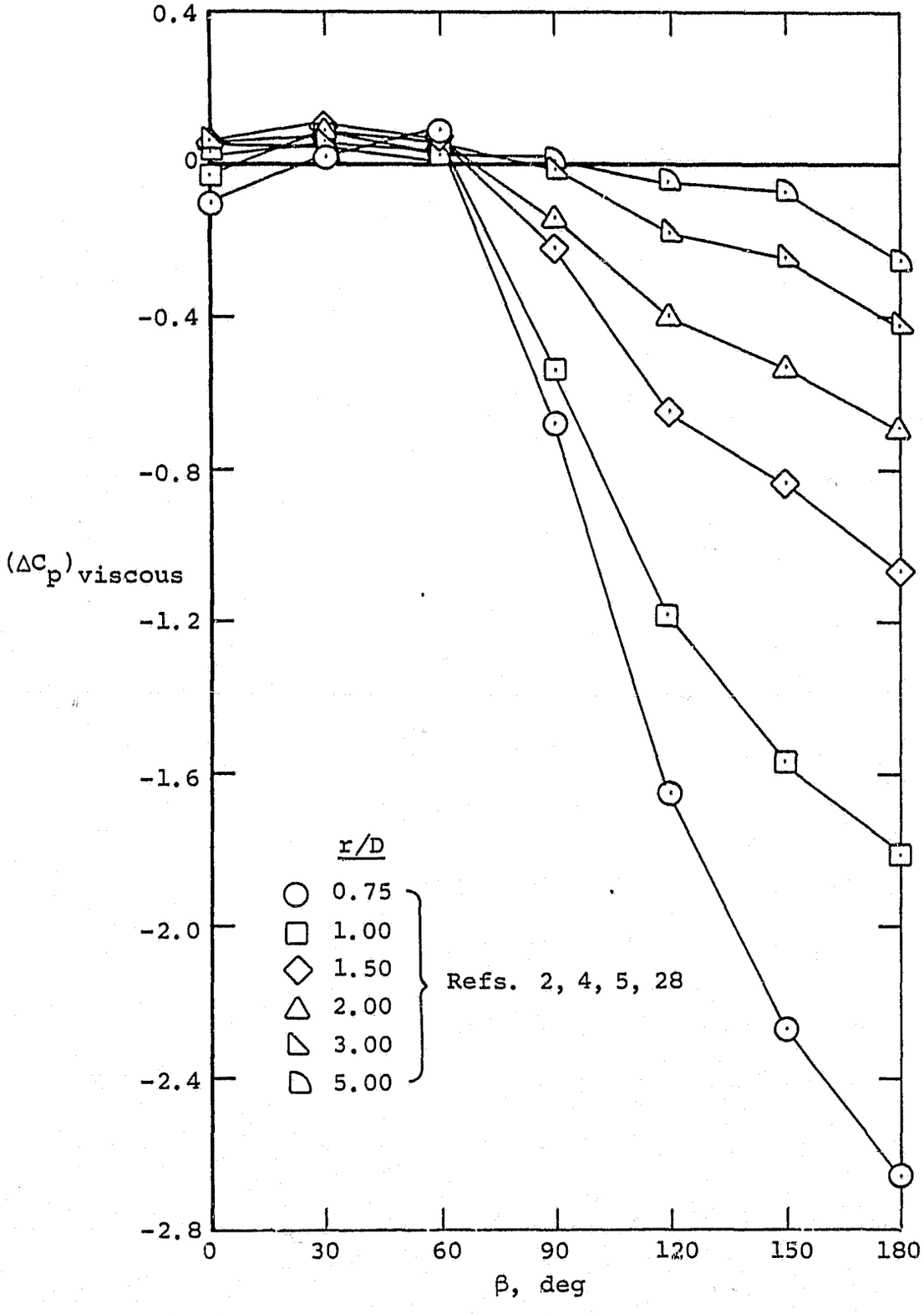

(b) $V_j/V_\infty = 3.9$

Figure 29.- Continued.

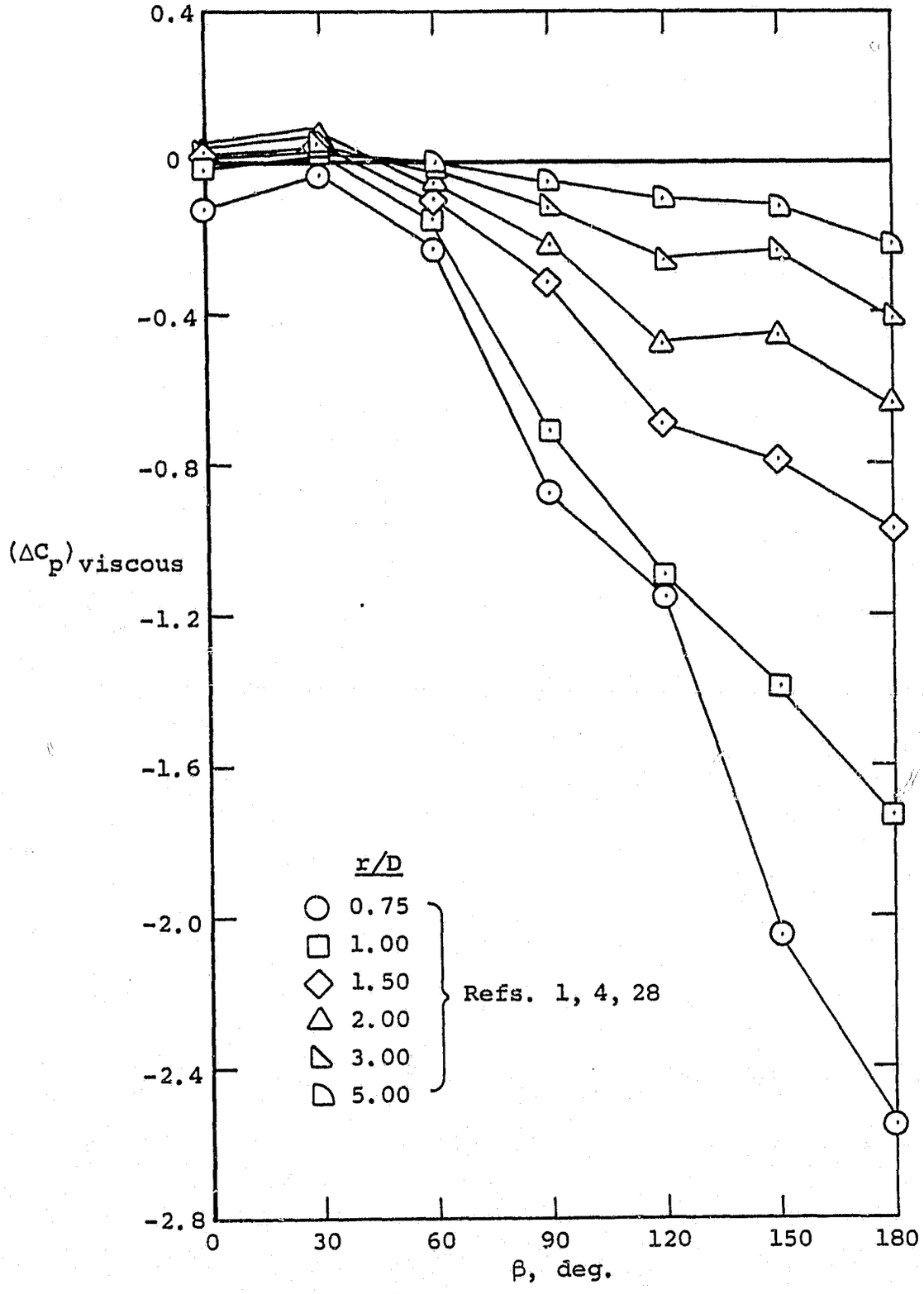

(c) $V_j/V_\infty = 5.0$.

Figure 29.- Continued.

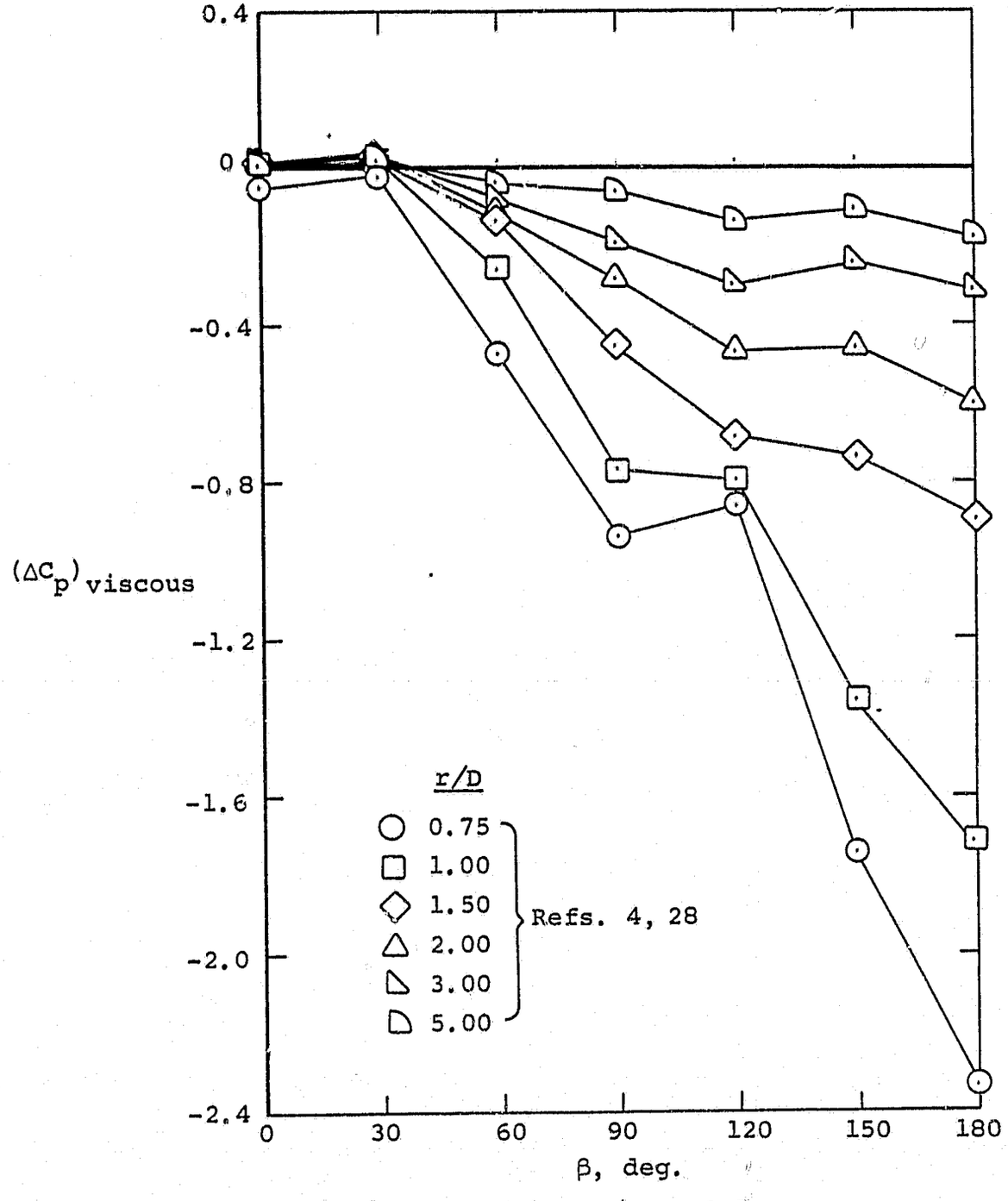

(d) $V_j/V_\infty = 6.1$.

Figure 29.- Continued.

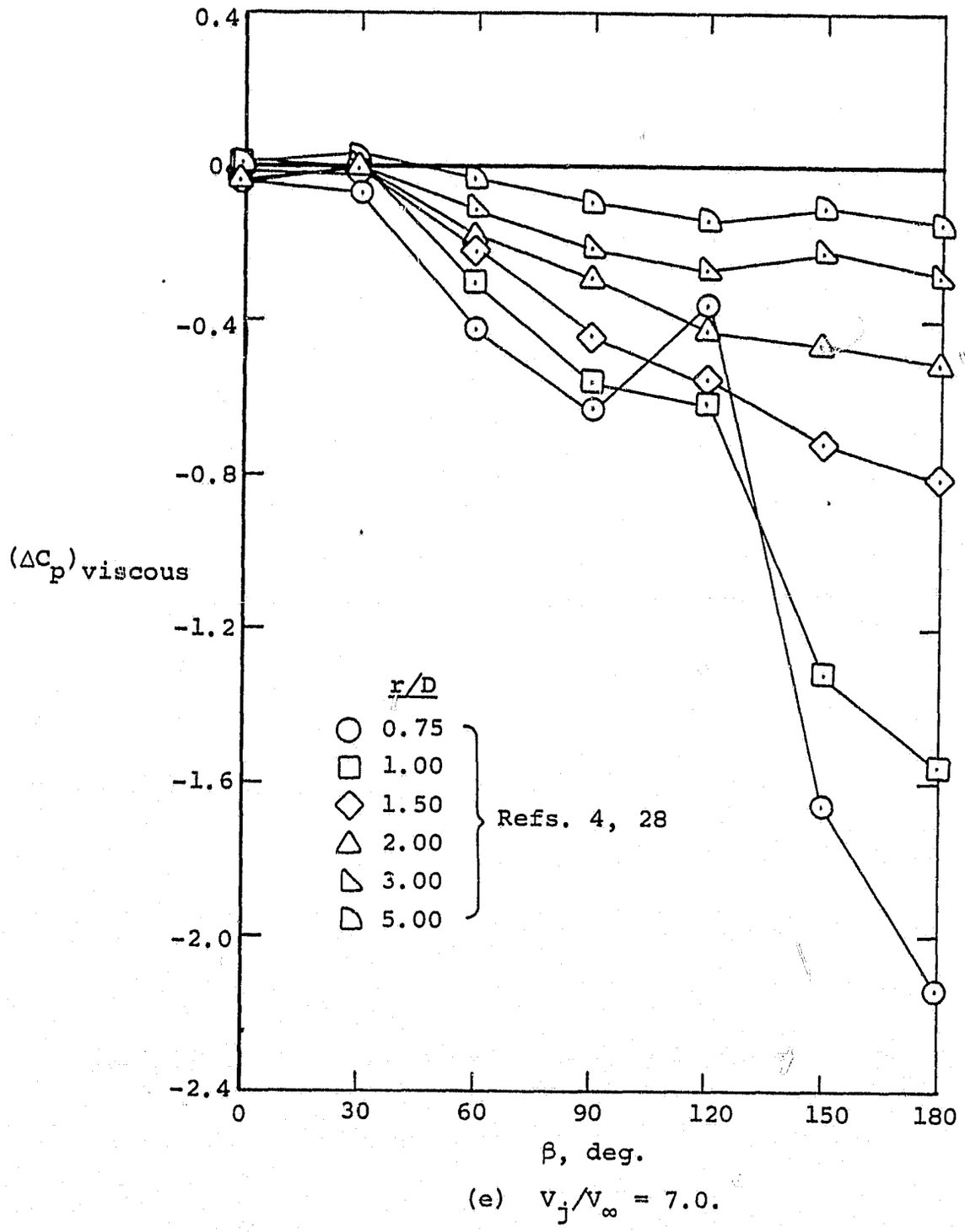

(e) $V_j/V_\infty = 7.0$.

Figure 29.- Continued.

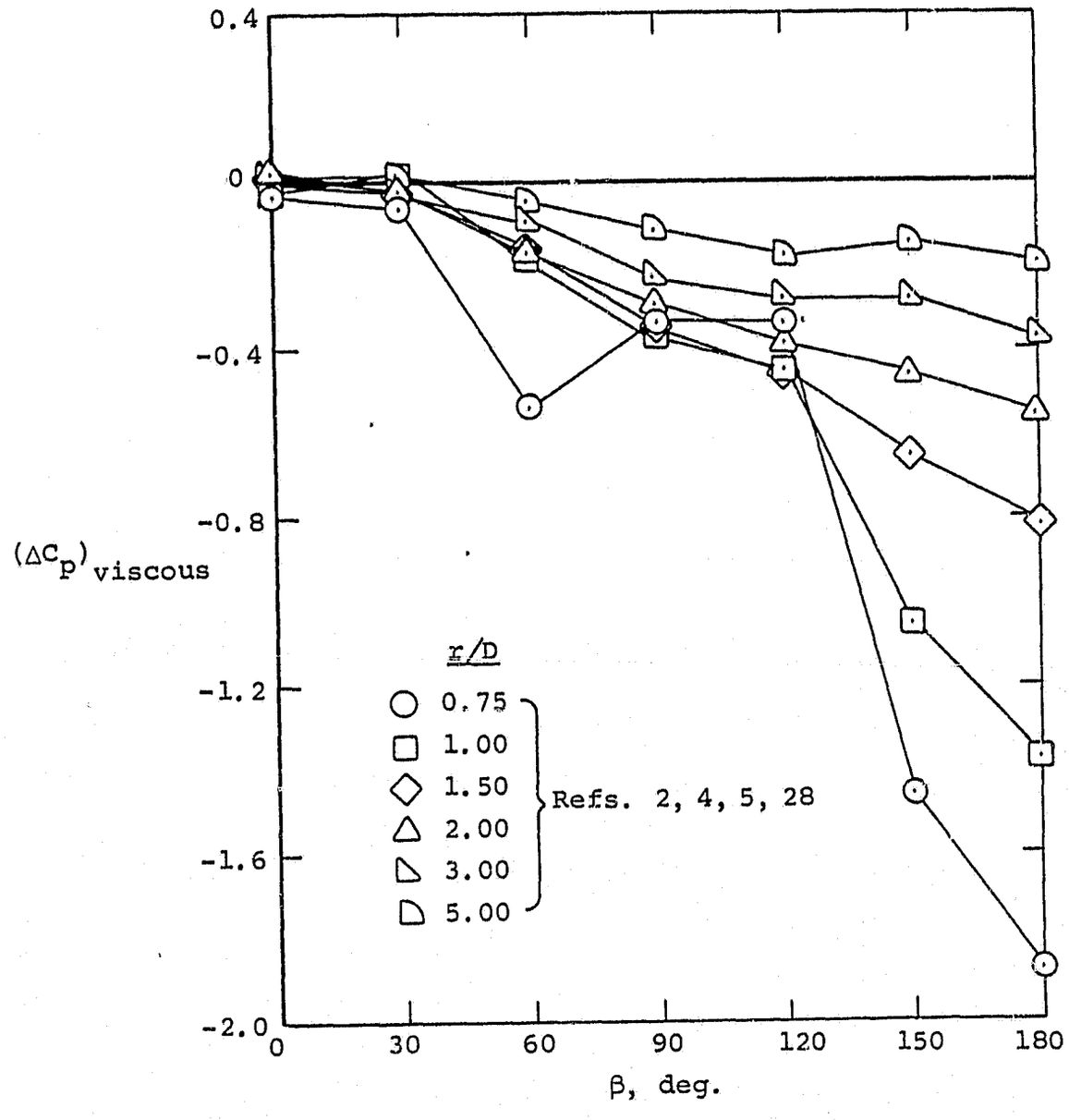

(f) $V_j/V_\infty = 8.0$.

Figure 29.- Continued.

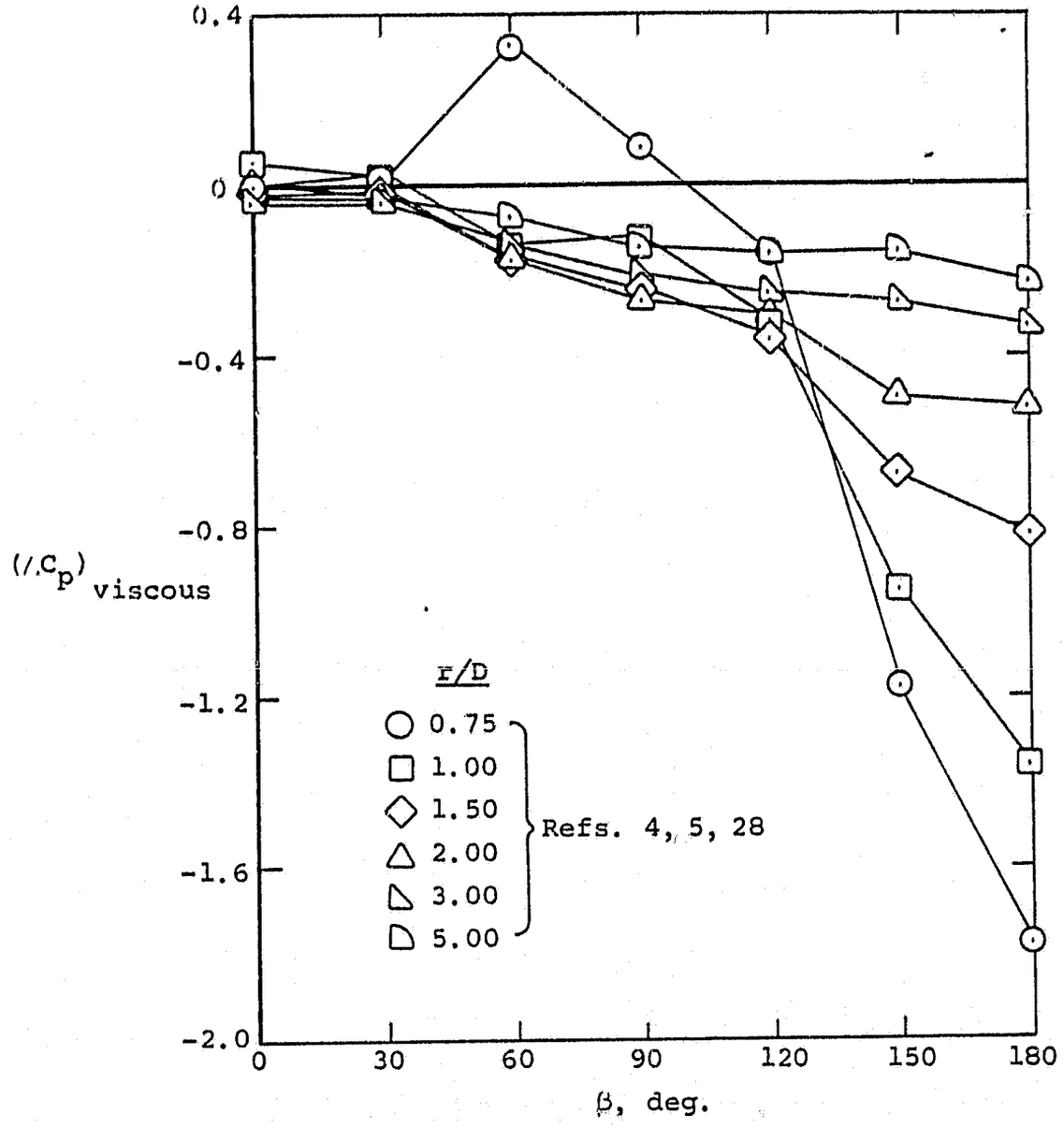

(g) V_j/V_∞ = 10.0.

Figure 29.- Concluded.

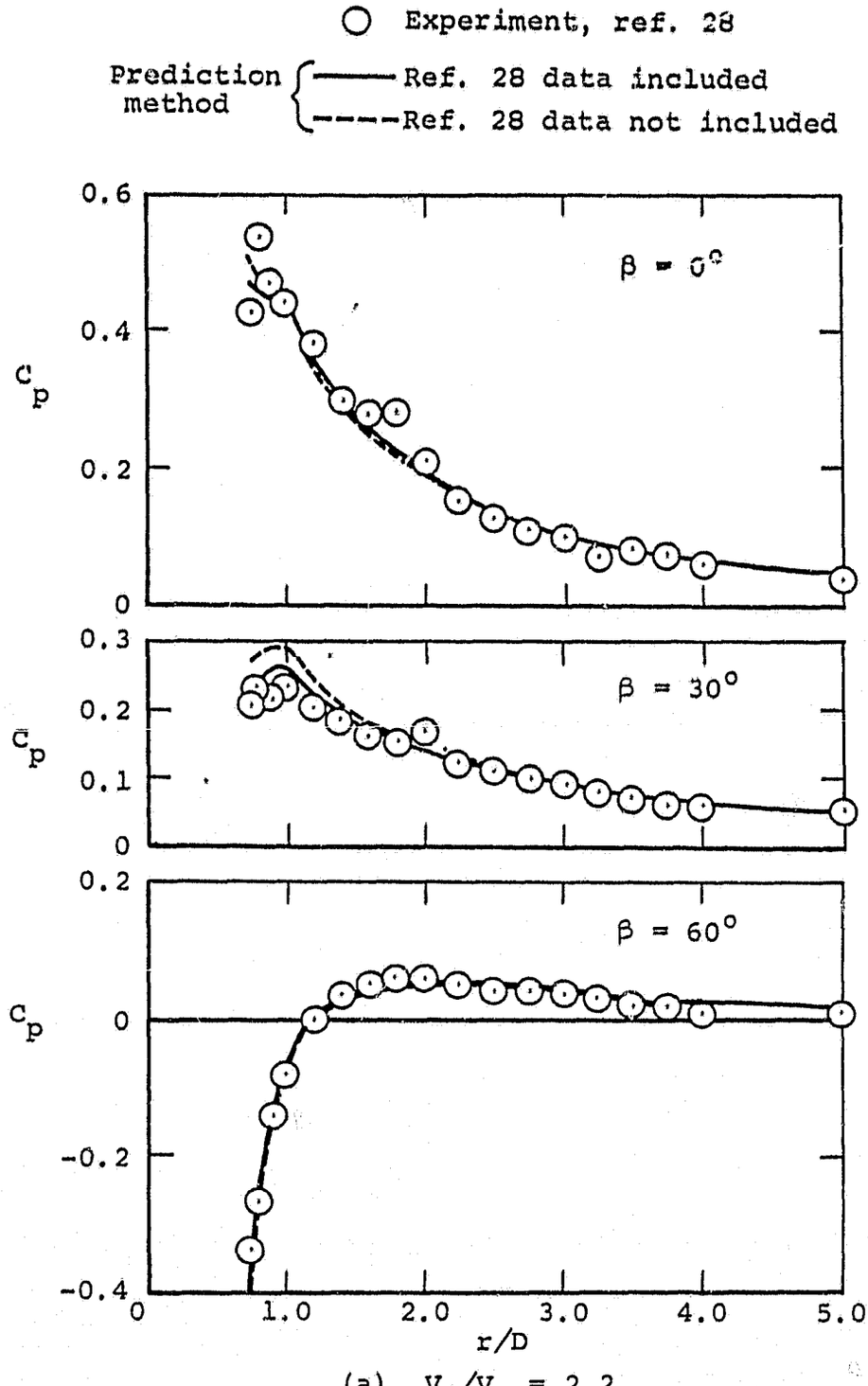

(a) $V_j/V_\infty = 2.2$

Figure 30.- Comparison of measured and predicted pressures on a flat plate from which a jet is exhausting into a crossflow, $\theta = 0°$.

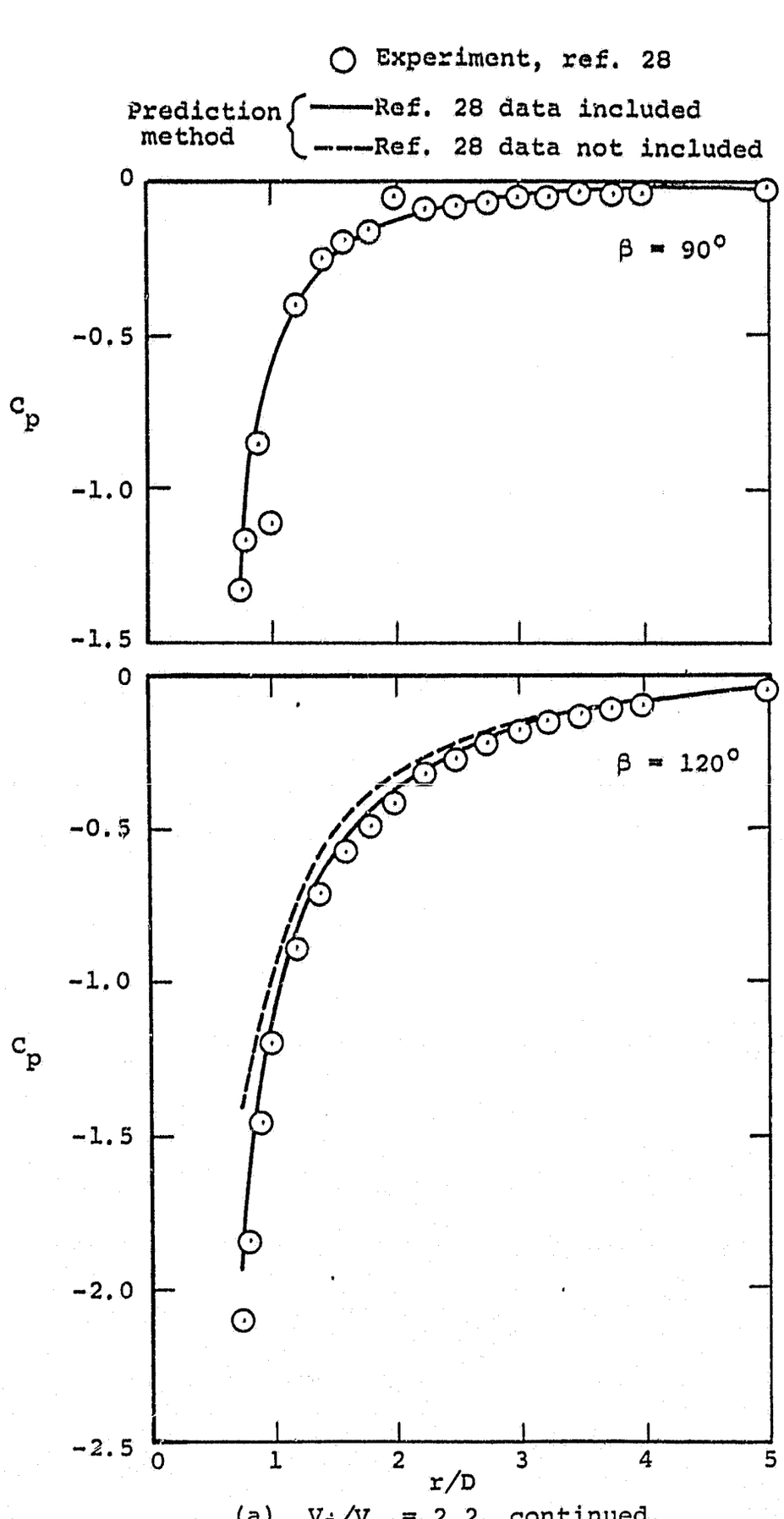

(a) V_j/V_∞ = 2.2, continued.

Figure 30.- Continued.

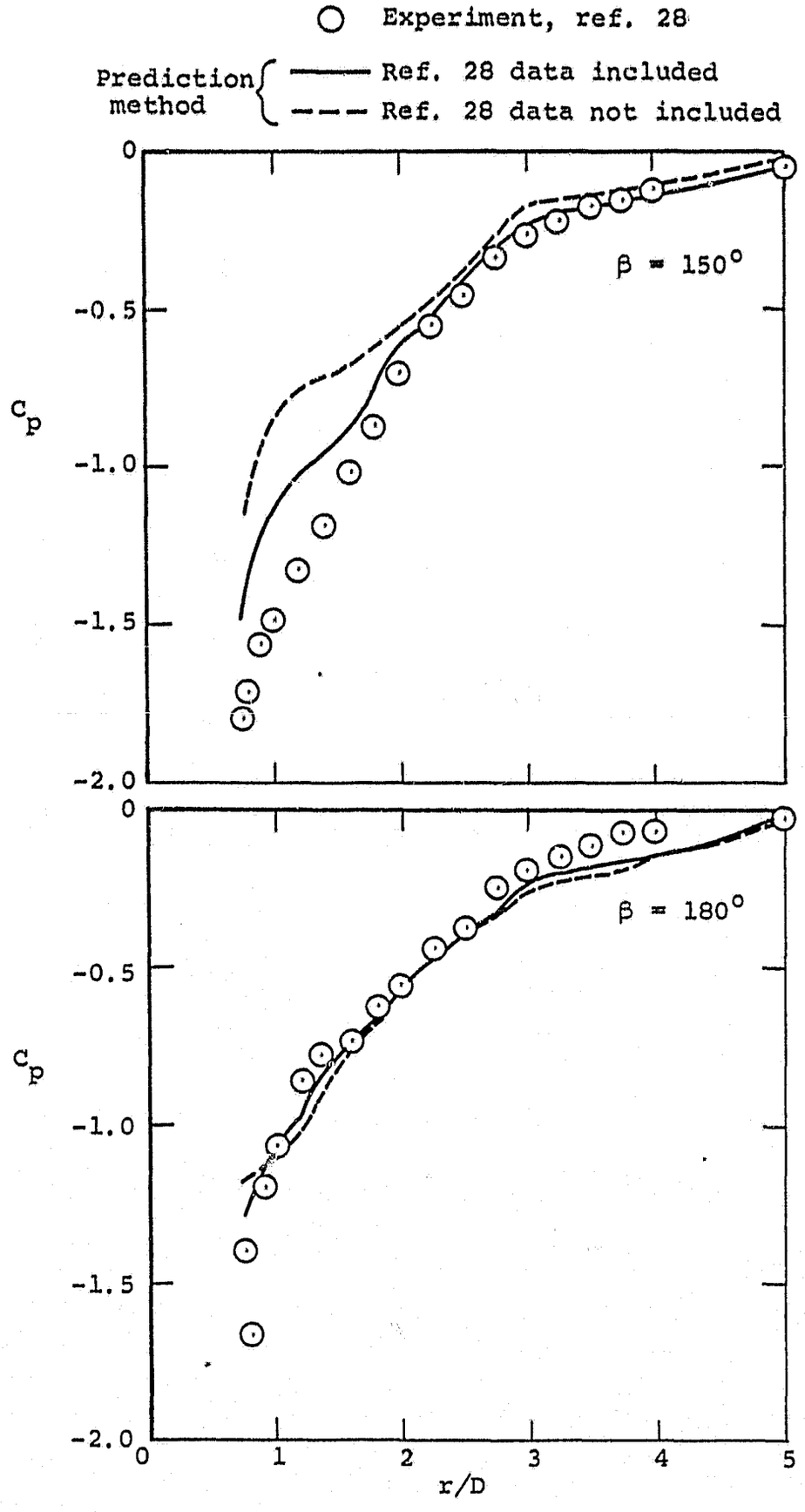

(a) $V_j/V_\infty = 2.2$, concluded.
Figure 30.- Continued.

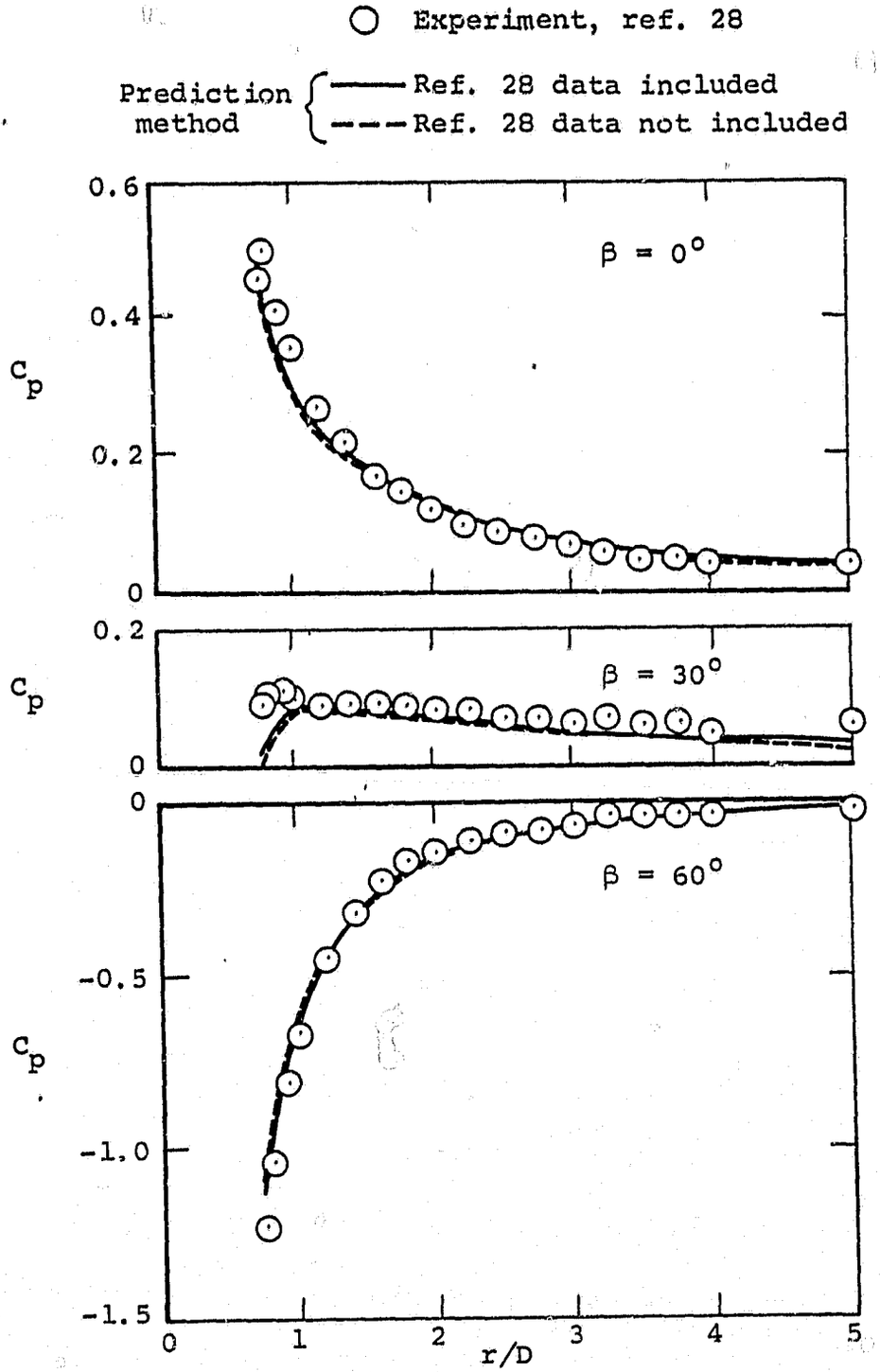

(b) $V_j/V_\infty = 3.9$

Figure 30.- Continued.

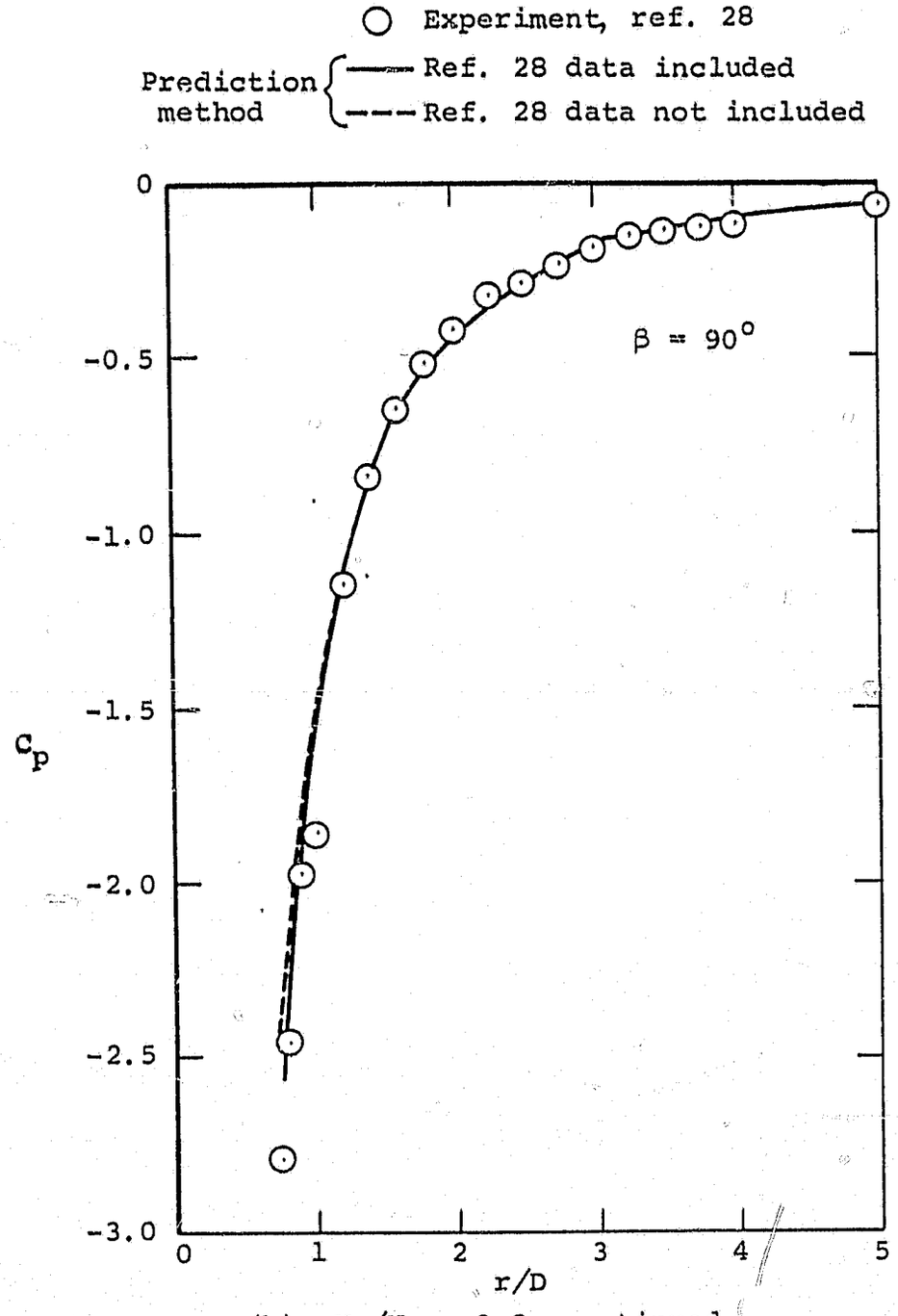

(b) $V_j/V_\infty = 3.9$, continued.

Figure 30.- Continued.

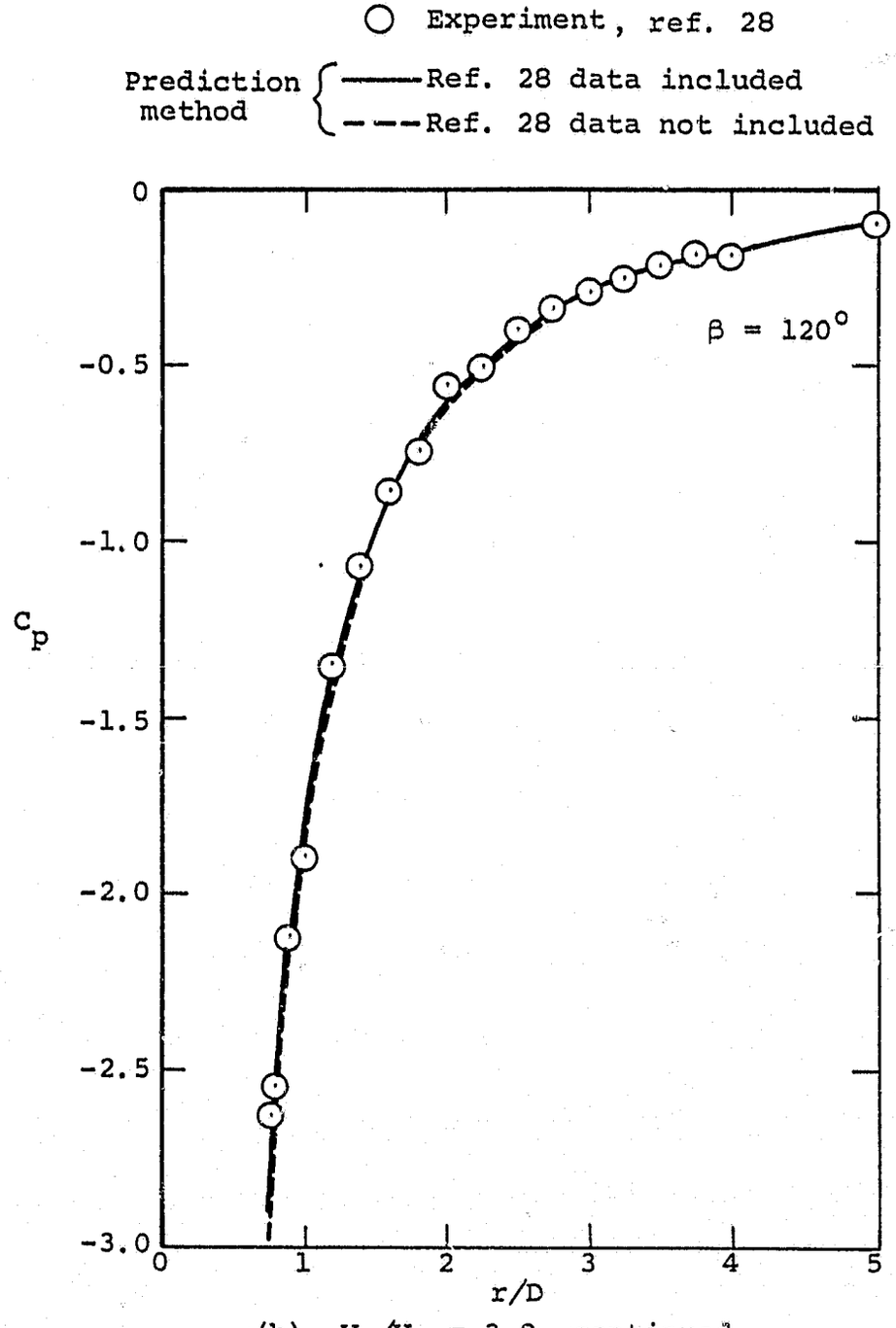

(b) V_j/V_∞ = 3.9, continued.

Figure 30.- Continued.

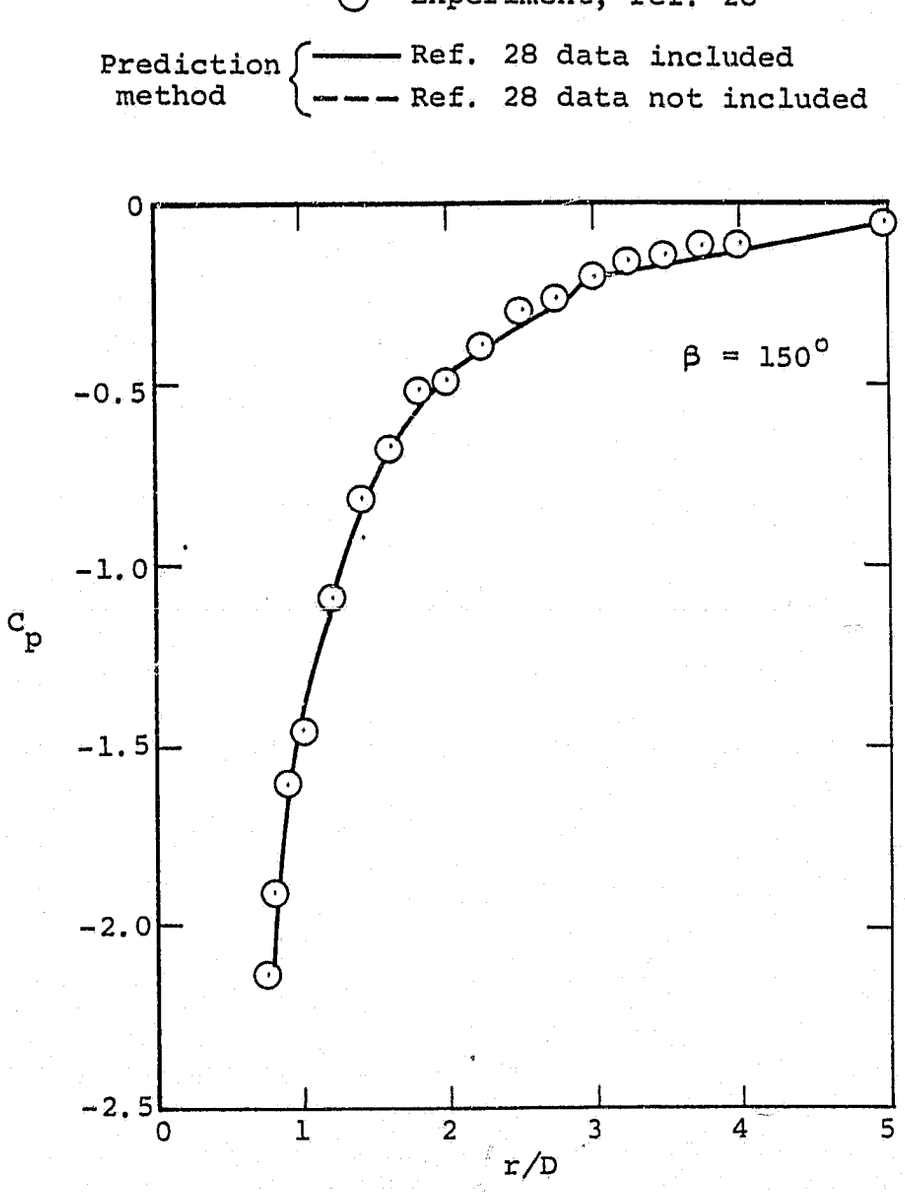

(b) V_j/V_∞ = 3.9, continued.

Figure 30.- Continued.

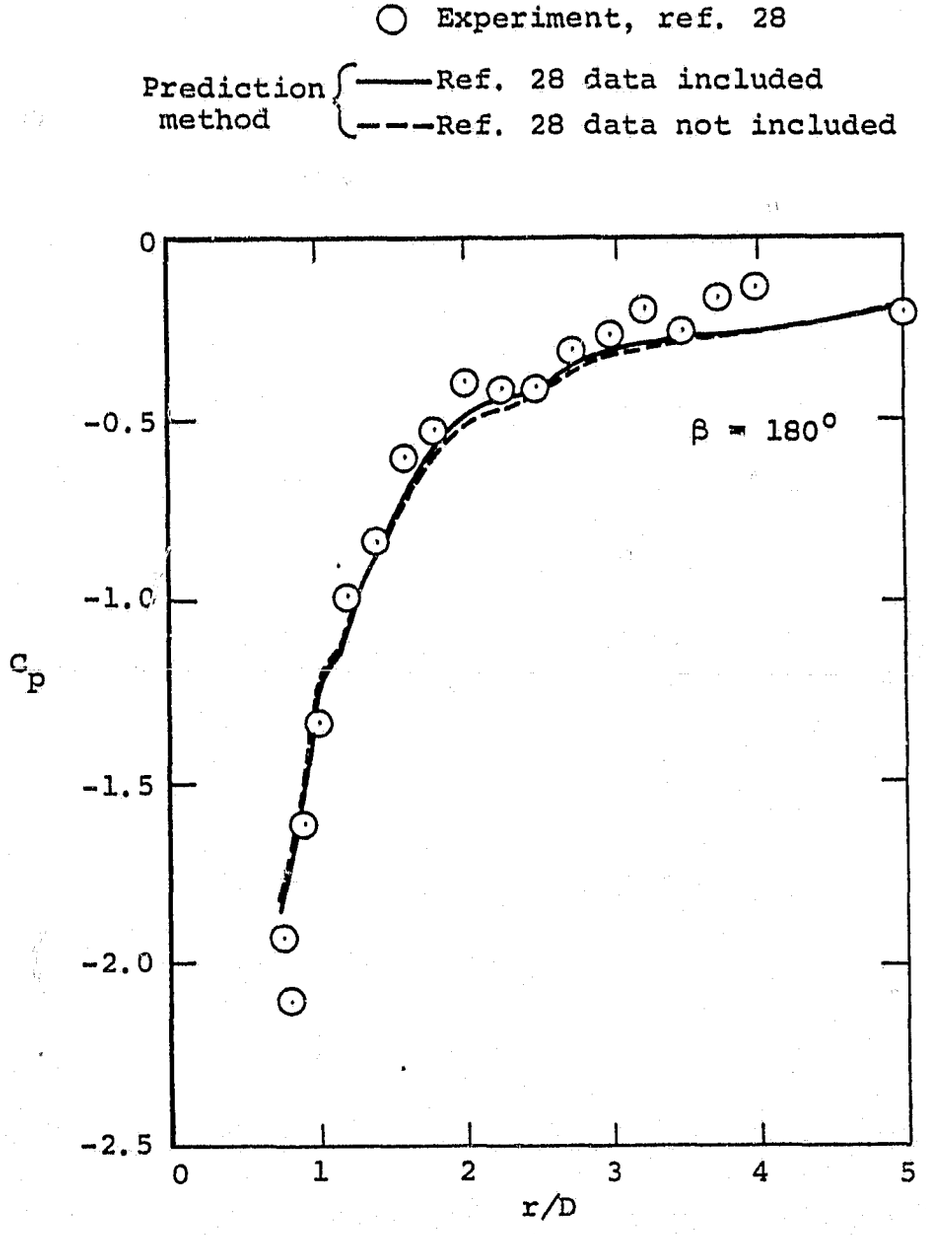

(b) $V_j/V_\infty = 3.9$, concluded.

Figure 30.- Continued.

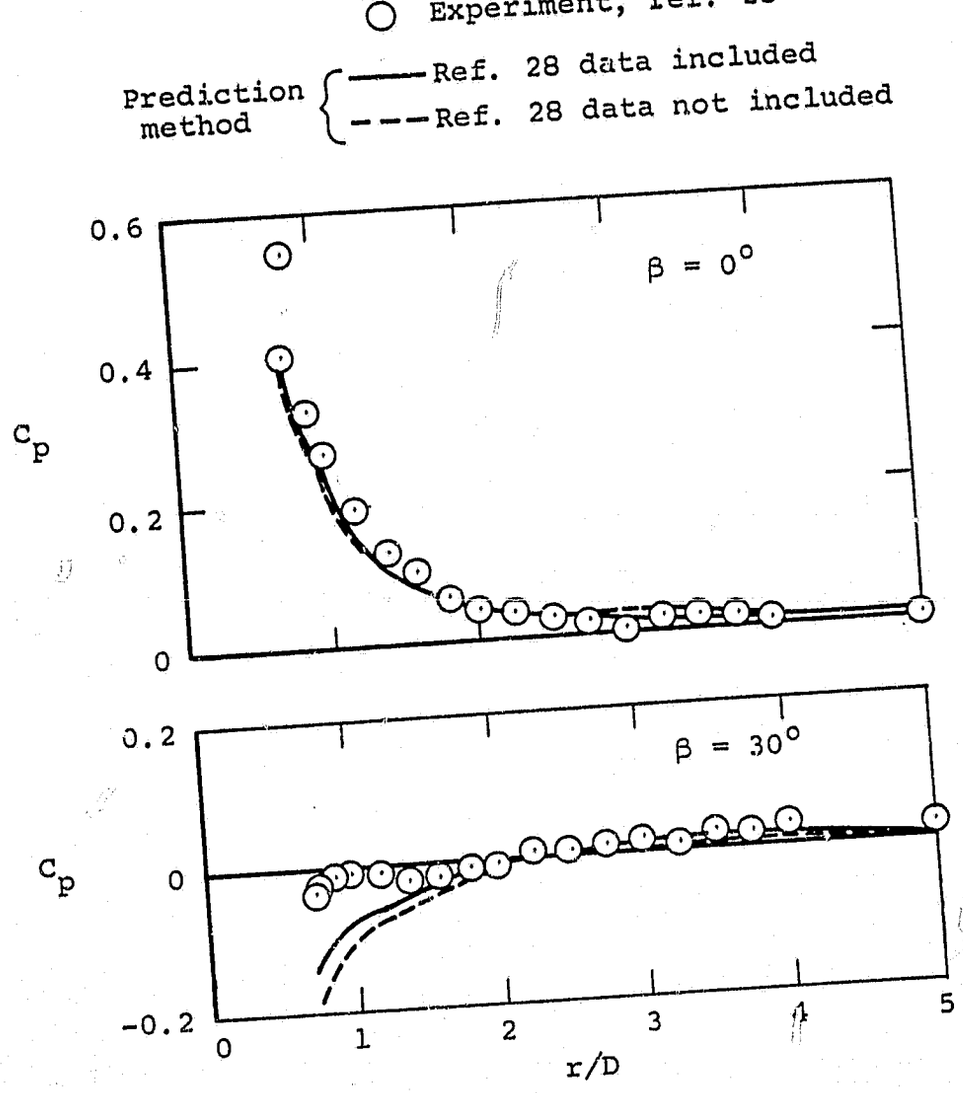

(c) $V_j/V_\infty \doteq 5.1$

Figure 30.- Continued.

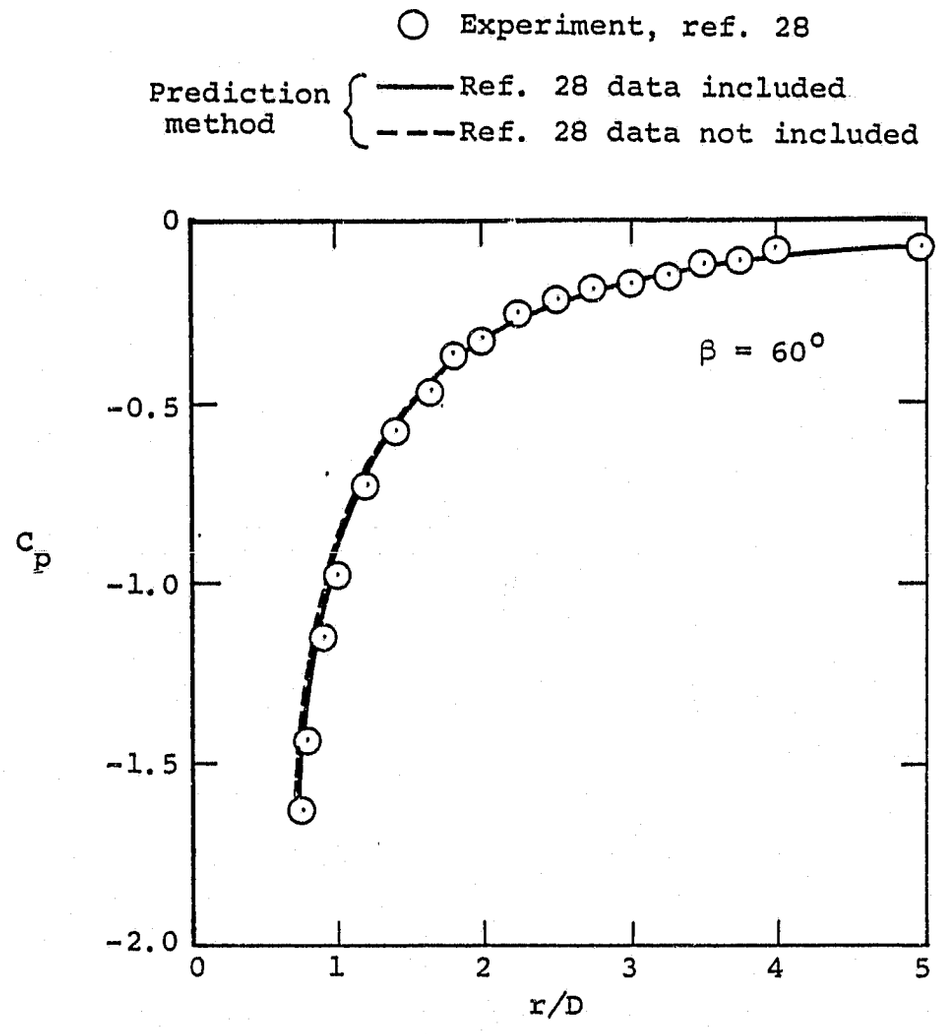

(c) $V_j/V_\infty = 5.1$, continued.

Figure 30. - Continued.

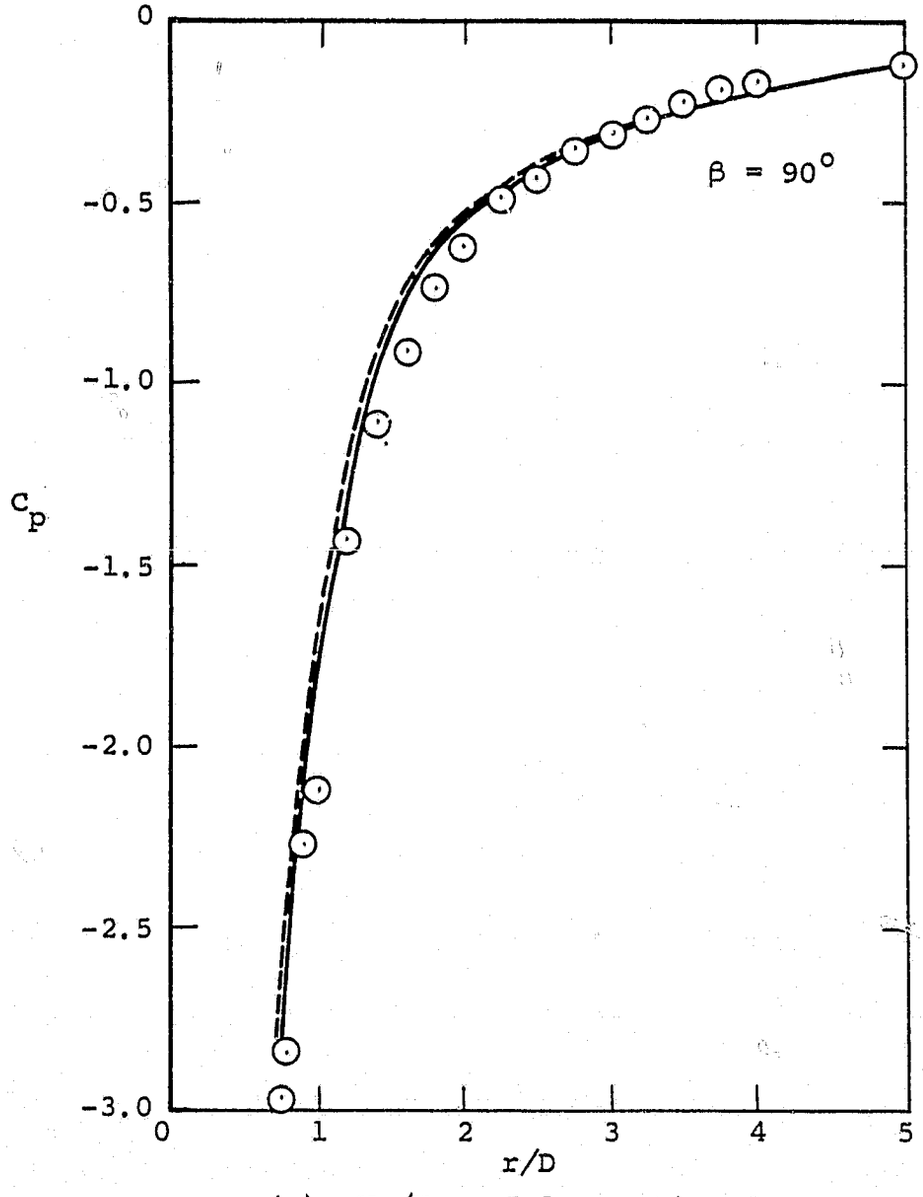

(c) V_j/V_∞ = 5.1, continued.

Figure 30.- Continued.

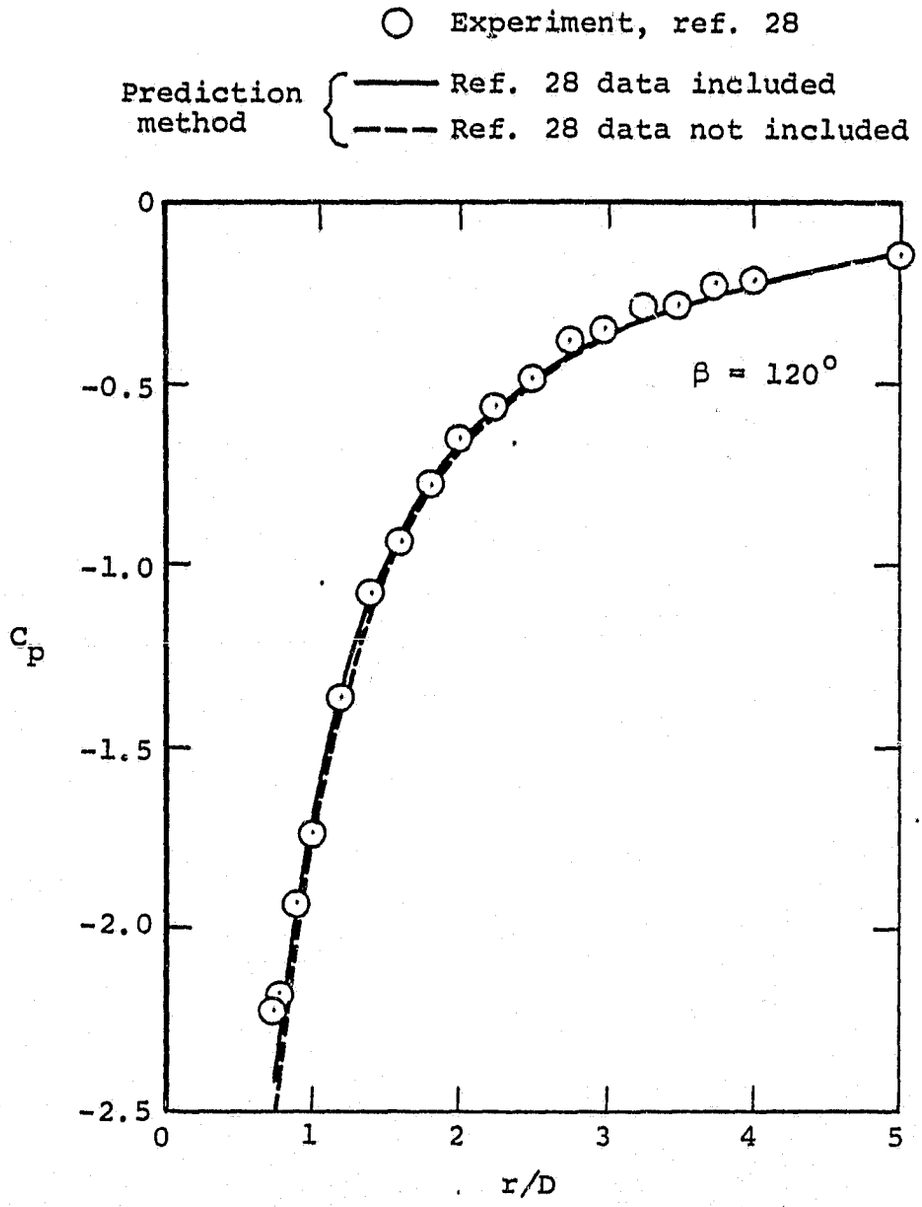

(c) V_j/V_∞ = 5.1, continued.

Figure 30.- Continued.

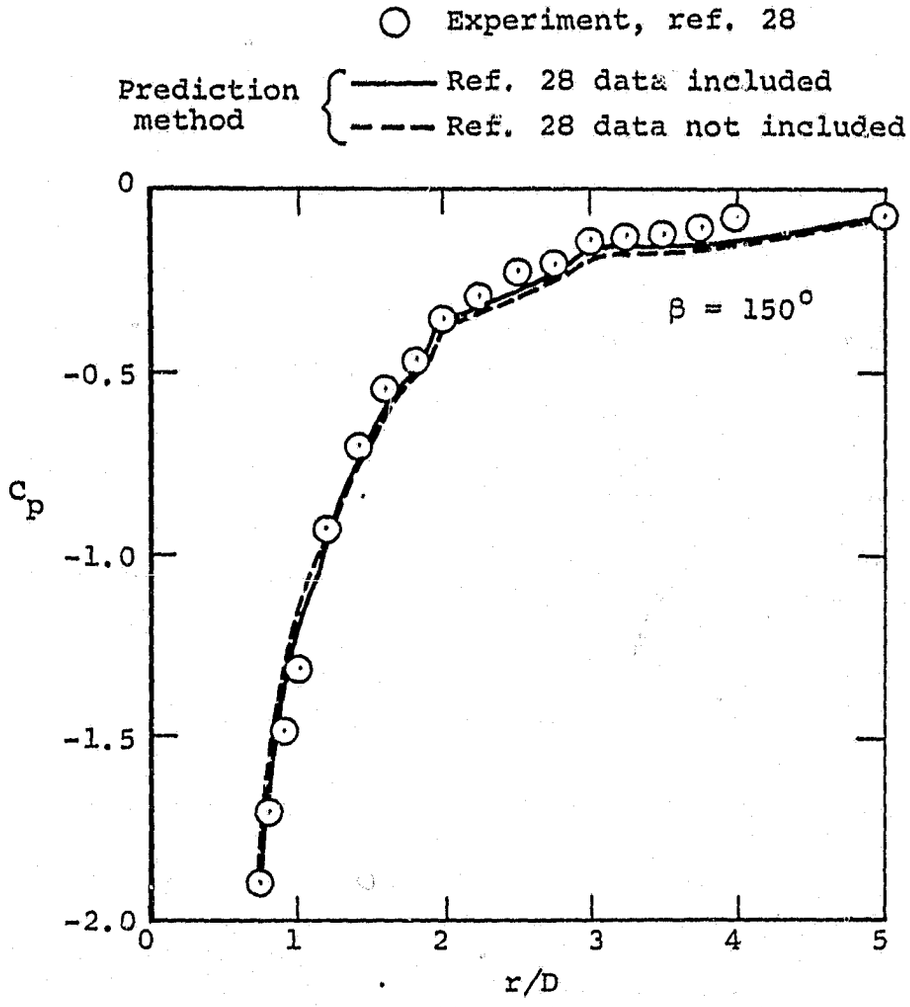

(c) V_j/V_∞ = 5.1, continued.

Figure 30.- Continued.

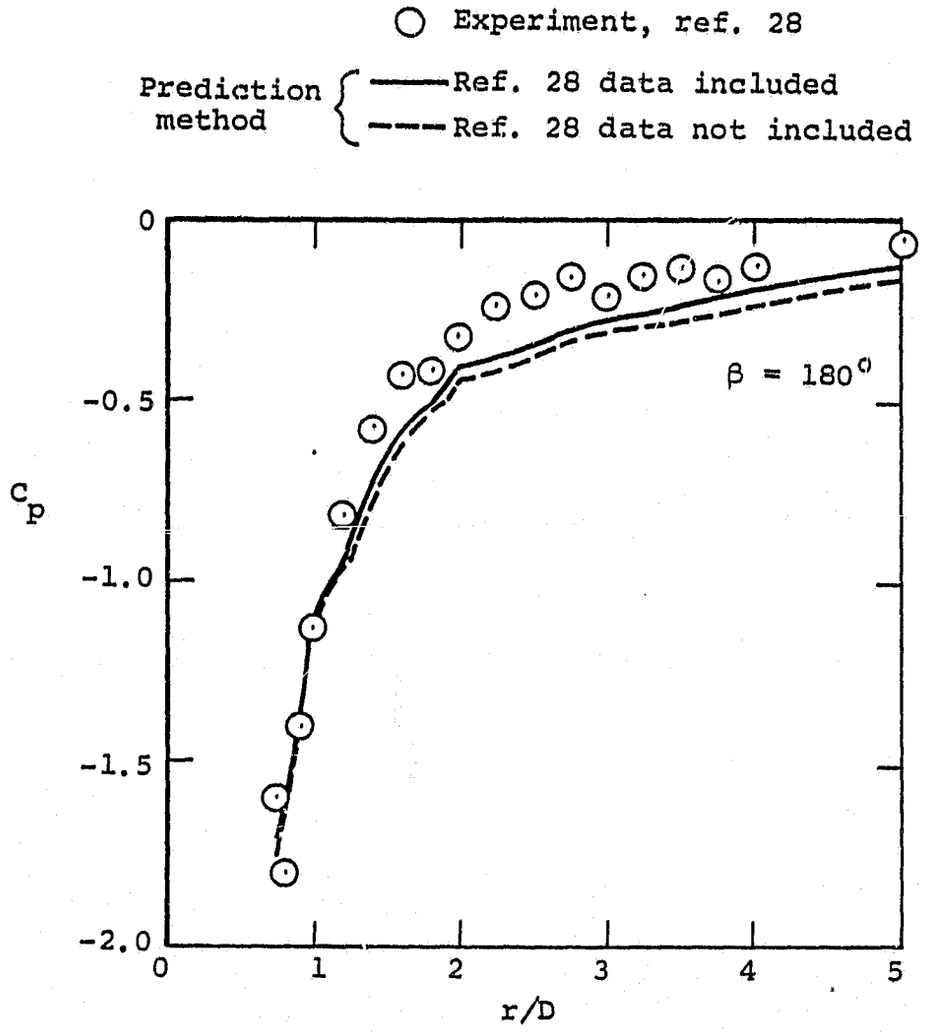

(c) V_j/V_∞ = 5.1, concluded.

Figure 30.- Continued.

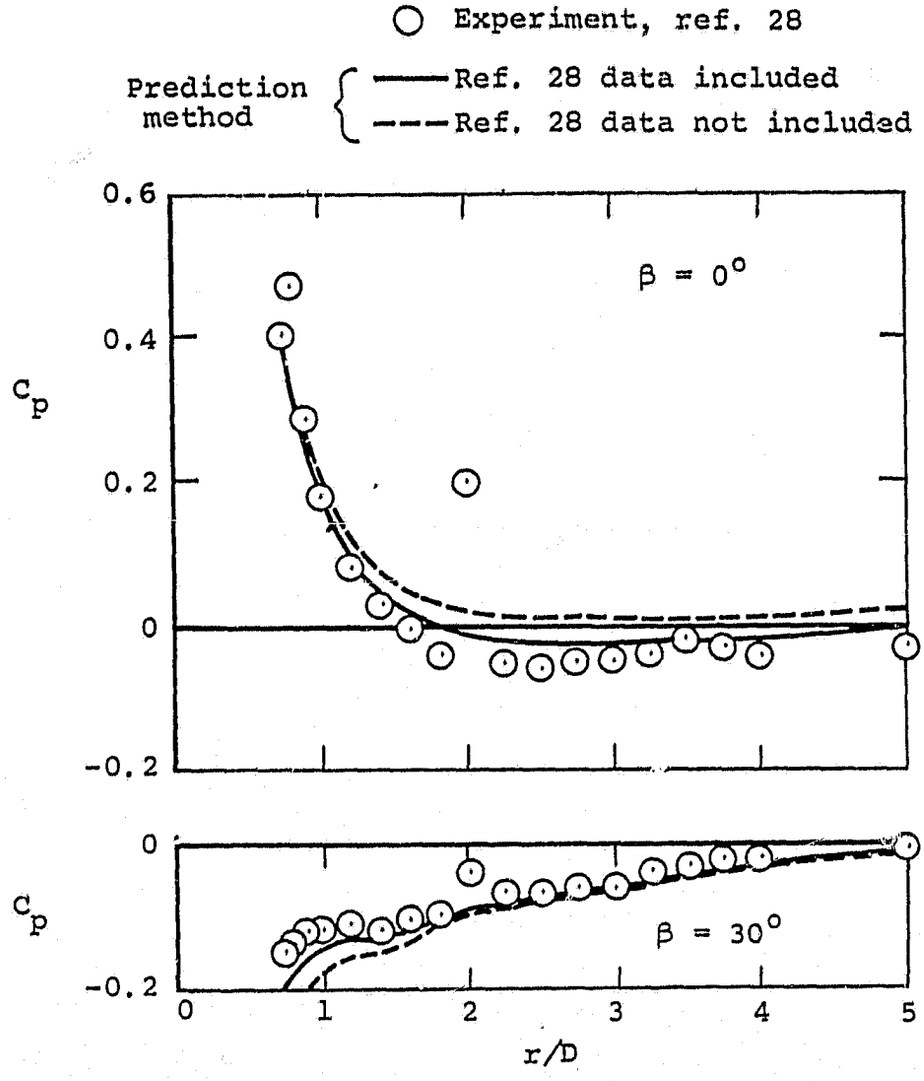

(d) $V_j/V_\infty = 6.1$

Figure 30.- Continued.

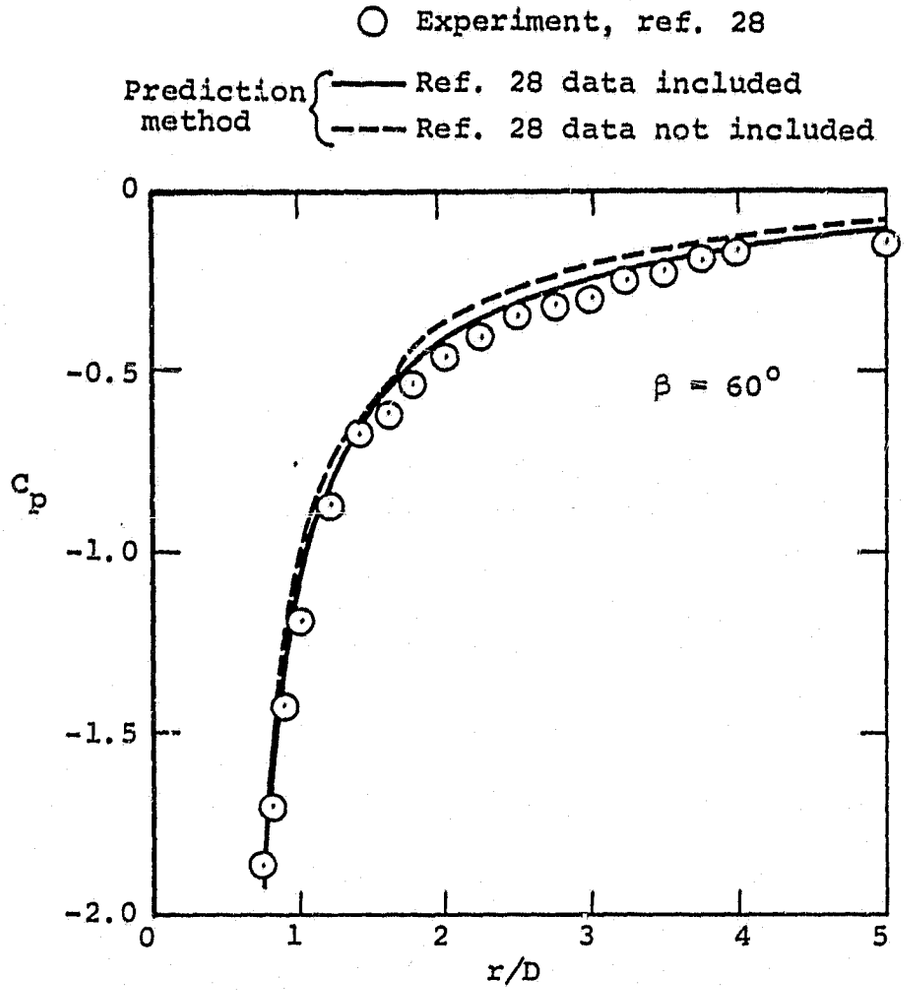

(d) V_j/V_∞ = 6.1, continued.

Figure 30.- Continued.

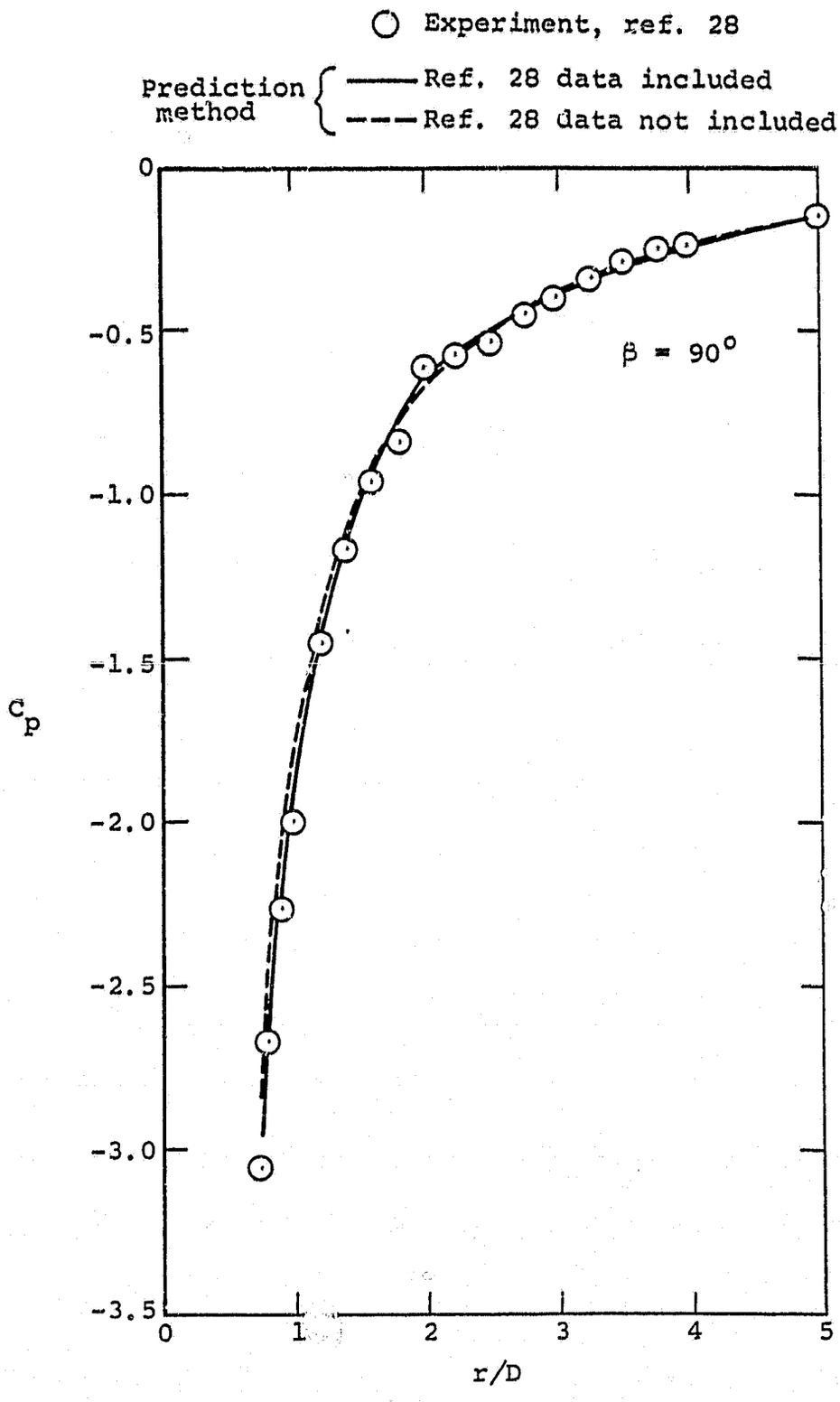

(d) $V_j/V_\infty = 6.1$, continued.

Figure 30.- Continued.

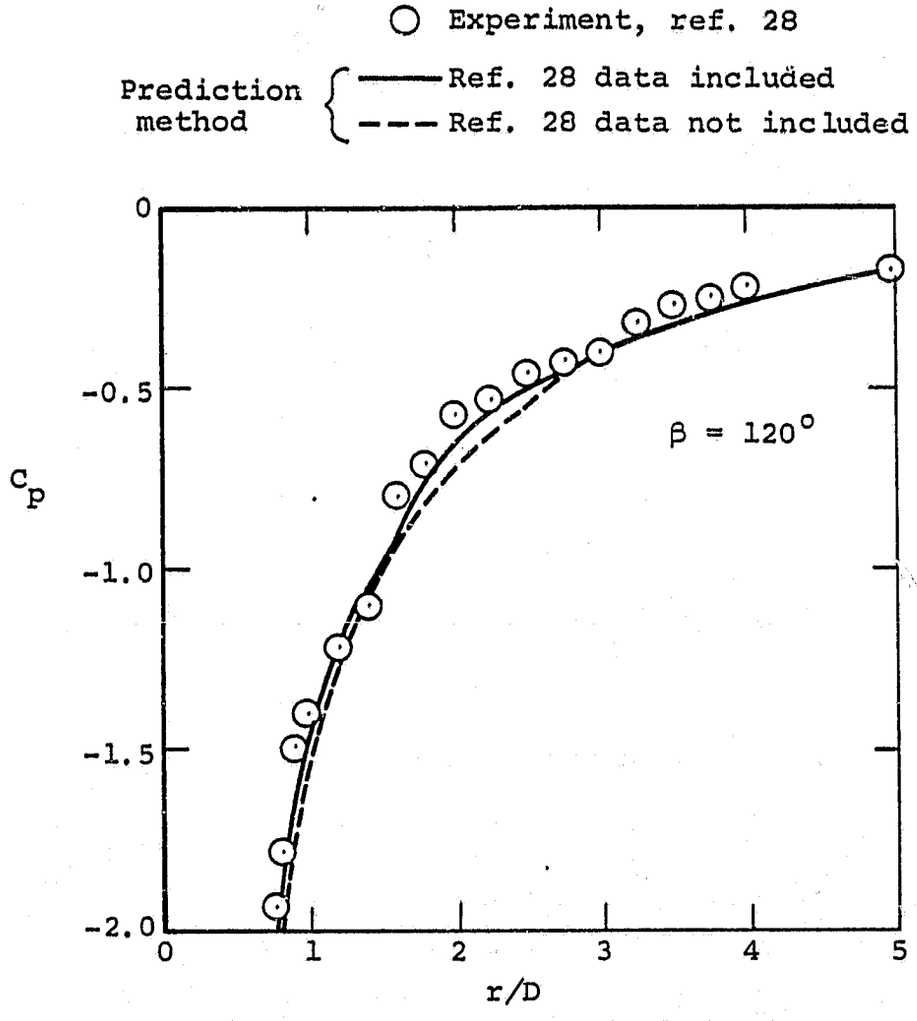

(d) $V_j/V_\infty = 6.1$, continued.

Figure 30.- Continued.

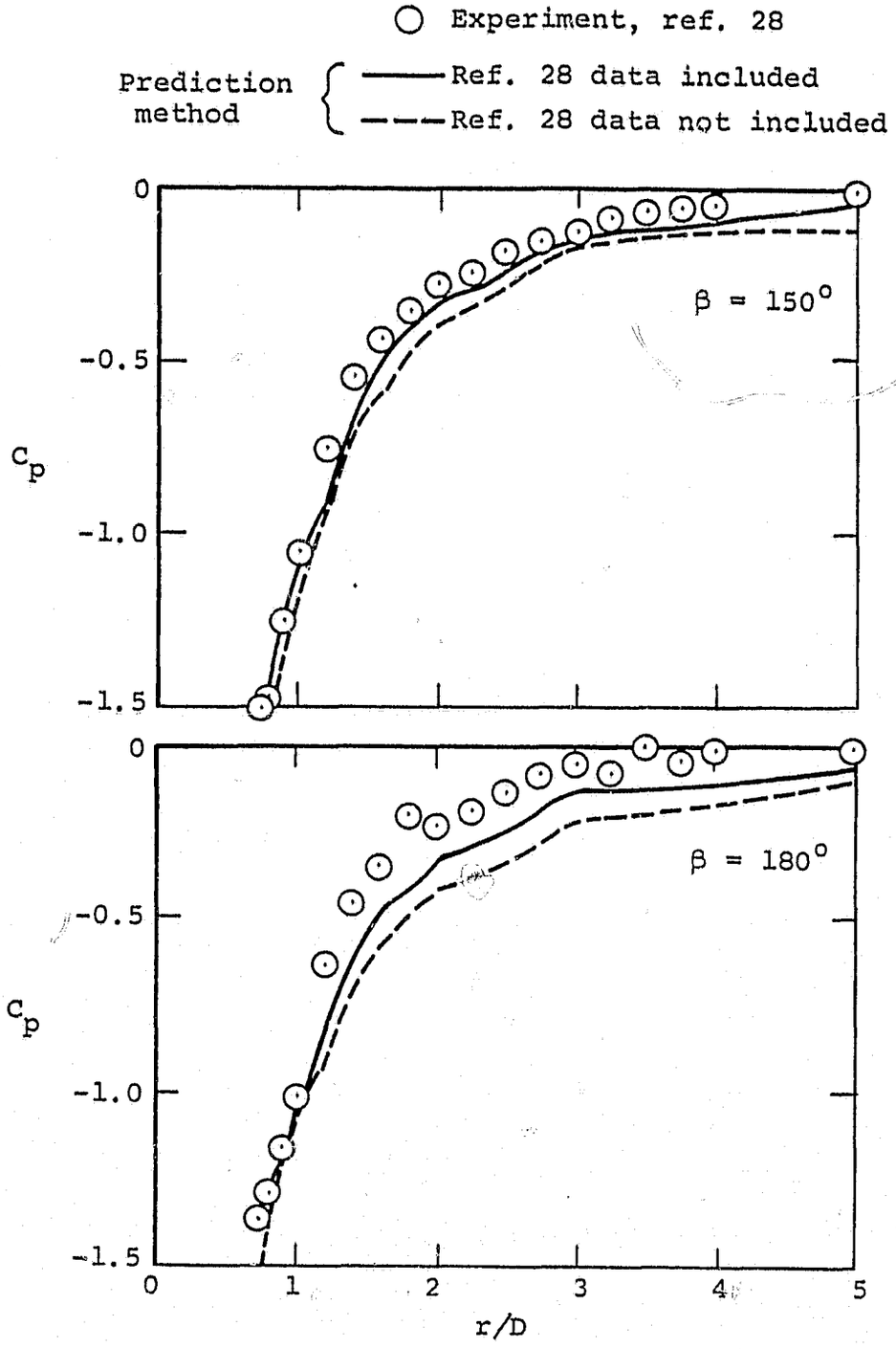

(d) V_j/V_∞ = 6.1, concluded.

Figure 30.- Continued.

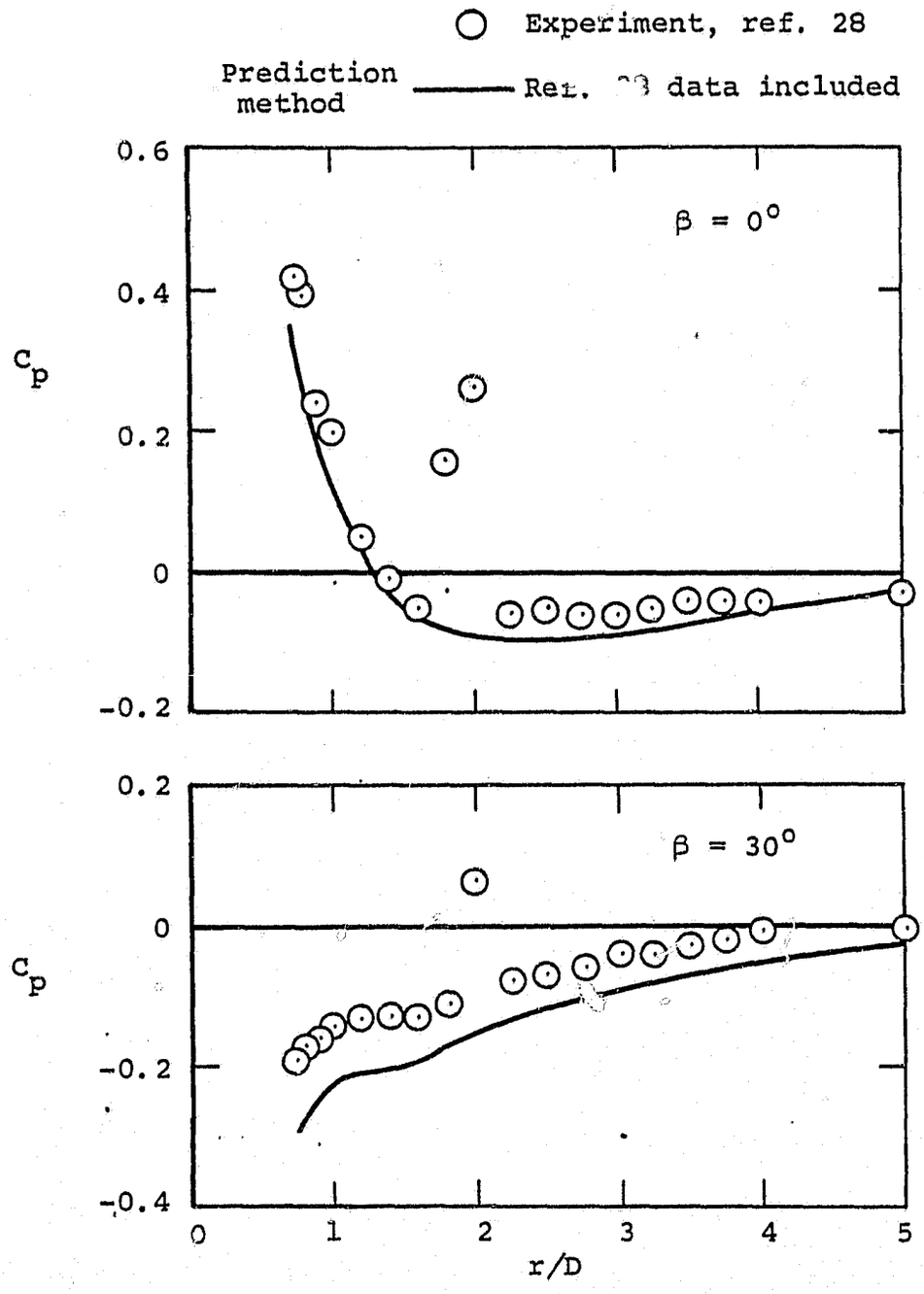

(e) $V_j/V_\infty = 7.0$

Figure 30.- Continued.

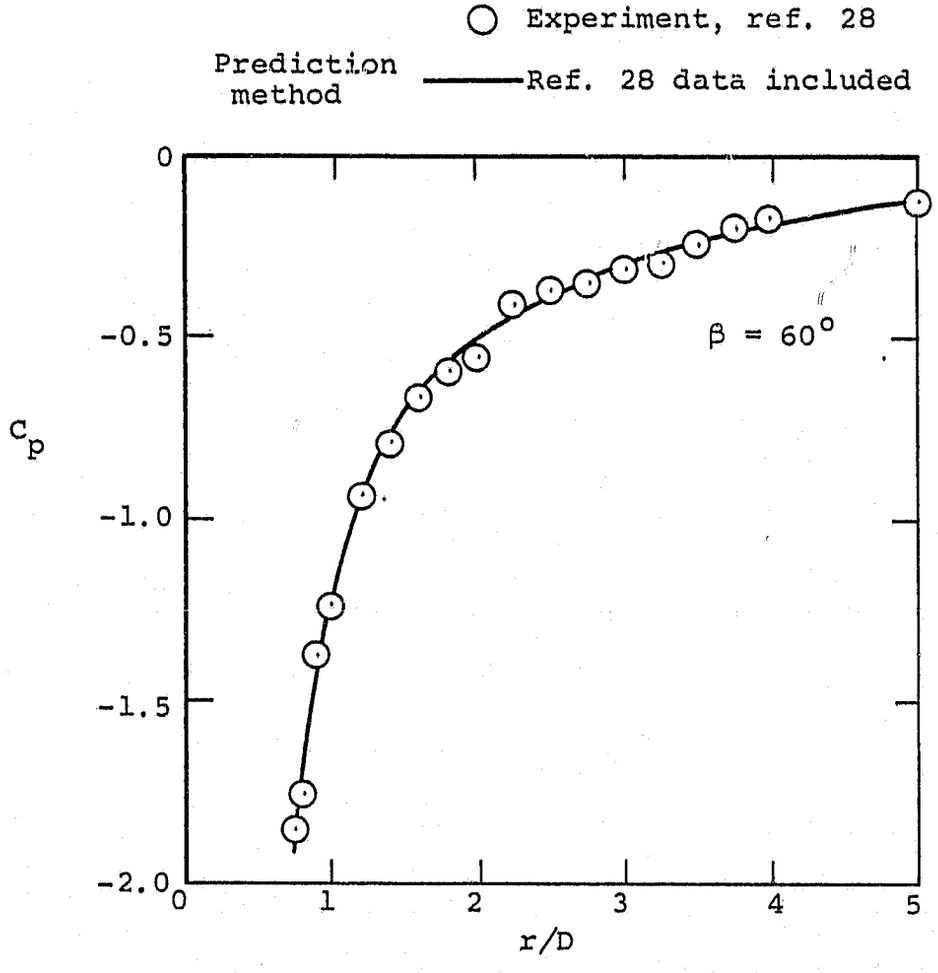

(e) $V_j/V_\infty = 7.0$, continued.

Figure 30.- Continued.

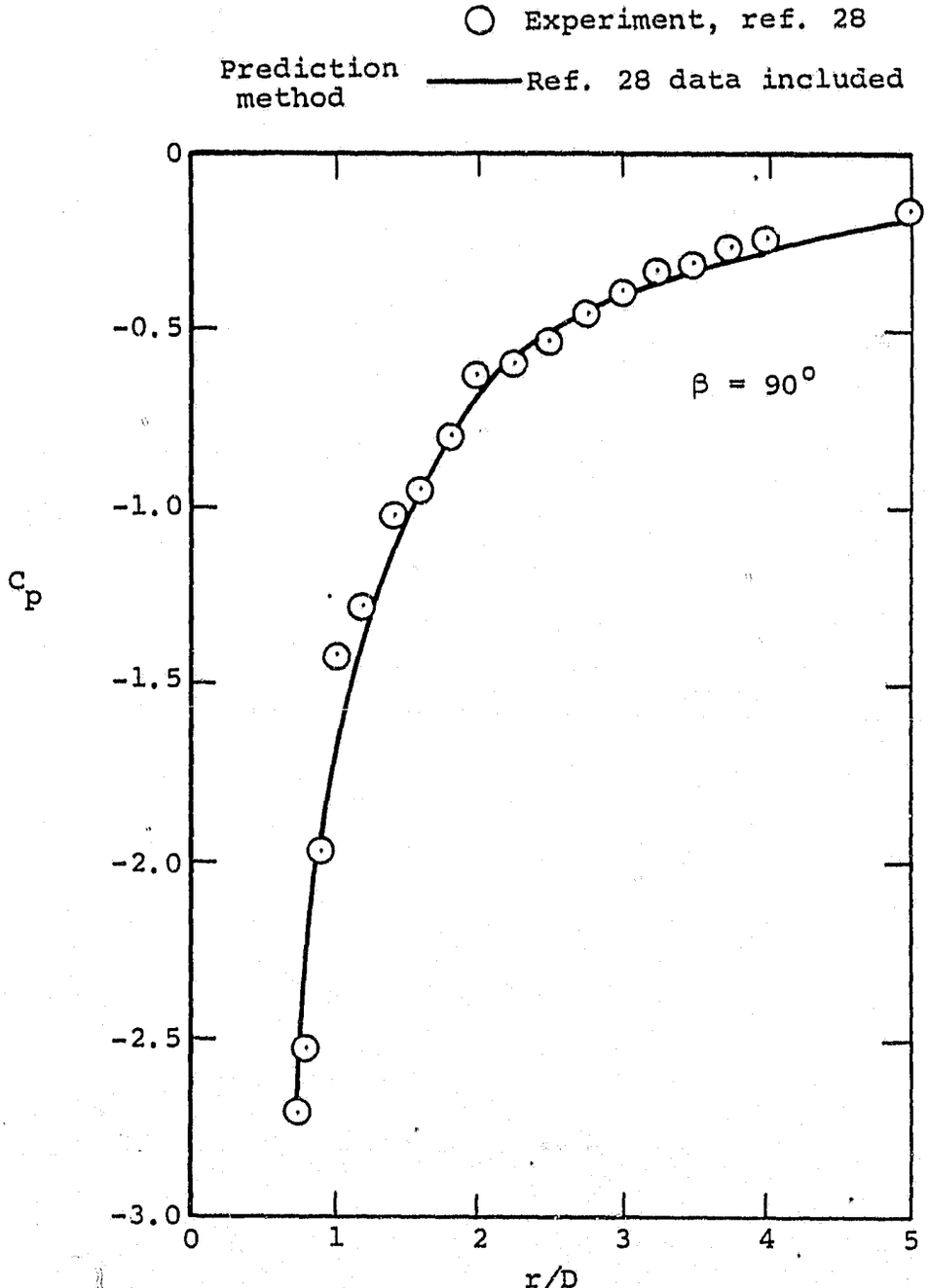

(e) $V_j/V_\infty = 7.0$, continued.

Figure 30.- Continued.

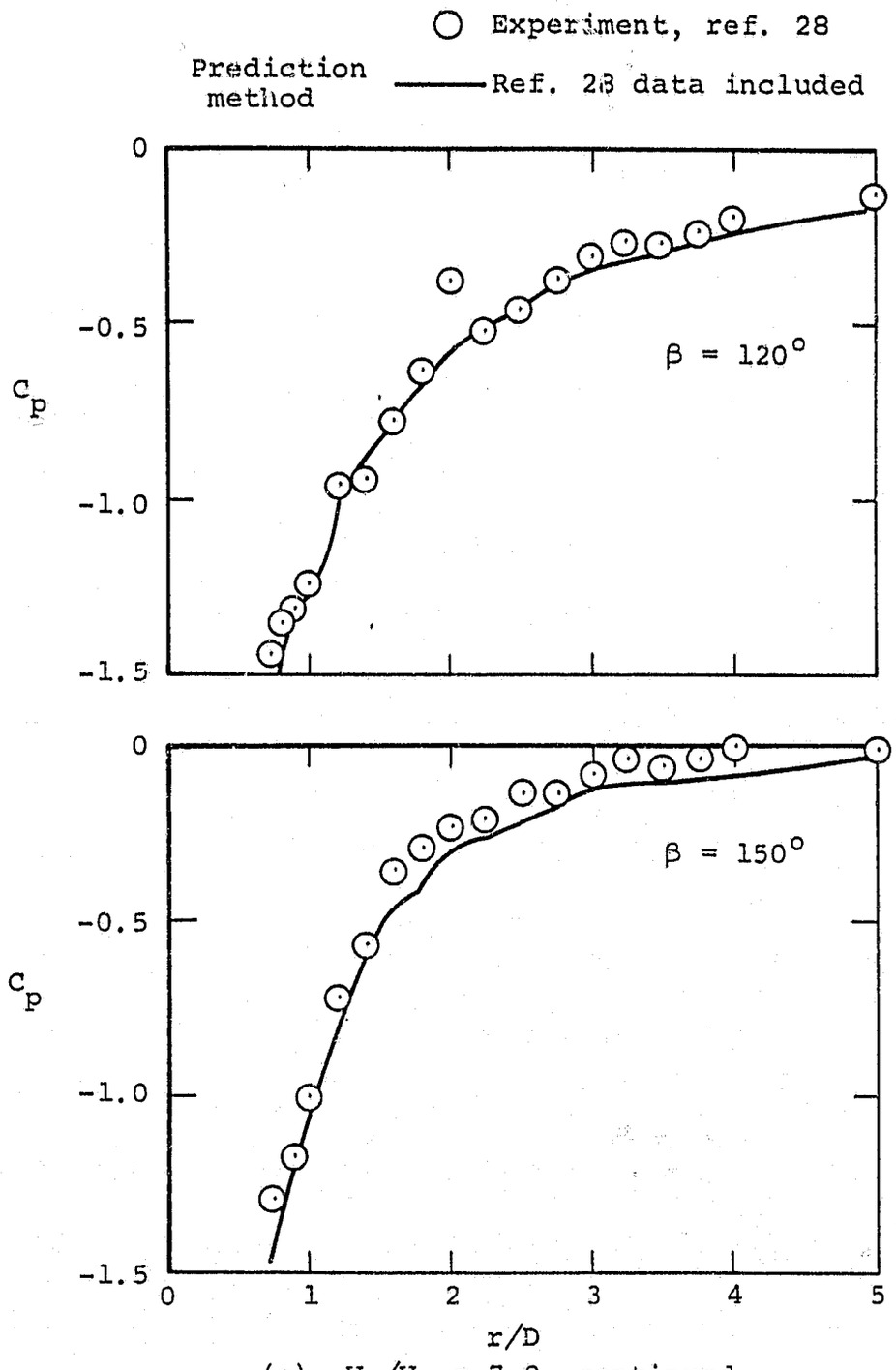

(e) V_j/V_∞ = 7.0, continued.

Figure 30.- Continued.

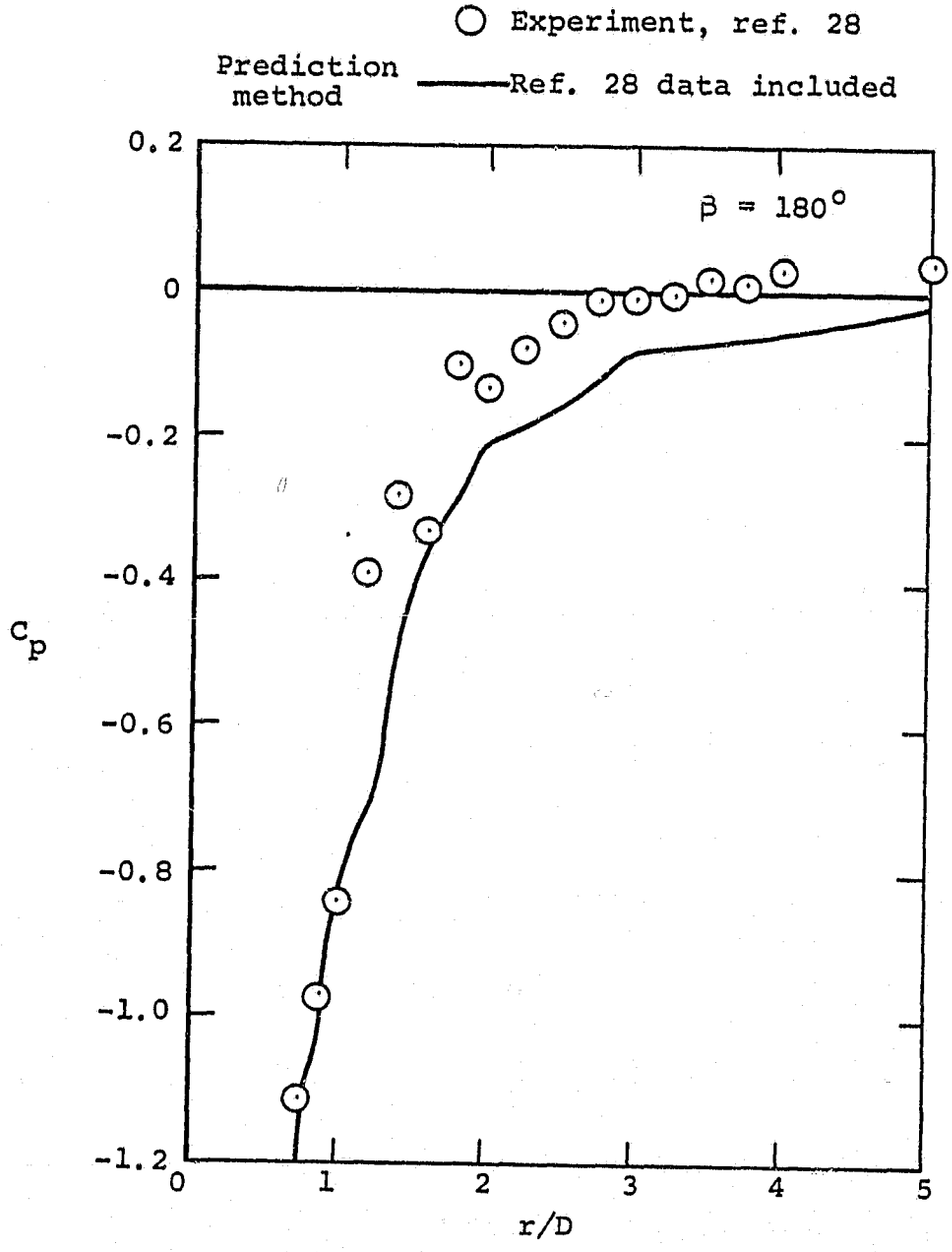

(e) V_j/V_∞ = 7.0, concluded.

Figure 30.- Continued.

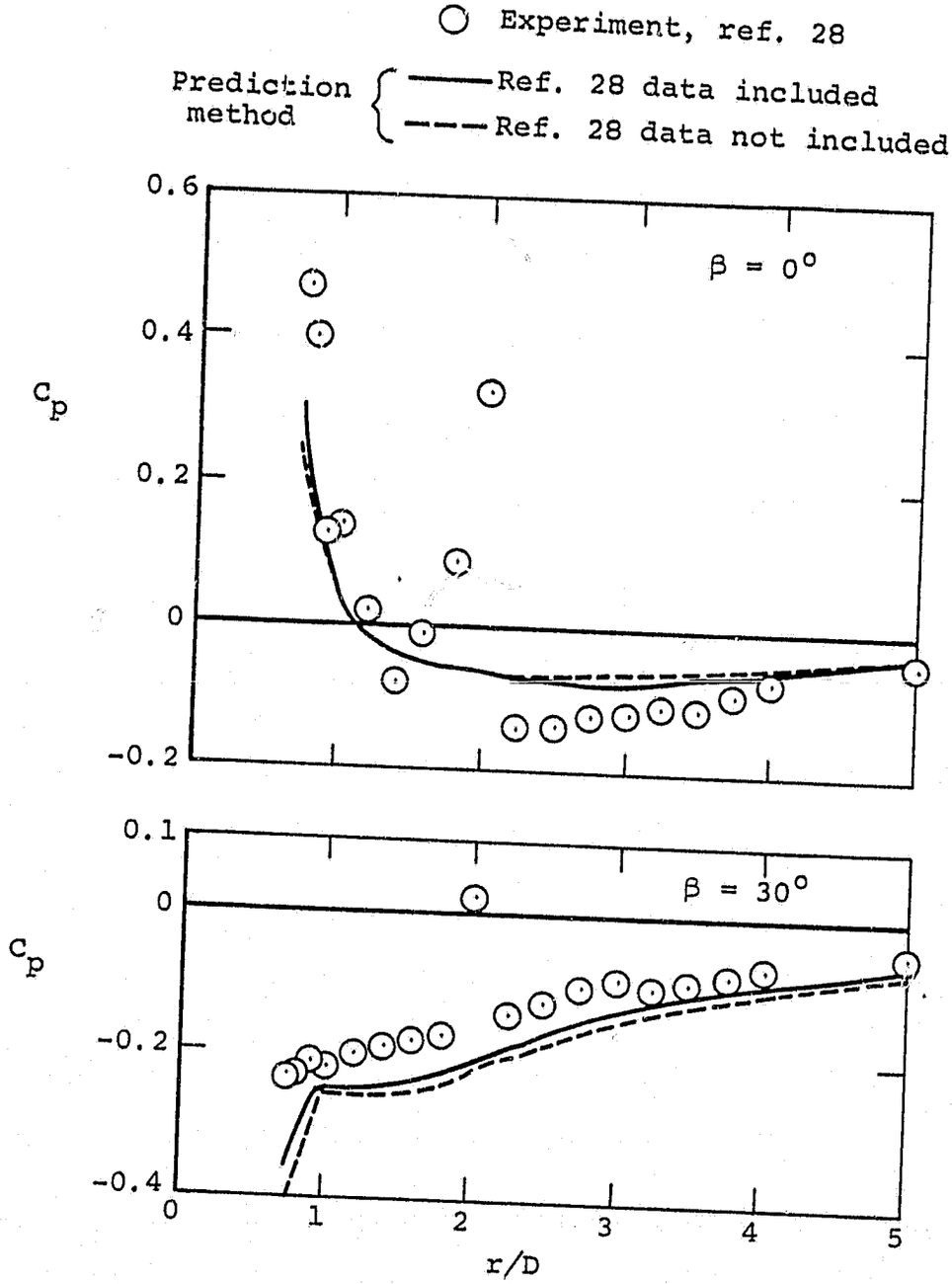

(f) $V_j/V_\infty = 8.0$

Figure 30.- Continued.

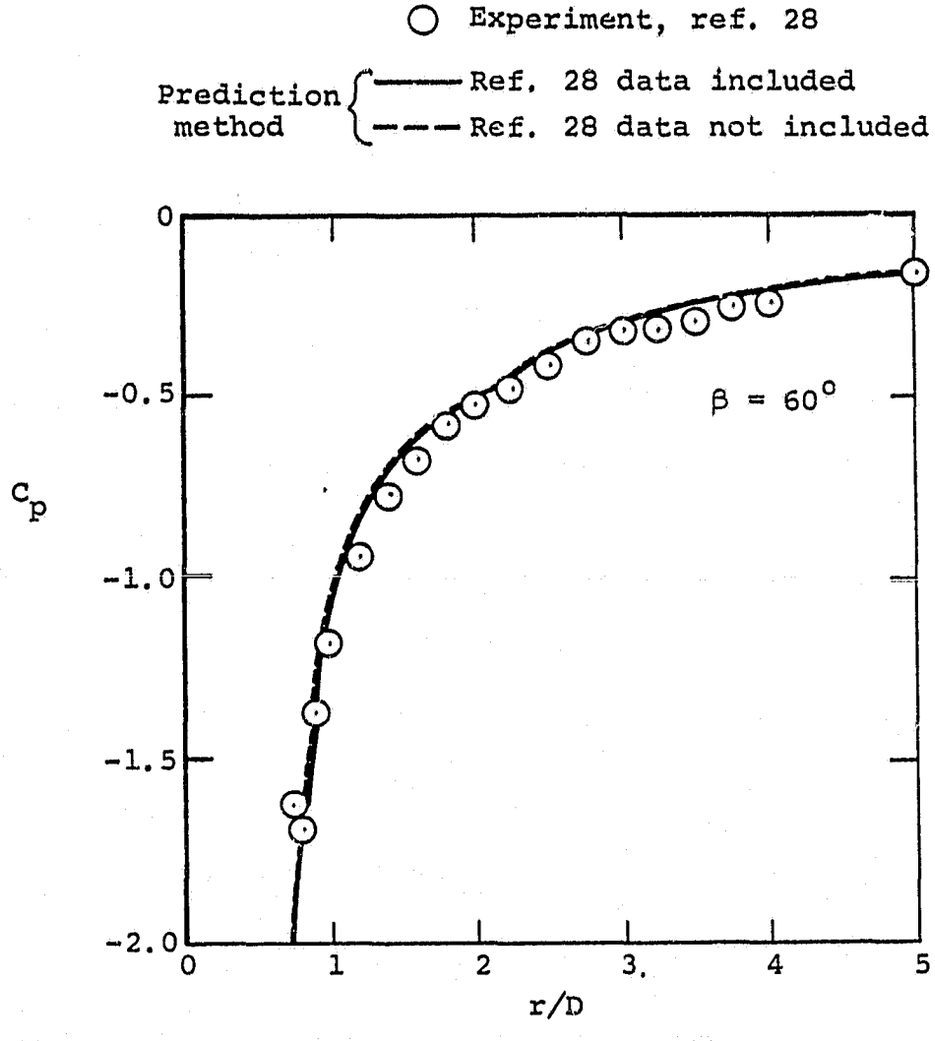

(f) $V_j/V_\infty = 8.0$, continued.

Figure 30.- Continued.

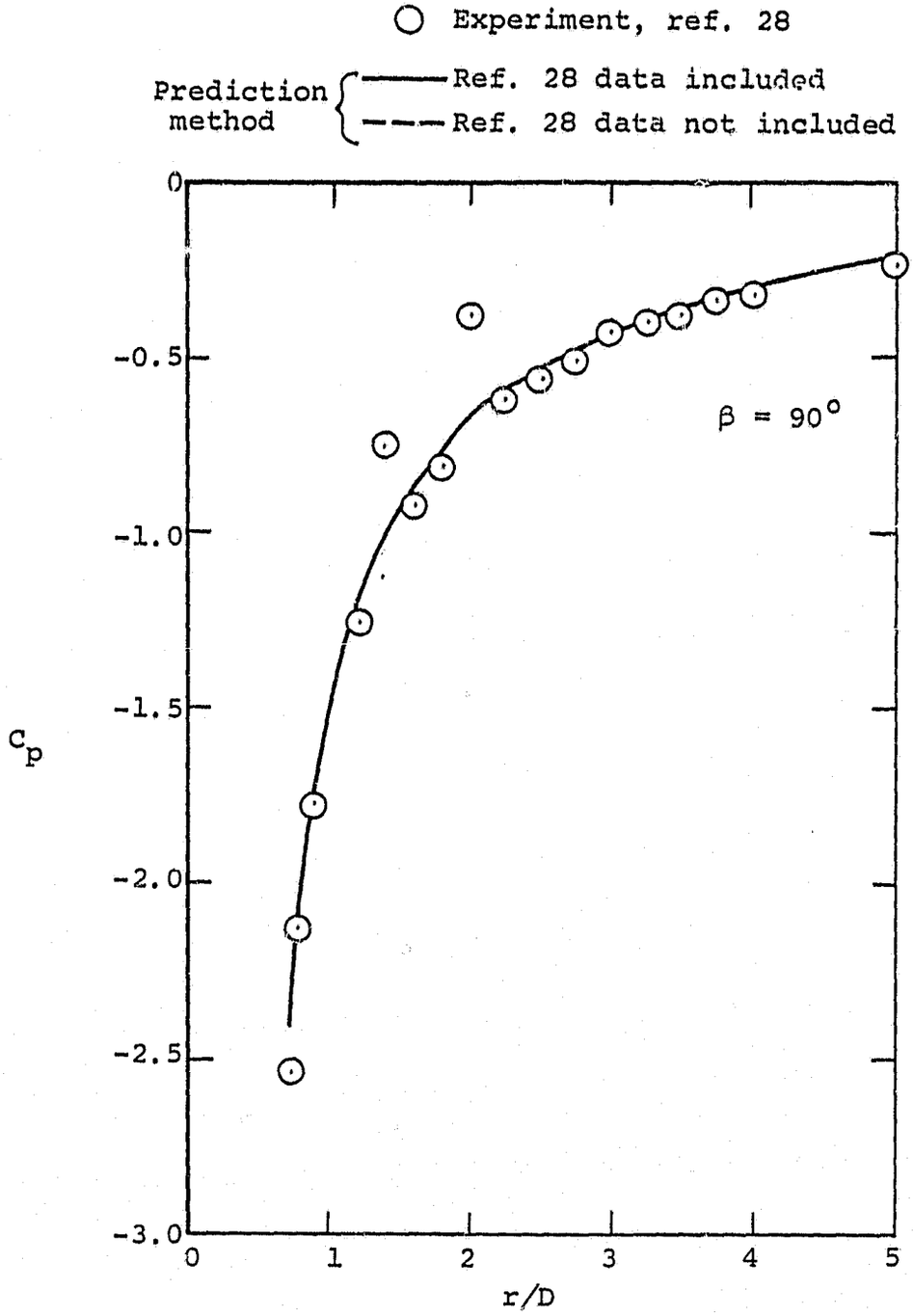

(f) V_j/V_∞ = 8.0, continued.

Figure 30.- Continued.

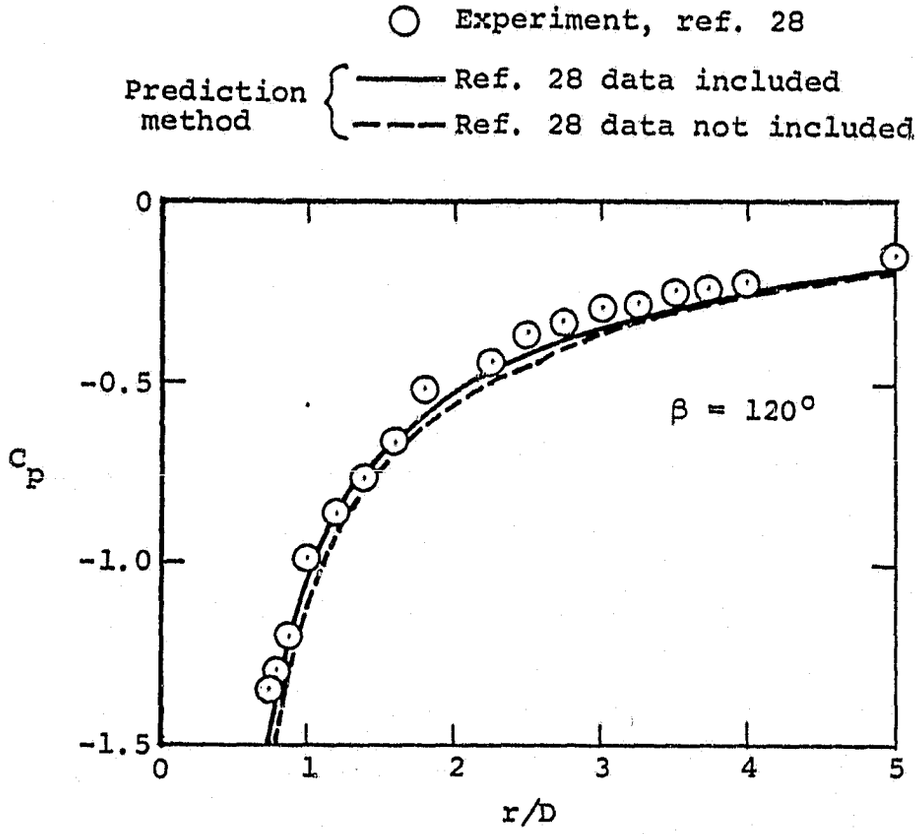

(f) V_j/V_∞ = 8.0, continued.

Figure 30.- Continued.

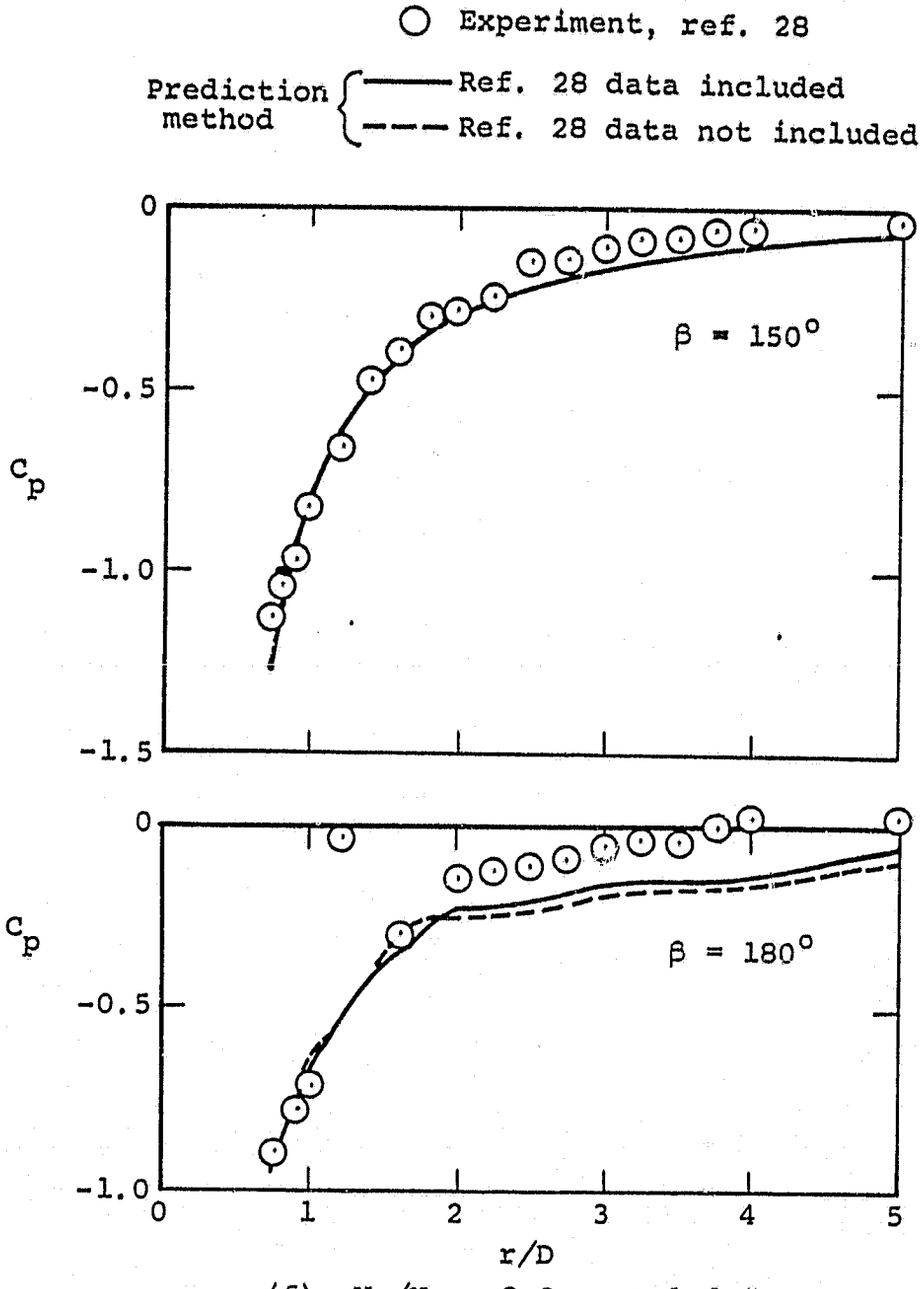

(f) V_j/V_∞ = 8.0, concluded.

Figure 30.- Continued.

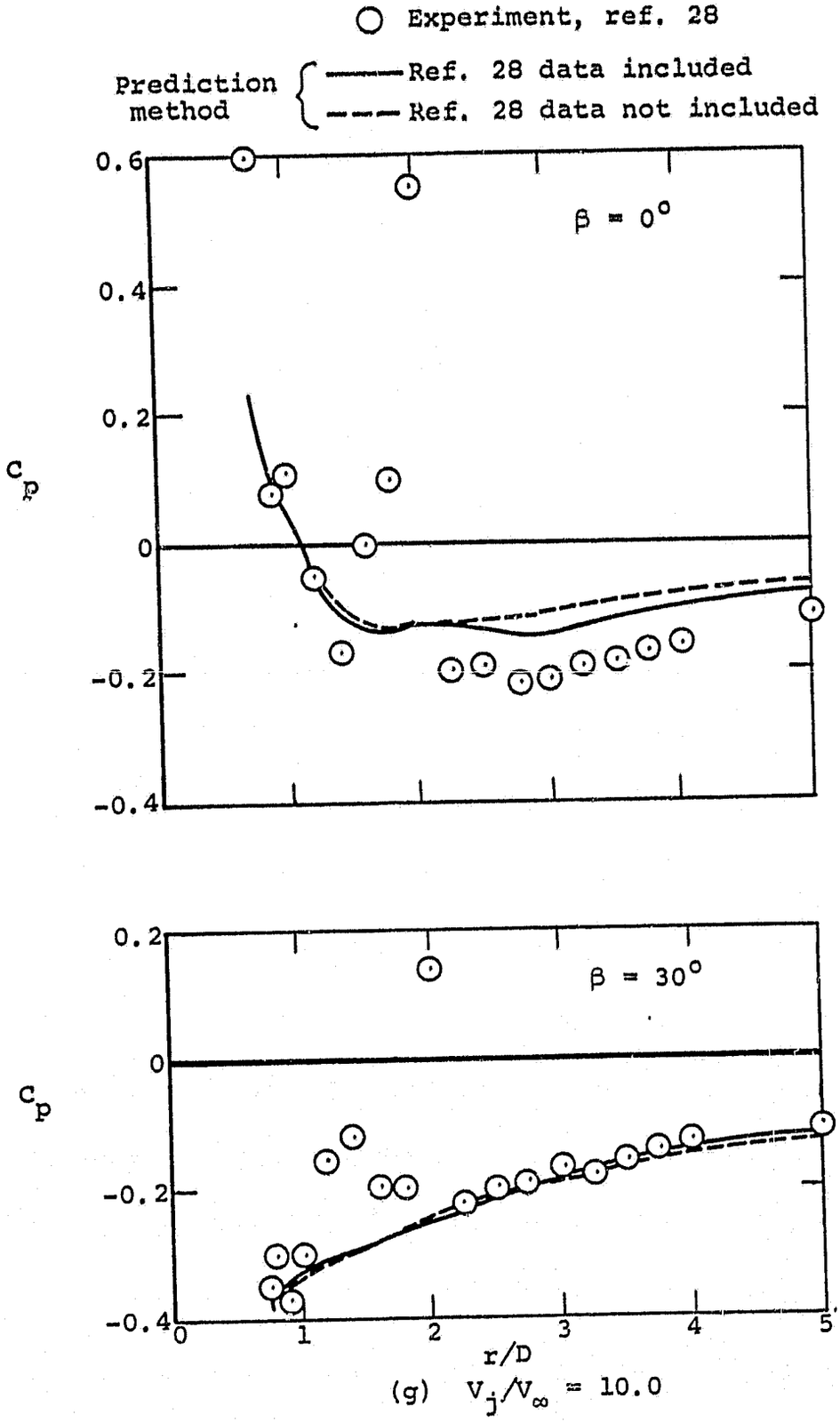

(g) $V_j/V_\infty = 10.0$

Figure 30.- Continued.

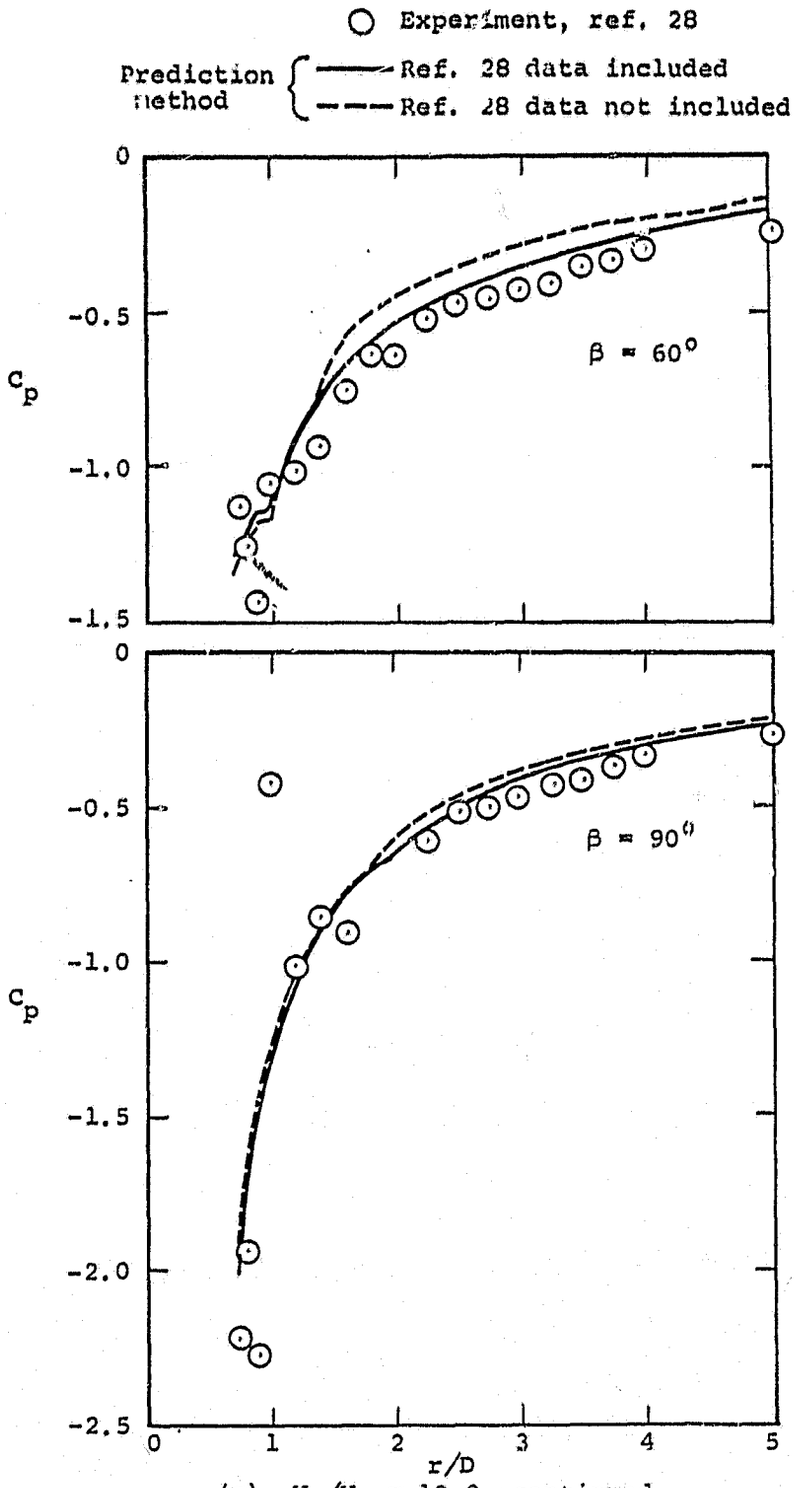

(g) V_j/V_∞ = 10.0, continued.

Figure 30.- Continued.

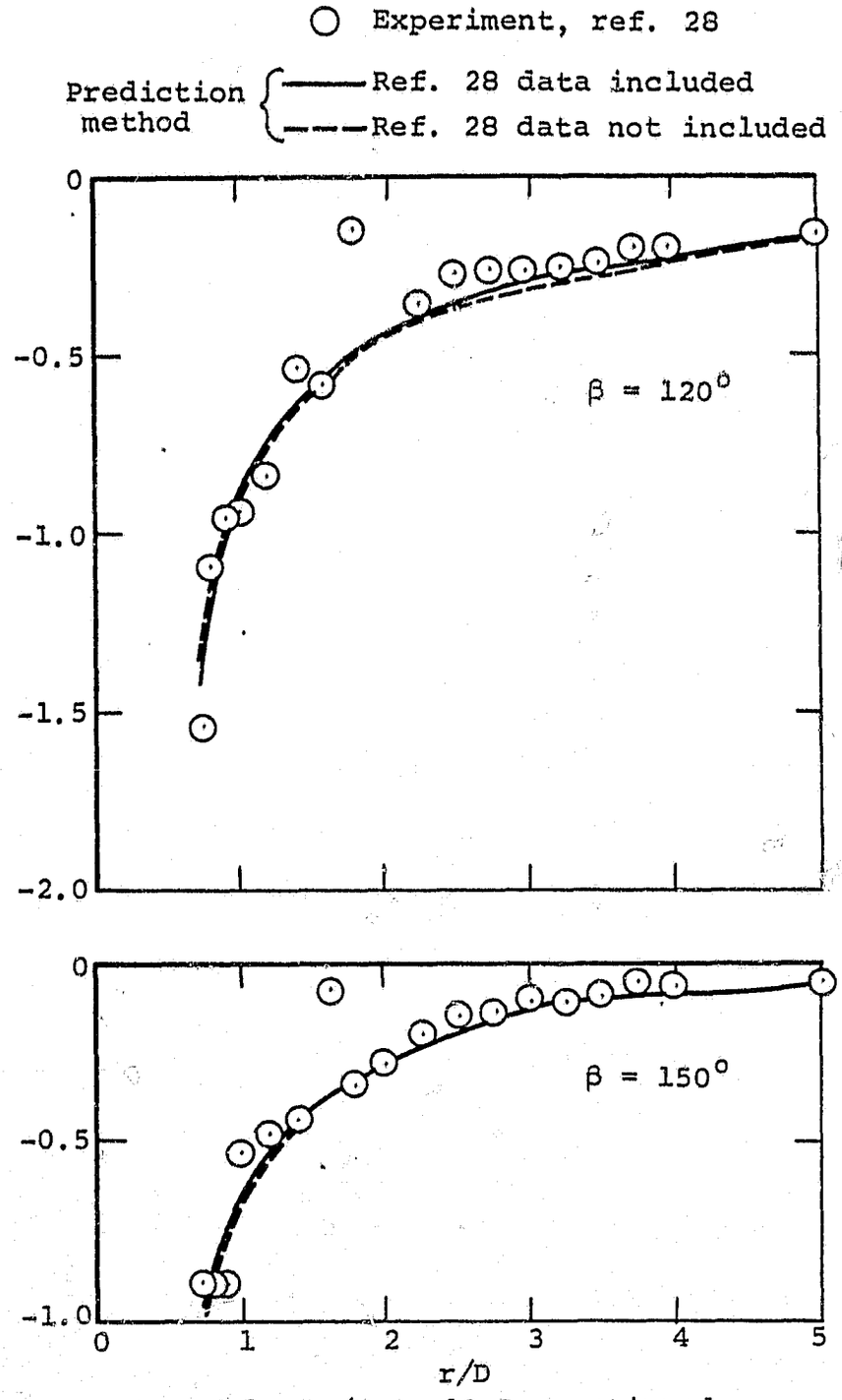

(g) V_j/V_∞ = 10.0, continued.

Figure 30.- Continued.

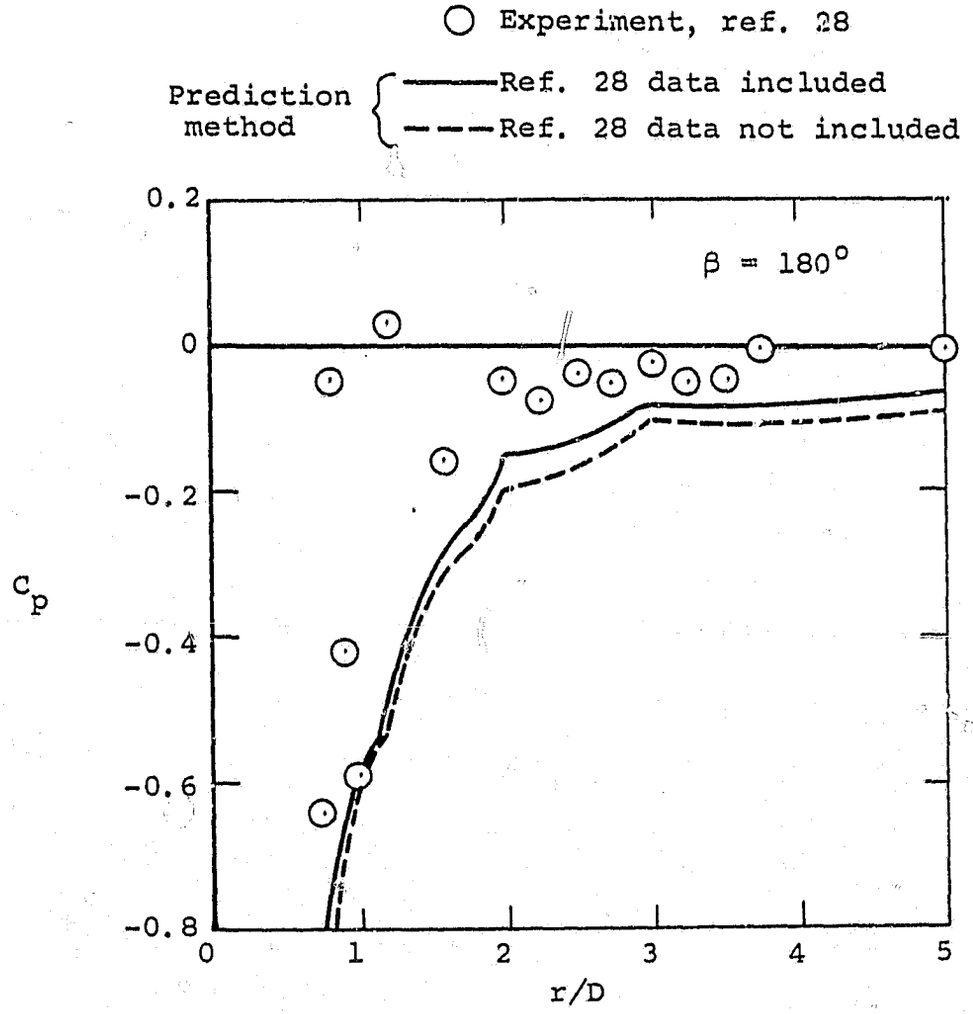

(g) V_j/V_∞ = 10.0, concluded.

Figure 30.- Concluded.

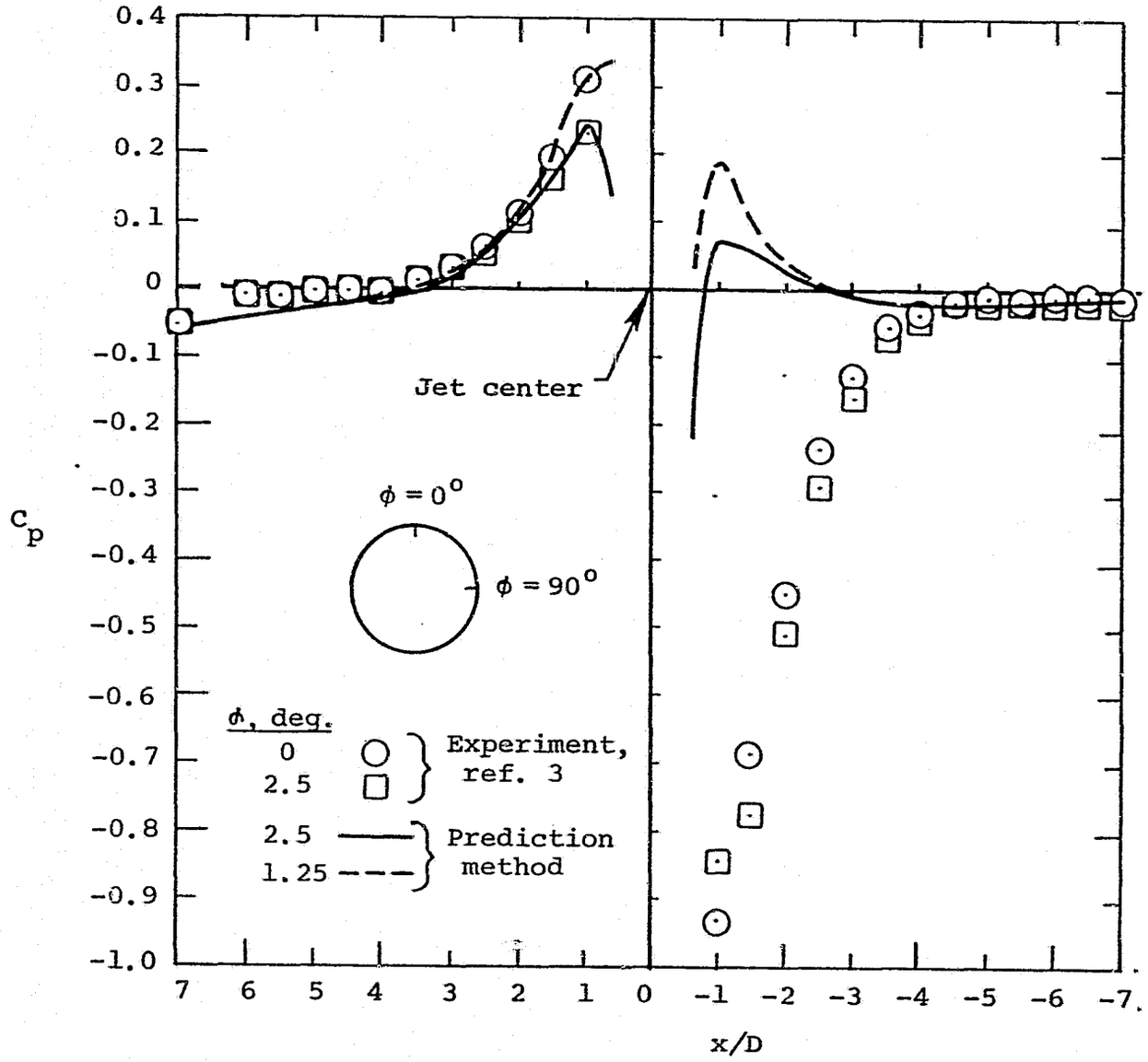

(a) $\phi \leq 2.5^o$.

Figure 31.- Comparison of measured and predicted axial pressure distributions along a cone-cylinder from which a jet is issuing (correlation factors not included in prediction method), $V_j/V_\infty = 1.96$.

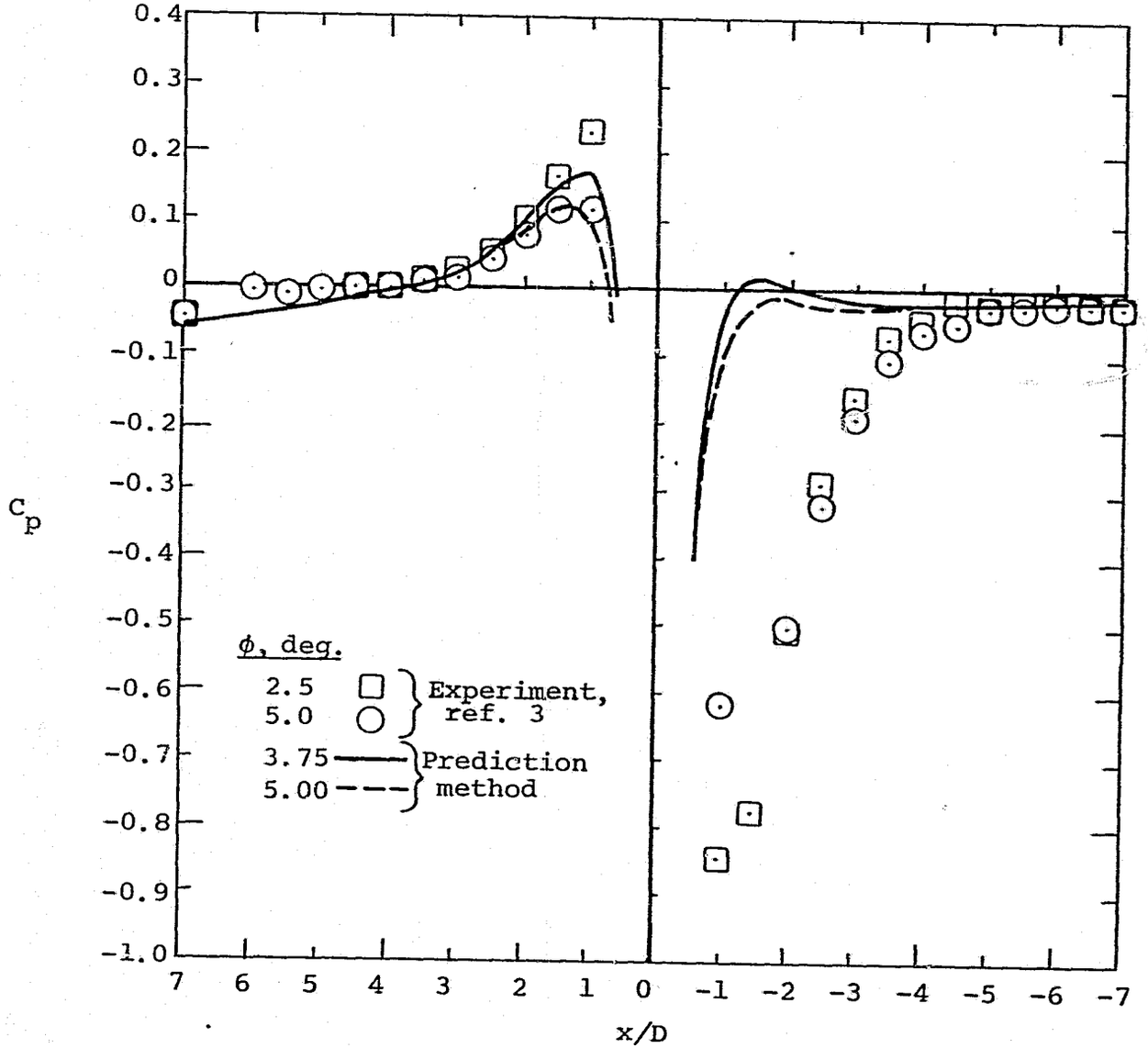

(b) $2.5^{\circ} \leq \phi \leq 5.0^{\circ}$.

Figure 31.- Continued.

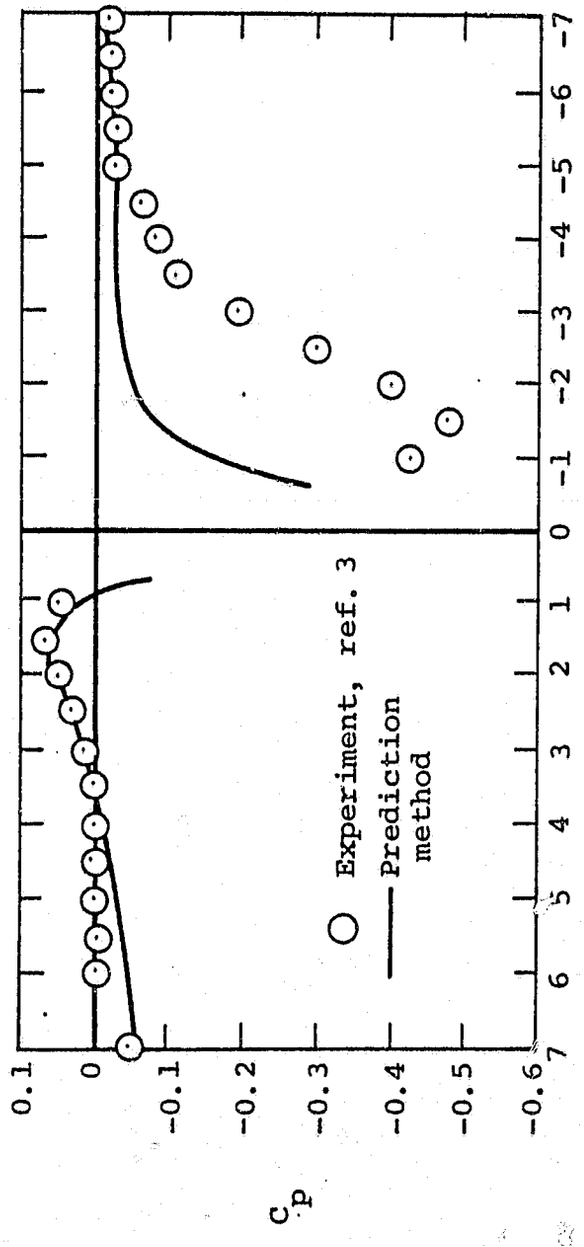

(c) $\phi = 7.5^{\circ}$.

Figure 31.- Continued.

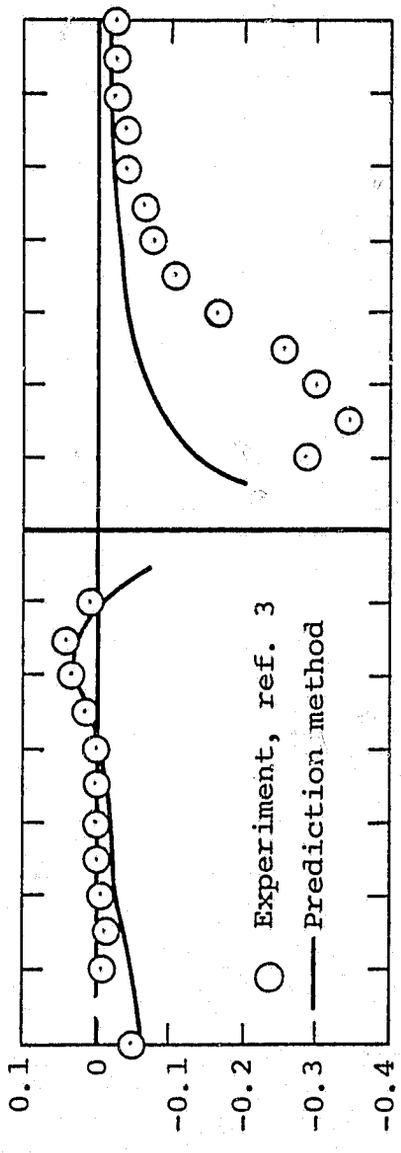

(d) $\phi = 10^{\circ}$.

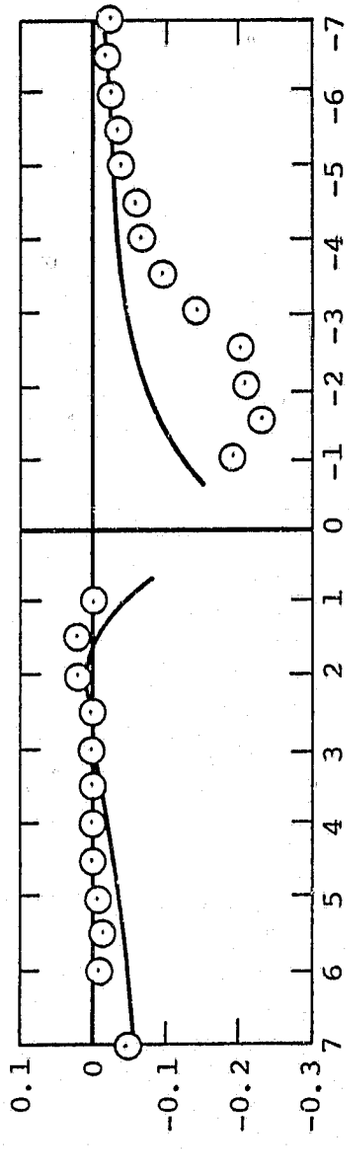

(e) $\phi = 12.5^{\circ}$.

Figure 31.- Continued.

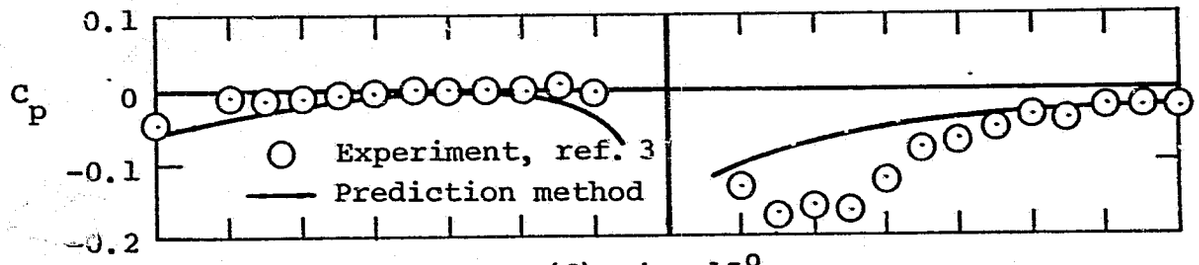

(f) $\phi = 15^{\circ}$.

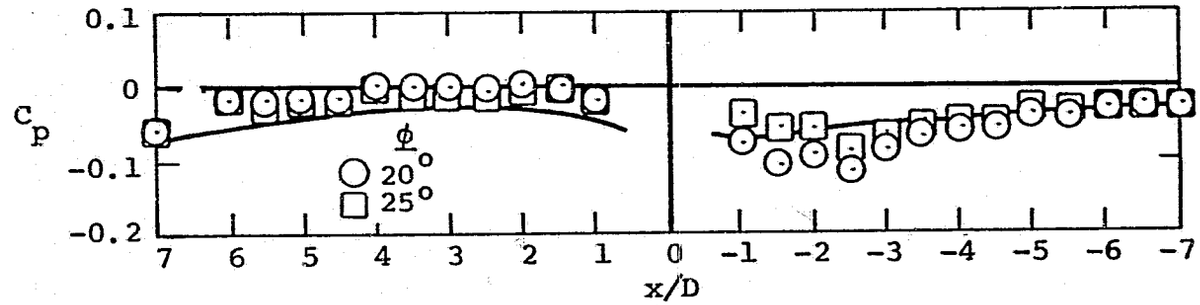

(g) $\phi \geq 20^{\circ}$.

Figure 31.- Concluded.

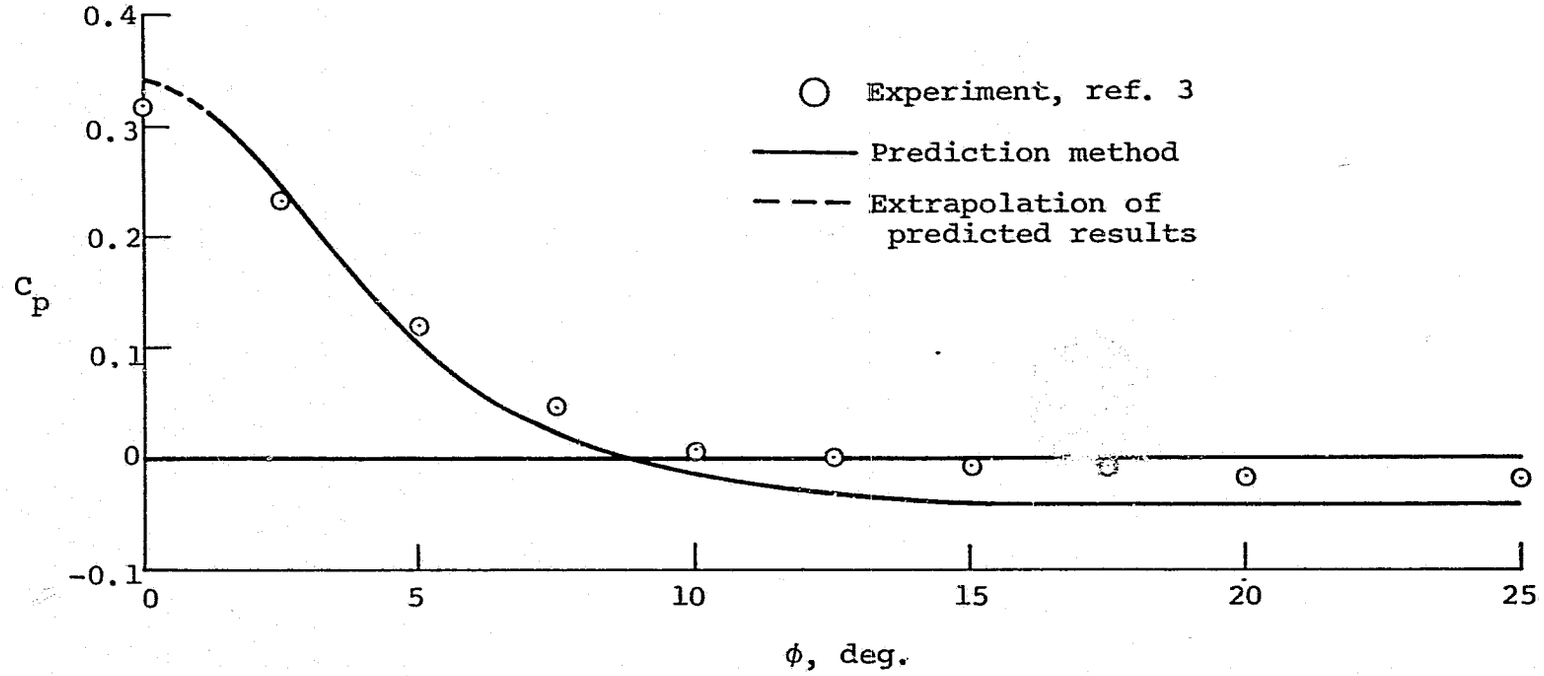

(a) x/D = 1.0.

Figure 32.- Comparison of measured and predicted circumferential pressure distributions on a cone-cylinder from which a jet is issuing, (correlation factors not included in prediction method), $V_j/V_\infty = 1.96$.

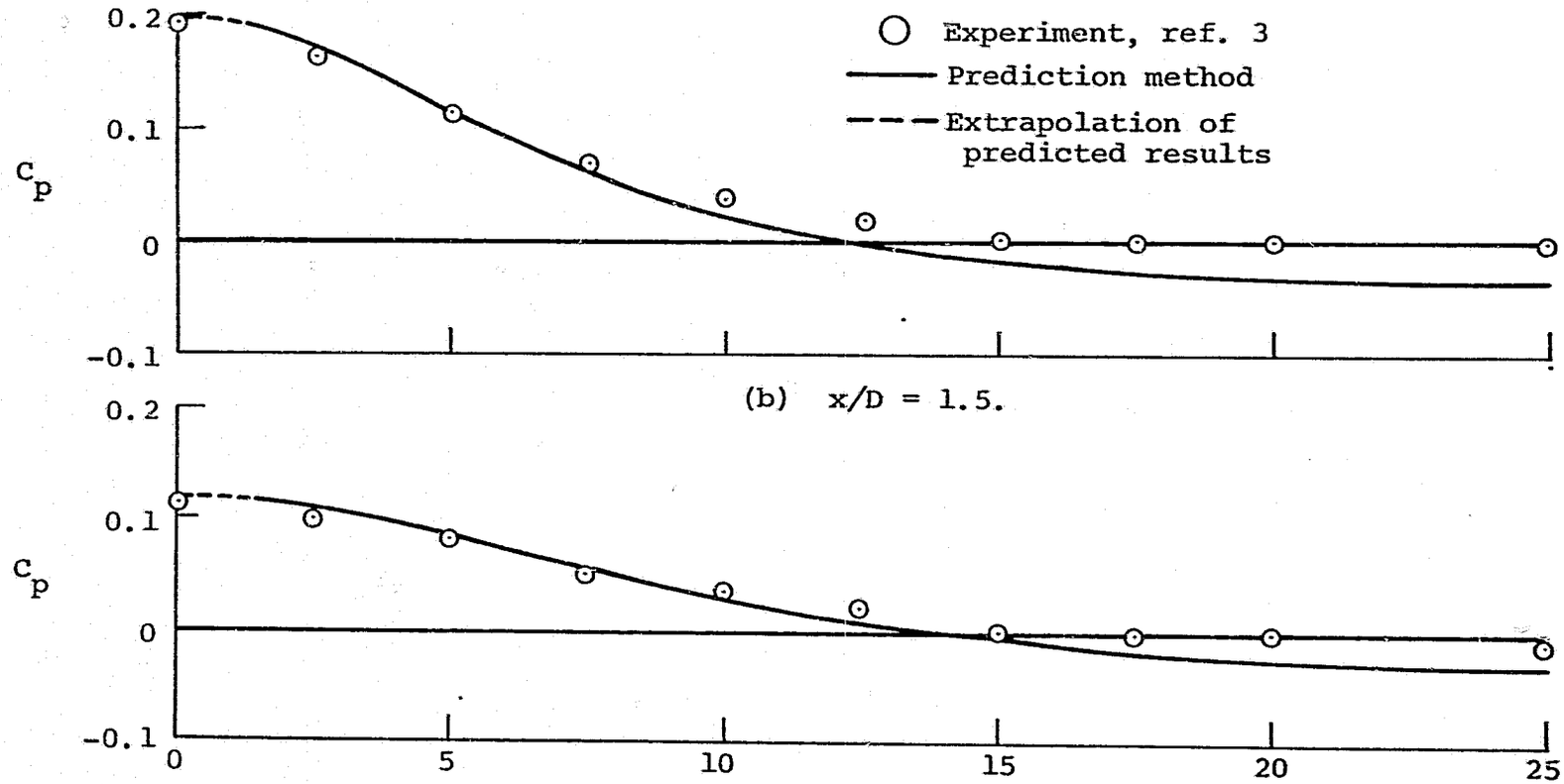

Figure 32.- Continued.

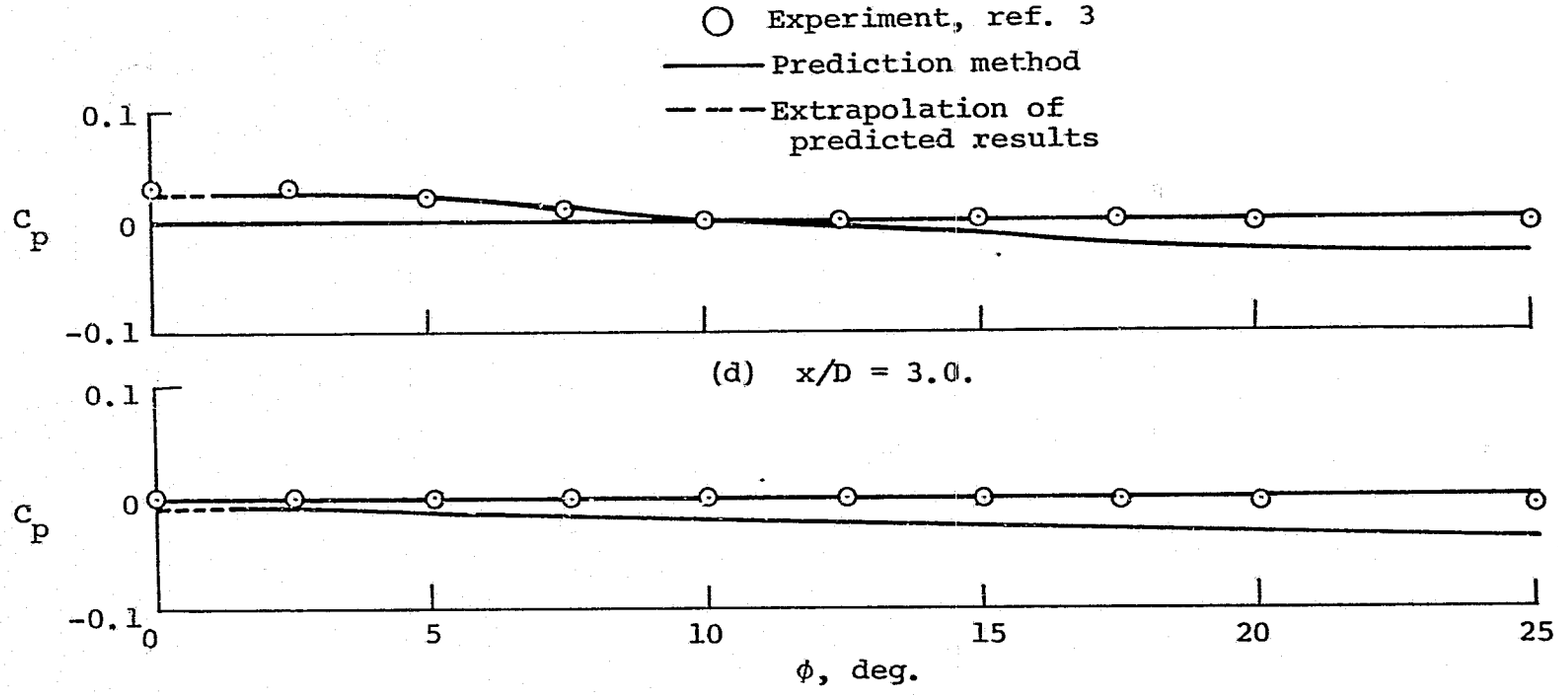

(d) x/D = 3.0.

(e) x/D = 4.2.

Figure 32.- Continued.

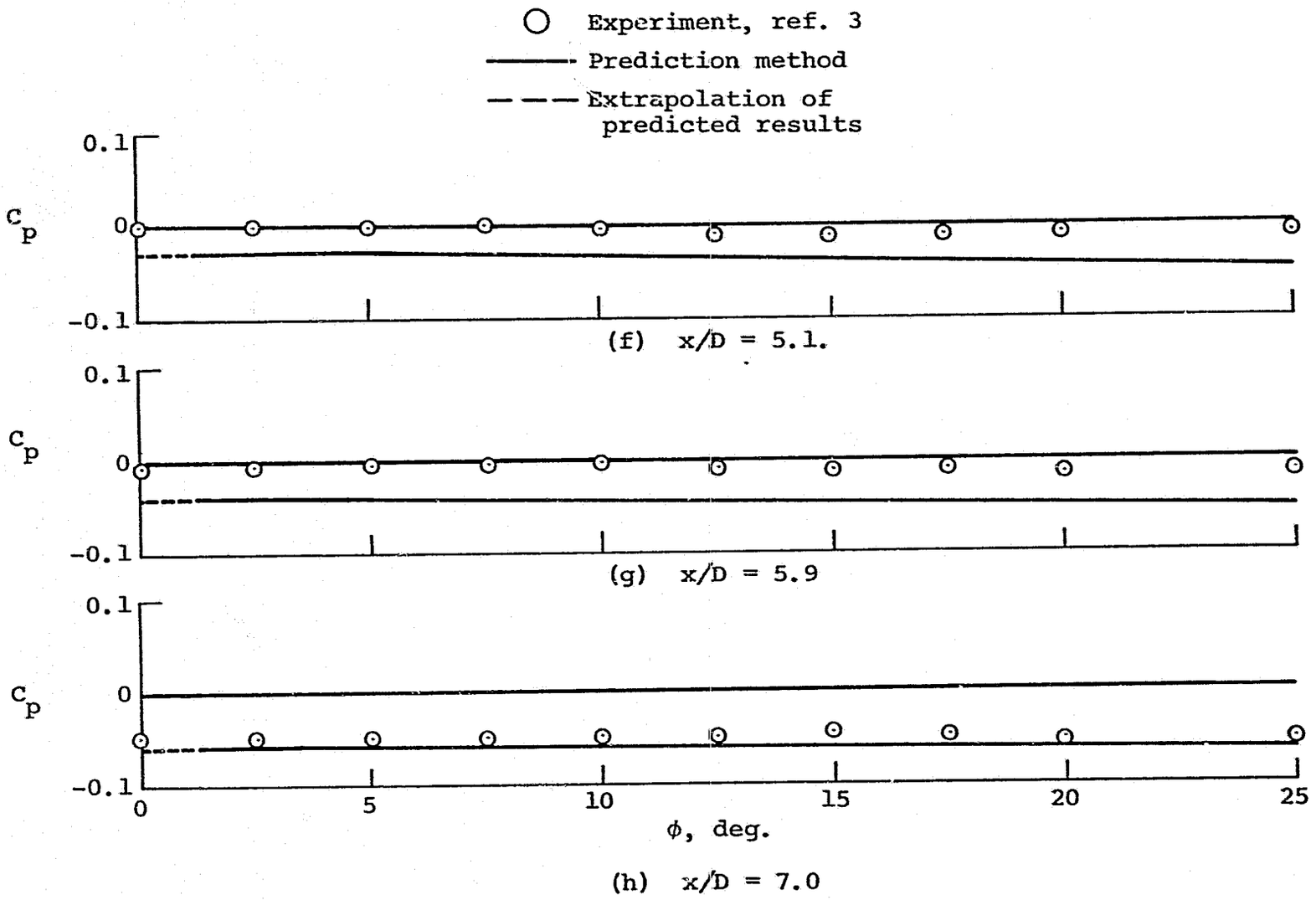

Figure 32.- Continued.

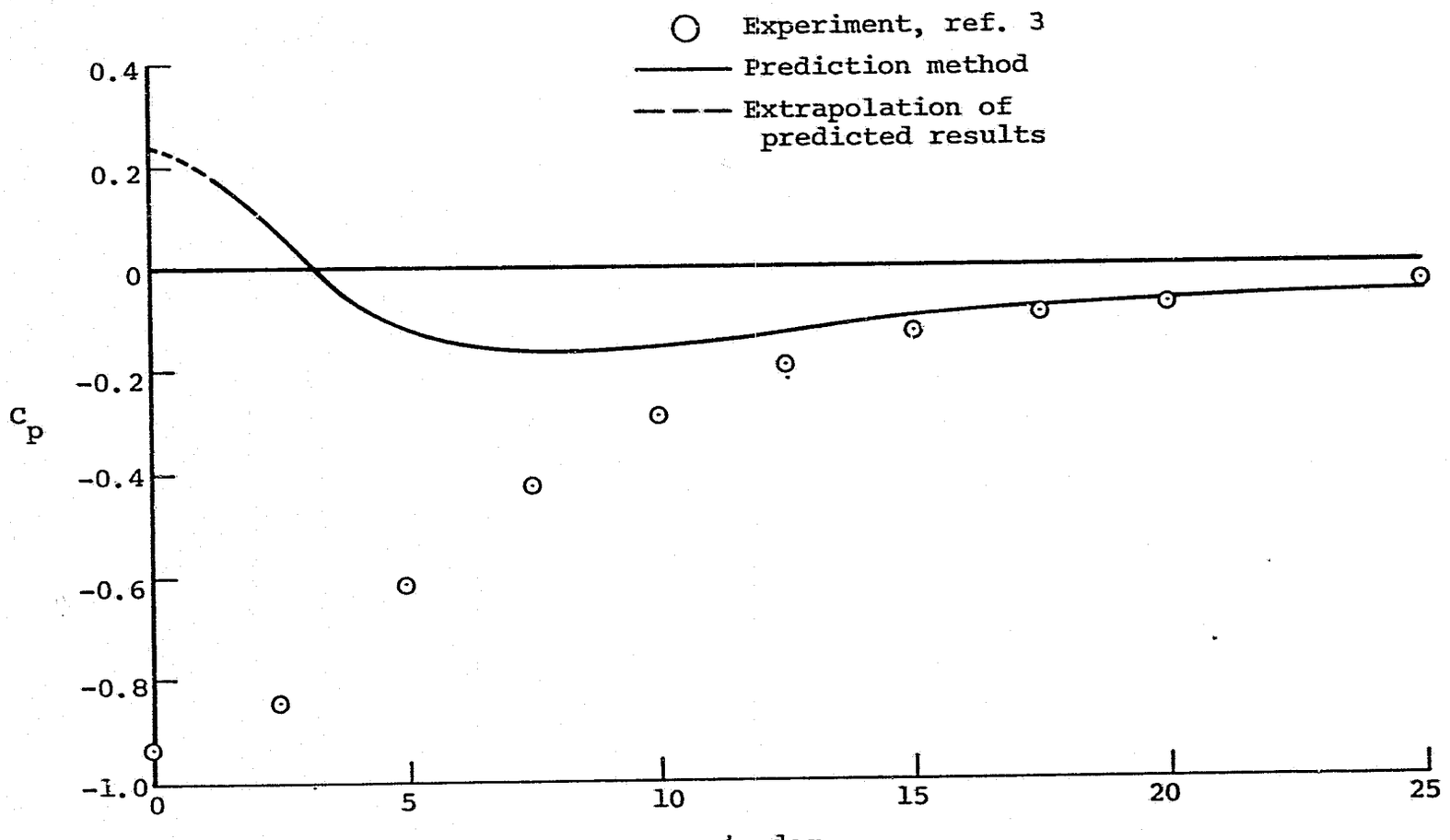

(i) x/D = -1.0.

Figure 32.- Continued.

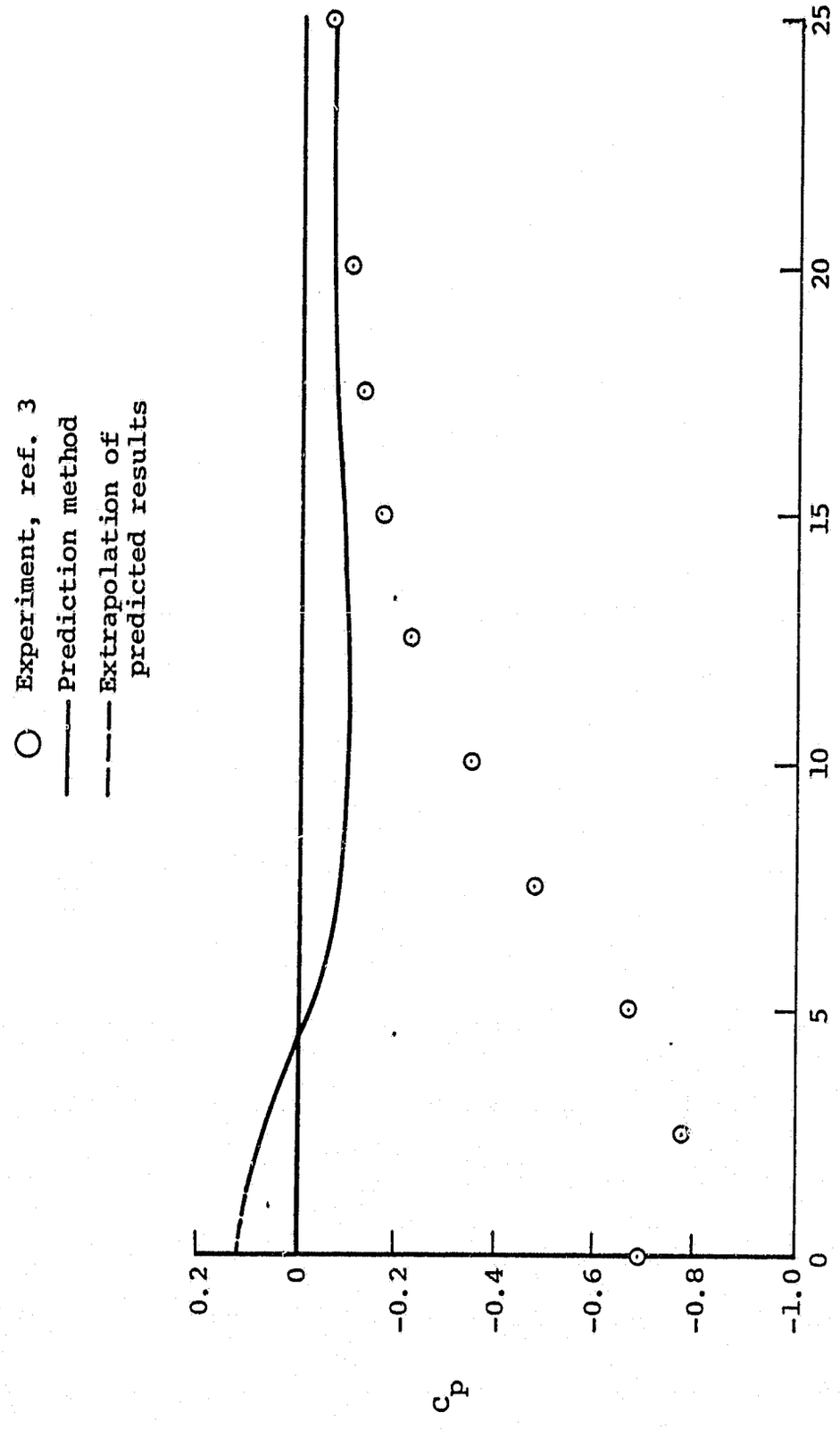

(j) x/D = -1.5.

Figure 32.- Continued.

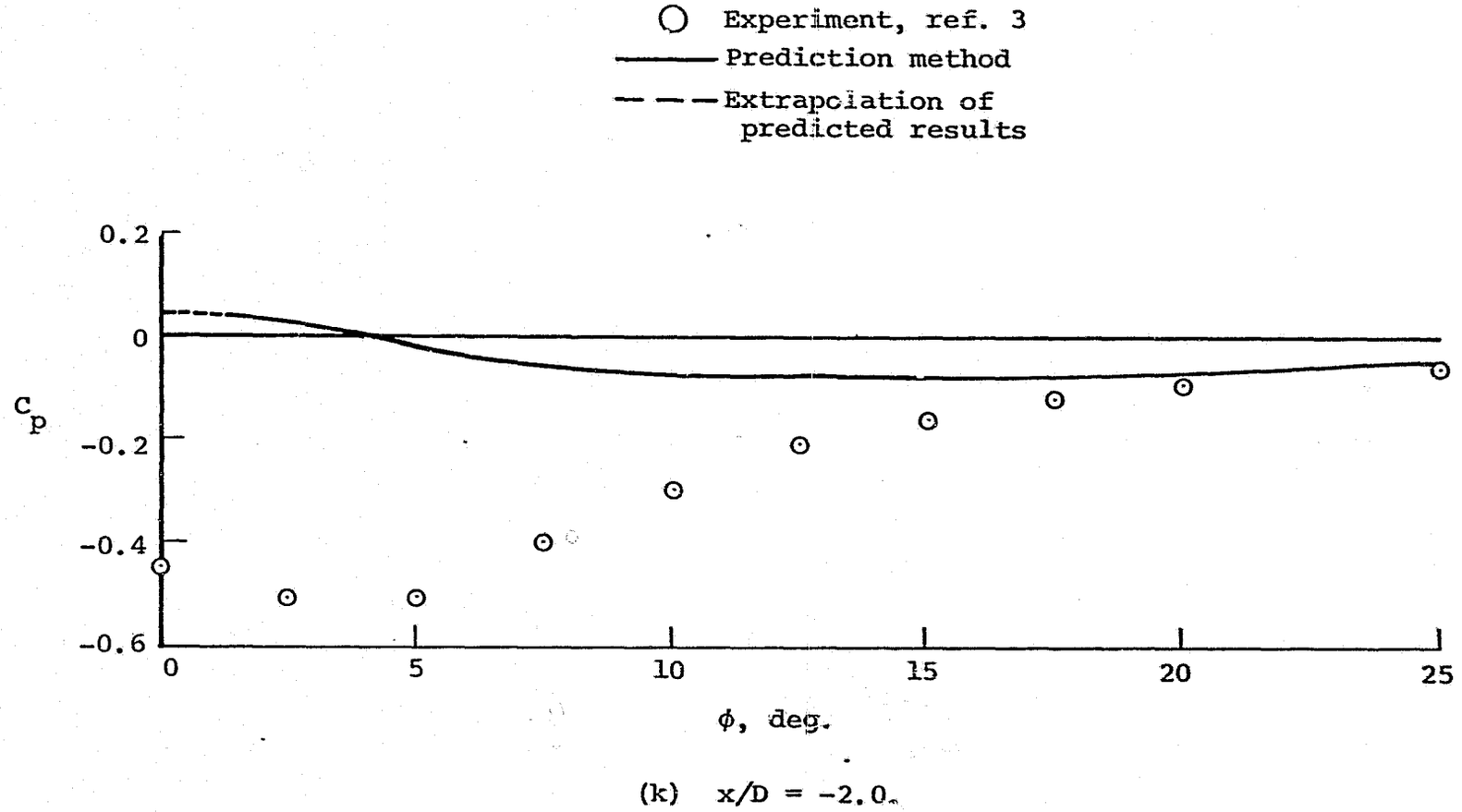

(k) x/D = -2.0.

Figure 32.- Continued.

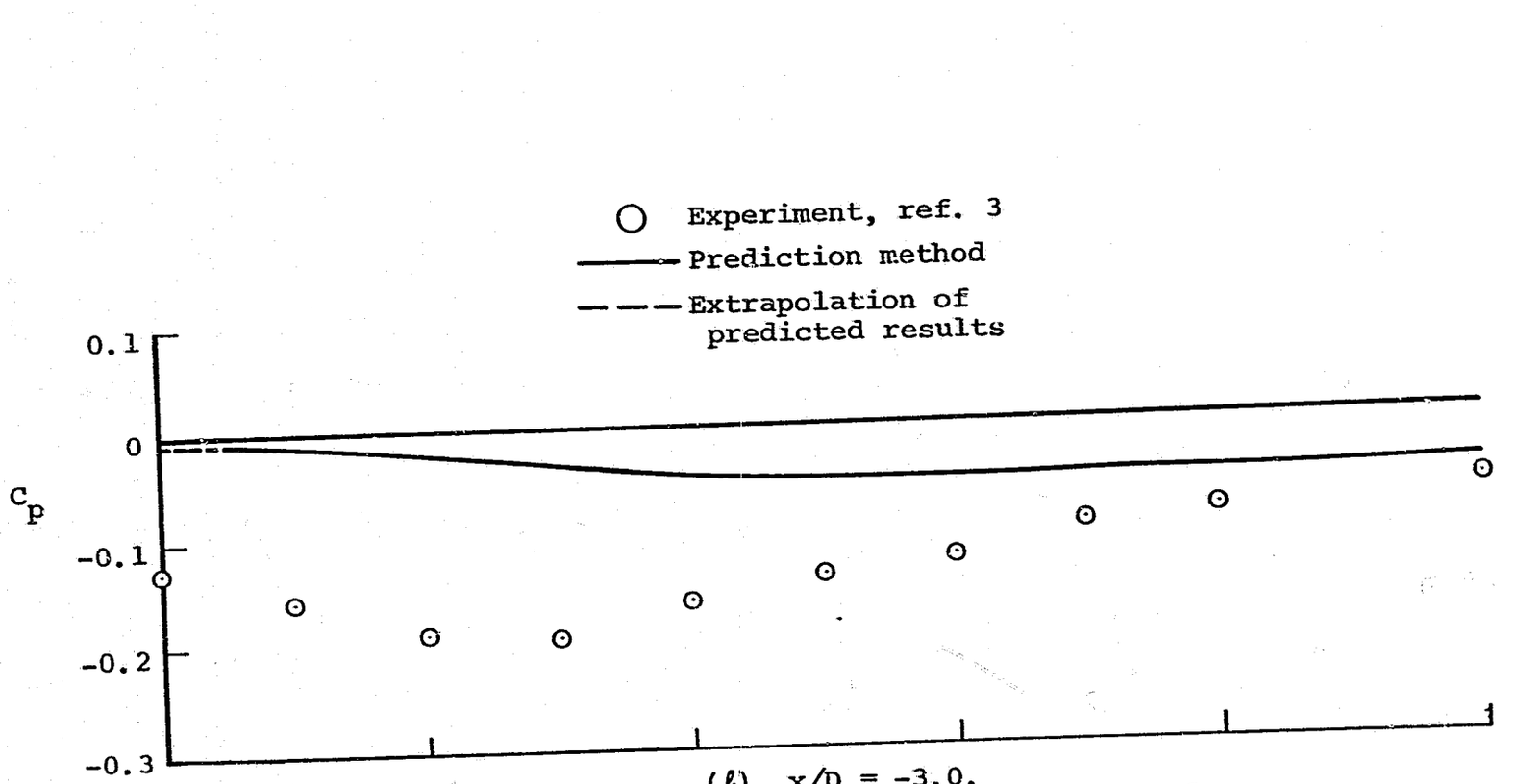

(ℓ) x/D = -3.0.

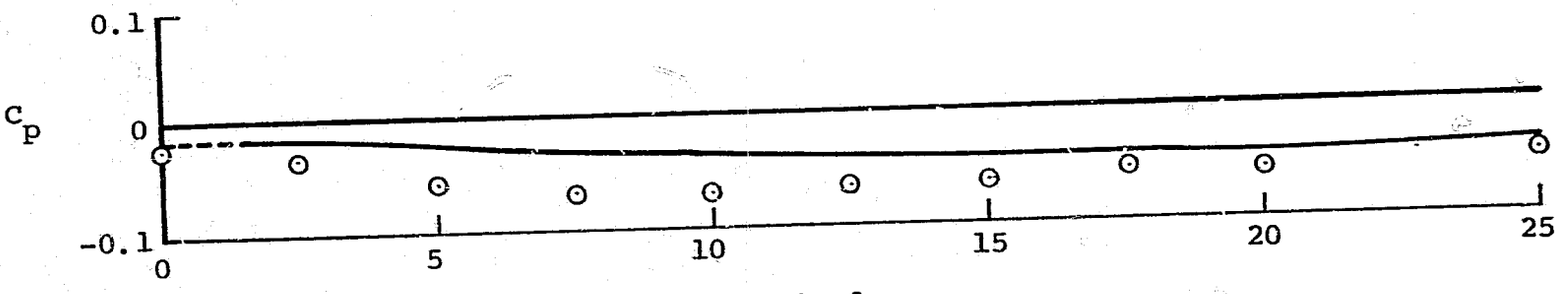

(m) x/D = -4.2.

Figure 32.- Continued.

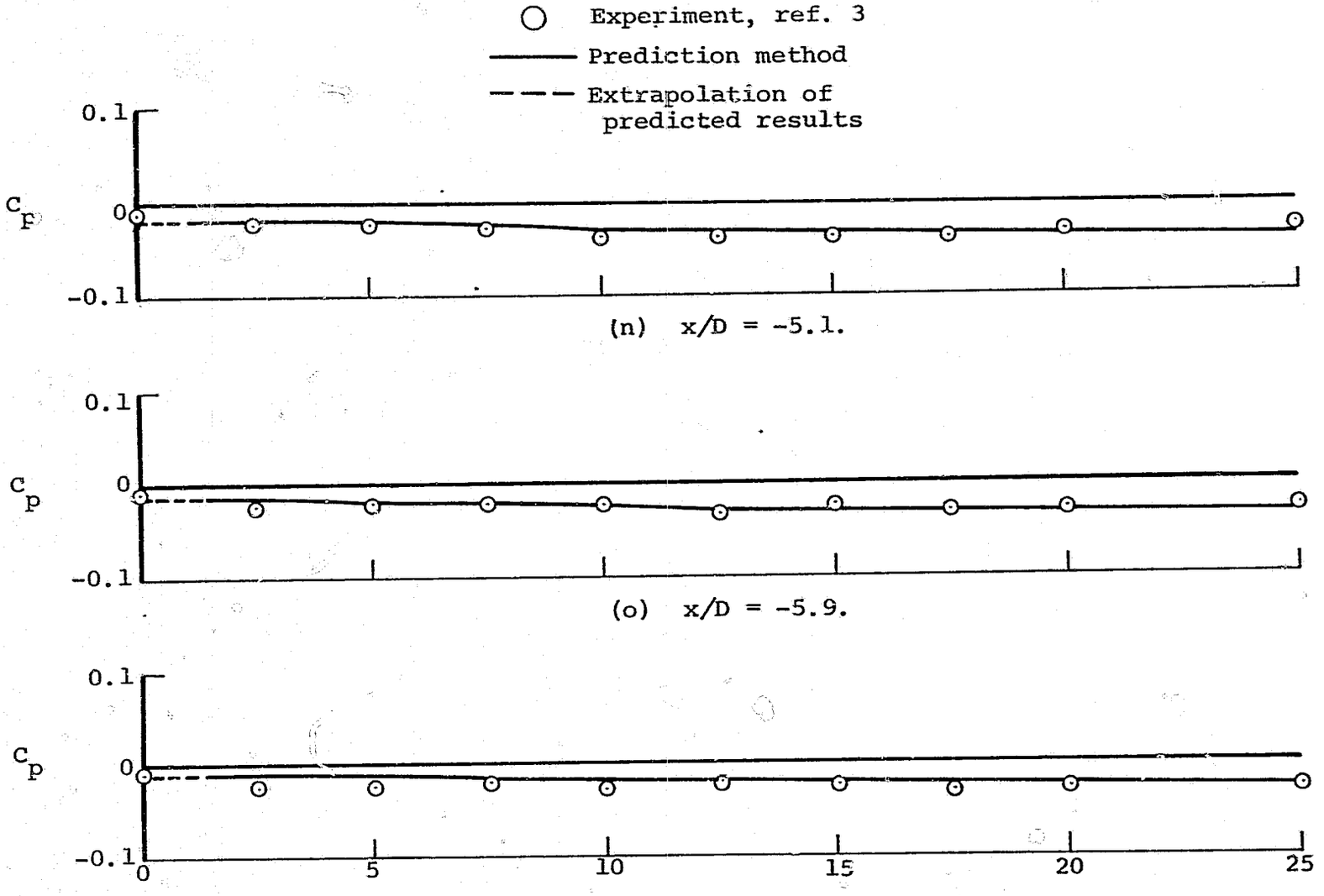

Figure 32.- Concluded.

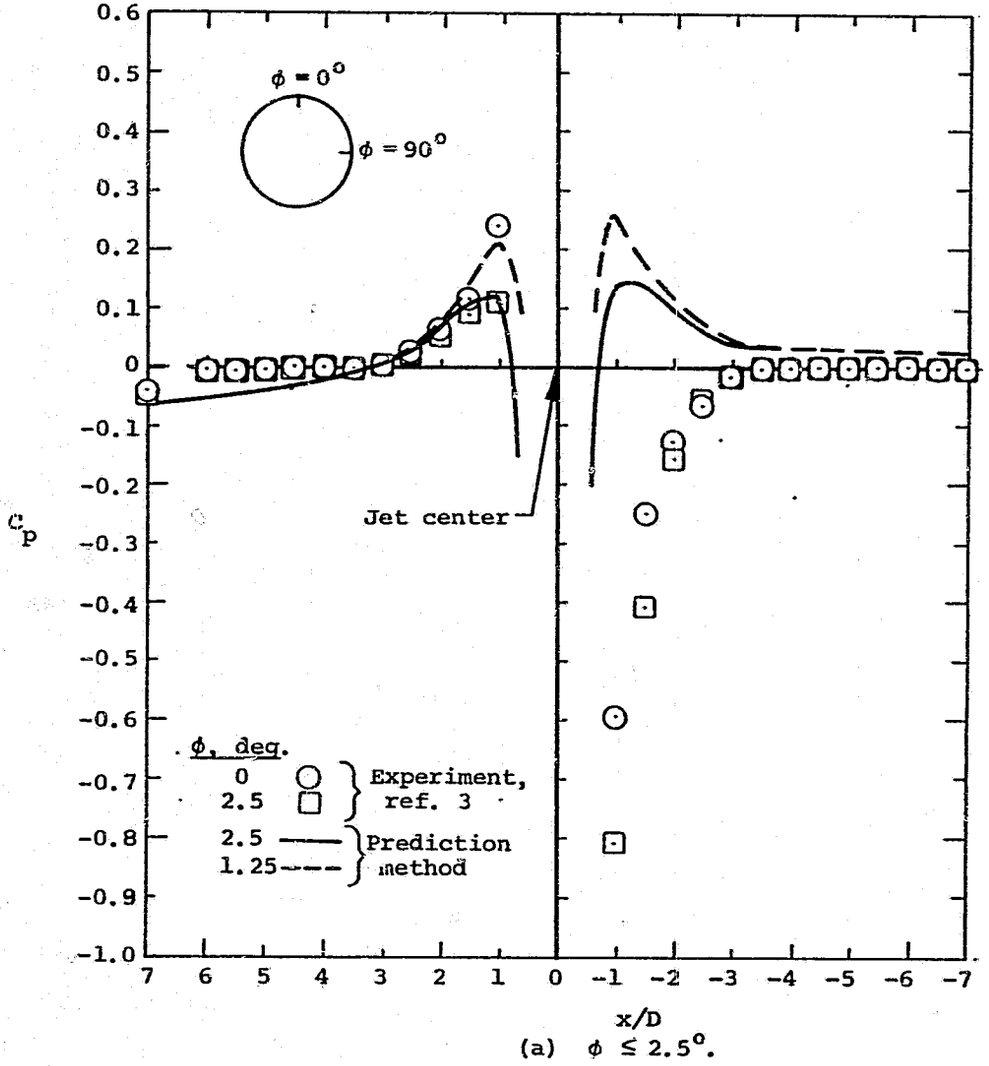

(a) $\phi \leq 2.5^o$.

Figure 33.- Comparison of measured and predicted axial pressure distributions along a cone-cylinder from which a jet is issuing (correlation factors not included in prediction method), $V_j/V_\infty = 3.43$.

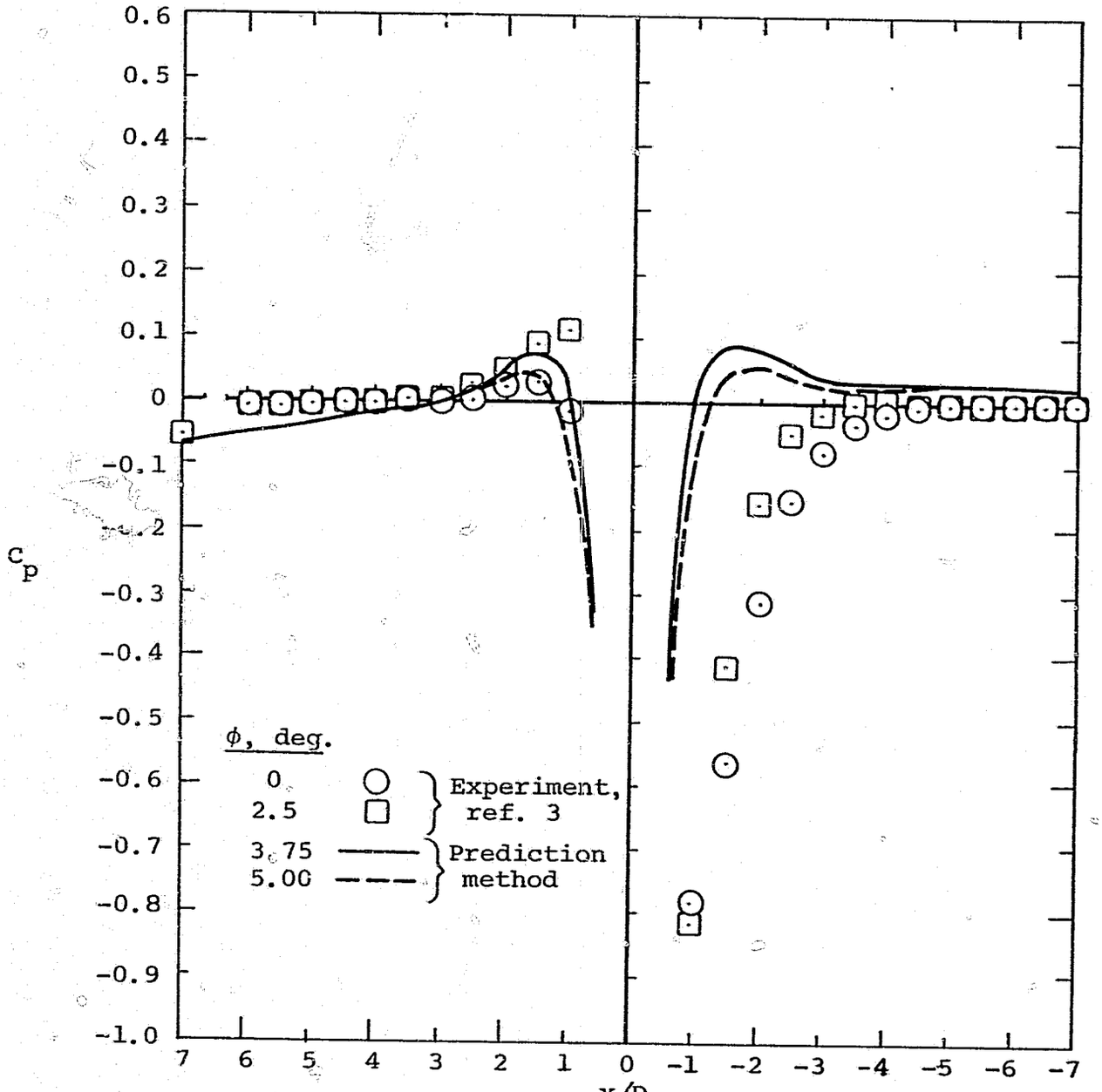

(b) $2.5^{\circ} \leq \phi \leq 5^{\circ}$

Figure 33.- Continued.

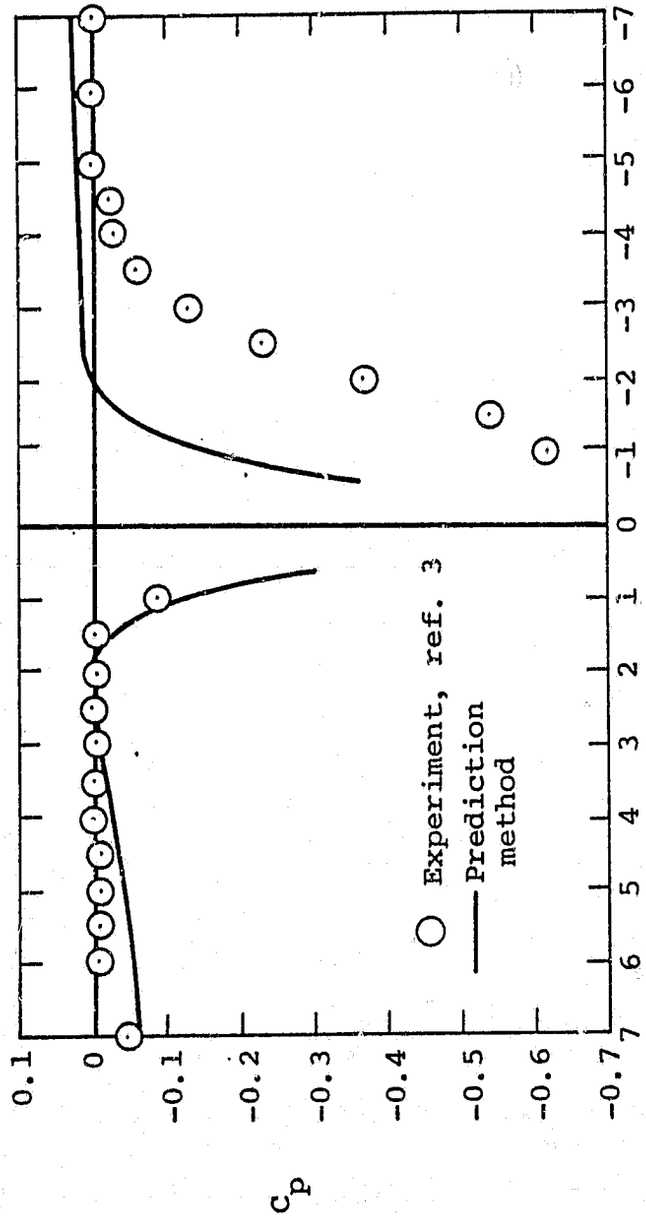

(c) $\phi = 7.5^{\circ}$.

Figure 33 - Continued.

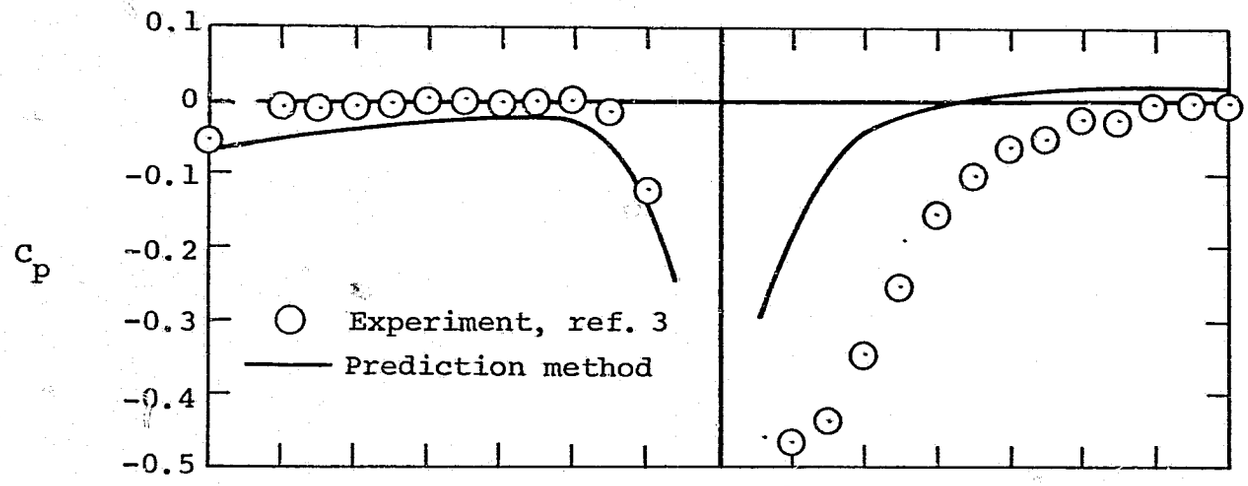

(d) $\phi = 10^o$.

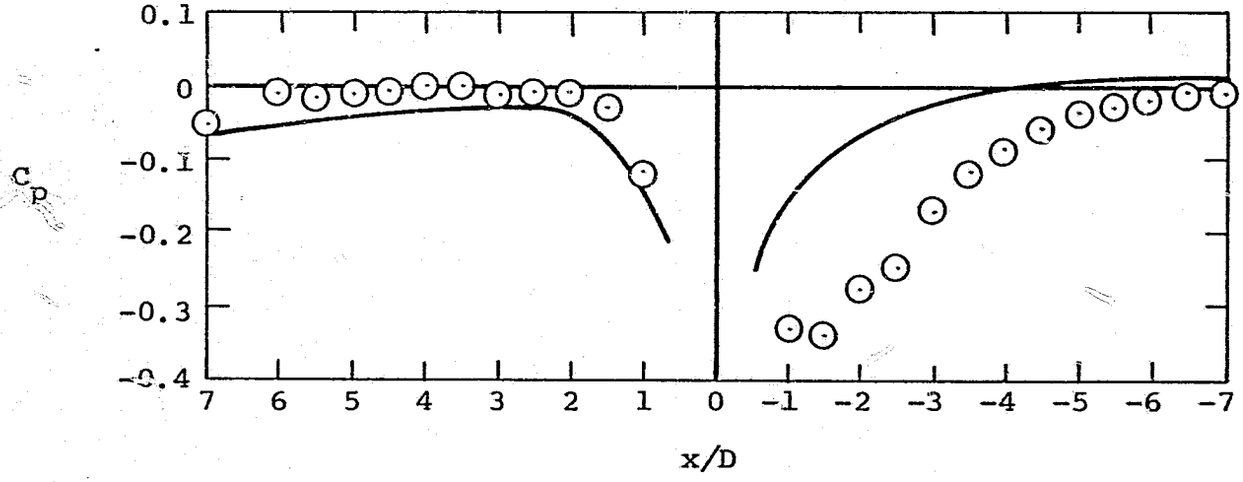

(e) $\phi = 12.5^o$.

Figure 33.- Continued.

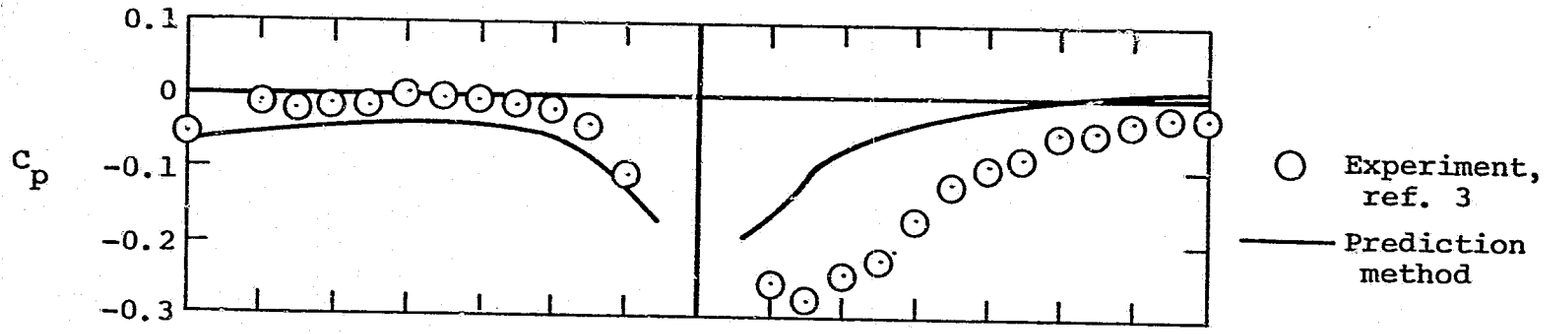

(f) $\phi = 15^{\circ}$.

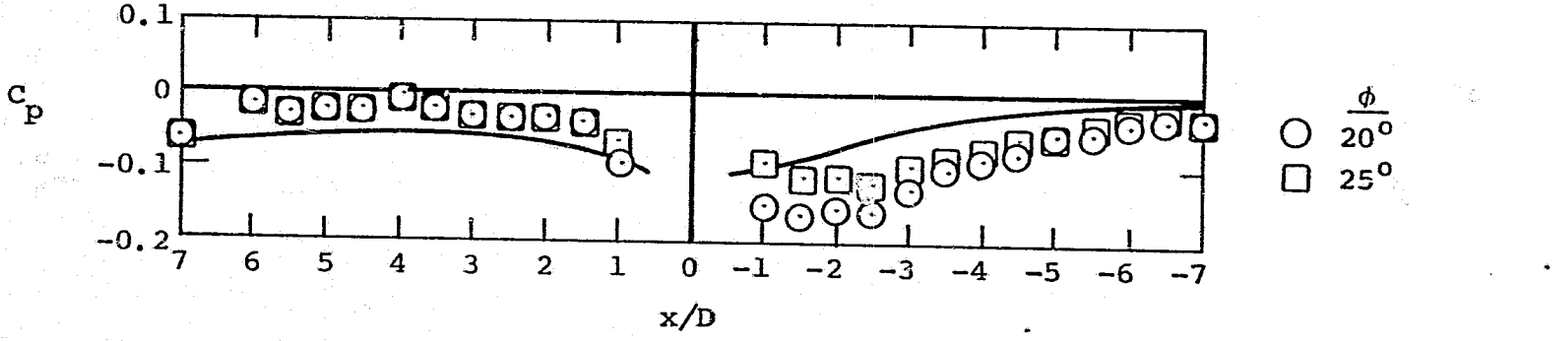

(g) $\phi \geq 20^{\circ}$.

Figure 33.- Concluded.

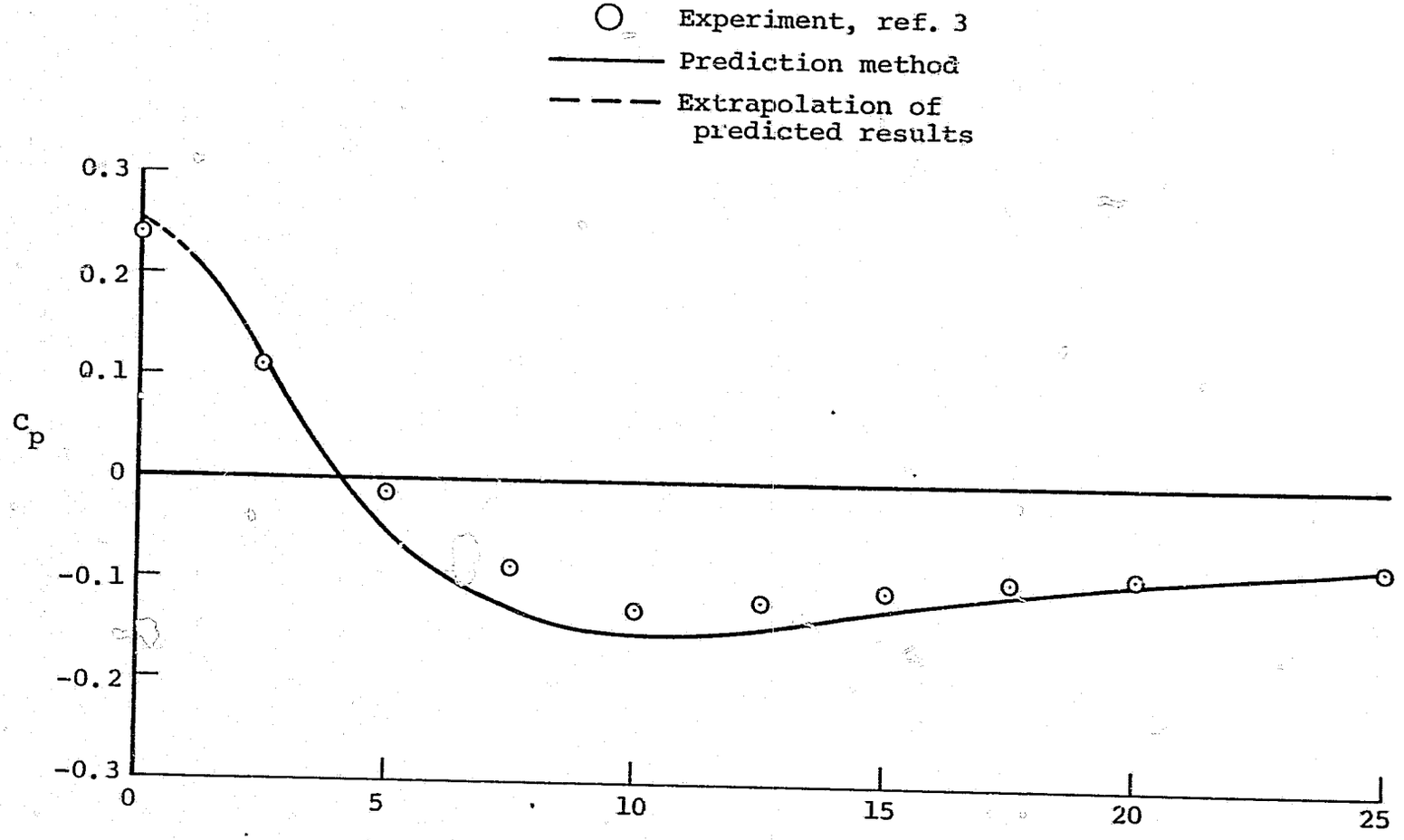

(a) $x/D = 1.$

Figure 34.- Comparison of measured and predicted circumferential pressure distributions on a cone-cylinder from which a jet is issuing (correlation factors not included in prediction method), $V_j/V_\infty = 3.43$.

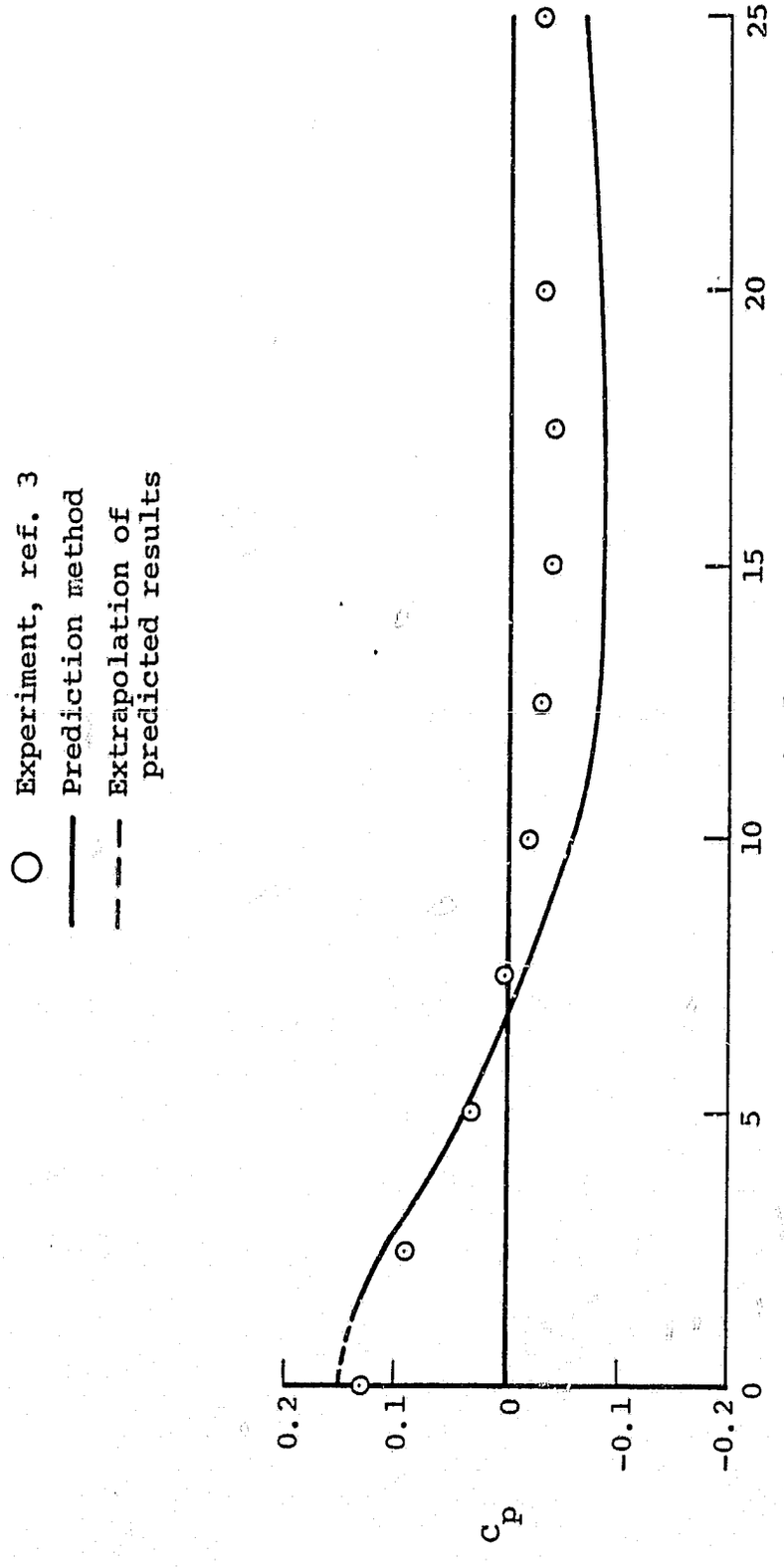

(b) x/D = 1.5.

Figure 34.- Continued.

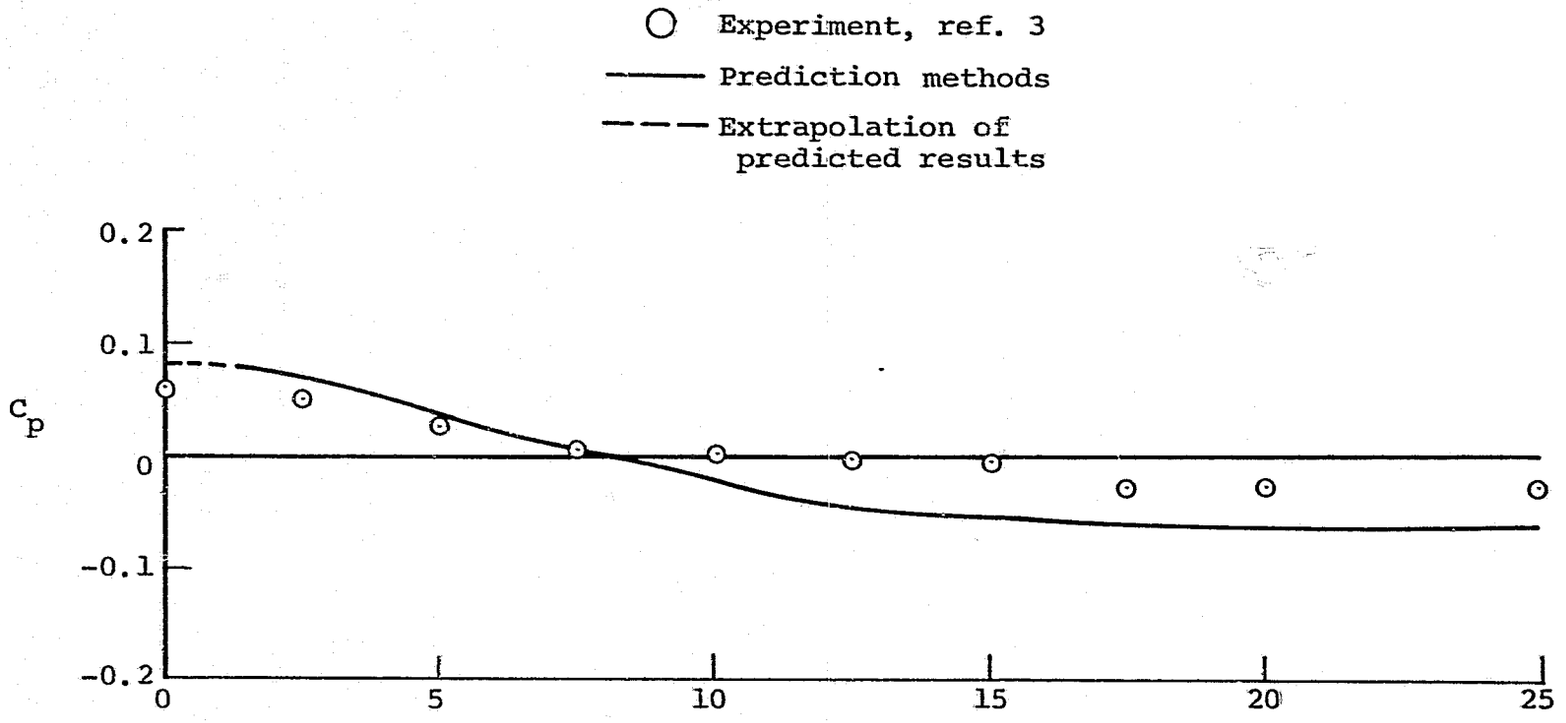

(c) $x/D = 2.0$.

Figure 34.- Continued.

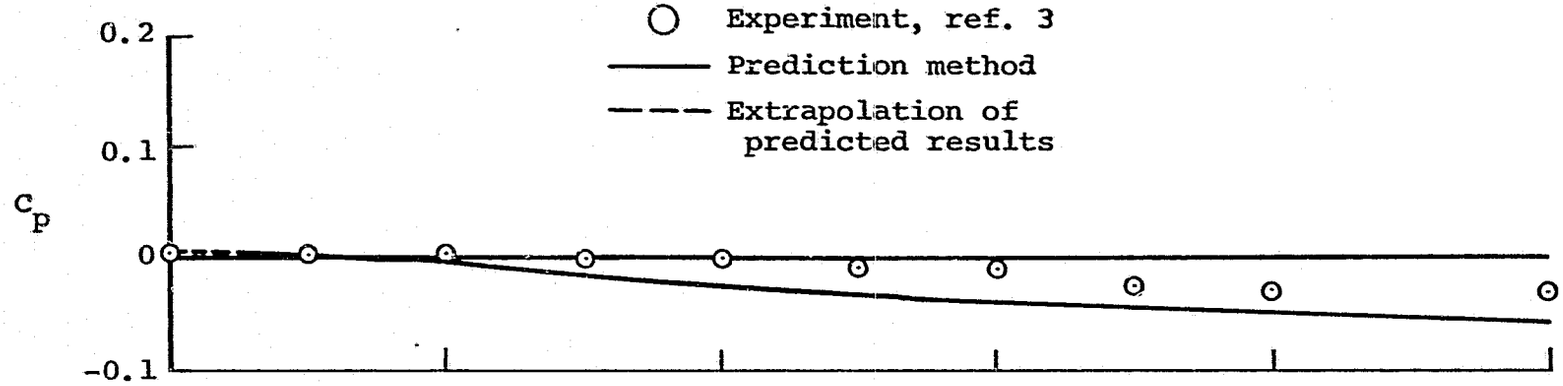

(d) x/D = 3.0.

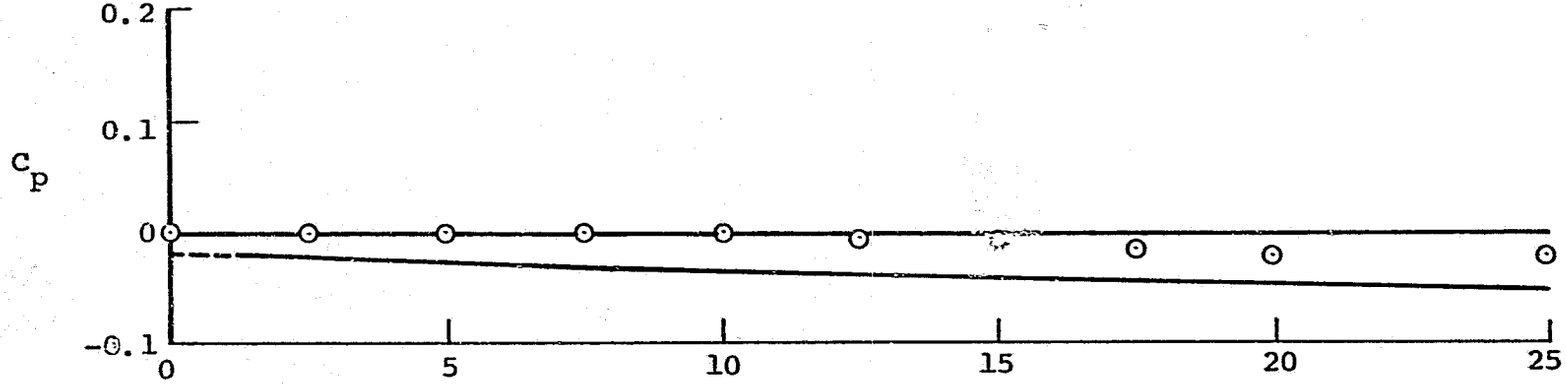

(e) x/D = 4.2.

Figure 34.- Continued.

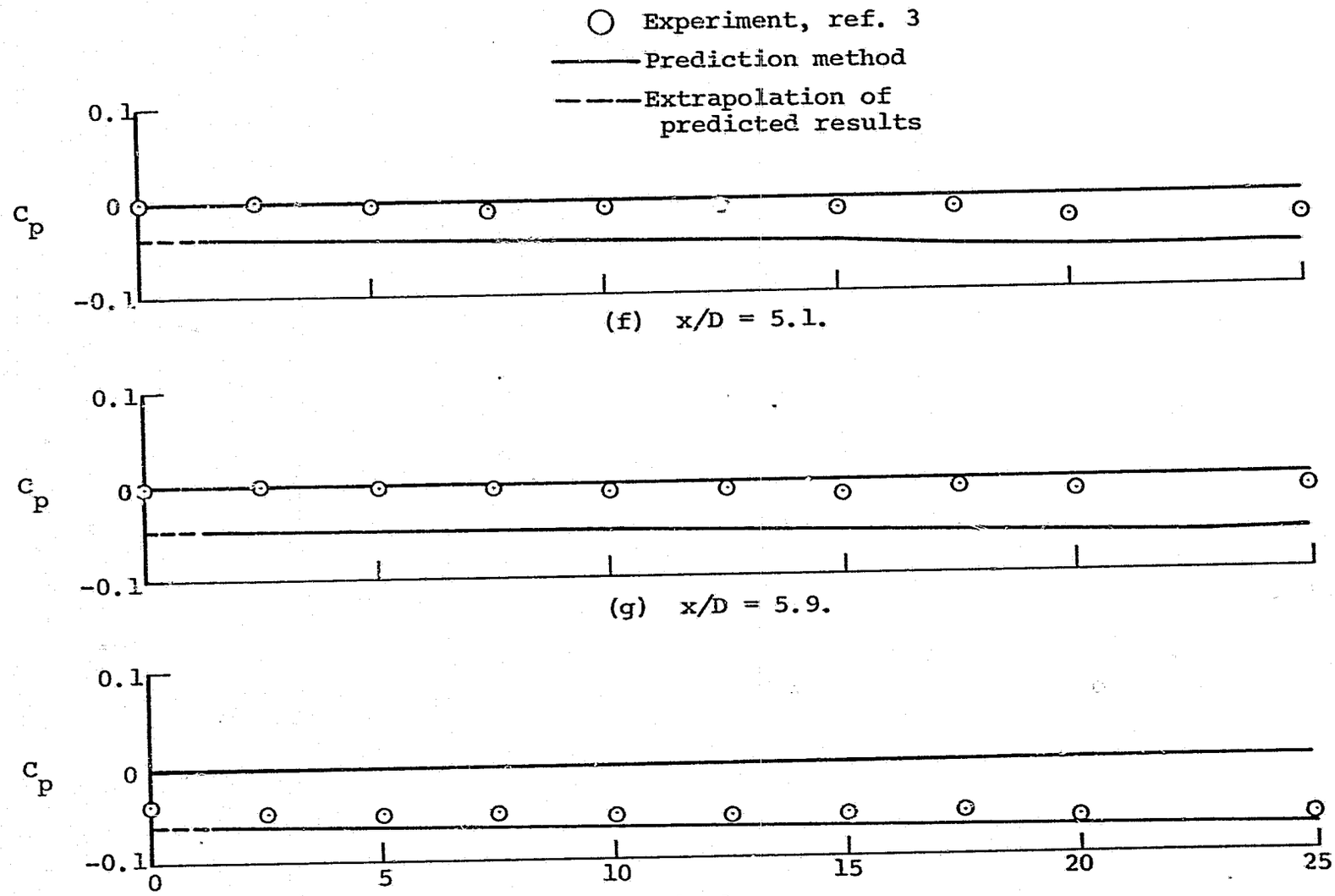

Figure 34.- Continued.

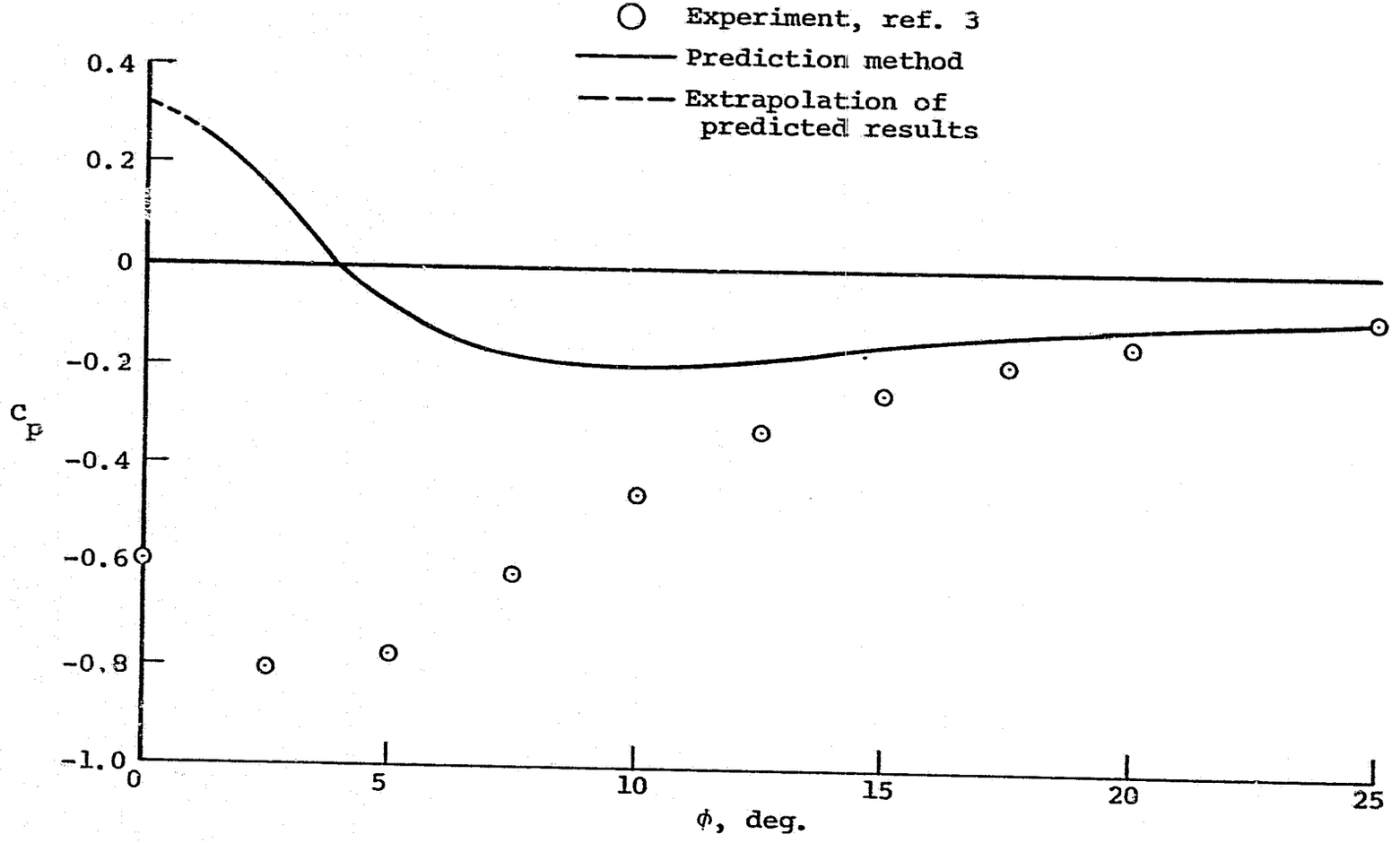

(i) x/D = -1.0.

Figure 34.- Continued.

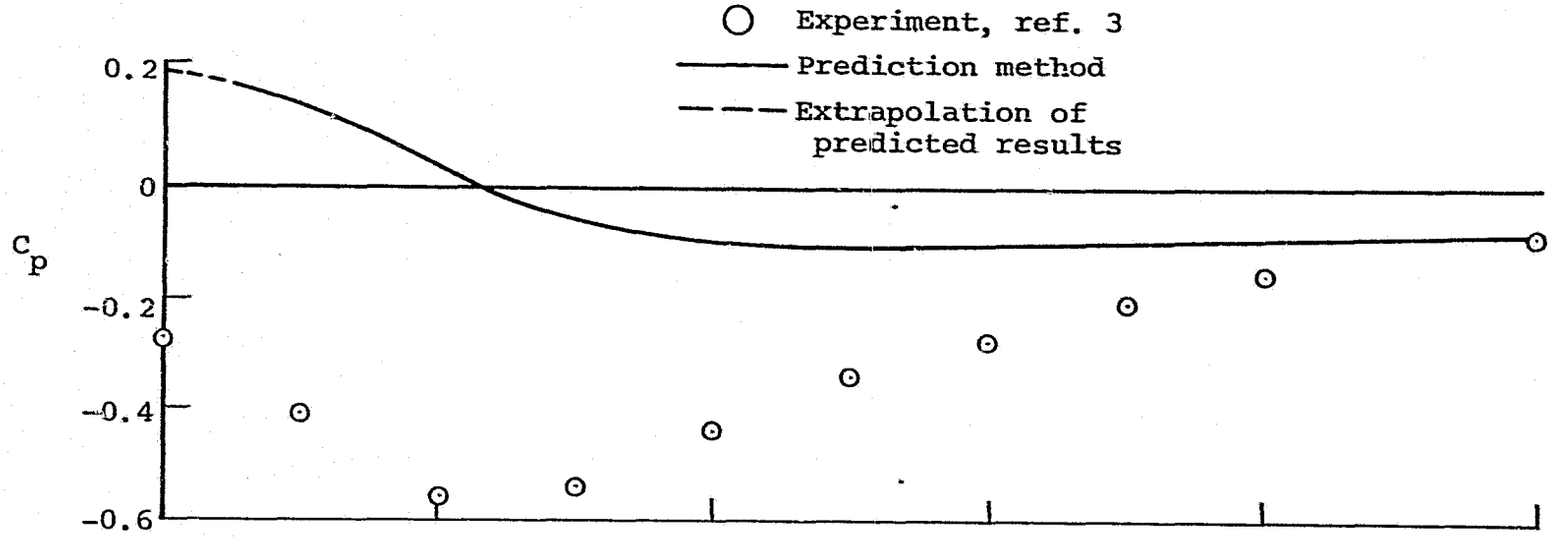

(j) x/D = -1.5.

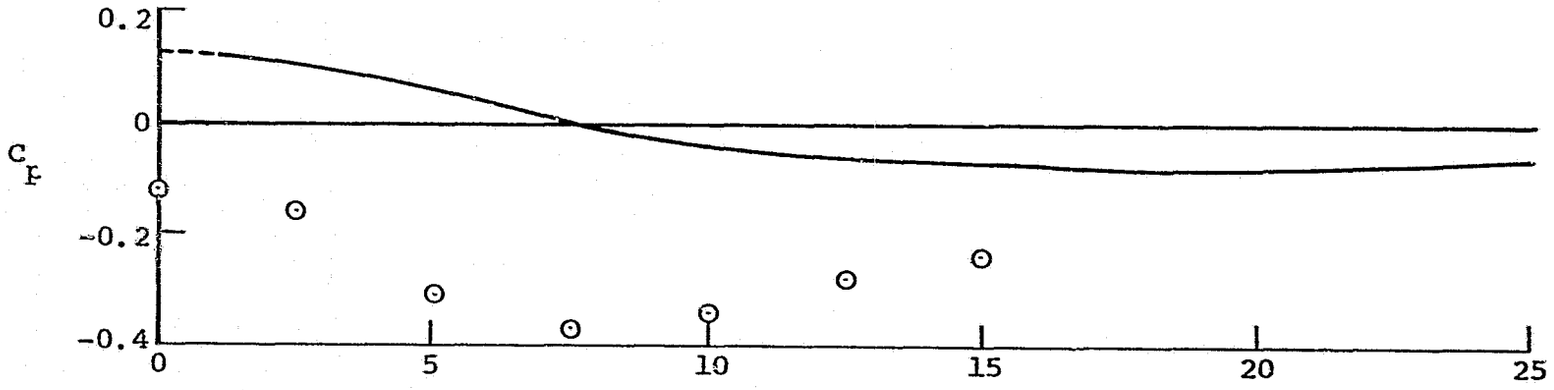

(k) x/D = -2.0.

Figure 34.- Continued.

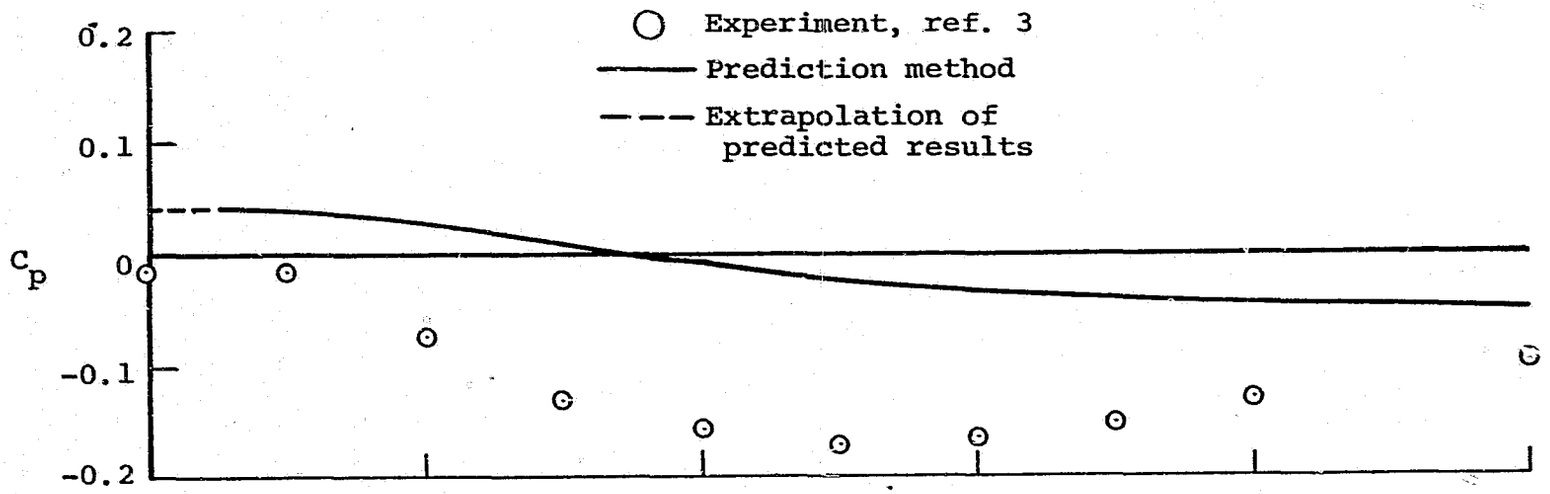

(ℓ) x/D = -3.0.

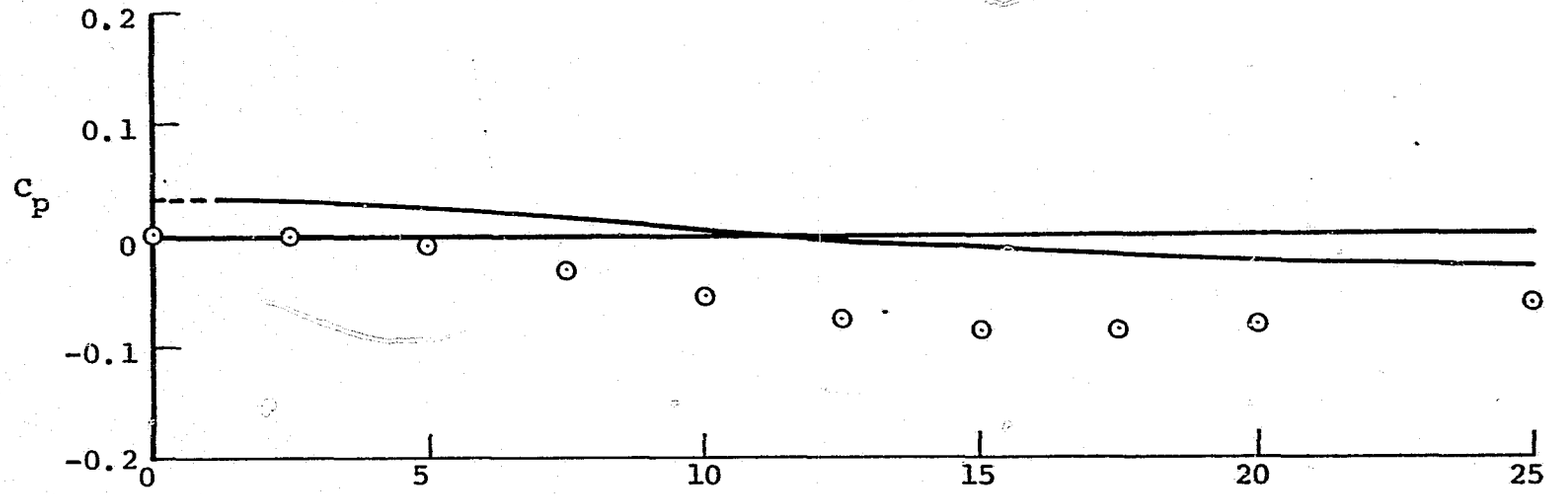

(m) x/D = -4.2.

Figure 34.- Continued.

C-3

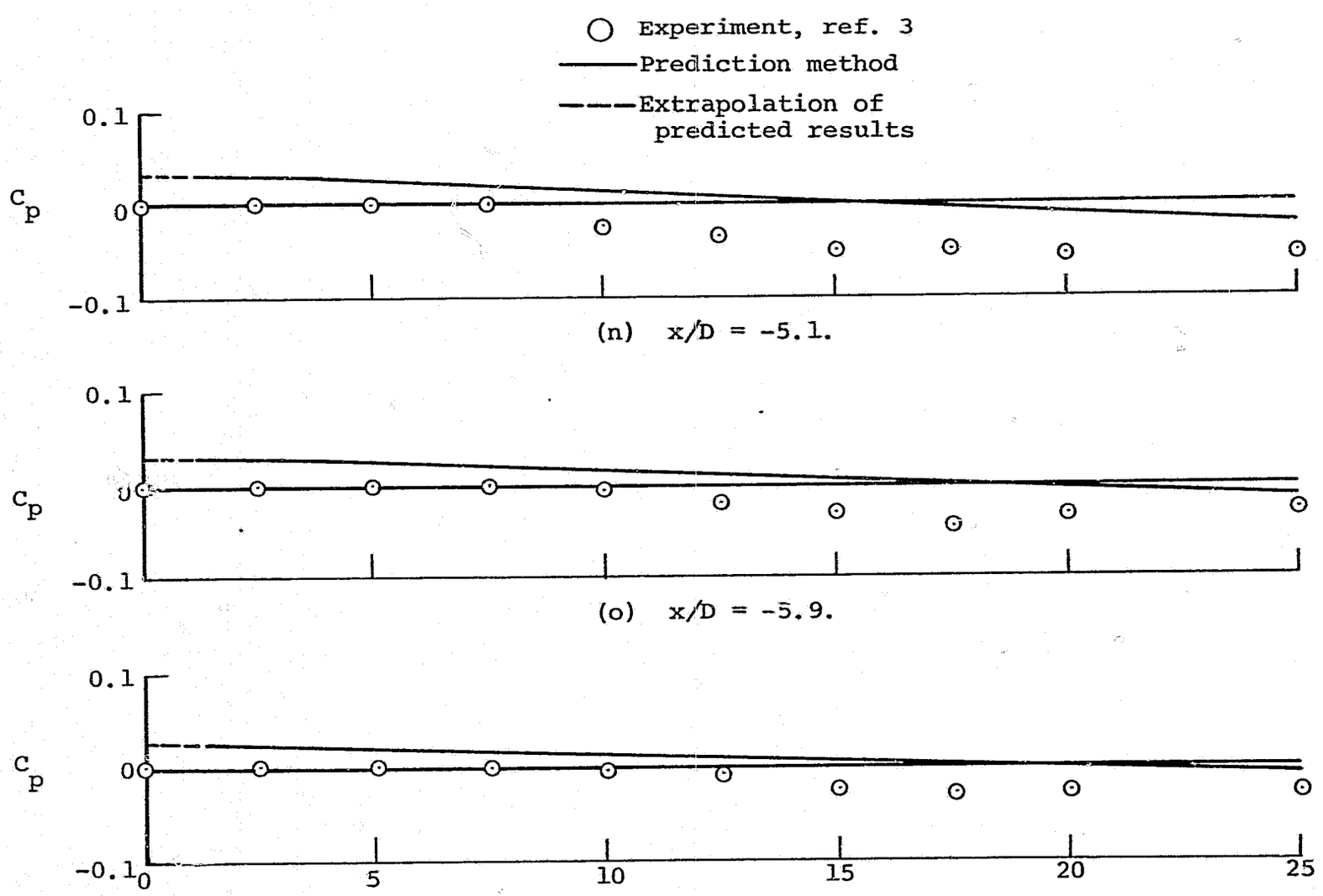

(n) $x/D = -5.1$.

(o) $x/D = -5.9$.

(p) $x/D = -7.0$.

Figure 34.- Concluded.

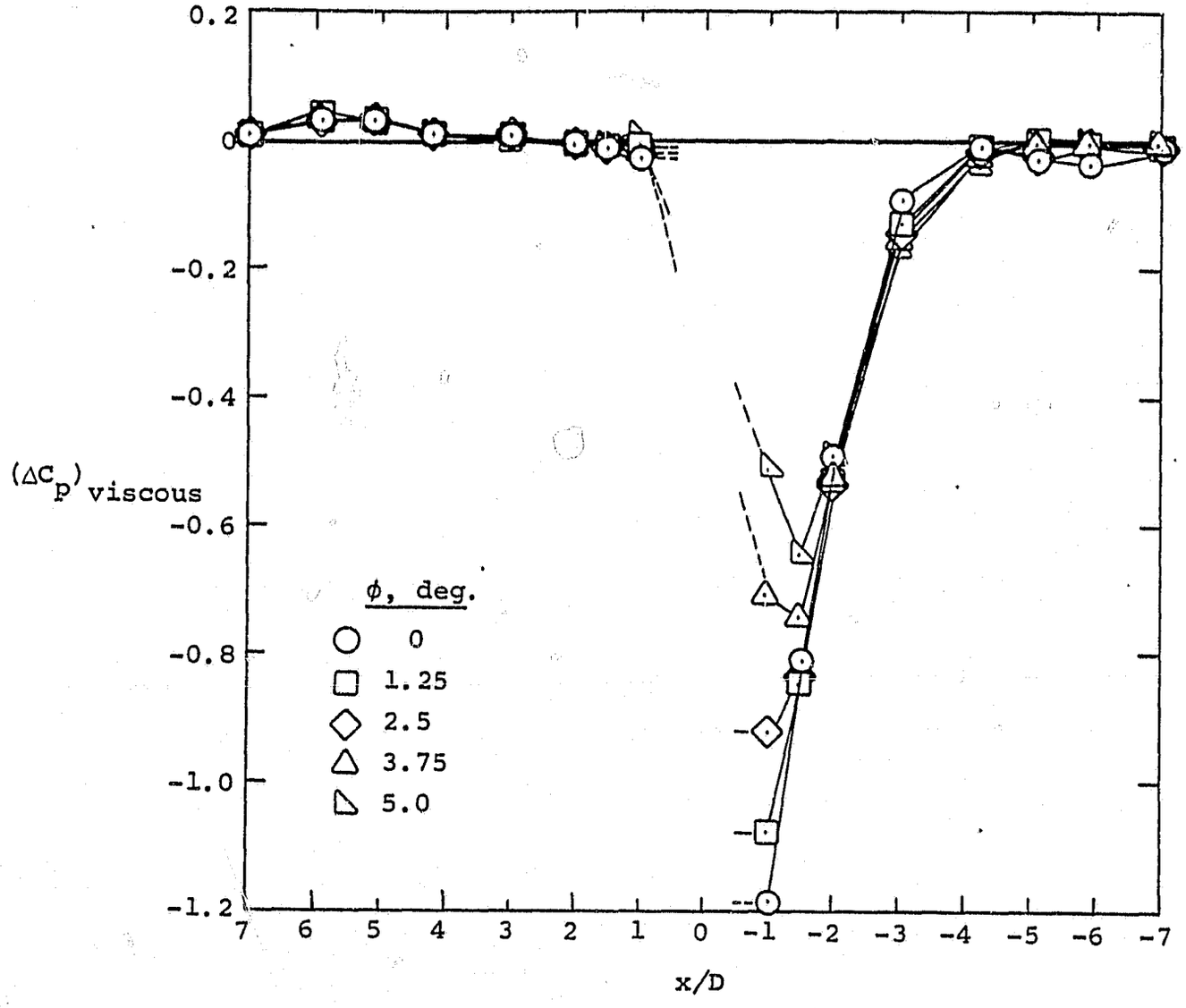

(a) $0^\circ \leq \phi \leq 5.0^\circ$.

Figure 35.- Correlation factors for viscous portion of the pressure coefficient induced on a body of revolution by a jet exhausting into a crossflow, $V_j/V_\infty = 1.96$, $\theta = 0^\circ$.

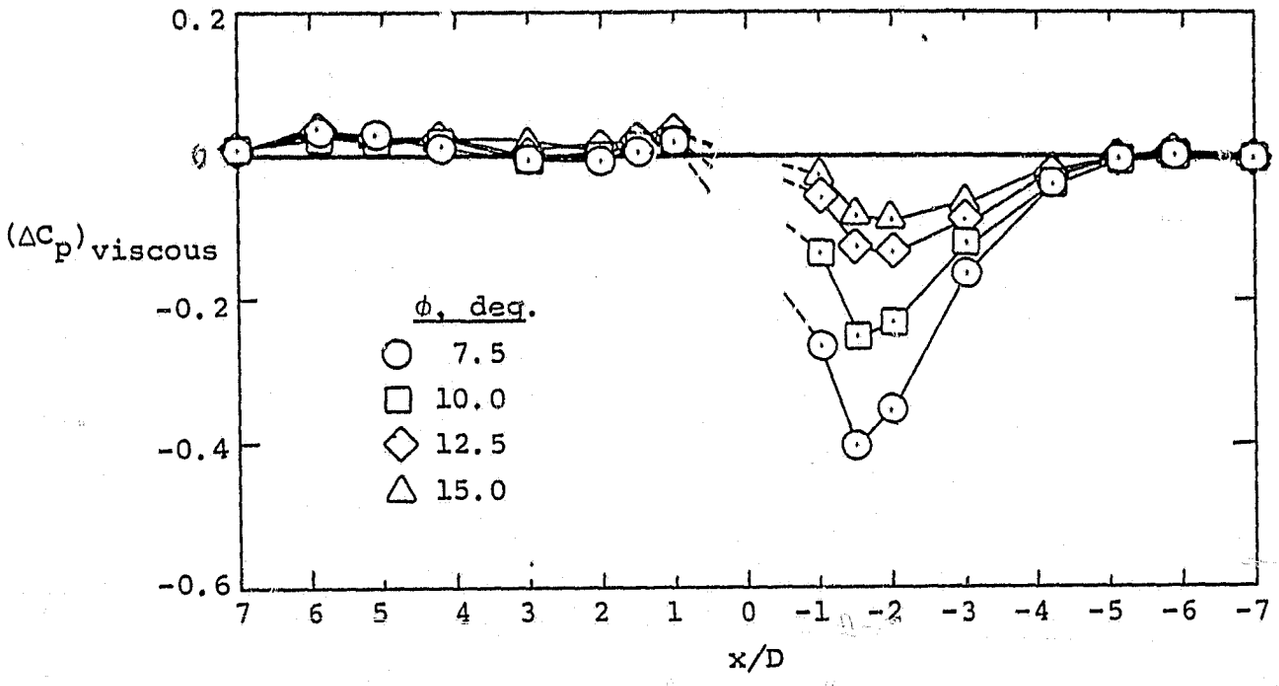

(b) $7.5^\circ \leq \phi \leq 15^\circ$.

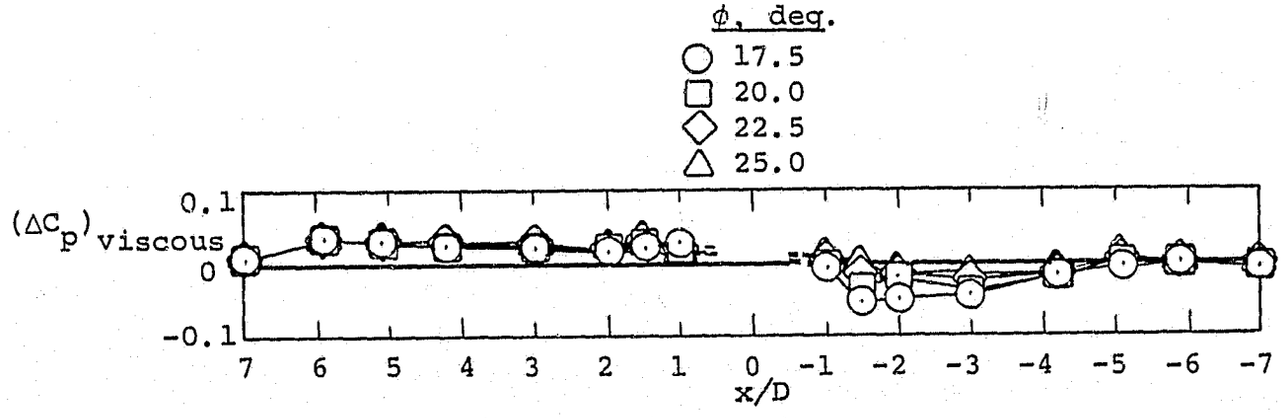

(c) $17.5^\circ \leq \phi \leq 25^\circ$.

Figure 35.- Concluded.

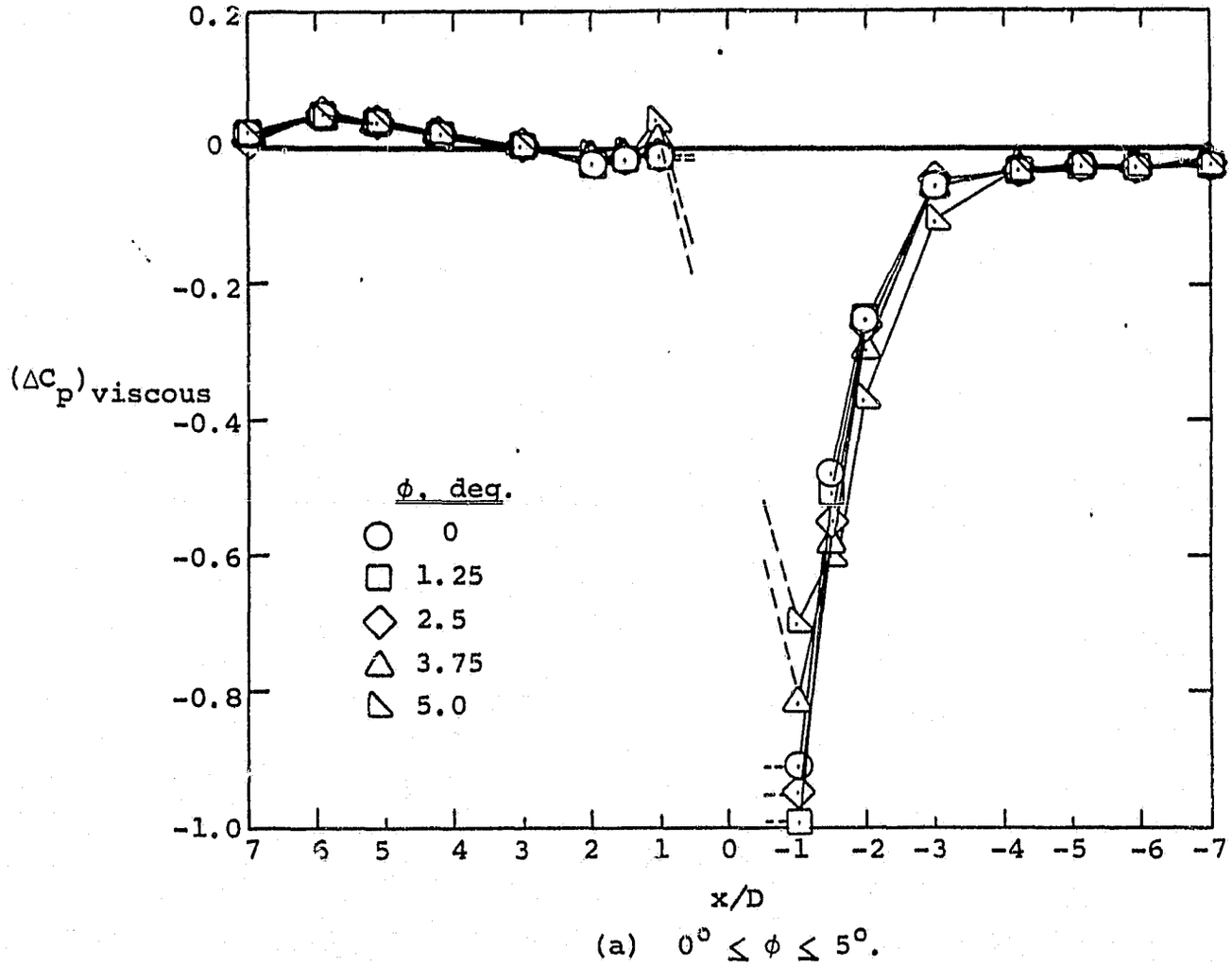

(a) $0^\circ \leq \phi \leq 5^\circ$.

Figure 36.- Correlation factors for viscous portion of the pressure coefficient induced on a body of revolution by a jet exhausting into a crossflow, $V_j/V_\infty = 3.43$, $\theta = 0^\circ$.

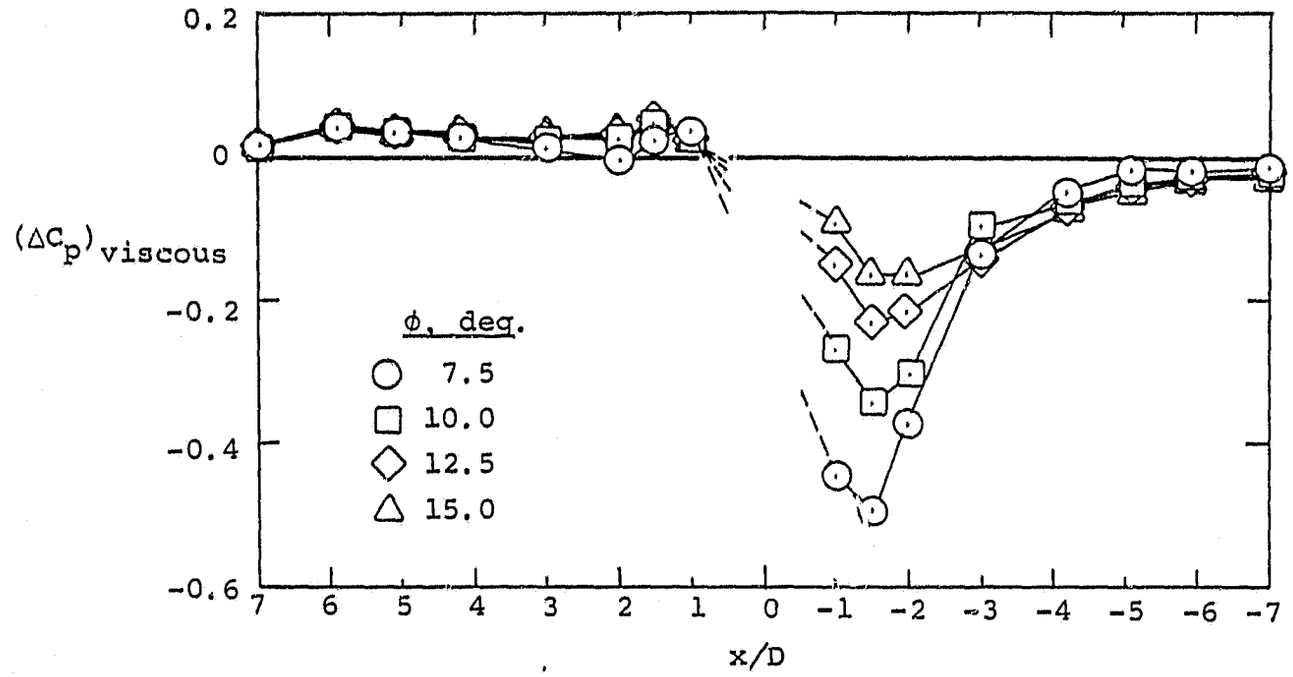

(b) $7.5^{\circ} \leq \phi \leq 15^{\circ}$

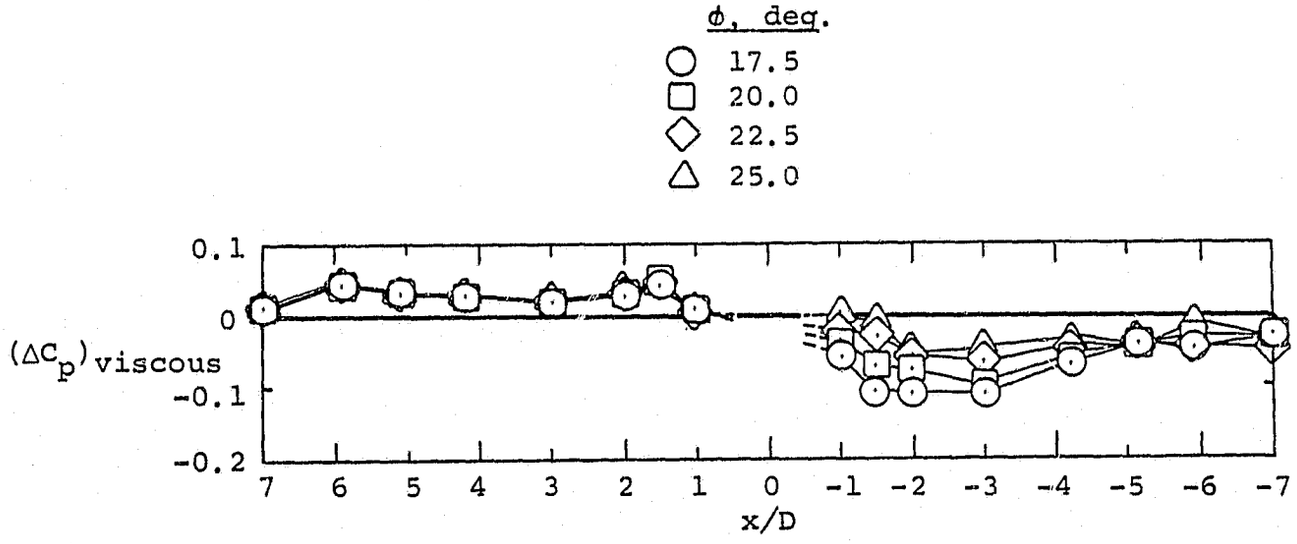

(c) $17.5^{\circ} \leq \phi \leq 25^{\circ}$.

Figure 36.- Concluded.